The Influence of Solid Additives on the Tribological Properties of Lubricants

Chuanli Zhao

A thesis submitted in partial fulfilment of the requirements of the University of Hertfordshire for the degree of Doctor of Philosophy

The programme of research was carried out in the School of Engineering & Technology, University of Hertfordshire, Hatfield, UK.

January 2013

Synopsis

The present work investigates the tribological properties of solid particles as lubricant additives in lubricants. Two types of solid particles, Ceria nanoparticles (CeO_2) and Zinc borate ultrafine powders (ZB UFPs), were used as the lubricant additives in this study. The friction and wear behaviours of these lubricant additives in different base lubricants were identified. With an appropriate application of these solid lubricant additives, the friction reduction and wear resistance properties of the lubricant have been successfully improved.

Without assistance of surfactant or surface modification, the two types of solid particles behave very differently. Evident performance was observed that pure ZB UFPs were capable of considerably reducing the friction coefficient of sunflower oil and liquid paraffin when they were used as a lubricant additive without further treatment. On the contrary, CeO_2 nanoparticles did not show noticeable contribution to friction reduction when they were used as the only additive in water. Only when surfactant Sorbitan monostearate was employed to enhance the dispersibility of CeO_2 nanoparticles in water, the application of this additive was capable of reducing friction coefficient of the water based lubricant effectively.

Surface modification of the solid particles was carried out to improve the dispersibility of these particles in base lubricants. Oleic acid (OA) and Hexadecyltrimethoxysilane (HDTMOS) were selected as the modification agents. Modified CeO_2 nanoparticles and ZB UFPs revealed outstanding wear resistance property. An improvement of up to 15 times was identified although this improvement on wear resistance, in this case, was often companied by a rise in friction coefficient.

Tribo-films generated by tribo-chemical reaction were observed on most of the worn surfaces and the formation of this tribo-film appeared to have played an important role in the friction

and wear behaviours of a system. A tenacious tribo-film with good surface coverage was only generated on the worn surface when HDTMOS modified solid particles were used as lubricant additives. The mechanical properties and elemental composition of the tribo-film were studied with nano-indentation and energy-dispersive X-ray spectroscopy (EDS). Finally, based on the experimental evidence, different functionalities of CeO_2 nanoparticles and ZB UFPs as solid lubricant additives were recognized

Acknowledgments

Foremost, I would like to thanks my supervisors, Dr. Yongkang Chen and Dr. Guogang Ren for their help and support throughout this project. Particularly, during this period, Dr. Chen guided me with great patience and cleared up the problems I encountered through the course of this PhD. My thanks also go to Dr Dr Andreas Chrysanthou and Mr Peter Thomson for all of their assistance and suggestions during this project. I would like to thank Mrs. Li Qiu at the Taiyuan University of Technology for her support in this project.

I would like to give a special thanks to Mr Yang Jiao and Mr Adil Loya for their help during the course in this PhD. They have been fantastic partners in the research and a real pleasure to work with.

A special thanks to many past and present colleagues in the Engineering & Science research group. Without the support of my colleagues, the work in this project would have seemed much harder. I also acknowledge the technical and administrative support at the School of Engineering & Technology.

Last but not least, I greatest gratitude must go to my family and my girlfriend for their support and unconditional love, not just through the past three years of my PhD, but up until now.

List of Contents

List of Figures and Tables

List of Abbreviations

AES	Auger electron spectroscope
AFM	Atomic force microscopy
ASTM	American society for testing and materials
DLVO	Deryaguin Landau Verwey Overbeek
DMT	Derjaguin Muller Toporov
DSC	Differential scanning calorimetry
EDS	Energy Dispersive Spectrometer
EP	Extreme pressure
EPMA	Electron probe micro analyser
FTIR	Fourier transform infrared spectroscopy
HDTMOS	Hexadecyltrimethoxysilane
HFRR	High frequency reciprocating rig
ICP-AES)	Inductively Coupled Plasma- Atomic Emission Spectroscopy
ISS	Ion-scattering spectrometer
L-B	Langmuir-Blodgett
LP	Liquid parrafin
NMR	Nuclear magnetic resonance
NP	Nano particle
OA	Oleic Acid
SEM	Scanning electron microscopy
SF	Sunflower oil
SIMS	Secondary ion mass spectrometry
STM	Scanning tunneling microscope
TCP	Tricresyl phosphate
TEM	Transmission electron microscopy
TGA	Thermogravimetric analyser
TLA	Thin Layer Activation
TXP	Trixylyl phosphate
UFPs	Ultrafine powders
wt. %	Weight fraction
XPS	X-ray photoelectron spectroscopy
XRF	X-ray fluorescence
ZB	Zinc borate
ZDDP	Zinc dithiophosphate

List of Symbols

a	Radius of contact area
A_l	Horizontal projection of the asperity contact
A_p	Vertical projection of the asperity contact
A_r	Real area of contact
D	Diameter
E	Young's modulus
E^*	Effective modulus
F	Friction force
H	Hardness
L	Length
p_m	Mean contact pressure
p_o	Maximum contact pressure
r	Asperity radius
R	Radius
W	Normal load
δ	Displacement
ε	Strain
τ	Shear strength
μ	Friction coefficient
μ_a	Coefficient of adhesive friction
μ_{def}	Coefficient of deformation friction
v	Poisson's ratio
θ	Attack angle
σ	Stress

Chapter 1. Introduction

1.1 Framework, Aims and Objectives

Lubricant additives have an important influence on the performance of lubricants. These additives are active ingredients which can be added during a blending process to base oils in order either to enhance the existing performance of the base fluids or to impart new properties that the base fluids lack. In modern industry, the ever growing demand on the duration and efficiency of machineries stimulates the research for lubricant additives with better performance. At the same time, industry is facing increasingly rigorous environmental regulations. Compared with the traditional organic lubricant additives that contain P, S and Cl elements, novel lubricant additives with environmental friendly feature are certainly becoming more desirable in the future, and research for the novel lubricant additives with good tribological properties and low environmental impact becomes important [1-3].

Most of lubricant oils at present contain several critical lubricant additives, including antiwear additive, dispersant, detergent, friction modifier, viscosity index improver and antioxidant. Traditionally, lubricant oils are presented as a single phase material in order to maintain a good consistency and dispersibility of the lubricant additives in the base oil. However, a great amount of research has been focused on introducing solid particles as a friction reduction or antiwear lubricant additive over recent years due to a number of incomparable advantages of the two-phase lubricant oils (liquid-solid), such as the superior thermal conductivity, the high pressure standing ability, high resistance to decomposition at temperature, low environmental impact, etc. [4-6]. Some of the solid lubricant additives, particularly in nano or submicron size, have even demonstrated better tribological

performances than the traditional organic additives, Zinc dialkyldithiophosphates (ZDDP) for instance.

Due to the diversity of the materials, there are still many controversies about how their behaviour in a base lubricant and their lubricating mechanisms although many potential candidates have been tested as the solid lubricant additives and many of them have shown the excellent tribological properties [7-9]. The major drawback of solid lubricant additives, the intrinsic poor stability in liquid base lubricant systems, has considerably restrained them from applications. Therefore the research on exploring novel solid lubricant additives and the techniques that would improve their dispersibility in base lubricants is certainly required.

In this study, CeO_2 nanoparticles, and zinc borate submicron particles have been selected as the solid lubricant additives and investigated. CeO_2 nanoparticles, as an important rare earth material have attracted much attention due to their special optical and electrical properties; however other information of this material, especially the tribological properties in lubricant base oil are still very limited. Similarly, the information of submicron size zinc borate powders, whose nanoparticles have showed outstanding lubricating performances, is also lacking.

Eventually, this research aimed to study the influence of these solid lubricant additives on friction and wear properties of the base lubricants, and to develop a new mild wear test method which can be applied to future exploration of different lubricant additives. This is achieved through the following objectives:

- Explore the influence of different types of solid lubricant additives on the friction and wear properties of the base lubricants.

2

- Improve the dispersibility of the solid lubricant additives by using surface modification technique and investigate the tribological properties of the surface modified solid lubricant additives.

- Interpret the mechanisms of the effects of these solid lubricant additives on tribological performances.

- Use advanced techniques to analyse worn surfaces and investigate the effect of particle dispersibility on the formation of tribo-films and the antiwear mechanism of the tribo-films.

1.2   Dissertation Outline

In Chapter 2, this thesis begins with a literature survey which aims to provide an understanding of the background knowledge and theories in tribology.

Chapter 3 provides a review regarding the previous studies on the solid lubricant additives. the tribological properties of different types of solid lubricant additives and the various mechanisms which have been proposed to explain their tribological behaviours are also discussed.

Chapter 4 describes the experimental techniques used to characterise the solid lubricant additives and to investigate the friction and wear behaviours of the solid lubricant additives in base lubricants as well as the mechanisms. The testing materials involved in this study including solid lubricant additives and the surface modification agents were also introduced in this chapter.

Chapter 5 presents the experimental results and observations which were obtained from tribology tests of using Cerium dioxide (CeO2) nanoparticles as the solid lubricant additive in water. The friction and wear reduction mechanisms of CeO2 nanoparticles in water were also discussed.

Chapter 6 reports the experimental results and observations of using Cerium dioxide (CeO2) nanoparticles as a lubricant additive in liquid paraffin. Oleic acid (OA) and Hexadecyltrimethoxysilane (HDTMOS) coupling agents were employed to modify CeO2 nanoparticle surfaces in order to improve the dispersibility in base lubricant. The tribological properties of the original and modified CeO2 nanoparticles in liquid paraffin (LP) was evaluated and compared.

Chapter 7 reports friction reduction and anti-wear properties of zinc borate ultrafine powders (ZB UFPs) as a lubricant additive in sunflower oil. The morphology and mechanical properties of worn surface as well as the tribo film generated on the surface were analysed.

In Chapter 8 surface modification to ZB UFPs were carried out using Oleic acid (OA) and Hexadecyltrimethoxysilane (HDTMOS) coupling agents to improve the dispersibility. Surface modification of ZB UFPs was verified using FTIR Spectrometer and Thermogravimetric analyser (TGA). The tribological properties of liquid paraffin with original and modified ZB UFPs were investigated and tribochemical reaction conducted on the worn surfaces was identified.

Individual interpretation and discussion sections were included in Chapter 5 to Chapter 8 to discuss the possible mechanisms of the tribological behaviour that the corresponding solid lubricant additive has demonstrated in base lubricants.

Finally, Chapter 9 summarises the main findings from the overall study and makes some suggestions for the future research in this area.

Chapter 2. Fundamental Theory of Tribology

2.1 Introduction

This chapter reviews the background knowledge and theories in tribology. It starts with a brief overview of the nature of a solid surface, the parameters to describe roughness and the fundamentals of contact models which have been developed to describe the encounter of real surfaces. The next section deals with the definition and previous studies of boundary lubrication, as surface sliding in this lubrication regime is the main focus of this thesis. A section that explains wear, wear mechanisms and its measuring approaches is included in the chapter. Finally the principles of friction and related mathematical models of different friction components are followed.

2.2 Solid surface

Tribology is the science that studies interacting surfaces in relative motion (all surfaces mentioned are referred to solid surface) [10]. The nature of the interaction of surfaces seriously influences the friction, wear and lubrication behaviours. Therefore a good understanding of the surface nature is essential in tribology study. This section reviews the nature of surface and surface contact.

2.2.1 Surface nature

Solid surfaces in general have complex structures and properties. The nature of solids, the method of surface preparation, and the interaction between the surface and the environment all have considerable influence on the structures and properties of solid surfaces. During friction practice, surface properties greatly affect the real contact area, friction coefficient,

wear, and consequently lubrication performance. Therefore, solid surface properties are critical to tribological functions.

No surface is perfectly flat. The solid surfaces, irrespective of the methods of formation, contain irregularities or deviations from the prescribed geometrical form [11, 12]. Shape deviation and reregulation of the order of inter-atomic distances obliterate the possibility of a molecularly flat surface.

Solid surface itself does not have a consistent structure like a bulk material. A solid surface is composed of several layers, which have different physic-chemical properties from the bulk material [13]. Generally speaking, surface material is distinguished to be five layers: Deformed layer, beilby layer, chemical reacted layer, physisorbed layer, and chmisorbed layer [14]. Details of these surface layers are presented as follow:

Deformed layer:

Deformed layer is referred to a strained layer that was formed during a material surface preparing process. This highly strained layer can be formed during grinding, lapping, machining and polishing processes, in which the surface layer can be plastically deformed and hardened [15-17]. Cook and Bhushan have demonstrated that the deformed layer can also be formed during friction [18].

The properties of deformed layer can be influenced by two factors: 1). the amount of work or energy that was put into the deformation processes; 2). the properties of the material. The closer the deformed layer gets to the surface, the more strained it becomes. The typical thickness ranges of the lightly and heavily deformed layers are 1-10 and 10-100 μm [14] as shown in Figure 2–1.

<u>Beilby layer:</u>

Beilby layer is the surface layer formed by quenching effect of melting surface flow deposited on the cool substrate material. The thickness of the Beilby layer ranges from 1-100 nm and it can be reduced by a fine finishing process [14].

<u>Chemically reacted layer:</u>

Chemically reacted layer is one of the most familiar surface layers. In atmosphere environment, oxide layers form on the surface of most metals and alloys due to the reaction with oxygen. The oxide layers can also be formed during machining and the friction process. Likewise, these metals and alloys will form other layers in different environment. The thickness of chemically reacted layers could vary with three factors: reactivity of materials to environment, reaction temperature and reaction time [14]. A typical thickness of chemically reacted layers is 10-100 nm. In the case where a lubricant is used during a friction process, the lubricant and its additive may result in the formation of a solid reaction film on substrate surface, and this film can play an important role in reducing friction or protecting substrate surface.

<u>Physisorbed layer:</u>

Physisorbed layer is a layer mounted on substrate material by physisorption. There is no electrons interchange between the chemisorbed components and the solid surface. Adsorbed layers can be formed on both metallic and non-metallic surfaces [14]. The most common constituents of adsorbate layers are molecules of water vapour, oxygen, or hydrocarbons from the environment that may be condensed and become physically adsorbed to the solid surface [19]. The thickness of the layer can be either polymolecular or monomolecular. Different from chemical reaction, during physisorption, no electron exchange takes place between

adsorbate and adsorbent. Bonding that is involved in a physisorption process is attributed to van der Waals force, which is relatively weak. With lubrication, oily and greasy film can be formed due to physical absorption of the lubricant applied. The thickness of the lubricant film can be as small as 3nm [14].
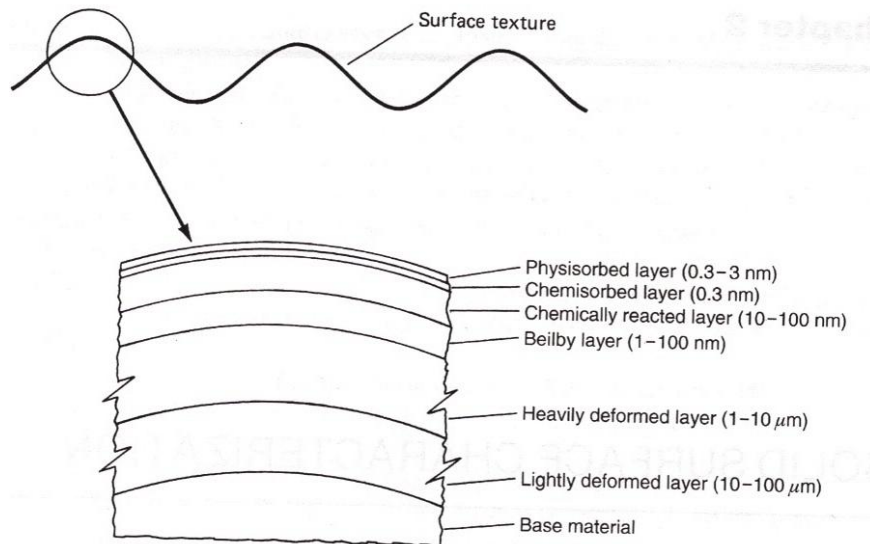
Figure 2–1 Solid surface layers [14]

Chemisorbed layer

Different from physisorption, electrons are shared and interchanged between the chemisorbed components and the solid surface in chemisorption. The bonding between the chemisorbed components and solid surface is covalent, which is much stronger than the Van der Waals force in physisorption [20].

In chemisorption, the chemisorption components remain their own identity. Therefore, the initial adsorbing components can be recovered through proper treatment. The difference between chemisorption and chemical reaction is that the chemisorption layer is limited to a monolayer. Chemisorption comes to an end as soon as the surface is covered with a layer. The formation of subsequent layer can be either physisorption or chemical reaction.

Compared with physisorption, chemisorption requires certain activation energy. As a result, chemisorption will only take place above certain level of temperature. Additionally, chemisorption will also be limited by the purity of the adsorbent surface, however, physisorption happens on all surface.

The comparison of Physisorption, chemisorption and chemical reaction is shown in Figure 2–2.
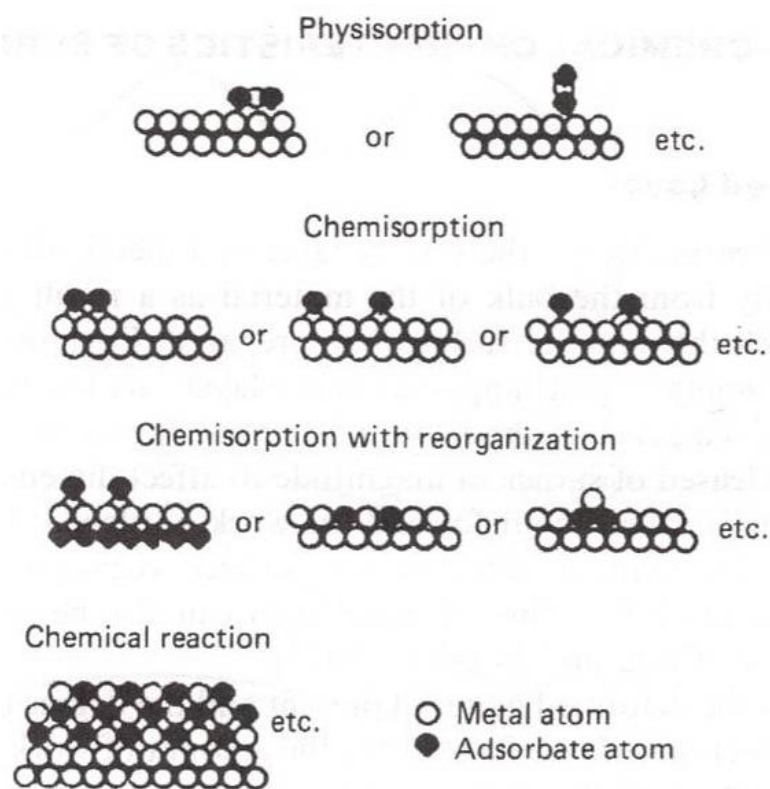
Figure 2–2 Schematic diagrams of physisorption, chemisorption, and chemical reaction [13]

2.2.2   Methods of surface analysis

A number of surface analytical techniques have been developed for the characterisation of surface layers [21]. The grain structure of the deformed layer can be determined by

examining the cross section area using powerful optical microscope or a scanning electron microscope (SEM). Transmission electron microscopy (TEM) can be used to examine microcrystalline structure and dislocation density of a sample prepared in very thin thickness. The crystalline structure of a surface layer can also be studied using X-ray, high-energy or low-energy election diffraction techniques (by firing electrons at a sample and observing the resulting, the properties of an element can be examined). Elemental analysis can be commenced by a range of analytical techniques, such as X-ray energy dispersive analyser (EDS) available with most SEMs, auger electron spectroscope (AES) [22], electron probe micro analyser (EPMA) [23], ion-scattering spectrometer (ISS) [24], Rutherford backscattering spectrometer (RBS), and X-ray fluorescence (XRF). The chemical analysis can be performed using X-ray photoelectron spectroscopy (XPS) and secondary ion mass spectrometry (SIMS) [25-27] .

Mass spectrometry, Fourier transform infrared spectroscopy (FTIR), Raman scattering, nuclear magnetic resonance (NMR) and XPS can also be used to conduct chemical analysis of adsorbed organic layers. XPS and ellipsomery (a powerful optical technique for the investigation of thin film) are the mostly used technique to measure the thickness of organic layers [14].

2.2.3   Surface roughness

2.2.3.1   Introduction of surface roughness

Surface texture is the description of the three-dimensional topography of a surface [28]. It includes three components: waviness, surface roughness and lay, as shown in Figure 2–3.

Lay is a description of the direction of the predominant machine finish [29]. Waviness is the measure of surface irregularities with spacing greater than that of surface roughness, which is

the surface irregularity in macro scale. Surface roughness is a measure of the finely spaced surface irregularities commonly in nano or micro scale. Surface roughness can be considered to be superimposed on the wavy surface [29].

In the tribology field, surface roughness is a factor mostly discussed and concentrated on. Roughness plays an important role in how a real object interacts with another. In machinery, high surface roughness usually causes high friction coefficient and wear rate. Machinery damage and unexpected energy loss are more likely to be introduced by the side products of friction, such as heat and wear debris, which is often caused by high surface roughness [30, 31].
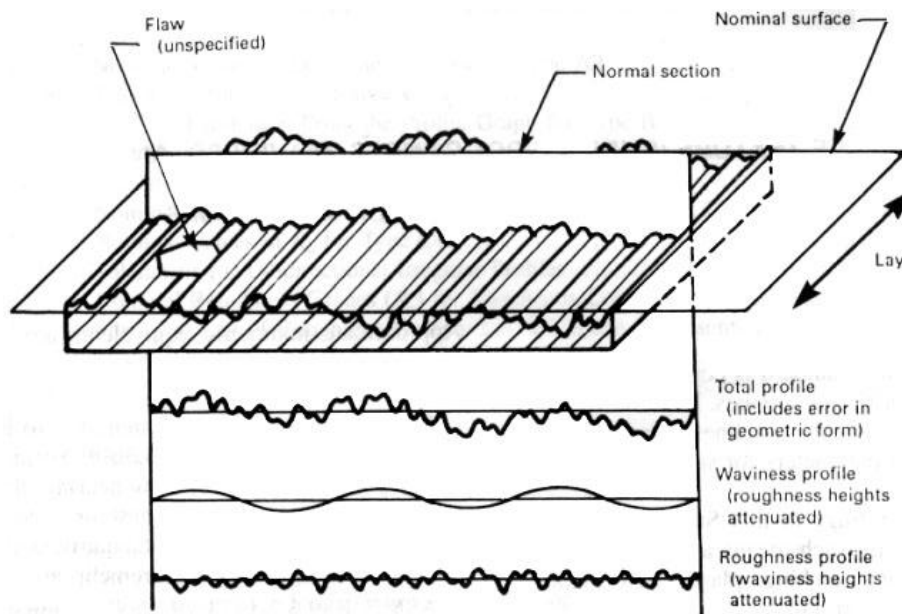
Figure 2–3 Concepts of surface roughness, waviness, and lay [32]

As a matter of fact, surface roughness has a very complicated relationship with wear. In 1938, America car manufacturer Chrysler suggested that low surface roughness would reduce the direct asperity contact so as to reduce abrasion [33]. If it was true, according to this theory, two perfect smooth rubbing surfaces would have no abrasion at all. However, in 1941 America car manufacturer Buick suggested that friction abrasion was mainly caused by

molecular interaction, consequently, certain level of surface roughness was required to protect machinery components from abrasion [33]. Mechanical department of former Soviet Academy of Sciences also studied effects of the surface roughness on wear rate, and they proved the existence of corresponding optimal surface roughness in different working conditions, as shown in Figure 2–4 and Figure 2–5. This theory has also been proved by many other scientific institutions [34-36].

The existence of optimal surface roughness indicates that: wear is caused by a coalition effect of mechanical interaction and molecular interaction. Mechanical interaction will play a predominating role when surface roughness is greater than the optimal figure. On the other hand, abrasion is mainly attributed to molecular interaction when surface roughness is smaller than the optimal value [14].
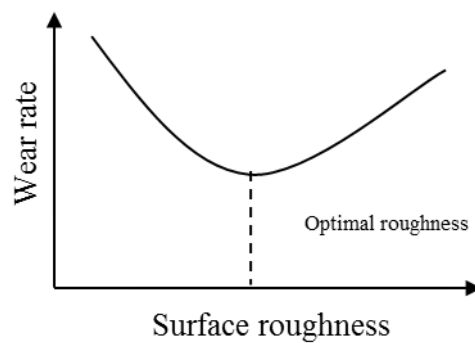
Figure 2–4 Relationship of wear rate and surface roughness [34]
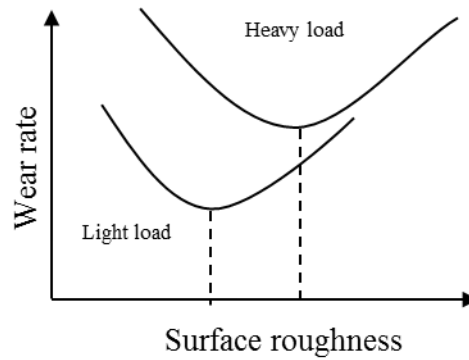
Figure 2–5 Optimal roughness at different loading conditions [34]

2.2.3.2   Roughness parameters

Surface roughness is a parameter that measures the texture of a surface. It commonly refers to the variations of asperities of surface compared with a reference line. It is usually described by one of the two statistical height descriptors advocated by the American National Standards Institute (ANSI) and the International Standardization Organization (ISO) [32, 37]. These two parameters are: (1) Ra, CLA (Center-line average), or AA (arithmetic average) and (2) the standard deviation or variance (δ), Rq or root mean square (RMS). As show in Table 2-1, there are other extreme-value height descriptors: R_t, R_p, R_v, R_v, R_z and R_{pm}.

Table 2-1 Roughness parameters

$\mathbf{R_t}$	maximum peak-to-valley height
$\mathbf{R_a}$	arithmetic average of absolute values
$\mathbf{R_q}$	root mean squared
$\mathbf{R_p}$	maximum peak height or maximum peak-to-mean height
$\mathbf{R_v}$	maximum Valley depth or mean-to-lowest valley depth
$\mathbf{R_z}$	average peak-to-valley height

The schematic presentation of a surface profile is shown in Figure 2–6. z(x) is a function of profile height measured from a mean line. The area of the profile above the mean line is equal to the area of the profile below the mean line.
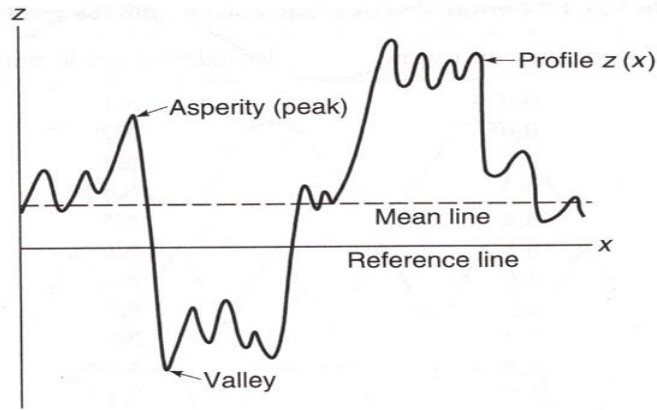
Figure 2–6 Schematic presentation of a surface profile [14]

Roughness Average Ra (also called AA and CLA) is an arithmetic average of the absolute values of the vertical deviation from the mean line to the profile. It can be written as:

$$Ra = CLA = AA = \frac{1}{L} \int_0^L |z(x)| dx \qquad (2\text{-}1)$$

where L is the profile length.

Rq or the Root Mean Square (RMS) is the square root of the arithmetic mean of square of the veridical deviation of roughness profile from mean line. It can be written as:

$$Rq = RMS = \sqrt{\frac{1}{L} \int_0^L z^2(x) dx} \qquad (2\text{-}2)$$

14

2.2.4 Surface contact

2.2.4.1 Introduction of surface contact

When two perfect flat surfaces are in contact, the normal force is supported evenly throughout the apparent contact area. However, the perfect surface does not exist. Even when the perfect finish was achieved to atomic level, a flat surface is still composed of spherical asperities because of the shape of atom. In real life, surface roughness makes contact only occur at certain contact spots as shown in Figure 2–7, where the spots in dark colour are the deformed asperities in contact. The real contact area is the sum of the contact areas of these spots. In most of the cases, when a load is applied, the real contact area will only be the small fraction of the nominal contact area. With an increase of the load, more asperities come into contact, and the real contact area also increases. Clearly real contact area is decided by surface texture, material properties and loading conditions. Friction and wear are contributed by interactions of asperities on contact pairs. The degree of these interactions greatly depends on the properties of real contact [38]. Therefore understanding of the contact mechanism is essential in study of tribology.
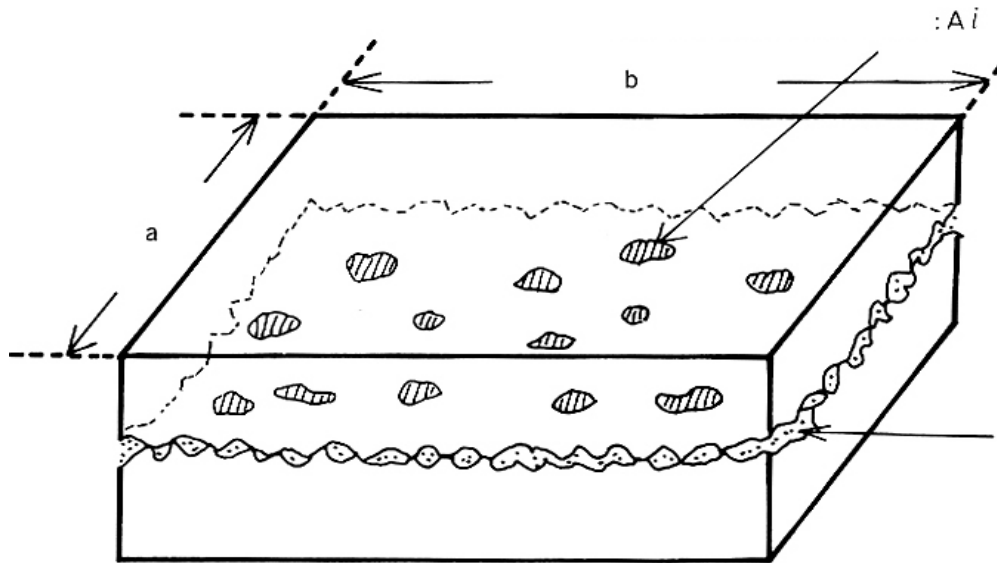
Figure 2–7 Surface asperity contact and deformation [39]

Both the uneven size and shape of surface asperities cause the uncertainty of the mode of surface deformation. When a small load is applied on an object, elastic deformation firstly occurs. The local stresses may exceed the elastic limit although sometimes the nominal stress is within the elastic range (yield strength) [38]. Similarly, in most of the cases, some asperities are conducting elastic deformation when others are experienced plastically. The overall deformation of the object is still elastic, but plastic deformation on the tip of some asperities has already taken place

Asperities on surface are not uniform. As a result, in order to avoid interference of asperities in different conditions, a contact analysis of contact focusing on single asperity is conducted. Due to the small size of each asperity, it is convenient to treat the tip of an asperity as spherical shaped.

2.2.4.1.1 Elastic contact

The first analysis of contact mechanics of two elastic solids was attributed to Heinrich Hertz in 1882 [40]. Such elastic contact is referred to as Hertzian contact. The analysis of such contact is based on 4 assumptions:

- The surfaces are continuous, smooth and nonconforming

- The strains are small

- Each solid can be considered as a elastic half-space in the proximity of the contact region

- The surfaces are friction less

A schematic model of two solid spheres in static contact is shown in Figure 2–8 [14]. The x-y plane is the contact plane. The point of first contact is taken as the origin of a coordinates system and the two spheres in contact have radii of R_1 and R_2. The objects are brought into contact when a normal load W is applied, and a circular contact area is formed due to the deformation of the spherical bodies. Hertz realised that the condition of the deformation was related to Young's modulus E, Poison's ratio v, and the geometry shape of both bodies, and the load W applied. Hertzian formulae for calculating the contact area radius, the maximum pressure and the approach of two distant points are given below:
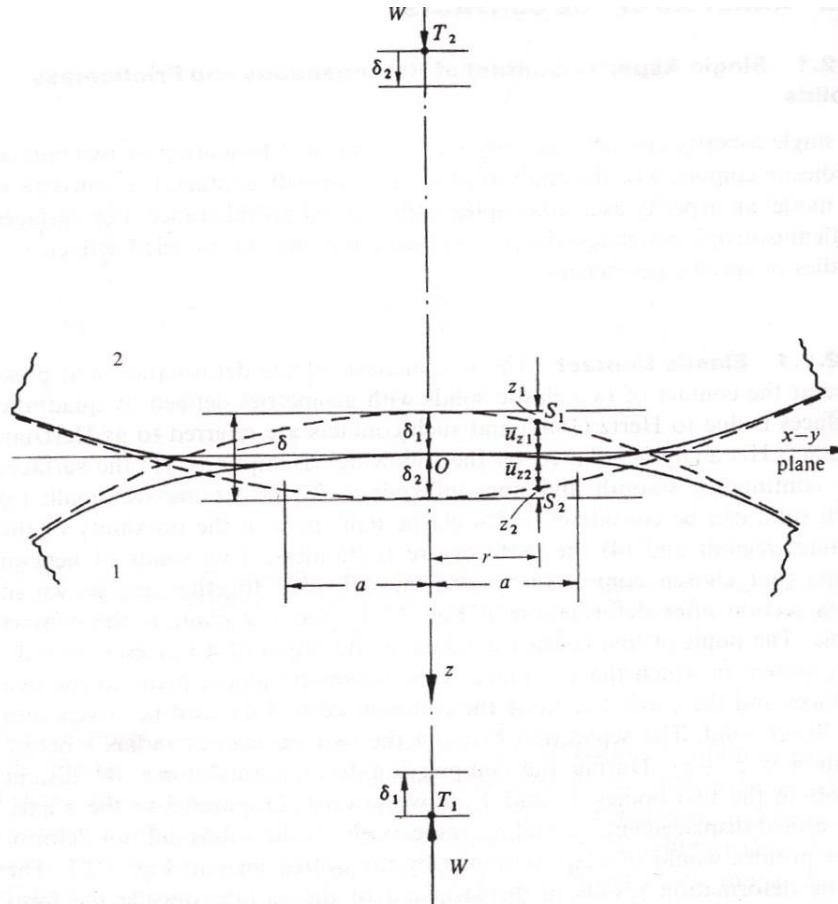
Figure 2–8 Two frictionless spherical solid in static contact [14]

The radius of contact area can be written as:

$$a = \frac{\pi p_o R}{2E^*} = \left(\frac{3WR}{4E^*}\right)^{1/3} \tag{2-3}$$

$$A_{contact} = \pi a^2 \tag{2-4}$$

where:

p_o is the maximum contact pressure, W is the normal load, R is the effective radius and E^* is the effective modulus.

Approach of distant points Compliance:

$$\delta = \frac{a^2}{R} = (\frac{\pi p_o}{2E^*})^2 R = (\frac{9W^2}{16RE^{*2}})^{1/3} \tag{2-5}$$

where the composite Young's modulus equals:

$$\frac{1}{E^*} = \frac{1 - v_1{}^2}{E_1} + \frac{1 - v_2{}^2}{E_2} \tag{2-6}$$

The composite curvature:

$$\frac{1}{R} = \frac{1}{R_1} + \frac{1}{R_2} \tag{2-7}$$

The maximum contact pressure p_o is achieved at the contact center with a value of 1.5 times of mean contact pressure p_m:

$$p_m = W/A_{contact} \tag{2-8}$$

$$p_o = \frac{3}{2} p_m = \frac{3W}{2\pi a^2} = (\frac{6WE^{*2}}{\pi^3 R^2})^{1/3} \tag{2-9}$$

The pressure distribution is elliptical:

$$p = p_o[1 - (r/a)^2]^{1/2} \tag{2-10}$$

In macro scale, there are many other contact forms, such as contact between a sphere and an elastic half-Space, contact between two crossed cylinders, contact between a rigid Cylinder and an elastic half-space, and contact between two cylinders with parallel axes. The calculations for these contact forms are all following the similar principle.

However, the classic Hertz contact model does not incorporate the effect of adhesion. In the theory any surface interactions such as near contact Van der Waals interactions, or contact

adhesive interactions are neglected. Based on the previous work, some improved elastic contact models were developed by other scientists.

2.2.4.2   Improvement of elastic contact

2.2.4.2.1   JKR model

With consideration of surface energy, Johnson *et al.* [41] have developed the JKR theory for elastic contact. In this theory they incorporate the adhesion effect in Hertzian contact. The contact area of JKR model is composed of two parts, one is attributed to the elastic material deformation, and the other one is introduced by interfacial interaction strength (adhesion strength). As a result of the adhesive contact, contacts can be formed during the unloading cycle also in the negative loading (pulling) regime. Schematic contact profile for the JKR model is shown in Figure 2–9.
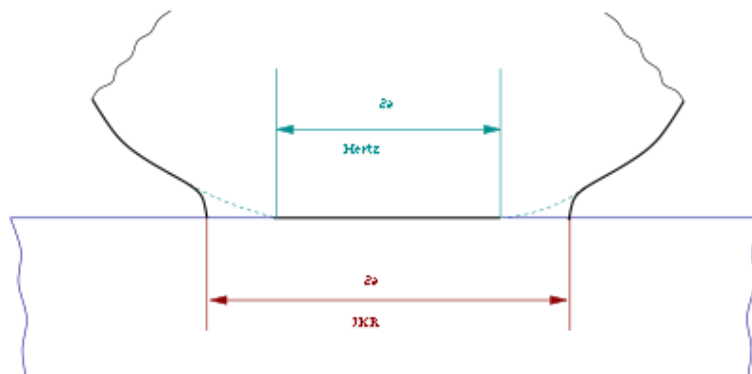
Figure 2–9 Contact profile of JKR model

2.2.4.2.2   DMT model

An alternative model for adhesive contact has been developed in Derjaguin Muller Toporov (DMT) model. According to DMT theory, the contact area remained the same as in Hertzian contact, but adhesion and Van der Waals played additional attractive interactions outside the

area of contact [42]. Schematic of contact profile for the DMT model is shown in Figure 2–10.
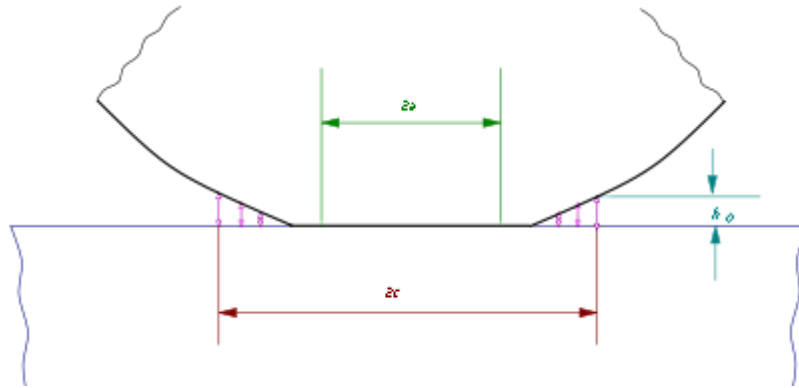
Figure 2–10 Contact profile of DMT model

2.3 Boundary lubrication

2.3.1 Introduction

Three distinguishing lubrication regimes can be observed when two rubbing counterparts are lubricated by liquid lubricants. These three lubrication regimes are defined by a relative thickness of the lubricant film formed between the rubbing components to the roughness of the component surface:

Hydrodynamic or fluid film lubrication is the condition when the load carrying surfaces are separated by a relatively thick film of lubricant. This is a stable regime of lubrication and metal-to-metal contact does not occur during the lubrication since the thickness of the lubricant film is bigger than the roughness of the surfaces. The lubricant pressure is self-generated by the moving surfaces and the lubricant is entrapped into the wedge formed by the moving surfaces at a sufficient velocity to generate the pressure to completely separate the surfaces and support the applied load [43].

Mixed lubrication is the condition when a lubricant film formed between two surfaces is thick enough to avoid most of the asperities in contact but not sufficiently thick to prevent the contact completely as in hydrodynamic lubrication regime. During this type of lubrication, the tallest asperities of the bounding surfaces will protrude through the film and occasionally come in contact. This lubrication regime often occurs at high load condition when insufficient entrainment speed and lubricant with low viscosity are applied [44].

Boundary lubrication is the condition when the fluid films are so thin and there are considerable asperities in contact. Compared with the other two lubrication regimes, boundary lubrication generally occurs at relatively severe operating conditions. Very low entrainment speed, very high load and the employment of lubricant with very low viscosity could all result in boundary lubrication [45].

A boundary film can be formed during boundary lubrication, and the physical and chemical properties of thin surface films are of significant importance. Lubricant additives can have important influence to the properties and the formation of boundary films. Therefore in boundary lubrication it is important to understand the characteristics of the lubricant additives and the boundary films. The morphology of boundary films is very random and depends on the lubrication condition. The boundary films can be either patchy or continuous [46, 47].

Extensive studies in boundary lubrication have been carried out over recent years, and various advanced techniques have been developed and employed. However due to many intrinsic difficulties the understanding of this type of lubrication is still not comprehensive. First of all, the study of boundary lubrication involves the understanding of the boundary films which generally have a very small thickness varying from few nanometres to hundreds of nanometres. Such small size introduces enormous difficulties on not only the scientific measurement but also the theoretical analysis. Secondly, boundary films are formed in a

closed environment and locked between two moving surfaces. This makes the real time observation difficult. Finally, there are many factors that would affect the formation and properties of the boundary films, such as: physical and chemical nature of metal surface, geometry of the contact, properties of the lubricants, environmental influences, lubricating conditions, *etc.*

2.3.2 Stribeck curve

Stribeck curve is often used to present the transitions between different lubrication regimes [48, 49]. In a Stribeck curve, as shown in Figure 2–11, friction coefficient is presented as a function of viscosity, speed and load. Stribeck curve can also be used to show how friction coefficient develops with a variation of lubricant film thickness since these are the parameters that control the lubricant film thickness.

Many sliding components are attempted to be designed to operate in hydrodynamic and mixed lubrication regimes, in which low friction coefficient and wear can be obtained due to the good separation of sliding surfaces by a lubricant film. However, for some components enduring very high pressure, especially in starting and stopping stage, boundary lubrication can be the dominant regime in which the system is operating and high friction and wear are expected in these circumstances. In boundary lubrication, a monolayer of adsorbed molecules could make a noticeable difference on the antiwear performance of a component. The performance of sliding components in boundary lubrication becomes crucial since it sometimes controls the durability of the components [50-54].
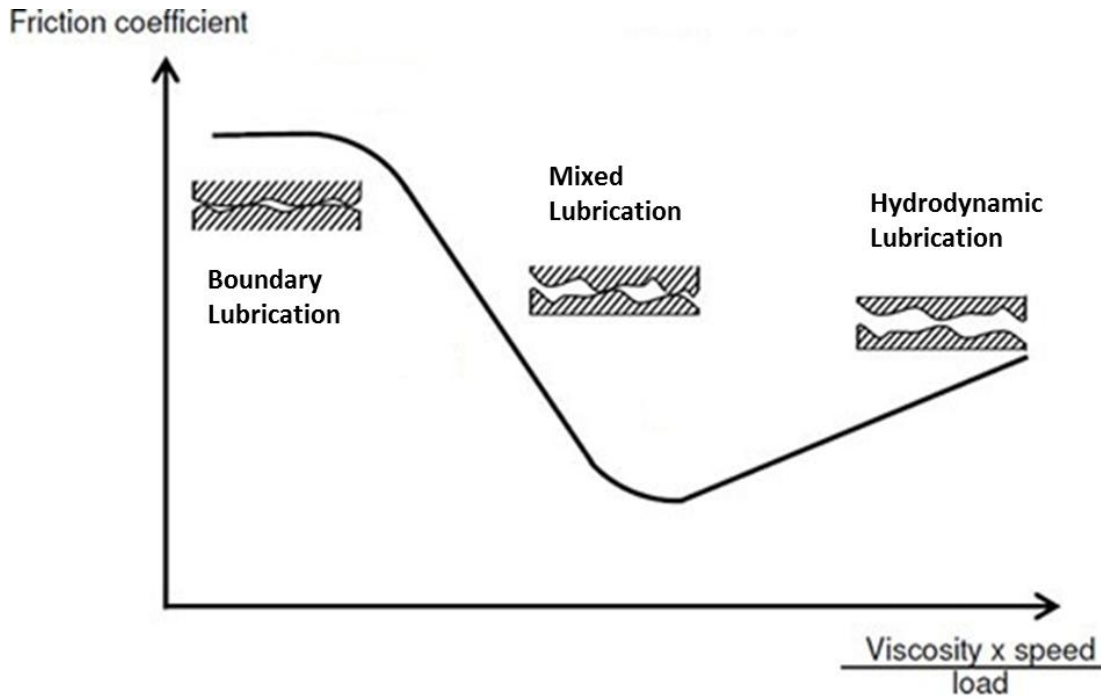
Figure 2–11 Stribeck Curve [55]

2.3.3 Current status on boundary lubrication

In hydrodynamic lubrication, the lubricating performance of the system greatly depends on the physical properties of the lubricant, such as viscosity. As suggested by Reynolds, since the two surfaces were separated by a complete lubricant film, the physical and chemical interactions of the lubricant with the solid bodies appeared to be relatively unimportant. However, in boundary lubrication, it is quickly realised that although two different lubricants have the similar viscosity they could deliver quite different performance of lubrication. It was thought that the lubricating performance of a lubricant was governed by 'oiliness', which was soon understood to be associated with the interaction of lubricant with solid surface. Interaction of the lubricant with solid surface is believed to play an important role in boundary lubrication.

Wells and Southcombe [56] in 1920 found that low concentrations of long chain surfactants reduced friction and wear in a boundary lubrication region. It was later discovered that the reduction of friction and wear was related to the adsorption of a monolayer or multilayer of surfactant on solid surface. This then attracted much attention of the researchers [57-60].

The term '*boundary lubrication*' was firstly used by Hardy and Doubleday [61] to describe the friction and wear reduction in sliding of two solid bodies. They believed that the solid bodies were separated by oiliness film composed of surfactant molecules. In the same period, Langmuir [62] found that surfactant molecules adsorbed on metallic surfaces to form vertically-oriented mono-layers, and consequently friction coefficient was reduced. The amount of wear and friction reduction was also proved to be dependent on the chain length of the surfactants.

Extensive studies have been done on the nature of the surfactant layers on the solid surfaces over 40 years. It was discovered that the oiliness films were made of near-vertically oriented molecules of long chain polar surfactants [63]. Langmuir-Blodgett (L-B) technique was developed to produce monolayers or multilayers on a surface [64]. This technique proceeds by transferring an insoluble monolayer floating on the surface of water to the surface of a solid. Bowden and Tabor [65] examined the influence of the number of the surfactant layer deposited on a surface to the friction coefficient. The results show that the greater the number of layers deposited on the surface the longer it takes to be worn off, hence the longer these surfactant layers will protect the surface from wear. The effect of chain length of the carbon atoms of paraffin, alcohols, and fatty acids on the coefficient of friction was also studied by Bowden and Tabor [65] and Zisman [66]. They observed a steady decrease in friction coefficient with an increase of carbon chain length when a stainless steel surface was sliding against a glass surface lubricated by a monolayer of fatty acid. Zisman [66] and Owens [67]

have also reported the improvement on durability of the lubricant films with a length grow of the film chain. In the later studies, there are consistent works showing that the lubricants may decompose chemically during rubbing, and a polymerized layer can be formed to protect the substrate surfaces. The thickness of this type of layer can even reach hundreds of nanometres [68].

In recent decades, many new techniques have been established to study the boundary films [69-71]. Different types of lubricant additives are also developed to improve the strength and the duration of boundary films formed during the usage. For instance, additional organophosphorus compounds in lubricant are found to be particularly useful to reduce wear [72, 73]. Many other organic additives such as tricresyl phosphate (TCP), trixylyl phosphate (TXP) and dilauryl phosphate have also been proved to have good anti-wear and extreme pressure (EP) properties [74-76]. Similarly to zinc dithiophosphate (ZDDP), they usually contain active elements such as sulphur, phosphorus or chlorine as well as polar group for strong adsorption. Under mild sliding conditions, a perpendicular orientated film will be formed on specimen surface to withstand the local contact pressure; On the other hand, under harsh conditions, those additives could react with specimen surface to form a protection film which protects interaction surface from further damage. ZDDP is one of the mostly used additives, and together with other popular additives they are still routinely used in lubricants today [51, 71, 77, 78].

However, there is always a downside for an employment of these active elements. Due to their corrosion effects on metal surface and pollution caused during manufacture, the use of these organic lubricant additives ought to be limited for environmental concern. More recently, inorganic solid lubricant additives have also been developed. The utilisation of nano sized or submicron sized particles as an inorganic lubricant additive is gradually earning their

attention in industrial applications, owing to their outstanding tribological properties and good environmental friendly feature compared with the traditional organic lubricant additives that contain P, S and Cl elements [1, 76, 79-82]. Like the traditional lubricant additives, some of the inorganic solid lubricant additives are also capable of forming a boundary film through so-called 'tribo-chemical' reaction to protect the rubbing surfaces. This boundary film may contain the materials from lubricant additives, lubricant, and substrate surface. [83, 84]

2.3.4 Types of boundary films and characterisation techniques

Boundary films can be generated in different forms. Based on the chemical and physical properties, thickness, and the structure orientation of the films, they can be categorized in to the following types as shown in Figure 2–12 [85].

Boundary films can also be sorted into two groups according to their physical states: solid-like boundary films and viscous or fluid-like boundary films [69]. The difference between the two groups of films can be demonstrated clearly in a Stribeck curve. As shown in Figure 2–13(a), the friction coefficient in boundary and mixed lubrication regimes (low speed) can be reduced with the presence of solid-like boundary films as a result of the low shear strength of the asperities of the films and the reduction of adhesive junctions [86]. Alternatively, in Figure 2–13(b), highly viscous boundary layer formed on the solid surface can be entrained into a contact easily, so that the mixed lubrication regime can be reached at relatively low speed, and therefore the formation of fluid-like boundary film is able to shift the Stribeck curve to the left [87].
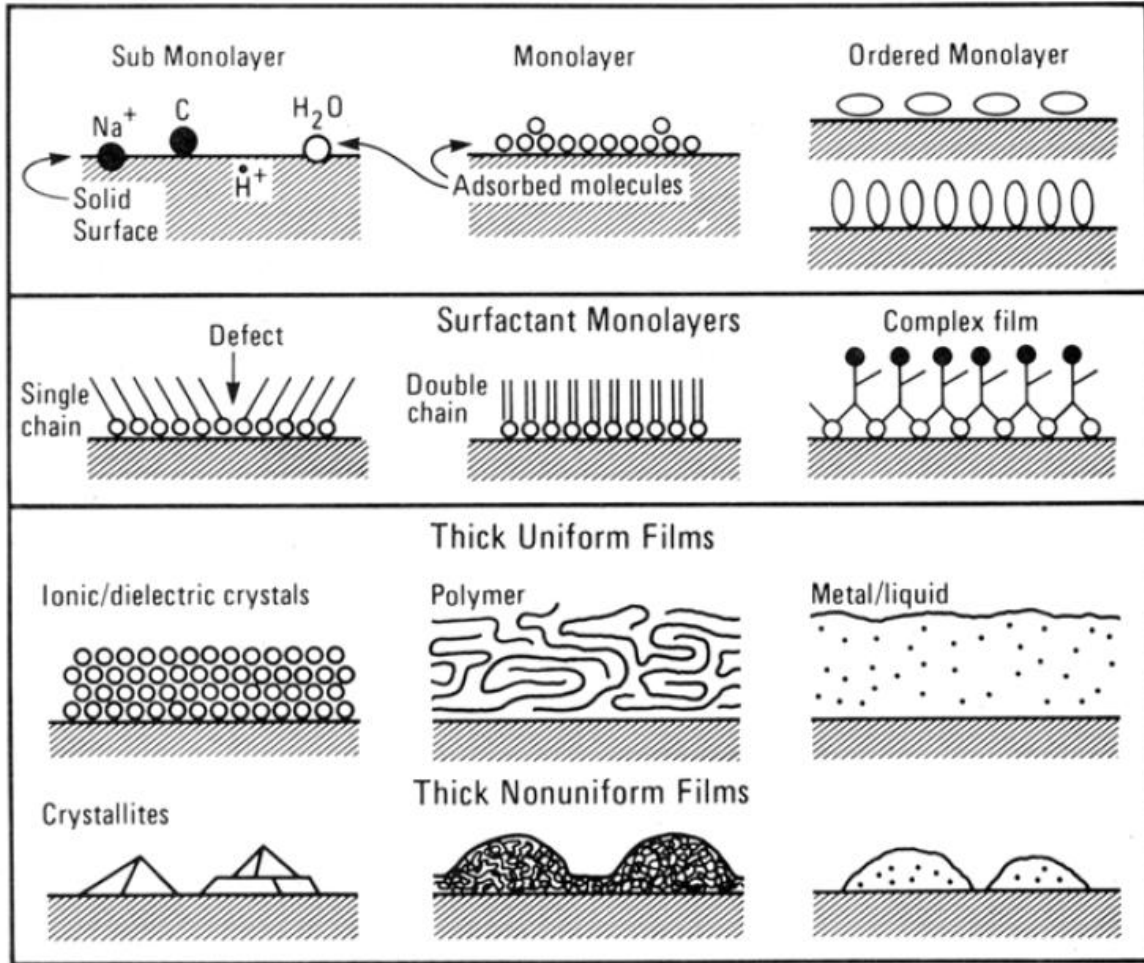
Figure 2–12 Types of boundary films on solid surfaces [85]

(a)

(b)
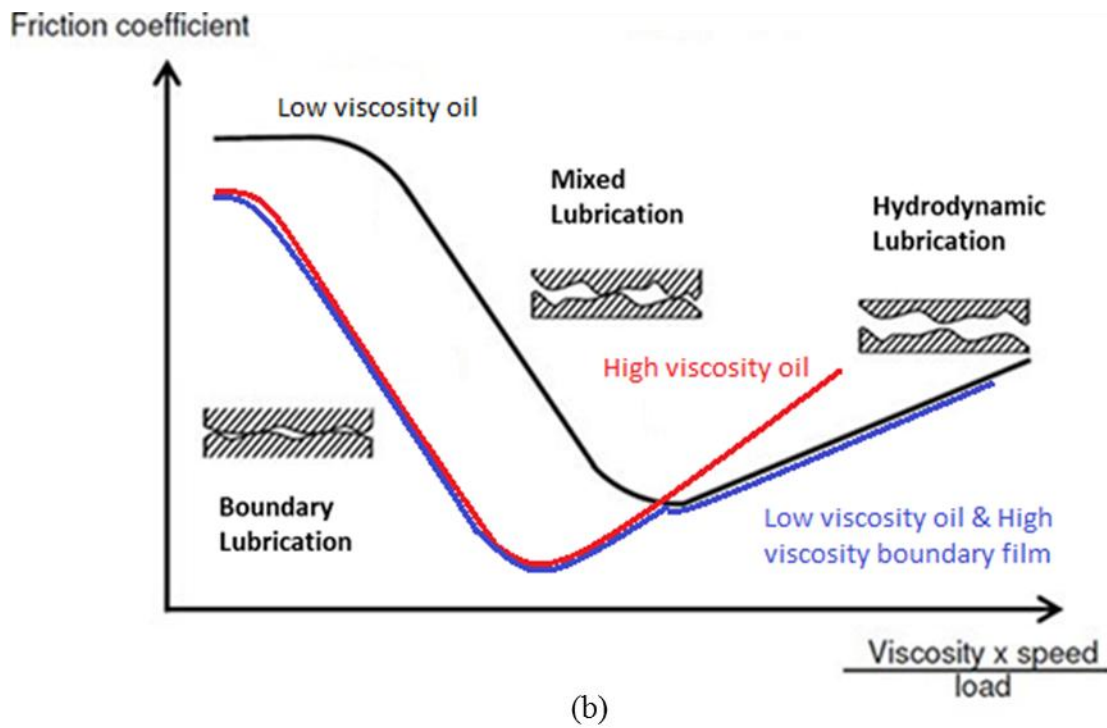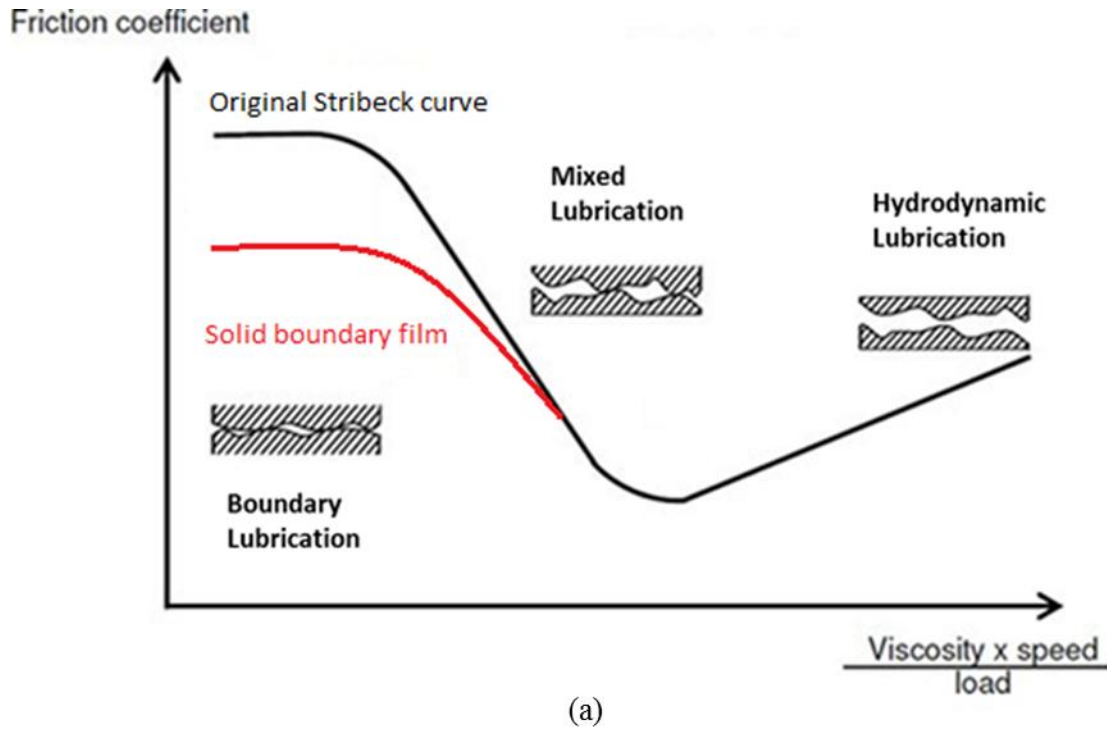
Figure 2–13 Influence of boundary films on lubrication regeme (a) solid-like boundary film and (b) viscous boundary film [87]

2.3.4.1   Solid-like boundary films

Solid-like boundary films are the most common boundary films formed on rubbing surfaces. Chemical reactions are often involved in the generation process of these boundary films [53]. There are several mechanisms of how the boundary lubricating film may function. Mainly these films functionalise as a sacrificial film or an easy shear layer. In the shear motion of the surfaces, the solid-like boundary films will be worn off gradually; therefore, replenishment character of the films becomes very important. The rate of film generation must be higher than the rate of film removal to ensure their efficacy [88].

Oxide layers

Oxide layers can be the most common boundary films. Normally, oxide layers would deliver lower friction coefficient and wear compared with bare metal surface due to reduced adhesion.

Layer-structure films

Layer-structure films are the boundary films with a layer lattice structure like graphite and molybdenum disulphide. Each two layers are attached together through Van der Waal force. The weaker attraction force between each layer cannot provide the structure a good resistance on shear deformation, and therefore imparts the layer-structure films, the lower shear strength.

Surfactant monolayers

Surfactant monolayers are composed of surfactant molecules. These surfactant molecules normally contain a polar group attached to a long, non-polar hydrocarbon chain. This polar end can attach to metal surfaces through Van der Waal forces. The long chain hydrocarbon

group can reduce the direct surface contact and reduce adhesion between asperities. Consequently reduction of friction and wear can be limited.

Active element additive films

In relatively severe conditions, lubricant additives that contain active elements such as sulphur, chlorine or fluorine may react with substrate metal and form boundary films containing the complex compounds [77, 89]. These boundary films have relatively low shear strength and are able to protect the sliding surface from seizure.

Boundary films generated by solid lubricant additive

Employment of solid inorganic lubricant additives has attracted much attention in recent years for technical and environmental reasons. Boundary films can be formed on the rubbing surface through two mechanisms: tribo-chemical reaction [90-93]; mixture of polymerised lubricant with additive particle filler [2, 53, 80].

2.3.4.2   Viscous, fluid-like boundary films

Viscous, fluid-like boundary film can be generated in the form of a monolayer of polymers adsorbed on the metal surface when some mineral oils which contain polar viscosity index improvers are used as lubricant. This layer of polymer has much higher concentration than the bulk solution, and therefore it has great influence on friction and wear performance at low speeds when the boundary film thickness reaches the similar dimension with the diameter of the polymer molecules. Lubricants of mixture of polar and non-polar components which have different viscosity can also form viscous, fluid-like boundary films. A viscous boundary film with a thickness of few nanometres was observed by Gao and Spikes in their study on mineral oil mixed with highly viscous polar ester [94].

2.3.4.3   Characterisation techniques of boundary film

Interferometry

Optical interferometry is the one of the best techniques that is capable of offering an *in-situ* observation of the formation of boundary films. This technique is originally applied in an investigation of elastohydrodynamic film in the 1960s [95]. As illustrated in Figure 2–14, it involves a metal ball or cylinder rolling or sliding a flat glass counterpart. During measurement, a beam of light is shone through the flat glass onto the contact zone. Two beams of light, one is from the underside of the glass and the other one is from the surface of the metal (due to the separation of the glass and metal surface by a lubricant film), are reflected back to the same side of the glass. An interference fringe pattern can be generated by these two beams of light. By calculating the parameters of the fringe pattern, the thickness of the lubricant film that separates the two surfaces can be achieved.

An improvement of the technique was made in the 1980s by coating a transparent solid spacer layer of around 100 nm to the flat glass, which significantly increased the accuracy of the film thickness measurement to 2 to 5nm [96]. This enables the application of the optical interferometry technique on boundary film observation [77, 97-99].

Spacer layer

Glass flat

To spectrometer

Inlet light

Outlet light
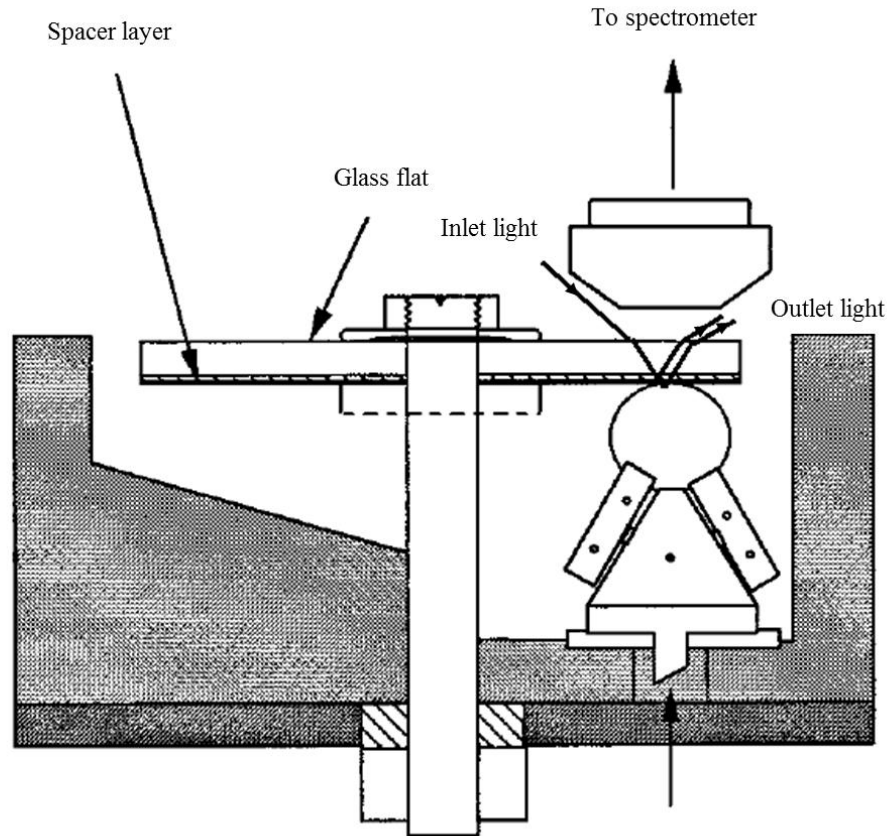
Figure 2–14 Set-up of optical interferometry [96]

Scanning Tunnelling Microscopy

A scanning tunneling microscope (STM) is an instrument that is able to image surfaces at the atomic level, which have made significant contributions to the study of the detailed topography of boundary films. The scanning tunneling microscopy was invented by Binnig in 1982 based on the concept of quantum tunneling [46]. When examining a surface with STM, a scanning tip is brought very close to, and voltage is applied between the tip and the surface so that electrons are able to tunnel through the vacuum between them. Information of the surface is acquired by monitoring the current as the tip's position scans across the surface [100]. The scanning tip used in STM is very sharp, typically has a radius of several nanometres. However, compared with other scanning microscopic techniques, STM has a big

drawback in the application of boundary film examination, as it requires extremely clean and stable surfaces, chemical variations of films formed on the surfaces may distort tunneling current and fail to give perfect compliance of the real topography of the surface [47].

Atomic Force Microscopy

Atomic force microscopy (AFM), also known as scanning force microscopy (SFM), is another type of scanning probe microscopy with very high resolution. The AFM is one of the most popular tools for surface imaging and measuring at the nanoscale. The AFM was developed to overcome the basic drawbacks of STM. The AFM consists of a cantilever with a sharp tip at one end that is used to scan the specimen surface. The force between the tip and a specimen surface is maintained constantly, and when the cantilever is dragged along a surface, the image of the surface can be generated by recording the deformation of the cantilever. Simplicity is the greatest advantage of AFM. It does not require complicated sample preparation such as conductive coating and can be applied on surfaces made of most of the engineering materials. AFM was employed in current study to map the morphology of tribofilm, the details of apparatus configuration and set-up will been discussed in Chapter 4.

2.4   Wear

2.4.1   Introduction

Wear is known as the progressive removal and deformation of material on a surface in a sliding, rolling or impact motion against its counterpart. In most of the cases, wear is not desired, since it may result in shrink in durability of machinery components, reduction of reliability and cost of replacement for failed machinery parts. Therefore it is of great interest for industry to carry out research on characterising and minimising wear.

Like friction, wear is not a material property. Wear of a system depends on many factors, such as working environment, type of motion, speed of motion, load, temperature, contact geometry, properties of the contact surfaces and so on [101]. Wear of a system is independent from the friction performance to some extent. High friction can be companied with little wear, and low friction does not necessarily suggest insignificant wear [14].

2.4.2 Mechanisms of wear

There are generally four types between wear: abrasive wear, adhesive wear, fatigue wear and corrosive wear. Based on the material removal mechanism, the four types of wear are listed as follow:

Abrasive wear

Abrasive wear occurs in sliding between two surfaces, where an asperity of one surface penetrates to the counterpart and removes materials from it. Abrasive grooves can be generated on a soft surface by the ploughing action of the asperities from a hard surface. The displaced material forms ridges adjacent to grooves. Wear debris can be produced and removed from the surface due to microcutting mechanism. For brittle material, wear debris can also be formed due to a crack propagation underneath the surface and eventually being peeled off from the surface [102]. Depending on material properties at the contact region and the contact mechanics, two types of abrasive wear can be released: two-body mode and three-body mode. As shown in Figure 2–15, two-body wear occurs when the asperities of a hard surface abrade a softer surface and remove material from the counterpart. While in three-body mode, the loose particles or debris are not constrained, and are free to roll and slide on a surface.
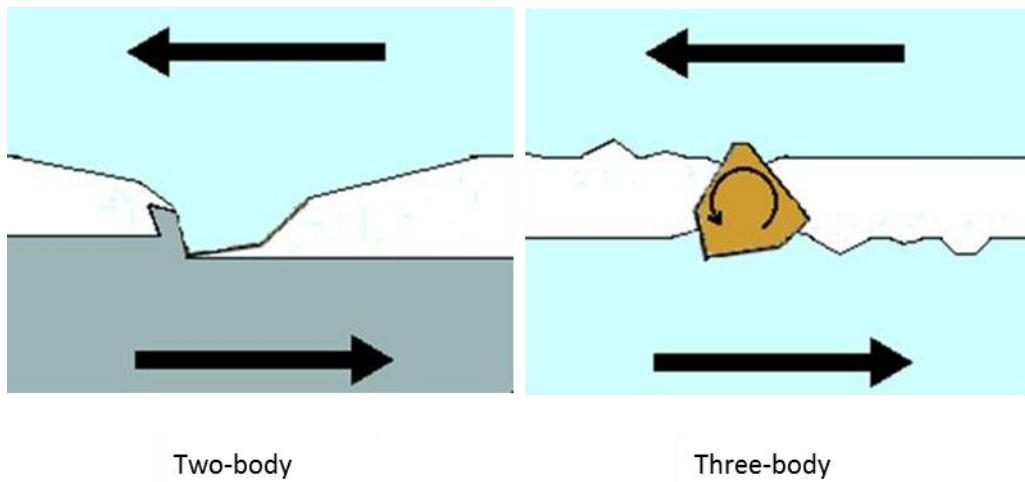
Figure 2–15 Schematic view of abrasive wear [102]

Adhesive wear

Adhesive wear takes place in sliding motion of two surfaces, when asperity contact undergoes adhesion or cold welding. Adhesive wear involves a detachment of material from one surface and an attachment of the same material to the other surface, as illustrated in Figure 2–16. Theoretically, wear does not occur in adhesive wear, materials are simply transferred from one body to the other. However, the transferred material is often weakly attached and will eventually be detached in microscopic particles. The result of adhesive wear is characteristically a matted, torn surface with grooves in the direction of sliding, and often with transferred ridges of material [103]. Adhesive wear can take place in both dry friction and lubricated friction conditions. Surface attraction and surface energy play an important role in adhesive wear. Some level of adhesion on contact surfaces happens in most solids. However, oxidation films, lubricants and contaminants on a surface can all suppress adhesion. Even with lubrication, severe adhesion may still occur under high load and high shear rate. Using lubricant additive that can interact rapidly with sliding surfaces and form a protective film is an effective approach to reduce adhesion and prevent adhesive wear [104].
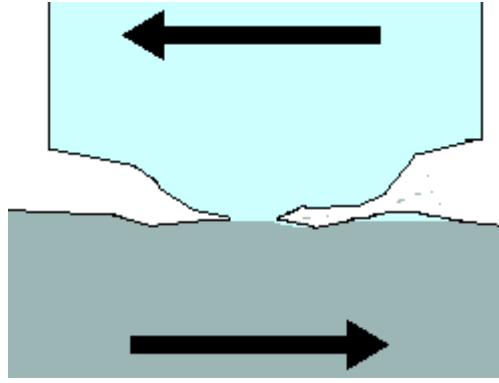
Figure 2–16 Schematic of Adhesive wear [104]

Corrosive wear

Corrosive wear is caused by a removal of layers of materials which are being continually formed on rubbing surfaces by chemical reaction. Corrosive wear takes place when surfaces are slide in a corrosive lubricant system or a lubricant system contains corrosive species such as water, oxygen, carbon dioxide, sulphur and other types of lubricant additives. The reaction product generated from chemical or electrochemical interactions is often weaker than the substrate material. Although the resultant usually prevents or reduces adhesive wear, it can be easily abraded away. As the fresh surface exposes, the reaction continues. Since the chemical reaction is the dominant mechanism for corrosive wear, the wear rate is controlled by the rate of chemical reaction.

Fatigue wear

As the name suggests, fatigue wear is a type of material failure caused by repeated stress cycles on an asperity contact. The repeated loading and unloading cycles that the materials are experiencing may induce cracks on surface or underneath surface [105]. Cracks can be initiated and propagated by fatigue wear even when the sliding is relatively too mild to prompt adhesive wear and abrasive wear. As shown in Figure 2–17, when these cracks reach a critical size, the top material will be removed and catastrophic wear will take place [105].
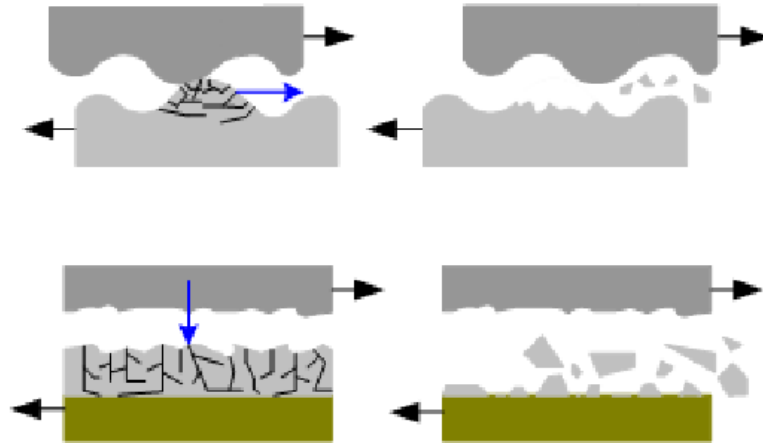
Figure 2–17 Schematic of Fatigue wear [104]

In a system, the dominant wear mode may not be constant at all time. There are a number of factors that may influence the transition of wear mode such as [106]:

- A change of contact geometry and

- Altering of the properties of the rubbing surfaces

- Lubricant additive empoyed.

2.4.3   Wear measurement

A number of ways developed to measure wear have been widely accepted and become the standard means to characterise and subsequently predict wear [107, 108]. These measuring techniques can be categorised into two groups: direct measurement and indirect measurement.

2.4.3.1   Direct measurement

Mass measurement

Evaluating wear by measuring tested samples directly is a broadly used quantification technique due to its convenience and simplicity. This technique involves weighting the

sample before and after a test, and the variance between the two measurements tells how much the wear is. However, in order to ensure a good accuracy, this technique is only suitable in measuring a system with relatively high wear rate and mass loss. The tested samples must be cleaned thoroughly and handled in a great care as deposit of oxidized oil, wear debris and contamination could all affect the reliability of the result. In particular, one downside of this method is that it does not provide any information on the distribution of wear on worn surface.

Dimension measurement

For some other specimens with a predictable geometrical change after tribological test, a dimension measurement is another way of quantifying wear. The dimension measurement includes linear, wear scar diameter and volume measurements of the specimens.

Linear measurement is often practiced in pin-on-disc test, where the reduction of pin length is recorded to reflect the wear rate. Same method also applies on measuring a change in diameter of cylindrical shafts, discs or bushes in wear tests.

Wear scar diameter measurement is generally used in 4-ball and ball-on-disc tests, and high frequency reciprocating rig (HFRR) where bearing balls are used to rub against a counterpart. Because of the spherical shape of the bearing balls, worn surface generated in the test will appear as a circle. Material loss can be quantified in volume with only one dimension of the circle due to the special spherical geometry. The biggest advantage of this method is that the measurement of the depth of the wear scar can be avoided; therefore a good accuracy can be achieved even in a low wear rate scenario.

The volume of the material loss can be obtained directly using atomic force microscope (AFM) [109, 110], light interferometer [111, 112] and stylus or optical 3-D profilometer.

With these sophisticated techniques very precise measurement becomes possible even for very mild wear. Gahlin [113] used AFM to measure the local wear volume and to map the distribution of wear by comparing the topography of the same surface region before and after a test. This technique promises to bring evaluation of wear to a new level of sensitivity and detail, in an order of 30nm. More importantly, the extremely high resolution endowed by these techniques may also improve tribological testing of real machine elements by reducing the need for excessively accelerated tests or an extremely long test duration [113].

2.4.3.2   Indirect measurement

Thin Layer Activation (TLA)

Thin Layer Activation (TLA) is originally a corrosion monitoring technique developed from nuclear science. It uses high-energy charged particles beam to produce a radioactive surface layer and gamma radiation will be emitted as radioisotopes decay. The change in gamma radiation emitted from the surface layer, which is associated with material removal from the surface, can be measured by suing a gamma detector. This technique promises a real time observation on wear phenomena, not only it can be employed in an experimental simulation but also in real machinery testing in industry [114].

Inductively Coupled Plasma- Atomic Emission Spectroscopy (ICP-AES)

Inductively Coupled Plasma-Atomic Emission Spectrometry (ICP-AES) is one of the most common techniques for elemental analysis. In ICP-AES, a plasma source is used to dissociate the sample into its constituent atoms or ions, exciting them to a higher energy level. Depended on the element present, the photons of a characteristic wavelength will be emitted when they return to their ground state. This light then can be recorded by an optical spectrometer and calibrated against standards to provide a quantitative analysis of the target

sample [115]. Since ICP-AES can only be used to detect metal elements, it is of particular interest to monitor the wear performance of a system contains metal by using this technique. Fan and Spikes [116] successfully used ICP-AES to monitor the concentration of iron in lubricant solution from which wear rates of system was determined.

2.5 Friction

2.5.1 Introduction

Friction is a resistant force generated when a body is in sliding or rolling motion against a counterpart. Friction force can be desirable in some cases such as gloves, brakes and clutches, but also undesirable in other scenarios such as bearings and gears. Friction is not a material property but a system response. Apart from material, friction of a system also depends on many environmental factors. For instance, in the same system the static friction force which is the tangential force required to initiate motion is often higher than the kinetic friction force which is the force required to continue the motion [117].

There are three most basic rules of conventional friction established by Leonardo da Vinci and Guillaume Amontons [118]. They are:

- In kinetic friction, friction coefficient (μ) is the ratio of the friction force (F) to the normal load (W) and is independent of normal load as described in equation below:

$$F = \mu W \qquad (2\text{-}11)$$

- The coefficient of friction (or friction force) is independent of the nominal area of contact

On top of these two rules, a third rule was added by Coulomb [119]:

- The friction coefficient (or friction force) is independent of the sliding velocity once motion commences.

These three rules that build the very foundation of tribology are entirely empirical. Although they are generally obeyed in wide range of applications, situations in which these rules are not followed do not suggest disagreement of more essential principle of nature [104].

2.5.2 Mechanism of sliding friction

The early investigators, including Amontons and Coulomb proposed that friction is the result of the mechanical interaction of asperities of the contacting surfaces. As shown in Figure 2–18 Coulomb model is one of the earliest friction models suggested. However, the mechanical interaction theory was abandoned since it could not provide a source of energy dissipation.
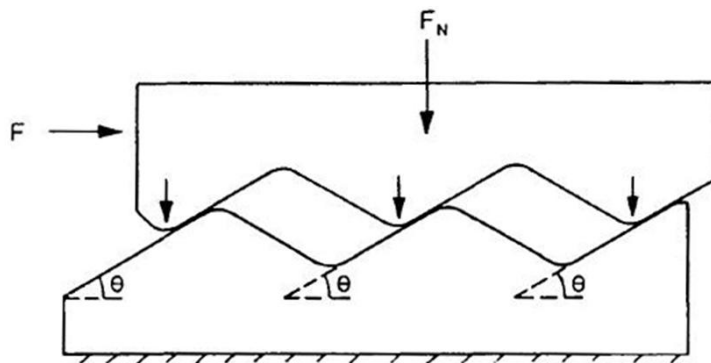
Figure 2–18 Coulomb friction model

One of the widely accepted friction theories for metals and ceramics is firstly raised by Bowden and Tabor [120]. In this theory, adhesion and ploughing are believed to be the two dominant mechanisms for friction. Therefore the total friction force of a system can be written as the sum of the forces required to shear adhered junctions (F_a) and conduct deformation (F_d):

$$F = F_a + F_d \qquad (2\text{-}12)$$

2.5.2.1 Adhesion term of friction

According to classical theory of adhesion, friction force contributed by adhesion can be written as [104]:

$$F_a = A_r \tau \qquad (2\text{-}13)$$

Where, A_r is the real area of contact, and τ is the shear strength of the softer of the two contacting materials. Based on the first law of friction, the coefficient of adhesive friction can be written as:

$$\mu_a = \frac{A_r \tau}{W} = \frac{\tau}{P} \qquad (2\text{-}14)$$

Where, P is the mean real pressure. For plastic contact which is the type of deformation takes place on asperities of a surface in most of the cases (at least at the tip of the asperities), P is the hardness of the softer of the contacting materials.

In general, the interfacial shear strength τ cannot exceed the bulk shear strength significantly. For ductile metals the hardness is normally around five times of the bulk shear strength. Therefore, the predicted values for the coefficient of adhesive friction should lie abound 0.2. However this assumption is not consistent with many experimental data which suggest a much bigger contribution on friction coefficient from adhesion. Two mechanisms could be the explanation for such disagreement: work-hardening and junction growth.

Work-hardening

Work hardening is the strengthening of a metal by plastic deformation. It happens when a metal is strained beyond the yield point. At this point, the metal appears to be stronger and harder to deform. During sliding between two metal surfaces, although the normal load is supported by plastic flow some distance from the immediate vicinity of the asperity junctions, the junction themselves will work-harden significantly, and increase the relative value of shear strength in comparison with that of hardness [101]. Therefore, coefficient of adhesion friction is increased.

<u>Junction growth</u>

For ductile metals, in most cases that involves plastic deformation, a growth of contact area will occur when a surface is subject to a combination of normal and tangential stress by as much as an order of magnitude [121]. In comparison with the scenario of an asperity compressed with a sole normal load, the application of shear stress lowers the critical normal pressure for plastic flow to take place. However, if the normal load remains the same the real area of contact must increase to maintain the plasticity [101].

2.5.2.2   Deformation term of friction

Deformation term of friction is the other dominant component of friction when plastic deformation and displacement of the interlocking asperities take place on the interface of two sliding surfaces. Although this component of friction is not considered as the primary contribution to friction in the classic theory suggested by Bowden and Tabor, it is demonstrated in the later of Tabor and Greenwood [122] that friction is mainly contributed by plastic deformation when adhesion is unlikely to occur.

During sliding of a hard surface against a softer counterpart, the asperities on the harder surface may penetrate and plough into the matching surface and produce grooves when the

shear strength of the softer surface is exceeded. Rigney and Hirth believed that the dominant mechanism of energy dissipation in metals was plastic deformation [123]. They were focused on the plastic work done in the near-surface region, and looked for a way to quantify the contribution of plastic deformation.

In the first model, an asperity is considered to be a rigid body which has a conical shape with an attack angle of θ pressed into a softer body, as shown in Figure 2–19. Then the load supporting area A_l which is the horizontal projection of the asperity contact can be written as:

$$A_l = \frac{1}{2}\pi r^2 \tag{2-15}$$

At an equilibrium condition, friction force is equal to the resistance produced by the ploughed area A_p which is the vertical projection of the asperity contact:

$$A_p = \frac{1}{2}(2rd) = r^2 tan\theta \tag{2-16}$$

Assuming that the yielding of the body is isotropic and the tangential force F, and normal load W required to carry out the plastic deformation can be treated as the indentation hardness H of the surface material, multiplied by the cross section area of the groove and the normal projection area of the asperity respectively:

$$W = HA_l \tag{2-17}$$

$$F = HA_p \tag{2-18}$$

Hence,

$$\mu_{def} = \frac{F}{W} = \frac{A_p}{A_l} \tag{2-19}$$

Finally,

$$\mu_{def} = \frac{2tan\theta}{\pi} \tag{2-20}$$

The slopes of real surfaces are usually less than $10°$, as a result, the value of μ_{def} can be expected to be close to 0.1 [101].
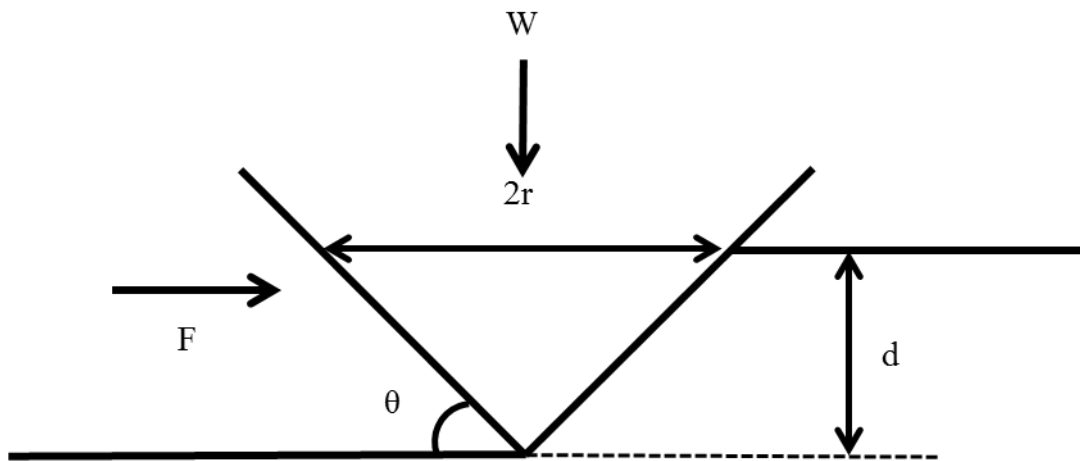
Figure 2–19 Schematics view of a conical asperity indenting and sliding
through a softer material

Similar model with different asperity shape has also been reported by Moore [124]. As shown in Figure 2–20, μ_{def} of a spherical asperity (with a radius of R) in contact with a softer body can be written as:

$$\mu_{def} = \frac{A_p}{A_l} = \frac{4}{3\pi}\frac{r}{R} \tag{2-21}$$
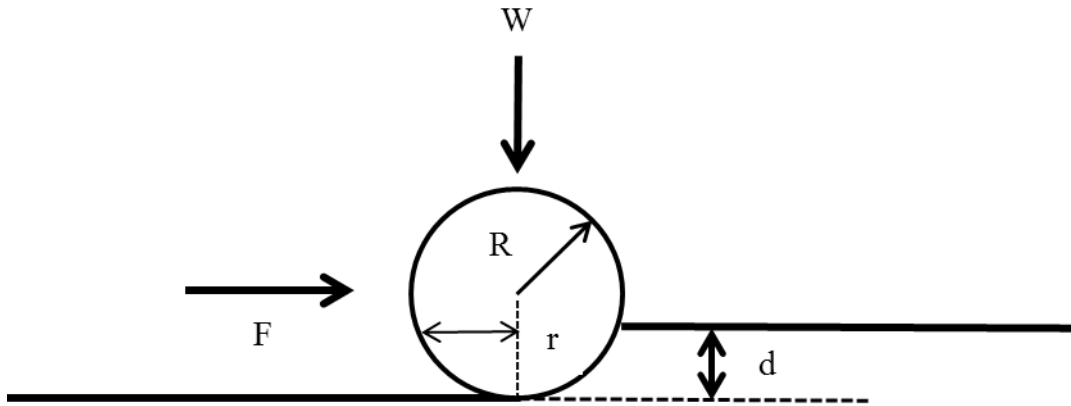
Figure 2–20 Schematics view of a spherical asperity indenting and sliding through a softer material

Base on the classical friction theory, Suh and Sin [125] extended the expression for μ_{def}. In this case, ploughing groove was considered to have large width compared with the radius of spherical asperity, hence they put the ploughing by wear particles into account:

$$\mu_{def} = \frac{2}{\pi}\{\left(\frac{R}{r}\right)^2 sin^{-1}\left(\frac{r}{R}\right) - \left[\left(\frac{R}{r}\right)^2 - 1\right]^{\frac{1}{2}}\} \qquad (2\text{-}22)$$

From the equation, it is clear that μ_{def} will surge sharply with a rise of the value *r/R*, this suggests that the coefficient of friction will increase as the sphere digs deeper [125].

2.5.2.3 Other mechanism of friction

Crystallographic structure of a material and Grain boundary effects may also affect the friction performance.

Rabinowicz [104] has suggested that the less number of slip planes in hexagonal close-packed metal than that in face-centred cubic metal is responsible for the low coefficient of friction and much less wear observed.

47

Sliding friction experiments across the surface of grain boundaries have been conducted by Buckley [126]. It is found that the presence of grain boundaries in a material hugely influences its tribological performance and strain hardening in the surficial layers caused by the accumulation of dislocations (blocked by grain boundaries in the sliding process) enlarges resistance for sliding, and hence increases the friction coefficient.

2.5.3 Friction transition in sliding

In this section the mechanisms of sliding friction are discussed. Adhesion and deformation are the dominant terms of friction, while crystallographic structure of a material and Grain boundary effects would also affect the friction to some extent. The fundamental theories and classic mathematical models are presented in the section. It is clear that low shear strength between contact surfaces is the key factor to obtain low friction force.

In a sliding experiment, temporary fluctuations in friction coefficient would commonly be observed shortly after the start of the action between freshly prepared samples. The phase of sliding is described as run-in or break-in. After some period, the friction coefficient stabilizes when the system enters the steady state of sliding. This friction transition caused by the change of the condition of mating surfaces is not necessarily a singular event; it can go on periodically more than two times before the system reaches the steady state.

Run-in has a big influence on the performance and life span of a sliding system. During run-in, high asperities will be smoothened out, initial surface films will be removed and replaced by the new steady films, and eventually better mating between two surfaces can be achieved. An appropriate run-in can lead to a desired state of sliding and significantly reduce the chance of system failure.

Blau [127] has given a systematically reviewed on the transition of friction, as shown in Figure 2–21, eight types of friction break-in curves have been described. Among them, Figure 2–21(a) and Figure 2–21(b) are the most seen curves.
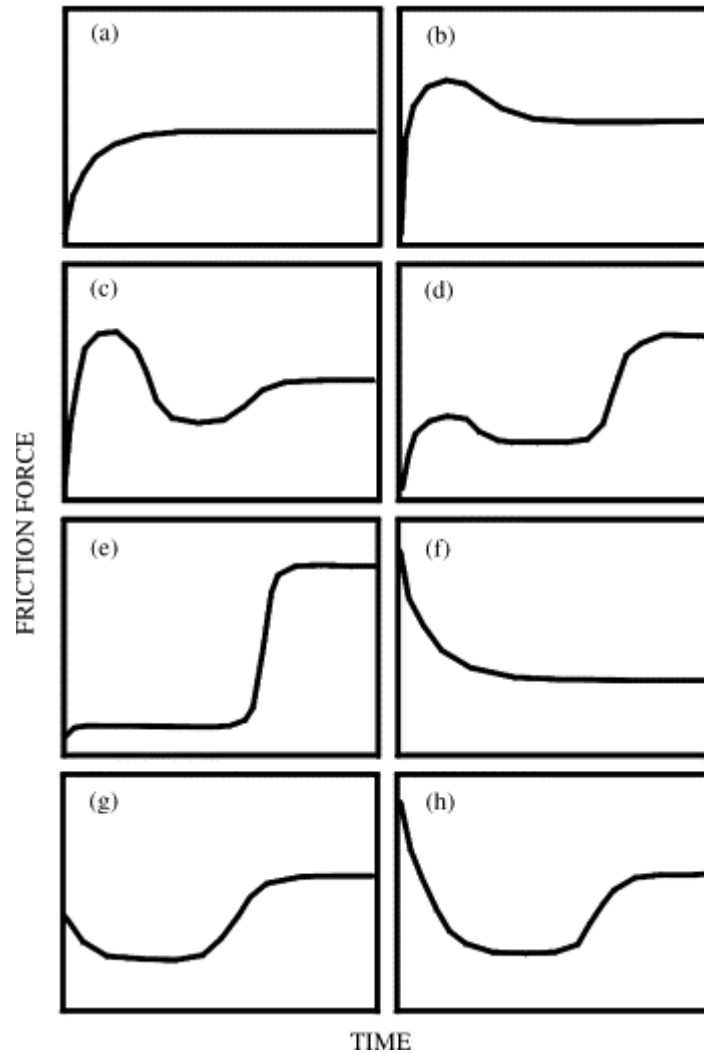
Figure 2–21 Typical types of run-in curve shapes [127]

Figure 2–21(a) is characteristic of sliding of a pair of metal components in a dry friction contact. A surface contamination, oxide, and adsorbed species reduce adhesion of two surfaces at the beginning of the sliding. As the sliding goes on, these substances are quickly worn away, and lead to a greater degree of adhesion, hereby a rise in friction [127]. Figure 2–21(b) is often seen in boundary lubrication. The first temporary rise in friction caused by the initial roughness of the surface is quickly replaced by a reduction in friction due to the

surface conformity and smoothing. Depending on the materials and conditions, surface texturing by shear and the development of a low-shear transfer film can also be responsible for reduction of friction after the initial rise [128].

Run-in is a complex process, and it is closely related to the condition in which a system is operating. Surface roughness and macro-conformity, thermal effects, vibration, microstructural effects such as work-hardening, fatigue damage and third body formation are all among the factors that are influential on running-in.

2.6   Summary

The present Chapter reviewed the nature of surface, fundamental subjects in lubrication, as well as the theoretical background of friction and wear. The basic principles of boundary lubrication were described. The important experimental techniques that are encompassed in tribology study were also summarised. The inclusion of this chapter on fundamentals helps obtain a comprehensive understanding of friction and wear mechanisms. Boundary lubrication regime is used in this study, where the solid lubricant additives may show their effectiveness. Suitable surface analysing techniques are selected and the details will be discussed in Chapter 4.

Chapter 3.   Solid Lubricant Additives and Surface Modification Techniques

3.1   Introduction

In modern industry, machinery parts operating under severe conditions require lubricants to be able to withstand high temperatures and pressure. Friction and surface damage caused in such conditions can be avoided or reduced by applying extreme pressure (EP) and anti-wear (AW) additives. However, when temperature is elevated under extreme conditions, the failure of the boundary films may cause direct contact of the moving surfaces and lead to adhesion and surface damage of the components. Sulphur, chlorine and phosphorous containing organic compounds were mostly used in the past. They were designed to react chemically with the metal surfaces, and to form easily sheared layers of sulphides, chlorides or phosphides, and thereby to prevent severe wear and seizure.

Back in 1960s, solid lubricant additives began to be used as antiwear and extreme pressure agents in gear oil. Graphite and molybdenum disulfide micron particles that have layered structurs were the firstly employed solid lubricant additives [129-132]. The good friction and wear reduction performances were observed due to the low shear strength of the materials as a result of their intrinsic crystal structure. However, introduction of a solid lubricant additive in lubricant oil caused another problem, stability. Solid particles generally are not stable in liquid media, especially for large particles. The flocculation of the solid lubricant particles cause them to separate from the lubricant by sedimentation, hereby reduce or remove the additive content from the base lubricant so that the benefits gained from the introduction of solid particles in the lubricant are therefore lost.

Nano sized and submicron sized particles began to be used as solid lubricant additives in the 1980s, thanks to the development of synthesis techniques. Compared with the large sized

particles, particles with smaller size have demonstrated intrinsic advantages. Typically, nano-sized and submicron-sized particles have the superior dispersibility in a lubricant base media. This greatly improves feasibility of solid particles in lubricant application and reduces the possible abrasion that the solid lubricant additives may cause to the substrate surface. Outstanding performance in friction and wear reduction was observed in some applications of the solid inorganic lubricant additives [1, 2, 80, 82, 84, 133-136]. Some of the solid inorganic lubricant additives even outperform the traditional organic lubricant additive ZDDP [83, 137].

Dispersing agent is often used to improve the dispersibility of solid lubricant additive in base lubricant. Surface modification technique is also broadly applied to change the surface property of additive particles so as to serve the same purpose. It is essential to understand the mechanisms of the surface modification and how the modification agents react with solid particles before the employment of such technique.

3.2   The roles of solid lubricant additives

The excellent tribological property of solid inorganic lubricant additives can be attributed to four mechanisms:

Tribochemical reactions --solid lubricant additives may interact with the surface material of friction pairs and form a surface protection film [93, 138, 139].

Ball effect--small spherical nano-particles enable to roll between friction pairs. These particles introduce a partial rolling friction into a pure sliding friction [4, 8, 140]

Mending effect--in most of the cases, surface roughness is greater than the mean diameter of nano-particles. Nano-particles can be deposited on the surface, and form a physical tribo-film which compensates the mass loss of materials [141, 142].

Third body effect—a large quantity of nano-particles help to reduce compress stress concentrations associated with high contact pressure by bearing the compressive force depressively[141, 143].

3.3 Layer structure solid lubricant additives

Solid lubricant additives with layer structure have been extensively studied and excellent tribological performance has been observed. These solid lubricant additives, including graphite, molybdenum disulfide (MoS_2), tungsten disulphide (WS_2) and boron nitride (BN) , have a lamellar crystalline structure, in which the bonding between molecules within each layer is strong covalent, while each two layers are bonded together by weak van der Waals forces. Due to such a unique structure, low shear stress is expected and an easy-shear mechanism is resulted when these additives are applied between sliding surfaces [81, 143-146].

Graphite powder is one of the mostly used solid lubricant additives, especially in harsh conditions with very high or very low temperatures. It can be used directly as a dry powder, as an additive in water or oil, or as colloidal graphite (a permanent suspension in a liquid). The special layer structure, as shown in Figure 3–1, provides a low shearing localized film between rubbing surfaces and leads to a significant friction and wear reduction. Conventional flake graphite has a particle size of several to several tens of microns meters and the large particle size means a problem in dispersion. Graphite nano-sheets are much smaller than the ordinary flake graphite, and their small size gives them better dispersibility in a base lubricant and superior tribological performance to the ordinary flake graphite. SEM morphology of graphite nano-sheets is shown in Figure 3–2. The tribological behaviour of nano graphite nanosheets as an additive in paraffin oil was investigated by H.D. Huang *at el.* with a four-ball and a pin-on-disk tribo tester [81]. The graphite nanosheets with an average diameter of

500 nm and a thickness of 15 nm were prepared by stirring ball milling. The maximum nonseized loads of the lubricating oil were determined according to the ASTM D2783 standard method. As a lubricant additive in oil, graphite nanosheets demonstrated better tribological properties than in pure paraffin oil when an appropriate additive concentration was used. Figures 3–3 - 3–5 illustrate the friction reduction, anti-wear and maximum non-seizure load properties of the lubricant improved by adding graphite nanosheets respectively. The low shear strength between the sliding surfaces resulted from the employment of graphite nanosheets with layered structure is responsible for the observed improvement on tribological properties. 1% was found to be the optimal concentration for the application of this type of solid lubricant additive [81].
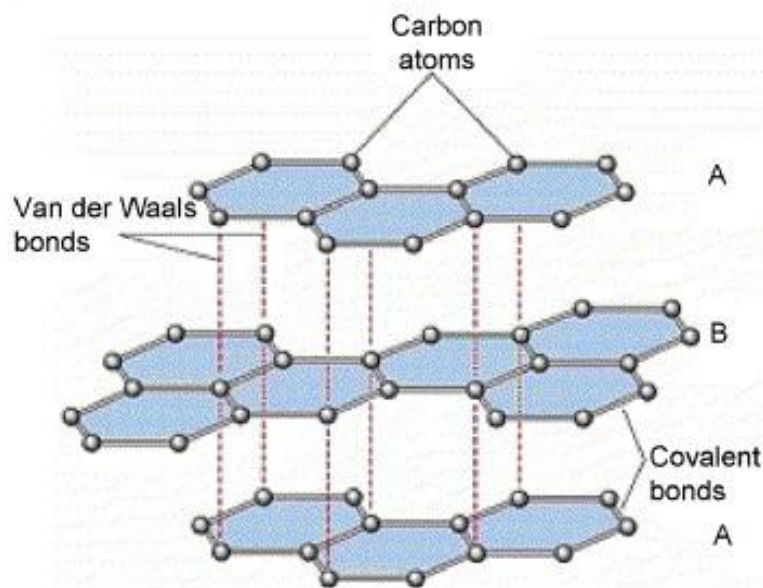
Figure 3–1 Atomic arrangement of lamellar graphite
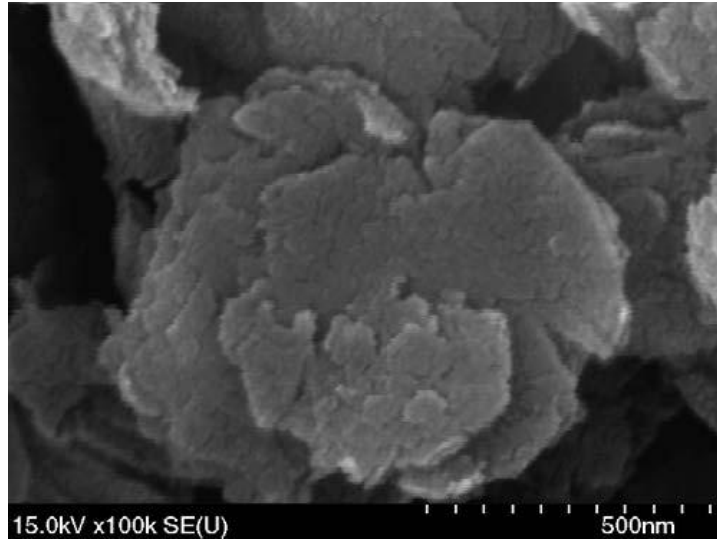
Figure 3–2 SEM morphology of graphite nano-sheets [81]
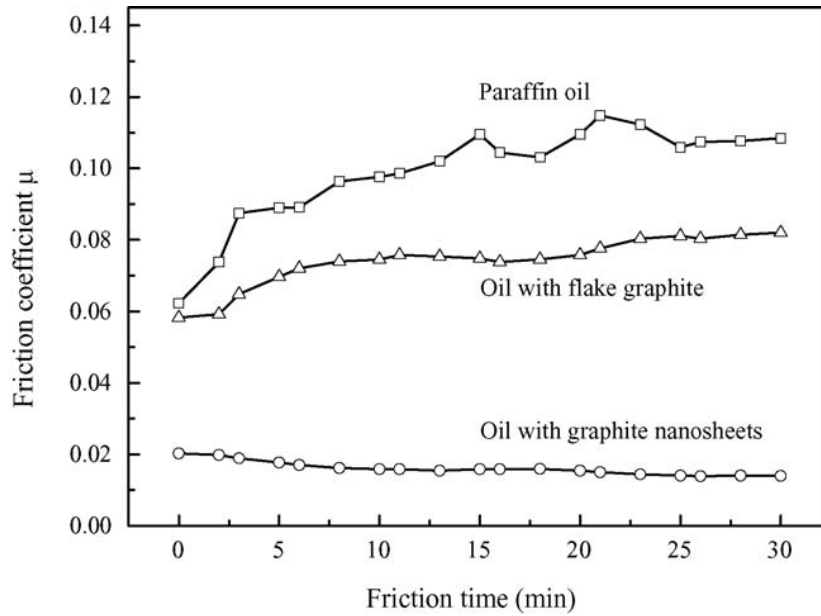
Figure 3–3 Effect of graphite nanosheets and flake graphite on friction coefficient [81]
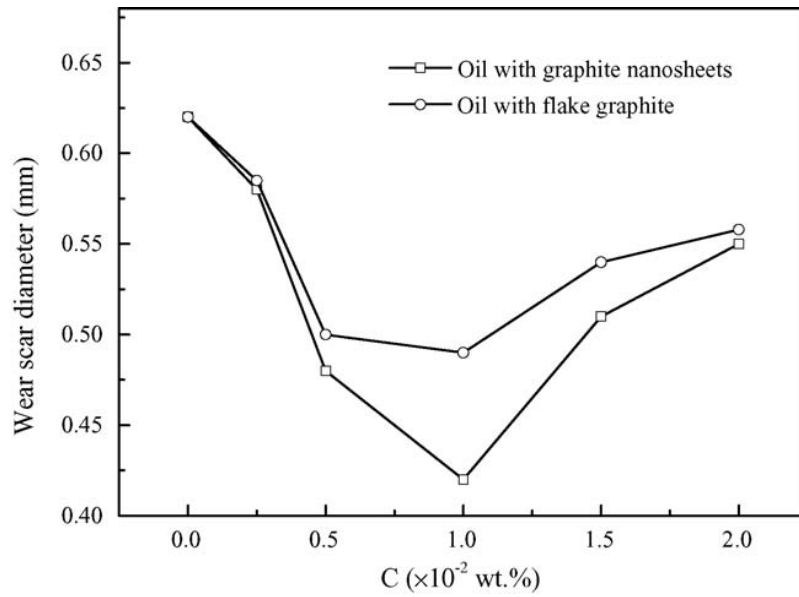
Figure 3–4 Wear scar diameter as a function of additive concentration [81]
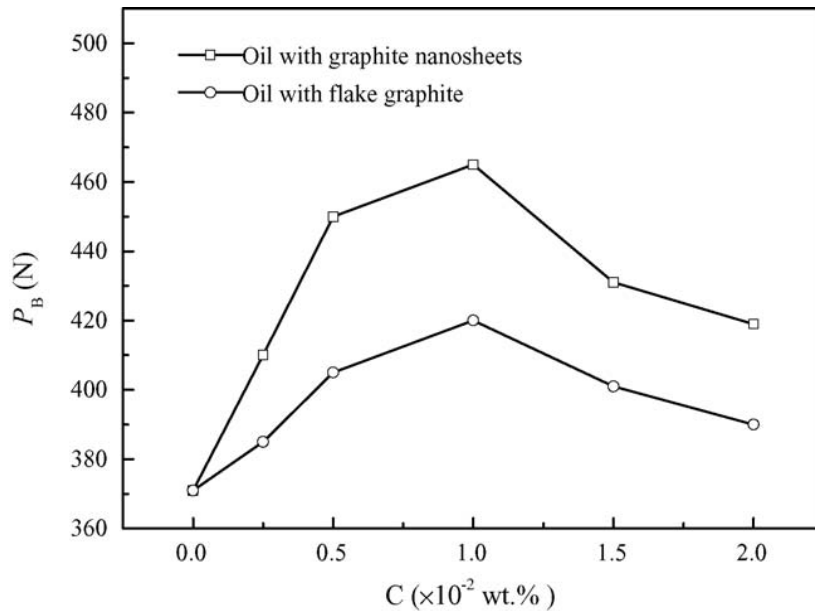
Figure 3–5 Effect of graphite nano-sheet and flake graphite concentration on
maximum non-seizure load [81]

J. Gansheimer [146], L. Rapoport [147] and Yoshitsugu Kimura [145] also reported the similar improvement on tribological properties, such as friction and wear reduction and the improvement on maximum non-seizure load, by using MoS_2, WS_2 and BN as solid lubricant additives correspondingly.

3.4 Metal particles as solid lubricant additives

Recent research has suggested that an addition of nano sized metal particles to a lubricant is effective for the reduction of wear and friction in mechanical systems. Numerous types of metal nanoparticles as lubricant additives have recently been investigated.

Nanoparticles of soft metals, such as copper (Cu), gold (Ag), and nickel (Ni) are the mostly studied materials. Wear and friction properties of Cu nanoparticles in commercial base lubricants at different loading and sliding speed conditions were studied by He-long Yu [148] and S. Tarasov [140]. As shown in Figure 3–6, an excellent mending effect of copper nano-particles has been demonstrated by the Scanning Electron Microscopy (SEM) observations. Compared with the surface lubricated by pure oil (Figure 3–6(e)), surfaces lubricated by the lubricants containing Cu nanoparticles have all revealed a smoother surface finish. As shown in Figure 3–7, He-long Yu has illustrated the effect of temperatures on the friction coefficient and wear scar diameter when 50CC pure oil and 50CC oil containing Cu nano-particles were tested. Clearly, 50CC oil containing 0.2% Cu nano-particles showed better friction and wear reduction performance through the whole temperature range. Most importantly, it can be seen that the higher the temperature went, the better the tribological properties Cu nano-particles demonstrated. S. Tarasov also found that the worn surface lubricated with motor oil containing copper nanoparticles were very smooth, whereas much rougher surface with wear grooves formed by wear particles were typical worn surfaces lubricated by motor oil without additive [140].

(a) 110N, 1.56m/s

(a) 184N, 1.56m/s

(c) 110N, 2.62m/s

(d) 184N, 2.62m/s

(e) typical SEM image of worn surface obtained after tests in pure oil
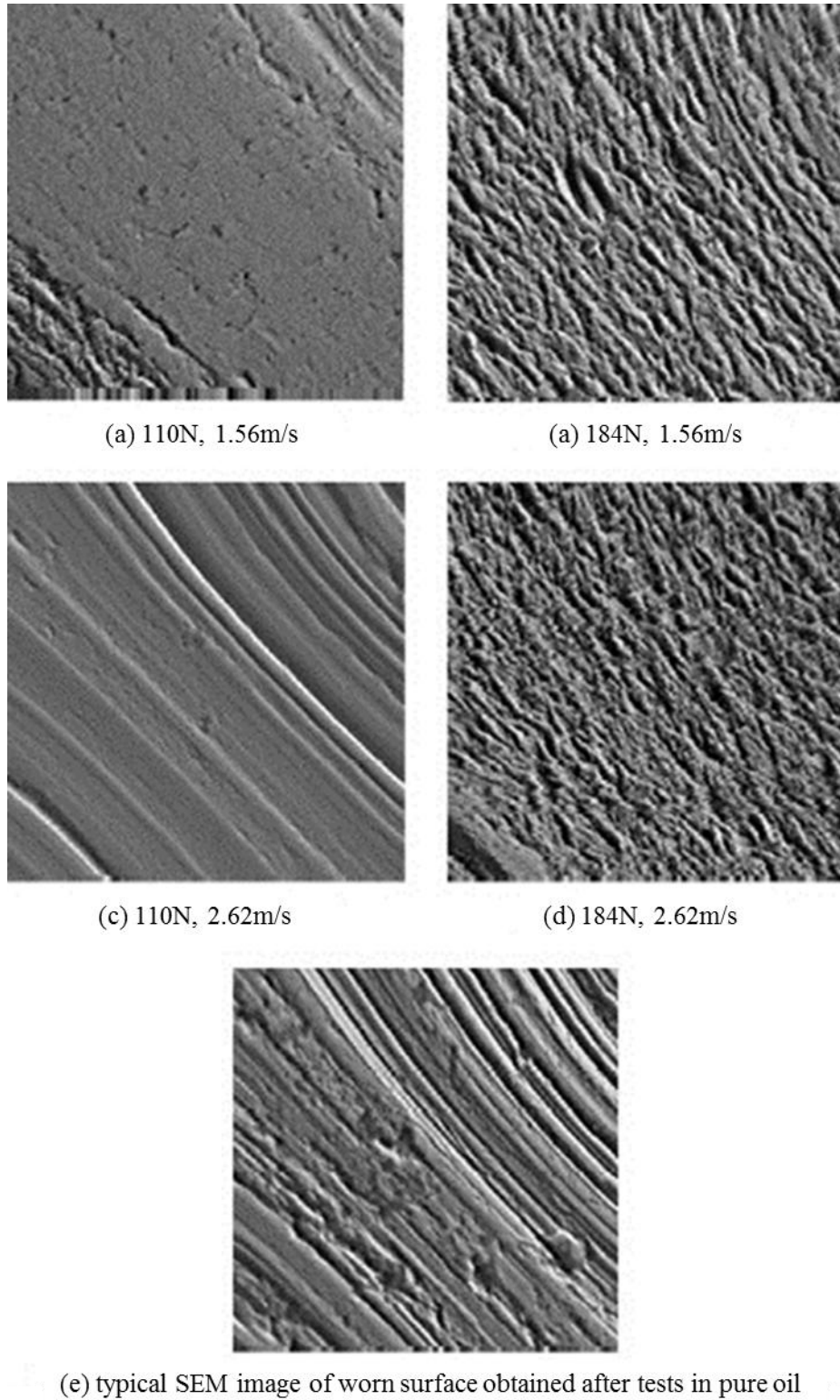
Figure 3–6 (a-d) SEM images of worn surfaces after friction tests with copper nanoparticles (e) worn surfaces after friction tests with pure oil [148]
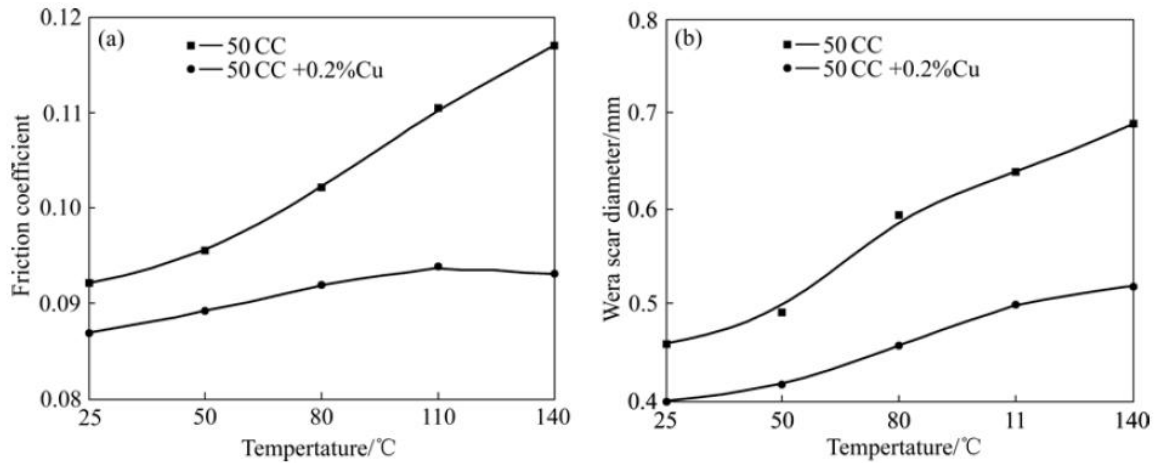
Figure 3–7 Tribological properties of 50CC oil and 50CC oil with 0.2% Cu nanoparticles at different emperatures: (a) Friction coefficient; (b) Wear scar diameter [148]

R. Chou studied the tribological properties of nickel nanoparticles in polyalphaolefin, and reported the similar friction reduction and antiwear performance[149]. As shown in Figure 3–8 and Figure 3–9, dramatic reductions in friction coefficient and wear loss were achieved at all additive concentrations. Highest improvement on tribological performances of the base oil was delivered by the employment of 0.5% nickel nanoparticles.
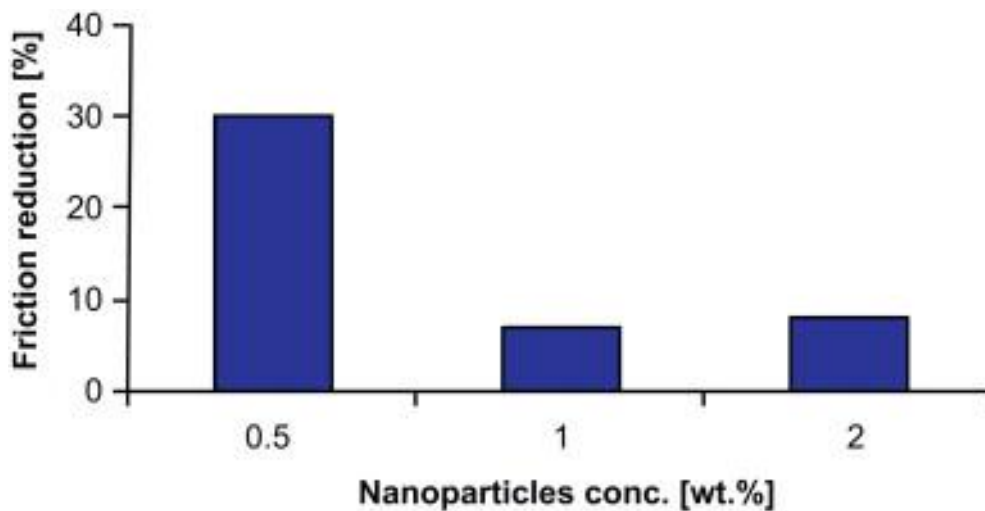
Figure 3–8 Friction reduction performance of nickel nanoparticles at different concentrations [149]
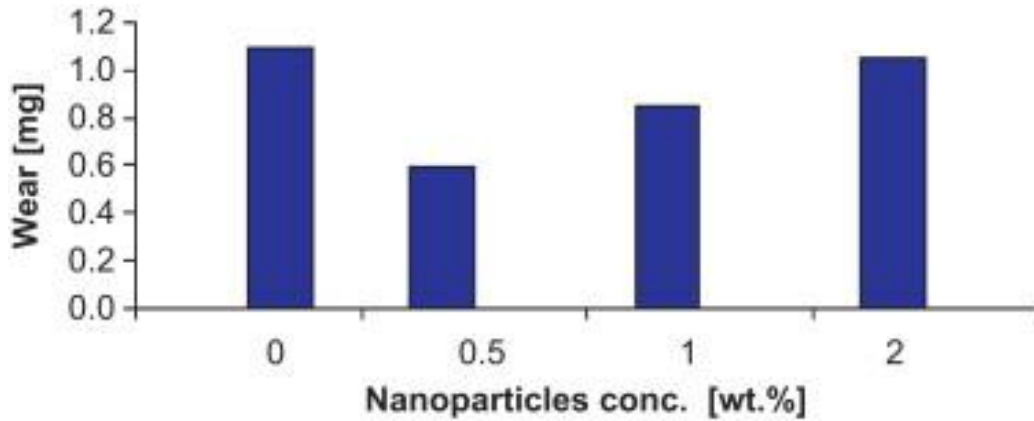
Figure 3–9 Wear reduction performance of nickel nanoparticles at different concentrations [149]

In order to interpret the mechanism of friction and wear reduction properties of copper nanoparticles in base lubricant, He-long Yu also analysed the mechanical properties of the worn surfaces after tribology tests. The nano-hardness, reduced modulus and elastic modulus of the worn surfaces were measured with a nano-indentation tester, as seen in Table 3-1.

Table 3-1 Micro mechanical property of copper film and worn surfaces lubricated with 50CC oil [148]

Temperature/℃	Nano-hardness/GPa		E_r/GPa		E_s/GPa	
	50CC oil	Copper film	50CC oil	Copper film	50CC oil	Copper film
25±2	13.08	12.15	190.20	160.827 6	210.15	172.40
50	12.94	11.74	185.90	146.424 3	204.47	154.72
80	13.15	11.58	193.45	140.360 6	214.40	147.40
110	13.01	11.55	184.62	149.141 5	202.80	158.41
140	13.3	11.4	186.30	140.861 8	205.17	148.21

The readings in the columns "50CC oil" describe the mechanical properties of the worn surfaces lubricated using 50CC oil, and the readings in the columns "Copper film" present the mechanical properties of the worn surfaces lubricated using 50CC oil blended with surface modified copper nano-particles. This low reduced and elastic modulus (E_r and E_s) achieved from using 50CC oil blended with surface modified copper nano-particles indicated that a protective film with less strength was formed on friction surfaces. The film material

60

provided a lower shear strength which led to a lower friction coefficient. Soft worn particles

would also be capable of getting through the contact area more easily, and therefore abrasive

wear would be consequently reduced. Furthermore, Soft film on the worn surfaces could also

increase the contact area and provide fast relaxation and reduction of contact stress.

3.5   Metal oxide solid lubricant additives

Metal oxides nanoparticles are one of the firstly studied solid lubricant additives and various

types of metal oxide nanoparticles have been tested before [2, 134, 150-152]. The anti-wear

performance of CuO, ZnO and ZrO_2 nano-particles blended in a polyalphaolefin (PAO 6)

were described by A. Hern´andez Battez *at el.* [151]. Micrographs of these three nano-

particles are shown in Figure 3–10.
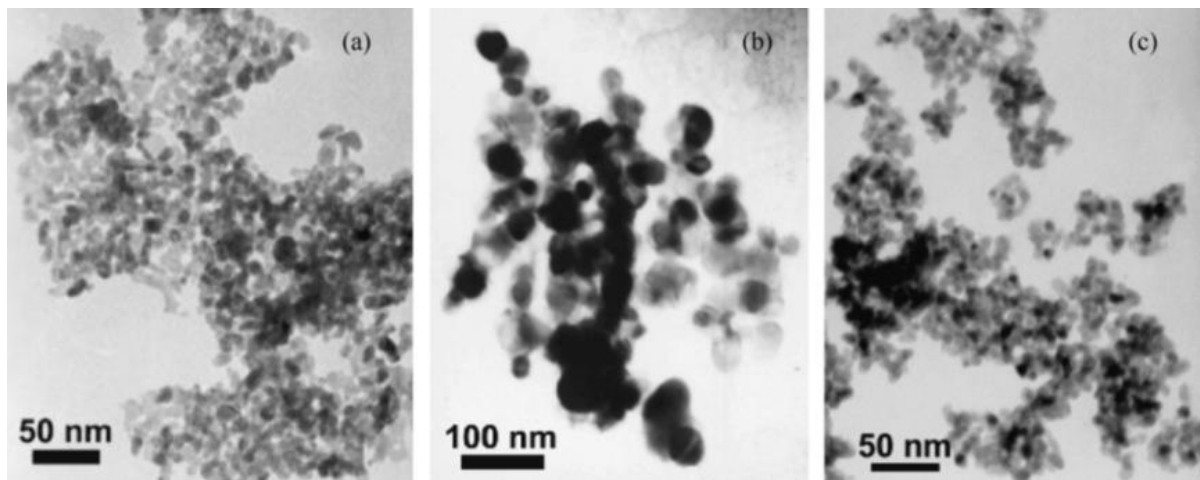
Figure 3–10 Micrographs of nanoparticles: (a) ZnO; (b) CuO; (c) ZrO_2 [151]

Friction coefficients of lubricant nano-particles in different concentrations were illustrated as

a function of sliding distance in Figures 3–11 - 3–13 [151].

Clearly, all nano-particles indicated obvious friction reduction, and the optimal concentration

that gave the lowest friction coefficient for each type of nano-particles was recorded.
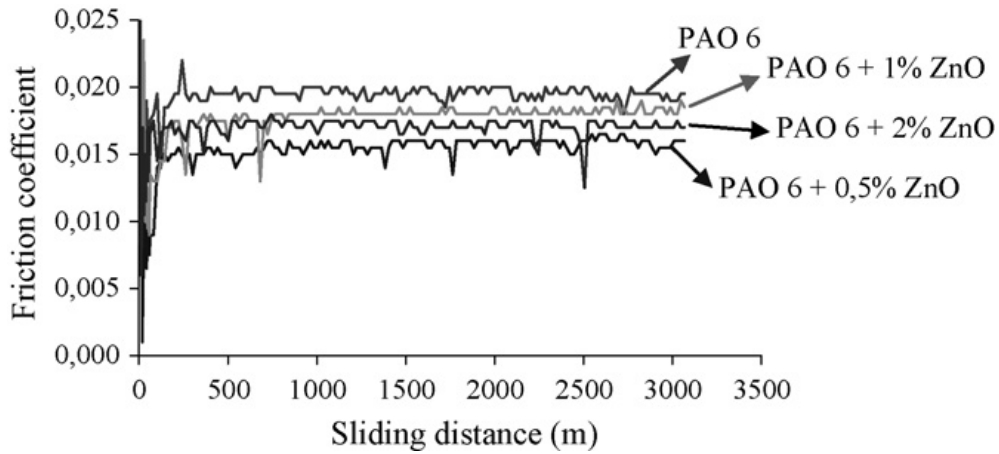
Figure 3–11 Friction as a function of sliding distance with PAO 6 + ZnO nano-particles [151]
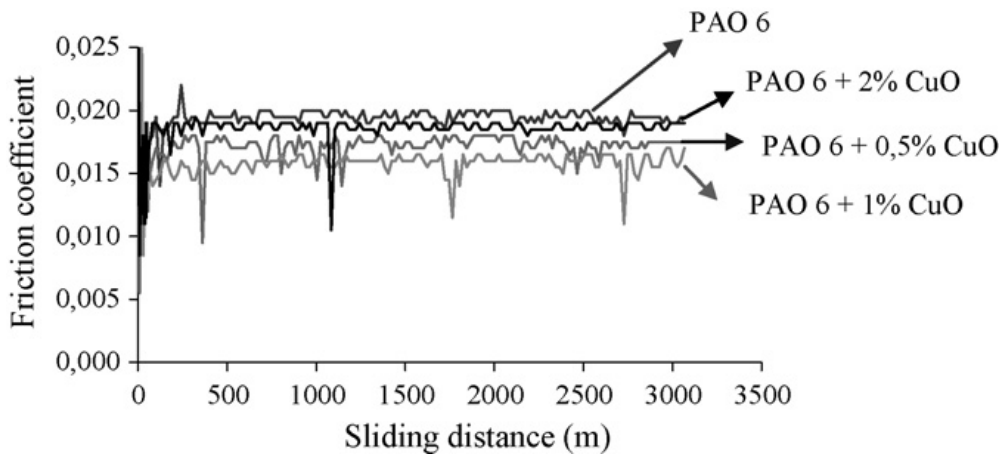
Figure 3–12 Friction as a function of sliding distance with PAO 6 + CuO nano-particles [151]

Figure 3–14 illustrated the overall comparison of CuO, ZnO and ZrO_2 nano-particles on wear reduction readings. It is evident that the nanoparticle concentration at which the optimal friction reduction performance was received did not necessarily contribute the best antiwear ability. The 2%CuO nano-particles in PAO 6 gave the highest friction coefficient, but the same combination also exhibited the least wear, with a reduction of about 60% in comparison with pure PAO 6. This phenomenon demonstrates the mending effect of CuO nanoparticles that tribo-film formed on friction surfaces compensates the wear loss and protects the surfaces.
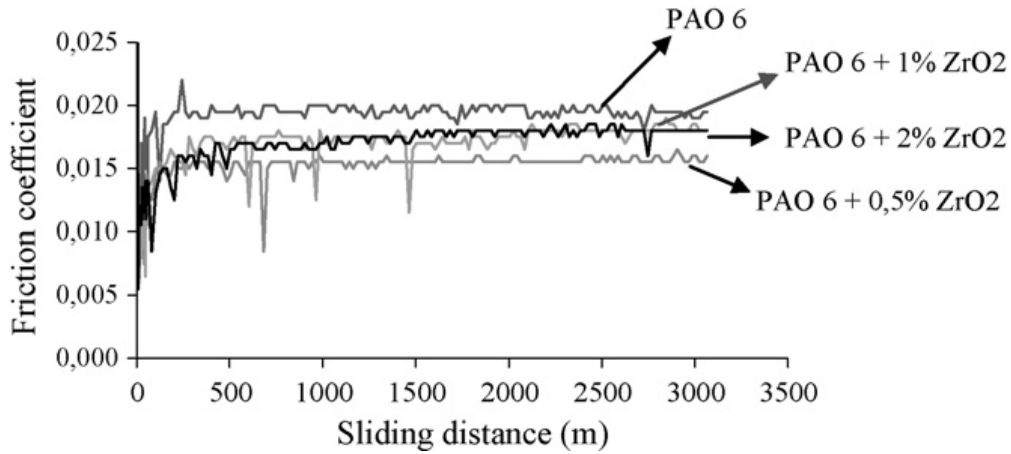
Figure 3–13 Friction as a function of sliding distance with PAO 6 + ZrO2
nano-particles [151]
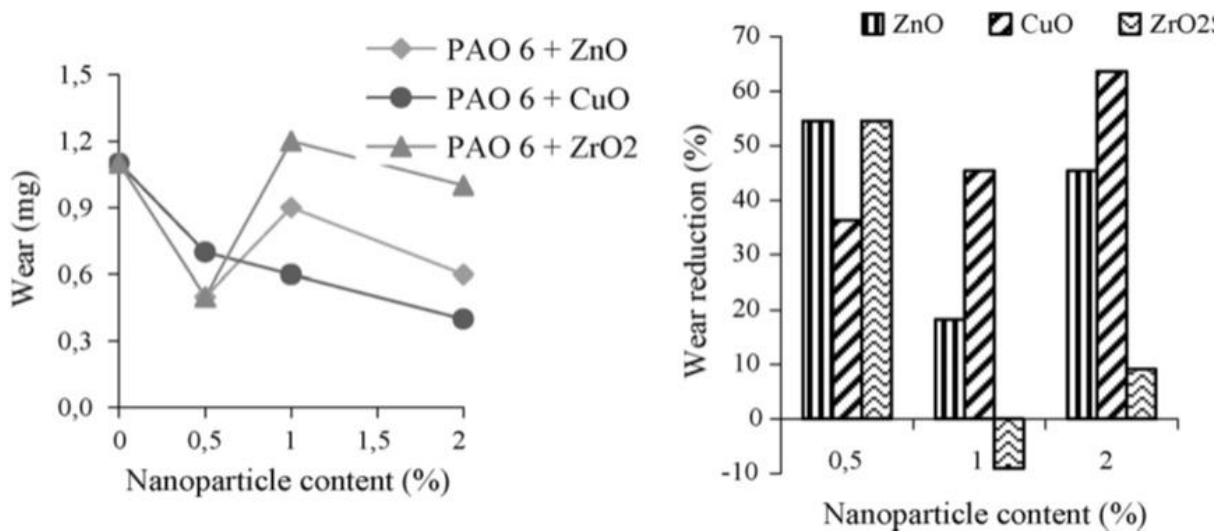
Figure 3–14 Overall anti-wear performance comparison [151]

It has also been reported that in an application of metal oxide nanoparticles as a solid lubricant additive, a reduction of friction coefficient was sometimes companied by higher wear rate. It is probably due to the high hardness of the metal oxide nanoparticles. As a result, high abrasive wear is caused on the contact surfaces.

The observed friction and wear reduction properties of metal oxide nanoparticles are generally attributed to the 'third body' mechanism and 'mending' effect of the additives

[153]. However complex physical and chemical reactions between the solid lubricant additive and substrate metal material may also have taken place, and therefore thorough research on this matter is still required.

3.6   Borate solid lubricant additives

Excellent wear and friction reduction performance of borate particles with various sizes, as well as their improving effect on the maximum non-seizure load of base lubricant has been widely reported in the literatures. It is well known that alkali metal borate is an excellent antiwear and friction reducing additive [12, 13, 154]. Alkaline earth metal borate possesses similar tribological properties to alkali metal, magnesium borate nanoparticles [91], strontium borate nanoparticles [138] and calcium borate submicron ultrafine powders [155] which all have demonstrated promising potential in wear and friction reduction aspect, as shown in Figures 3–15 - 3–17
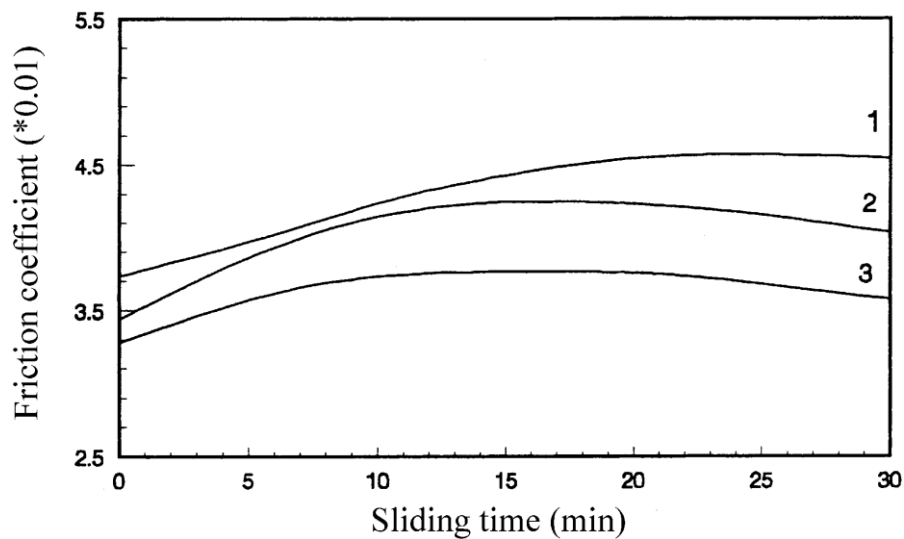
Figure 3–15 Effect of magnesium borate nanoparticles on friction coefficient of a lubricant oil. (1) Base oil with dispersing agent; (2) base oil; (3) oil with dispersing agent and magnesium borate [91]
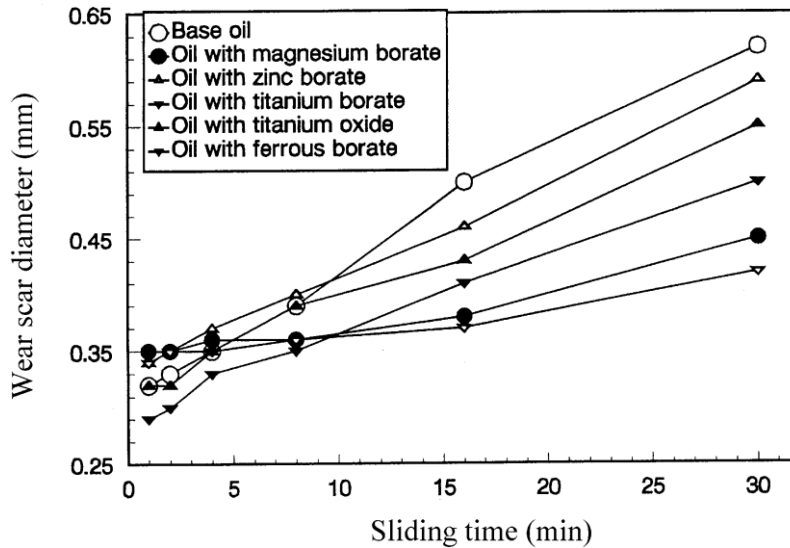
Figure 3–16 Effect of nanoparticle magnesium borate on wear scar diameter
[91]
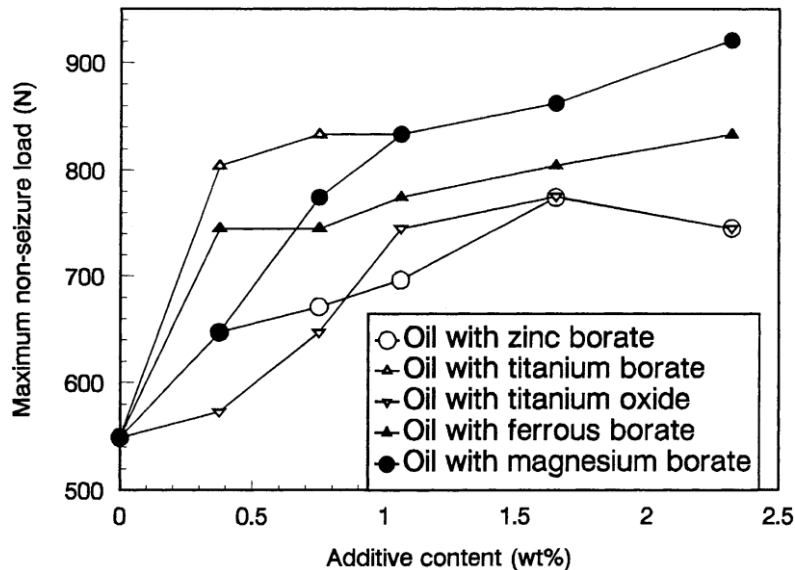
Figure 3–17 Effect of nano-particle magnesium borate content on maximum
non-seizure load of lubricant base oil [91]

Many other metal borate nano-particles can also be used as lubricant additives. Nanoparticles

of Zinc borate [84], Titanium borate [156], Lanthanum borate [139] and Cerium borate [92]

have been tested as solid lubricant additives in literature and proved to have the effective

friction and wear reduction properties. During an elemental analysis of the wear scar some

boron was generally detected in all applications of borates solid lubricant additive. The

chemical state of the boron is given in Figure 3–18 and the binding energy indicates that there

are diboron trioxide (192 eV) and FeB (187.9 eV) on the wear scar. Tribochemical reactions were observed in the application of borates particles as a solid lubricant additive. Figure 3–19 gives a schematic diagram of the friction and wear reduction mechanism. Diboron trioxide was firstly formed and deposited in the rubbing surface owing to tribochemical reaction of borate particles. Then, Fe_2B and FeB formed due to further reaction between diboron trioxide and Fe of the substrate metal. A decrease of shearing stress due to a gradual deposition of friction product of borate solid lubricant additive on the rubbing surface is the possible explanation in the friction reduction behaviour. Also the protective film generated through tribochemical reaction is capable at some level of protecting the surface from wear.
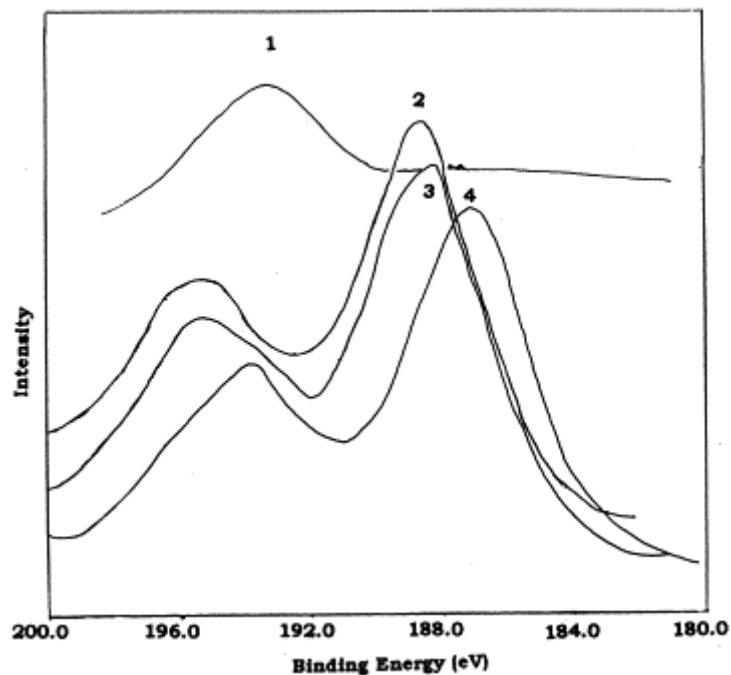
Figure 3–18 XPS spectra of boron on rubbed surface: (1) cleaned using ultrasonic bath with ligroin; (2, 3, 4) cleaned using ultrasonic bath with ligroin and then with distilled water, sputtered by Ar ions for 5, 10, 30 min respectively [84]
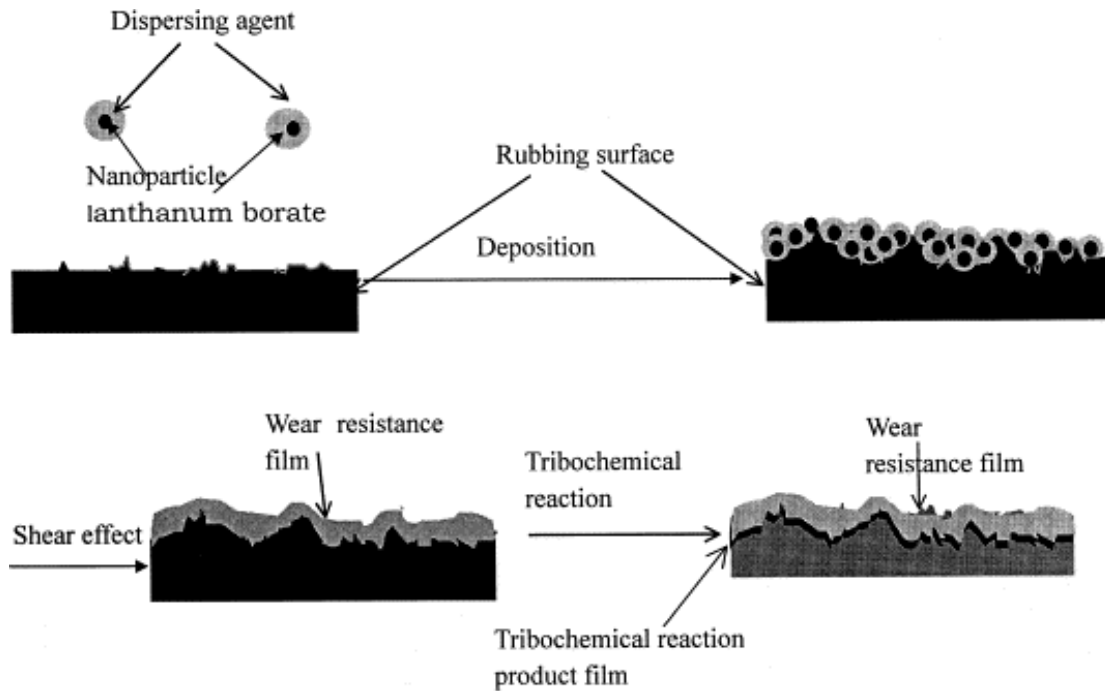
Figure 3–19 Schematic diagram of the friction and wear reducing mechanism
of borate nanoparticles [139]

3.7 Particle surface modification

Lubricants with solid lubricant additive are two-phase systems, with one phase (solid phas) dispersed in another (liquid phase). Some important issues have to be tackled in a two-phase system and one of the most important issues is the stability of the system. The intrinsic poor dispersibility of solid particles in base oil greatly restrains their lubricating performance and the development in practical applications and still remains a big challenge to achieve desired stability of solid lubricant additive in base lubricants

3.7.1 Stabilization of solid lubricant additive in base lubricant

Dispersibility of a solid lubricant additive describes the capability of the additive particles to be dispersed evenly in a base lubricant and to remain as they are. The two phenomena that control the dispersibility of a solid lubricant additive are agglomeration and sedimentation. Small particles have large surface area and therefore high surface energy. As a result the

tendency to form agglomerates is quite strong. Minimising agglomeration is of major importance in improving the dispersibility of solid lubricant additive in a base lubricant.

As illustrated in Figure 3–20, electrostatic stabilization and steric stabilization are the two main mechanisms for stabilization against agglomeration:

Electrostatic stabilization

In general, different phases have different charge affinities, so that an electrical double layer can form at any interface. Base on DLVO (named after Derjaguin and Landau, Verwey and Overbeek.) theory[157], agglomeration of small particles can be reduced by tuning the surface potential of particles using a surface modification agent. The mutual repulsion of alike electrical charges on particle surfaces can partially counteract attraction and hereby reduce particles agglomeration.

Steric stabilisation

Steric stabilization involves covering the particles in polymers, which physically separates the particles spatially and prevents the particles from getting close to each other.

Steric stabilization   Electrostatic stabilization
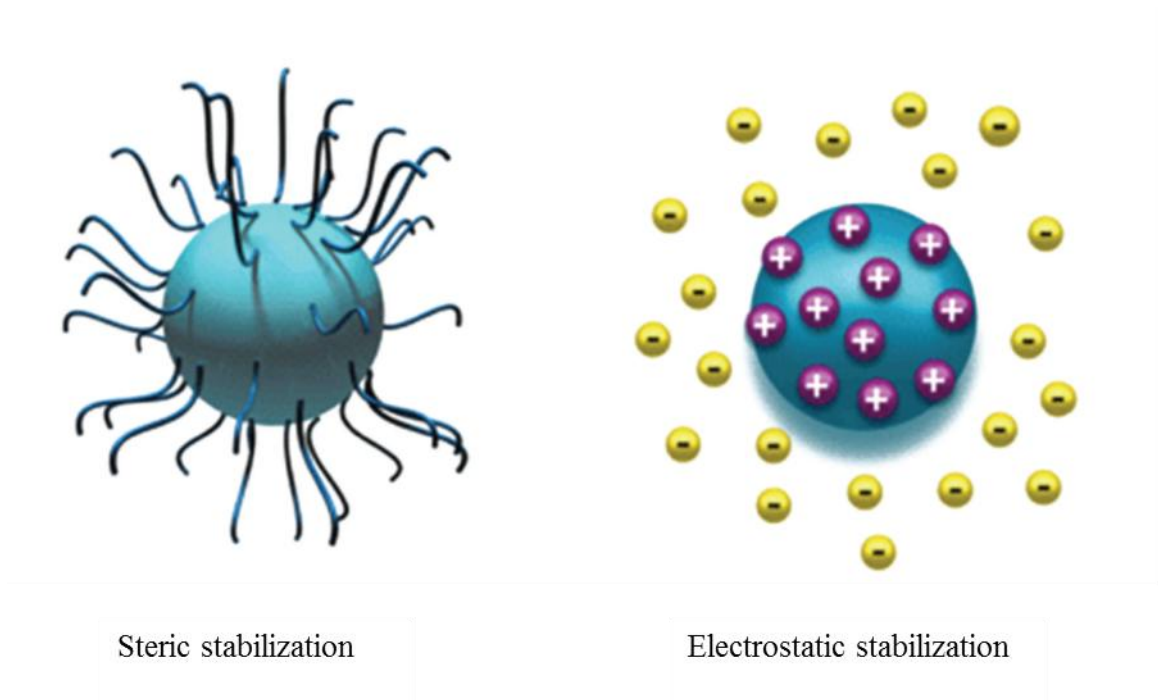
Figure 3–20 Stabilization mechanisms [158]

3.7.2 The methods to enhance the stability

3.7.2.1 Surfactants and application with solid particles

Using surfactants is a simple and economic approach to improve the dispersibility of solid lubricant additives in base lubricants. Even small amount of surfactant is able to markedly affect the inter-surface properties of a system. One surfactant molecule is composed of two parts; a hydrophobic tail portion, usually a long-chain hydrocarbon at one end, and a hydrophilic group at the other end. Surfactants are able to improve the contact quality of two materials by locating onto the surface of solid particles and introducing a degree of continuity between the solid particles and the fluid environment

According to the composition of the hydrophilic end, surfactants are divided into four categories [158]:

- Nonionic surfactants without charge groups in its head (including polyethylene oxide, alcohols, and other polar groups).

- Anionic surfactants with negatively charged head groups (anionic head groups include long-chain fatty acids, sulfosuccinates, alkyl sulfates, phosphates, and sulfonates),

- Cationic surfactants with positively charged head groups (cationic surfactants may be protonated long-chain amines and long-chain quaternary ammonium compounds).

- Amphoteric surfactants with zwitterionic head groups (charge depends on pH).

Water-soluble surfactants are generally selected to stabilise solid lubricant additive in polar solvent otherwise. Vice versa, oil-soluble surfactants are used for nonpolar solvent.

Although surfactant addition is an effective way to enhance the dispersibility of solid particles in liquid media, surfactants might cause undesired concerns. For example, the amount of surfactant used to effectively improve the dispersibility of the solid particles could have a big impact on the viscosity of the base liquid [159]. Also foams can be produced by additional surfactants during heating up, which needs to be avoided in a system where heating and cooling are a routine process[5].

3.7.2.2   Surface modifications of solid particles

Surface modification is a technique to prepare particle additives by attaching an organic layer onto the particle surface. Similar to using surfactant, the organic layer coated on particle surface helps to minimise particle/particle interaction and to enhance particle/matrix interaction. Functionalising solid particles has proved to be a promising approach to achieve long-term stability of solid particles in a lubricant. Dispersion of surface modified particles does not require additional surfactant therefore the problems associated with the application of surfactant can be avoided.

3.7.2.2.1 PyDDP

Yang and Liu presented a work on the synthesis of novel MoS_2 nanoparticles which were "capped" by dialkyldithiophosphate (DDP) molecules [160]. This capped nanoparticles were prepared by an ion modification method and the modified particles obtained had good solubility in organic solvents such as acetone, DMF, THF, and others [160]. Similar modification agent was also successfully applied on other solid lubricant additives such as PbS [161], ZnS [162], Cu [9], Ag and LaF_3 [76]. As shown in Figure 3–21, Pyridinium di-n-hexadecyldithiophosphate (PyDDP) was used as a modification agent. However active elements of S and P are contained in this modification agent, and therefore its manufacturing and employment may become a potential hazard for the environment concern.
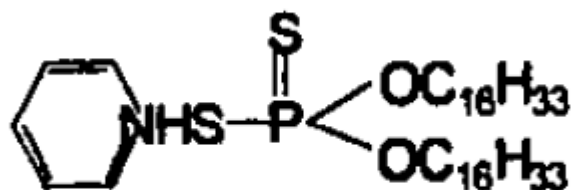
Figure 3–21 Chemical formula of PyDDP

3.7.2.2.2 Succinimide

Some Nitrogen (N) containing organic compounds have also been found to adsorb competitively on the metal surface to give good compatibility with the lubricant oils and also deliver effective antiwear ability. The chemical formula of succinimide is shown in Figure 3–22. Succinimide was used as modification agent and desired interaction with LaF_3 was observed [137].
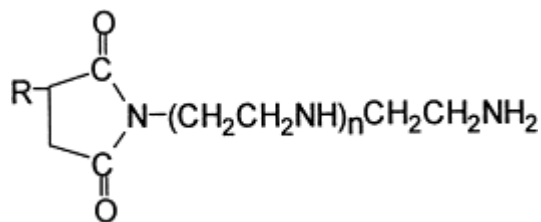
Figure 3–22 Chemical formula of Polyisobutylene Succinimide

3.7.2.2.3 Carboxylic acids

Carboxylic acids are the group of the mostly used surface modification agents. As shown in Figure 3–23, they are a type of organic acid that contains at least one carboxyl group. During modification, carboxylic group (-COOH) reacts with the Hydroxyl (-OH) on the surface of the solid particles and forms a covalent bond, which strongly attaches the other part of the carboxylic acid to the surface of the particles. Similar to other modification agents, the carbon chains at the other end of the carboxylic acids provide better interaction with base lubricants hence a better dispersibility of the modified particles can be achieved [163]. Many types of solid lubricant additives have been successfully modified using stearic acid [164, 165], oleic acid[163, 166], 2-Ethylhexanoic acid (EHA) [82] and linoleic acid. Stearic acid is the mostly used carboxylic acid modification agent currently. It is very cheap and easy to access since it is the main ingredient for soap production. However, stearic acid has a straight carbon chain, it is not easy to tangle with the surrounding hydrocarbon chains and its steric stabilizing effect is far from perfect [167].
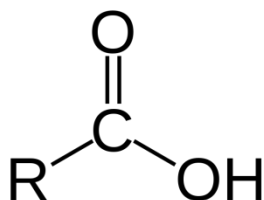
Figure 3–23 Chemical formula of carboxylic acids

3.7.2.2.4 Silanes

Silanes are often used as a surface modification agent most recently and they have demonstrated some superior stabilization performance than the classic carboxylic acids [168, 169]. Sharing the same principle as carboxylic acid modification, the hydroxyl group on solid particle surface is commonly the group that silanes react with. During modification, the alkoxy groups of the trialkoxysilanes are hydrolyzed to form silanol-containing species. Reaction of these silanes involves four steps [170]. Initially, hydrolysis of the three labile groups occurs, followed by the condensation to oligomers. Then the oligomers form hydrogen bond with OH groups on the particle surface. Finally a covalent linkage can be formed with the particles, and at the same time produces water. The reactions after the initial hydrolysis step can occur simultaneously. At the interface, for each silicon atom of the silane, there is usually only one linkage formed to the substrate surface. The two remaining silanol groups can appear either in condensed or free form. The modification reaction is shown in Figure 3–24.
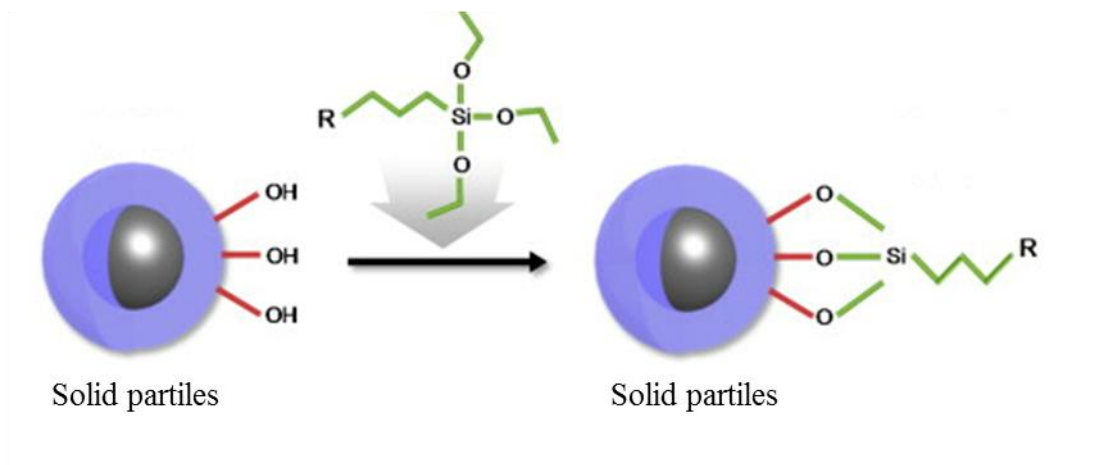
Figure 3–24 Surface modification with silanes [171]

3.8 Summary

The present chapter has reviewed previous studies regarding the application of solid lubricant additives. Various types of solid lubricant additives have demonstrated outstanding tribological properties such as friction reduction, wear resistance and improvement on maximum non-seizure load.

In general, it can be categorized into three ways by which solid lubricant additives are capable of improving the tribological performance of a lubrication system. The first approach is to employ their easy shear crystal structure. Solid lubricant additives that have such lubricating mechanism include graphite, Molybdenum disulfide (MoS_2), Tungsten disulphide (WS_2), Boric acid, and Boron nitride (BN). These solid lubricant additives create a layer of material with low shear strength, and therefore reduce the force required to activate the sliding manoeuvre, and consequently reduce friction. The second approach is by mending or third body effect. Solid lubricant additives that have such lubricating mechanism include metal nanoparticles, metal oxide nanoparticles and other inert solid particles with small particle size. These particles may deposit onto the contact surfaces, fill up valleys and work as the separation material, ultimately reduce direct "substrate to substrate" contact and protect contact surfaces. Finally, the third approach is associated with tribochemical reactions. Solid lubricant additives that have such lubricating mechanism include borates, sulfides, chloride and other materials that contain active elements such as Sulfur (S), Phosphorus (P), Chlorine (Cl) and Fluorine (F). These lubricant additives react with base oil and substrate material and form a protective film (tribo film) with low shear strength on contact surfaces. Exfoliation and replenishment of tribo film are the typical phenomenons involved in tribo chemical reactions.

Although many materials have been tested as the solid lubricant additives and many of they have shown the good tribological properties, there are still many controversies about their lubricating mechanisms. Therefore the research looking for new materials that are potentially suitable for a lubricant additive certainly needs to be continued. It is well known in literatures that the dispersion of the additives in base oil, in the application of solid lubricant additives, plays an important role on the tribological performance. Exploitation on new modification techniques is also an essential part of the research on solid lubricant additive.

Chapter 4.   Experimental Techniques and Materials

4.1   Introduction

In this study, the tribological properties of the selected solid lubricant additives were investigated by measuring friction and wear using a pin-on-disc configuration and comparing these parameters with the according base lubricants. In order to understand the mechanism of the modifications that the solid lubricant additives brought to base lubricants, several test rigs were also employed to post analyse the worn surface of the pins and the discs. The key test equipments involved in the study are introduced in this chapter.

4.2   Experiment outline

Common experimental procedures were applied to study the tribological performance of solid lubricant additives in lubricant base oil. Firstly, the solid lubricant additives were dispersed in base media. Subsequently the prepared lubricants were used to lubricate the pure sliding contact carried out with a pin-on-disc tribo tester, and the real time friction coefficient was recorded during a test. Wear of material was determined by measuring the wear scar diameter of the bearing balls (the upper pin) or the wear track depth on the lower discs. Post analysis on the worn surface generated in a tribology test was then conducted. A number of testing equipment were involved to determine the chemical and mechanical properties of the worn surface as well as the tribo film generated on the surface. By comparing the test results from pure base lubricants and the lubricants that contain solid lubricant additives, the friction and wear properties of the solid lubricant additives in base lubricants and the associate mechanisms can be identified. After the tribology tests, the worn surfaces were analysed by various types of laboratorial devices including nano-indentation, scanning electron

microscope (SEM), energy-dispersive X-ray spectroscopy (EDS) and atomic force microscope (AFM).

4.3   Experimental apparatus

4.3.1   Pin-on-disc tribo tester

The tribological properties of all lubricant samples were evaluated using a POD 2 Pin-on-disc tester (Teer Coatings Ltd.) as shown in Figure 4–1. Friction force can be measured automatically by a strain gage with a sensitivity of 0.02N on friction force measurement. Based on the literature study, suitable test conditions were selected. All the tests were carried out with a sliding speed of 50mm/s under 10-50N (1.54-2.63GPa Hertz pressure) normal load for a testing period of 30/60 minutes at the ambient temperature of 22°C. The bearing balls with 5mm diameter used as the pin in the experiments were made of AISI52100 chrome steel with HRC of 59-61. The disc samples used in this study was made of the identical material. At the initial stage of the study, disc samples with the dimensions of 27mm in diameter and 12mm in thickness were prepared. These discs were polished using progressively finer grades of emery paper at intervals of 400, 800, 1200 to achieve a uniform surface roughness Ra of around 30nm. However at the later stage of the study, automatic polishing device was adapted for consistent quality of samples in polishing. In order to meet the specification of the polishing device, the thickness of the disc samples was reduced from the original 12mm to 3mm instead. Accordingly, polishing technique was then changed to use diamond suspension on polishing 'Multicloth' (from Metprep, UK) since the disc samples with smaller thickness were no longer suitable for the original polishing technique and surface roughness Ra of 15nm was achieved using the second polishing technique. It has been verified that no noticeable influence on friction and wear results was made by changing polishing techniques due to the highly similar degree of finishing both two polishing techniques achieved.
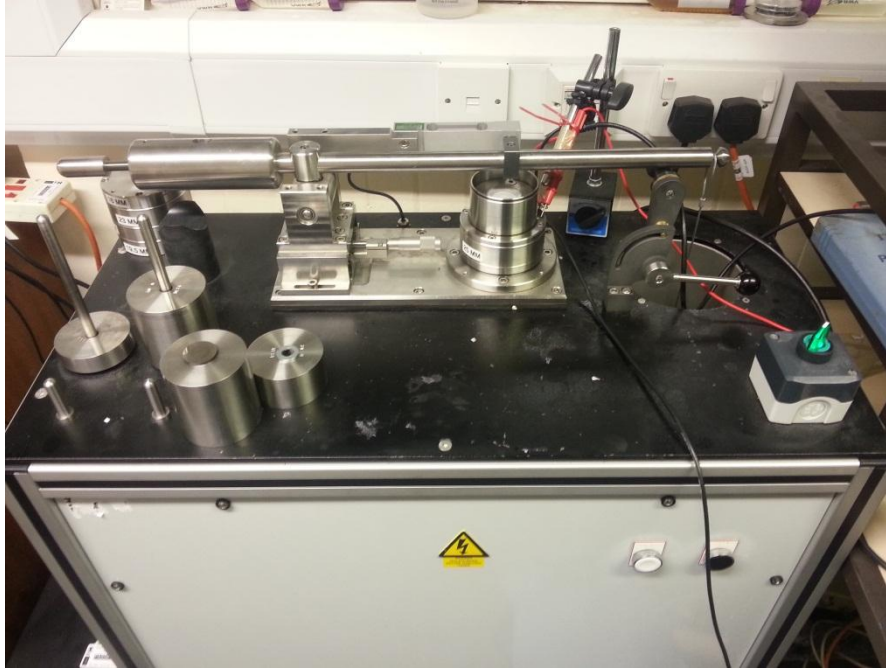
Figure 4–1 Pin-on-disc tribo tester used in this study

4.3.1.1   Repeatability of pin-on-disc test

In order to investigate the repeatability of the pin-on-disc tests, five preliminary tests were carried out using liquid paraffin. The test conditions were listed as follow:

- 10N applied load
- 50mm/s sliding speed
- Operating temperature 22°C
- One hour test duration

The sliding speed and operating temperature are identical with the systematic pin-on-disc tests and 10N load (1.54GPa Hertz pressure) was employed to demonstrate the repeatability of the test rig at the least sensitive condition. At the end of each test, the stabilized friction coefficient was recorded and they are shown in Table 4-1.

Table 4-1 Friction coefficients of the preliminary pin-on-disc tests

	Test 1	Test 2	Test 3	Test 4	Test 5	Average	Standard deviation
Friction coefficient	0.086	0.092	0.087	0.091	0.091	0.0894	0.0027

Standard deviation was calculated to describe the repeatability of the pin-on-disc tests of these five tests, the relatively low standard deviation (0.0027), compared with the mean friction coefficient of 0.0894, suggests that the data points tend to be close to the mean value. Therefore the results have demonstrated a good repeatability.

4.3.2   Electrical contact resistance

In order to investigate the alteration in contact conditions during sliding of two surfaces under lubrication, a device was designed to measure the electrical contact resistance (ECR). A constant current of 0.1Amp was selected as the power source (Figure 4–2(a)), and a 'Picoscope' (Figure 4–2(b)) was used to measure the voltage distribution between contact surfaces and to log the data into a computer. Then ECR was easily be calculated according to Ohm's law. The electrical circuit of the device set up is illustrated in Figure 4–3. The system was calibrated with standard resisters and a system error is less than 5%.
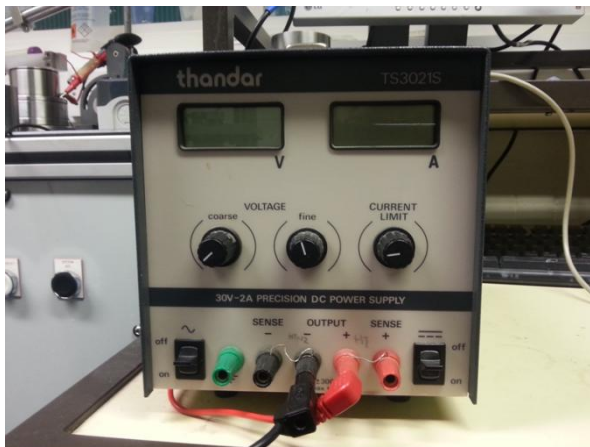
(a)   (b)
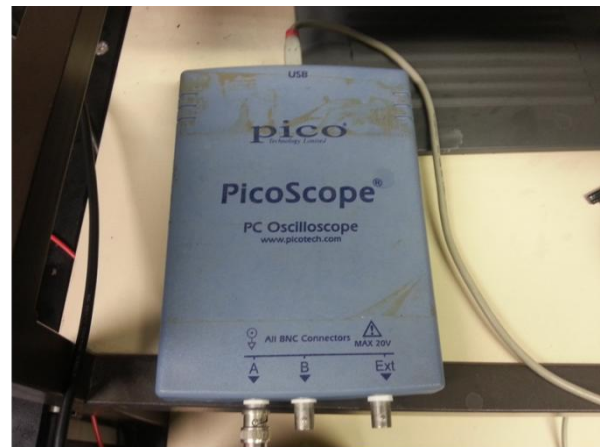
Figure 4–2 Main conponents of the ECR device (a) constant current power supply and (b)picoscope used for voltage measurement
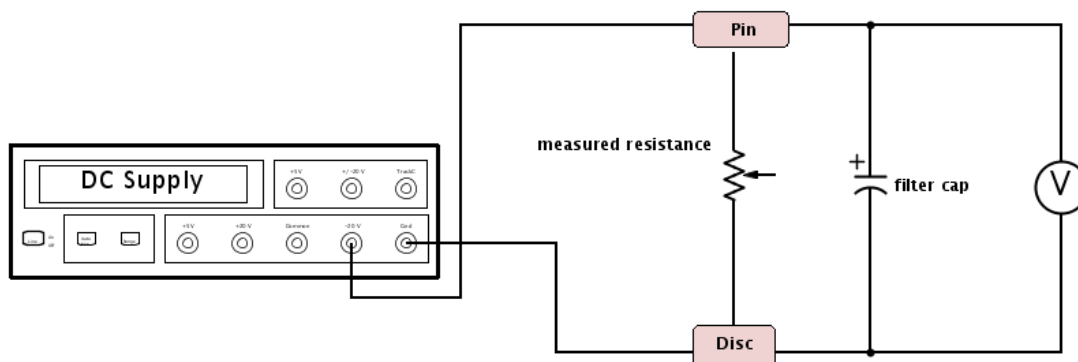
Figure 4–3 electrical circuit of ECR measuring device

4.3.3 Fourier transform infrared spectroscopy (FTIR)

FTIR is one of the most powerful tools for identifying types of chemical bonds (functional groups). In infrared spectroscopy, a beam of infrared radiation containing many frequencies of light is passed through a sample. Some of the infrared radiation is absorbed by the sample and some is passed through (transmitted). Different materials or chemical bondings have a unique absorption and transmission spectrum which is the fingerprint of the material. Therefore by analysing an infrared spectrum received from the material, the chemical bondings of this material can be identified. In this study, the FTIR device, as shown in Figure 4–4, was employed to investigate the surface modification of the solid particles. The Infrared spectroscopy measurements were conducted using a Perkin-Elmer Spectrum 100 FTIR Spectrometer. Samples were prepared as powder-pressed KBr pellets. The spectra were collected in a wave range from 600 to 4000 cm^{-1} with a resolution of 4cm-1 in a transmission mode.
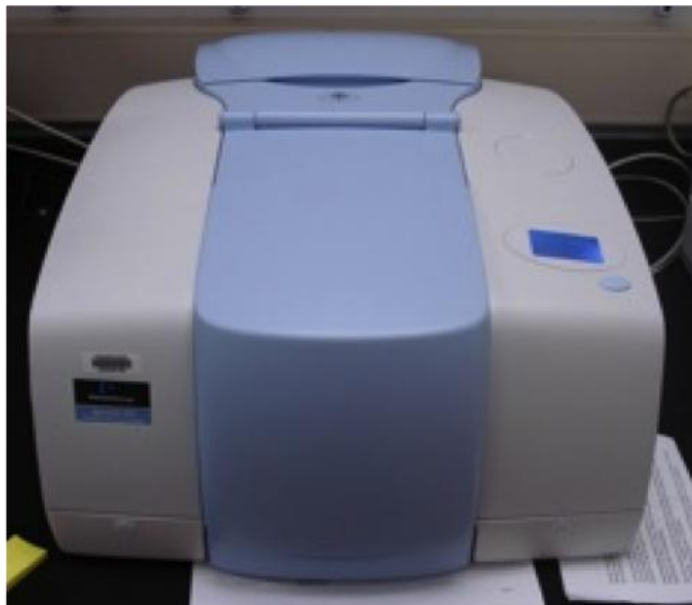
Figure 4–4 The inferred spectrum facility used in this study

4.3.4 Thermogravimetric analysis

Thermogravimetric analysis (TGA) is a technique that measures the amount and rate of change in the weight of a material as a function of temperature or time in a controlled atmosphere. The TGA device as shown in Figure 4–5 was employed to verify the surface modification carried out to the solid lubricant additives. At elevated temperature, solid particles have a better stability than the surfactant attached on the particle surface through surface modification process. As the temperature rises, the attached surfactant will be burn out first which leads to a reduction in sample weight. By comparing the sample weight before and after the heating process, the amount of surfactant that has been attached onto the particles` surface can be identified. Thermogravimetric analysis (TGA) was carried out with a SETARAM TG-DSC 1600 instrument (Caluire, France). For each test, approximately 10mg sample placed in an aluminium crucible was tested with a heating rate of 5 °C/min from 80 to 500 °C in atmosphere. Prior to the tests, an accurate calibration using the melting points of highly pure metals as standard reference materials was conducted.

Figure 4–5 The thermo gravimetric analyser used in this study

4.3.5 Zeta-potential & Dynamic light scattering

Particle conglomerate size in organic solvent was measured using a Dynamic Light Scattering device (DLS) (Malvern Zetasizer-Nano Series) as shown in Figure 4–6. This method determines the particle size by the scattering of light caused by the Brownian motion of the particles in concentrated suspensions using an autocorrelation function [172]. Three repeat readings on each sample were taken to deliver an average diameters record.

Zeta-potential, which is known as an important parameter that affects the stability of suspension, was also measured with the same device. When solid particles were dispersed in a solution, a rearrangement of local free ions in the solution will be initiated by the surface charge of solid particles. This rearrangement of ions gives a region of nonzero charge near the interface between the solid and the liquid. The zeta potential reflects the charge at the interface between the thin layer of immobile counter ions next to the solid and the mobile counter ions [173]. Zeta potential is related to electrostatic repulsion and high value of zeta potential can be the indication of stability for charge stabilised nanoparticles [174]. In current

study Zeta-potential of the suspensions that contain solid lubricant additive was obtained to reflect the magnitude of the repulsion or attraction between particles. Three repeat readings on each sample were taken to deliver an average value of Zeta-potential results.
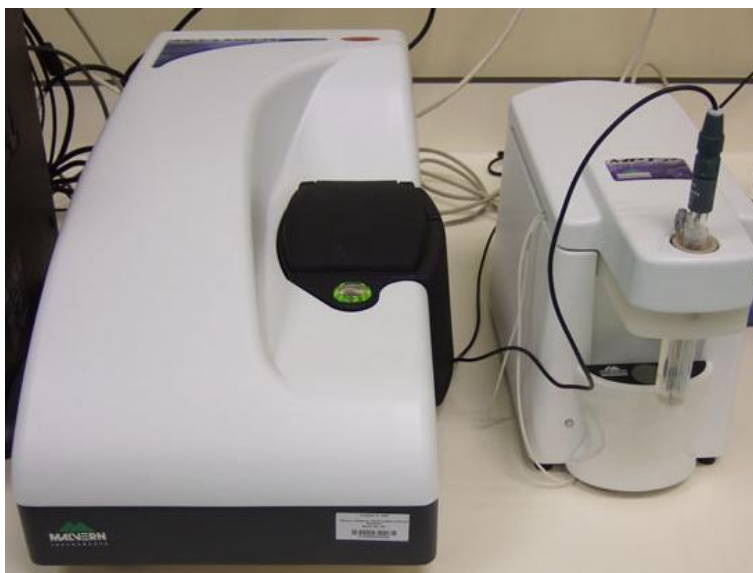
Figure 4–6 The Malvern Zetasizer-Nano Series used in this study

4.3.6   Atomic force microscopy

An atomic force microscope (AFM) was used to observe morphology of the tribo film generated on worn surfaces. The AFM used in this study was a MultiMode scanning probe microscope, 'Nanosurf Easyscan 2' from Nanosurf (Liestal, Switzerland) as shown in Figure 4–7. In an observation, a three dimensional image of the object surface can be constructed via a tip scanning across the surface under static force in contact mode. Contact force was set to be 20nN to avoid any scratching damage when probe was driven crossing the object surface. A silicon probe with a 5 nm-diameter tip was used in the AFM observation and all images were captured at 512×512 pixel resolution at a scanning rate of 1 Hz. A measuring accuracy of 0.3nm was achieved with the current setup.
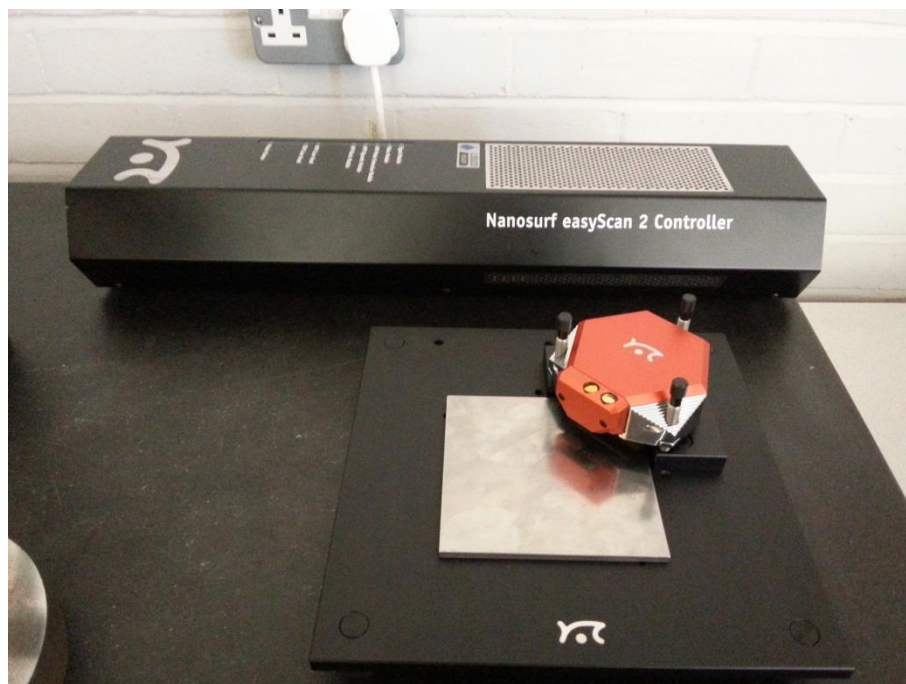
Figure 4–7 The atomic force microscope used in this study

4.3.7 Scanning electron microscope

The solid lubricant additives and wear scars of the pins (bearing balls) after the Pin-on-disc tests were inspected using scanning election microscopy (SEM JSM-6010LA) (Jeol Ltd., Tokyo, Japan) as shown in Figure 4–8. Tested bearing balls were first ultrasonically cleaned in acetone for five minutes, and then mounted onto SEM sample substrates using carbon conductive adhesive tabs.

The typical accelerating voltage was set at 5-20 kV and the working distance between the electron gun and observing object was around 6 mm. A thin layer of gold coating on the examining object was sometime necessary to improve the conductivity of the sample. A sputter coater, Emitech SC7620 (Fig 52(b)), equipped with a gold target, was set at 75 mA for 30 seconds to do the coating process. Also conductive silver paint was used to ensure an electrical conductivity from the surface to the sample stub.

(a)   (b)
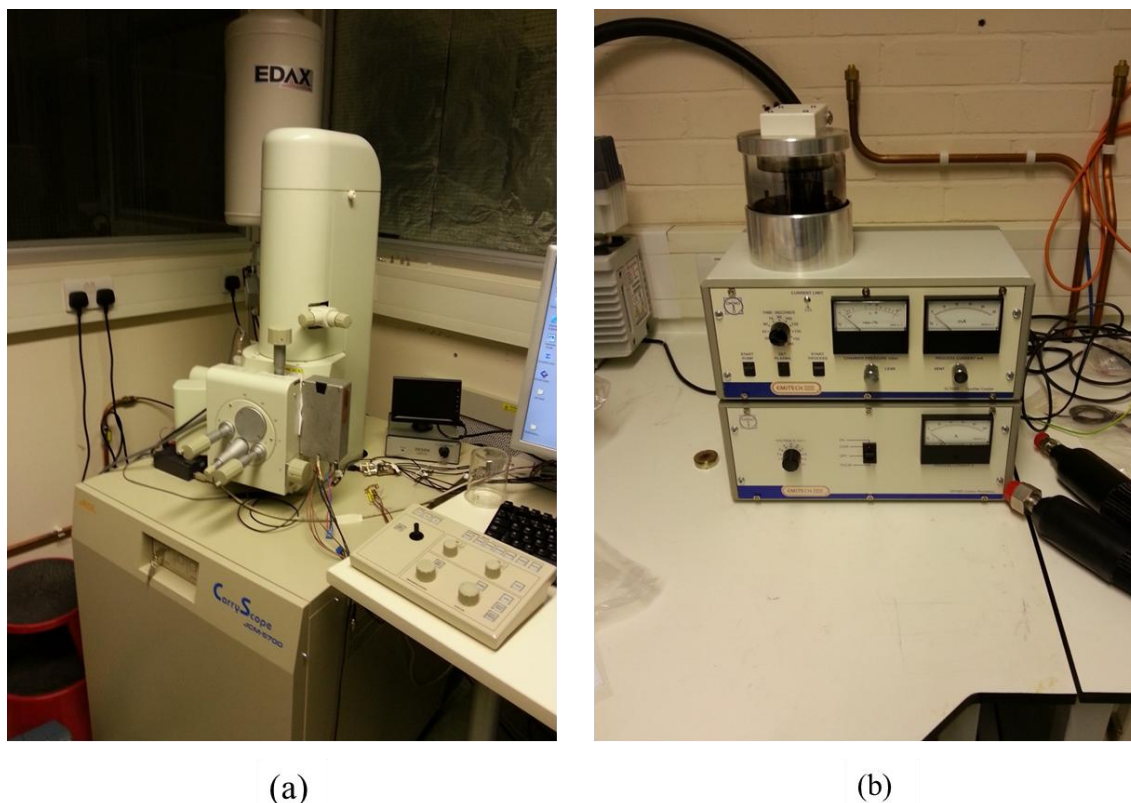
Figure 4–8 (a) The scanning election microscopy and (b) the sputter coater
used in this study

4.3.8   Nano-indentation

Mechanical properties of the tribo-film were determined using a Nano indentation device, 'nano tester', from Micro Material Ltd (Wrexham, UK) as shown in Figure 4–9. A Berkervich indenter with a tip diameter of 50nm was employed for the experiment. Supported by an on board microscope, the 'nano tester' is able to carry out indentation on a specific point. All indentation experiments were conducted inside an environmental chamber, and a constant temperature of 20 degree Celsius was maintained. The 'nano tester' is also capable of generating topography of a surface under 'scanning mode'. This function was employed to determine the wear track depth in the first series of the experiments. Before a test, the force calibration of the device was carried out using standard weight, and the diamond area function of the indenter was achieved by applying a hundred of indents with various indentation forces on a piece of standard fused silica.
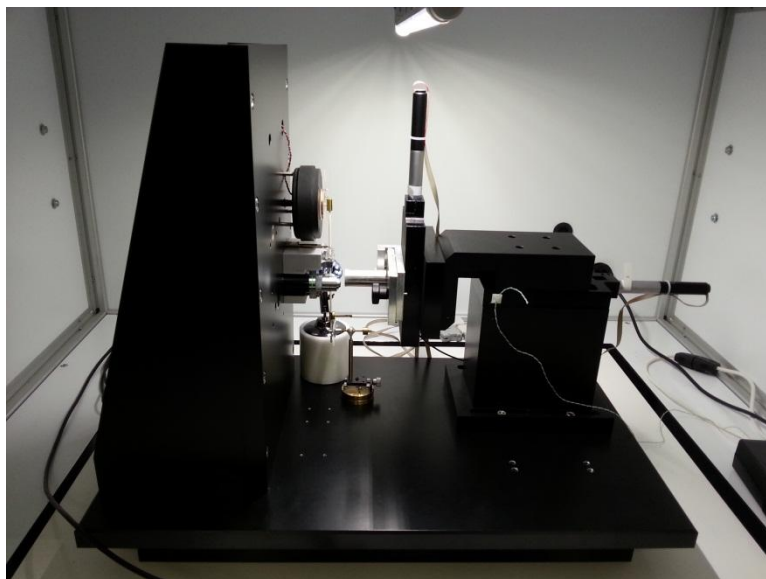
Figure 4–9 The nano indentation device used in this study

4.3.9   Materials

4.3.9.1   Base lubricants

Water, sunflower oil and liquid paraffin were selected as the base lubricants in this study. The

viscometric properties of these base lubricants are measured by author and listed in Table 4-2.

Table 4-2 The viscometric properties of the base lubricants

Description	Viscosity at 40 °C (m Pa s)	Viscosity at 100 °C (m Pa s)
Water	0.6	0.2
Sunflower oil	27.2	5.7
Liquid paraffin	24.0	4.8

4.3.9.2   Selection of solid particles

The utilisation of nano sized or submicron sized particles as an inorganic lubricant additive

has received much attention over recent years, owing to their outstanding tribological

properties and good environmental friendly feature compared with the traditional organic lubricant additives that contain P, S and Cl elements [1, 76, 79-82]. Tribological properties of metal oxide nanoparticles such as TiO_2 [82, 150, 152], SiO_2 [163], Al_2O_3 [175], Fe_2O_3 [134], ZnO [176], CuO [177] and ZrO_2 [80] used as oil lubricant additives have all been investigated. Considerable improvement in the tribological performance of the base oils have been demonstrated when these nanoparticle additives are used. Furthermore some of the rare earth metal oxides have also been studied. Together with $CaCO_3$ nanoparticles, CeO_2 nanoparticles were tested in 40CD oil [178]. It is reported that the additional $CaCO_3$ and CeO_2 nanoparticles in 40CD oil have improved anti wear property of 40CD oil by 33.5% and friction reduction property by 32% respectively [178]. However despite the fact that CeO_2 nanoparticles have the excellent wear resistance property, chemical erosion resistance and good polishing effect as abrasive [179, 180], information of the tribological properties of solely CeO_2 nanoparticles in lubricants are still very limited.

Many interests have also been put on the application of borate nanoparticles as solid lubricant additive. Particularly, tribological properties of titanium borate [156], ferrous borate, magnesium borate [91] and zinc borate [84] nanoparticles together with dispersing agent sorbitan monostearate have been investigated, and the outstanding lubricating performances were observed. However the expensive and complicated preparation process of nanoparticles hinders their mass application. Compared with nanoparticles, submicron sized particles have won their attention in industrial application due to relatively low cost and simple preparation process although submicron size particles are more thermodynamically unstable in liquid media.

For above reasons, two types of solid particles, Ceria (CeO_2) nanoparticles and Zinc borate ultrafine powders (ZB UFPs), were selected as solid lubricant additives in this study.

CeO_2 nanoparticles of 10-40nm diameters and 99.9% purity (Shandong Yitong, China) are shown in Figure 4–10. ZB UFPs (Molecular Formula: $2ZnO\ 3B_2O_3\ 3.5H_2O$) with the particle size of 500-800nm (Shandong Jiqing Chemical Co.,Ltd, China) are shown in Figure 4–11.
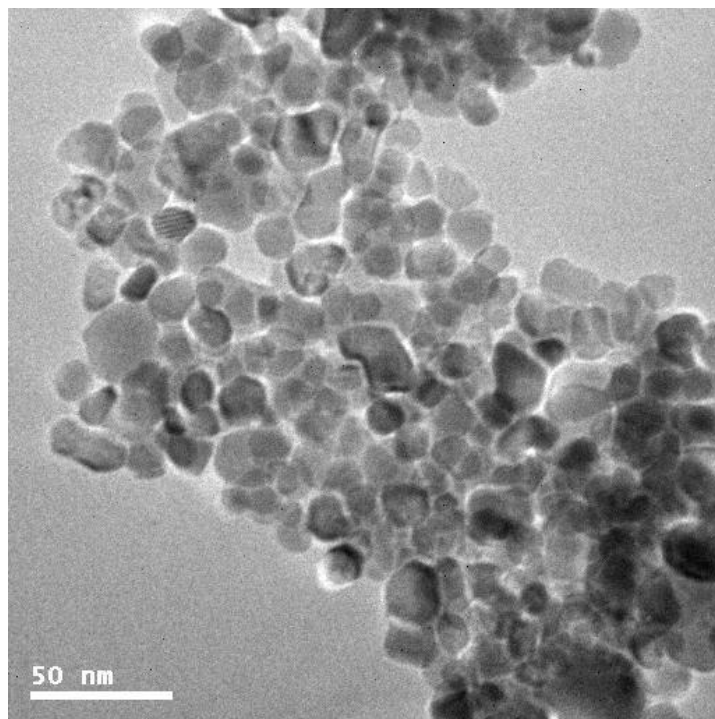
Figure 4–10 TEM micrograph of CeO_2
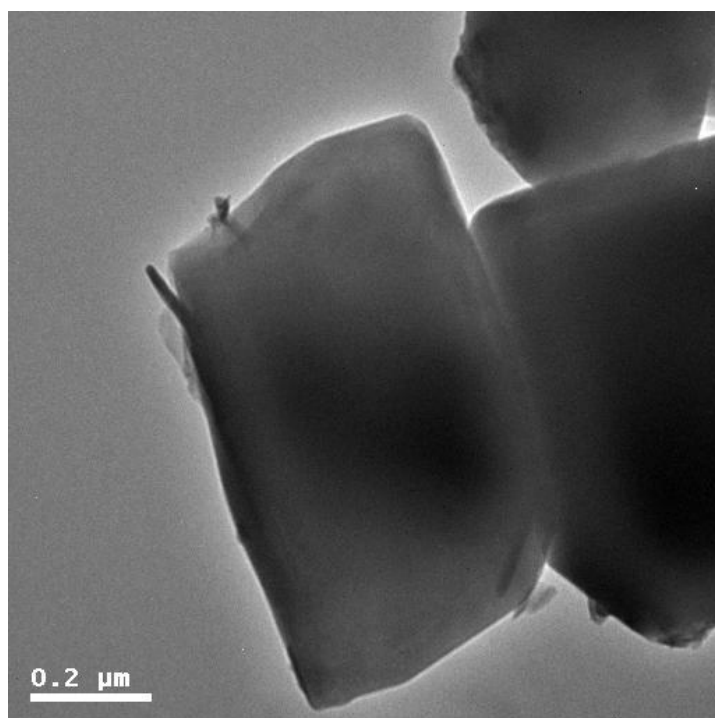
Figure 4–11 TEM micrograph of ZB UFPs

4.3.9.3   Surfactant and surface modification agents

Based on the literature study of the surfactant and modification agents, Sorbitan monostearate and Oleic acid used in this study were supplied by Sigma-Aldrich Co. LLC, St. Louis, USA. The Chemical formulas of Sorbitan monostearate and Oleic acid (OA) are shown in Figure 4–12 and Figure 4–13
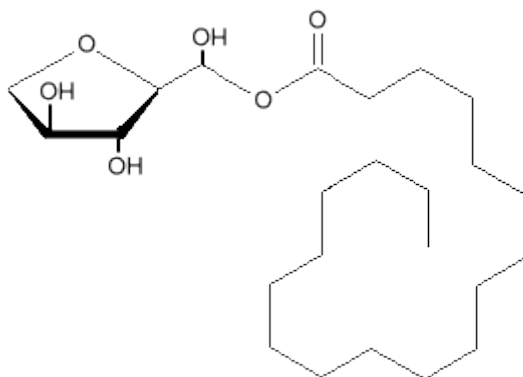
Figure 4–12 Chemical fomula of Sorbitan monostearate
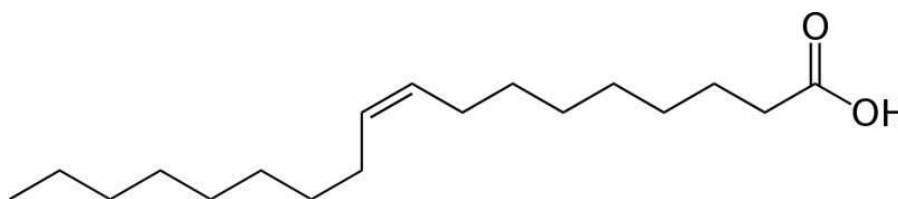
Figure 4–13 Chemical fomula of Oleic acid

Hexadecyltrimethoxysilane (HDTMOS) used as the surface modification agent in this study was supplied by Gelest, Inc., (PA, USA). The Chemical formula of Hexadecyltrimethoxysilane is given in Figure 4–14.
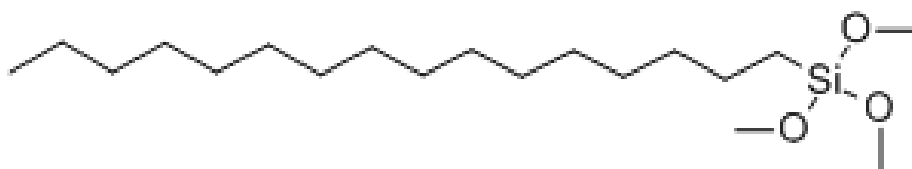
Figure 4–14 Chemical fomula of Hexadecyltrimethoxysilane

All surfactant and surface modification agent employed in this study have a distinguishing chemical structure. There are hydroxyl groups at one end of the molecules and a long carbon chain at the other end. During surface modification, the hydroxyl groups react with the –OH bondings on the surfaces of the solid particles and attach the carbon chains onto the surfaces. Eventually, the solid particles covered with organic substance (long carbon chains) can be synthesised.

4.4   Summary

This Chapter presented the main laboratory devices which were employed to characterise the prepared lubricants and the specimens lubricated with these lubricants. The test outline was briefly described. The base lubricants and solid lubricant additives involved in the tribology tests were also introduced, as well as the chemical agents employed in surface modification of solid lubricant additives. In the following Chapters, the experimental results for different lubricants modified with various solid lubricant additives will be discussed.

Chapter 5.   Tribological Properties of Ceria Nanoparticles in Water

5.1   Introduction

This chapter presents the experimental results and observations which were obtained from tribology tests of using Cerium dioxide (CeO_2) as the solid lubricant additive in water. Water as an important lubricant has rarely been studied in recent years, despite its great potential in engine cooling/vehicle thermal management, polymer, wood, metal, ceramic, glass machining and similar circumstances where oil contamination must be avoided. A stable dispersion of nanoparticles in the fluids was achieved with an appropriate percentage of surfactant Sorbitan monostearate. The stability of particle dispersion and additive conglomerate size in water were measured using a Malvern Zetasizer. It has been observed that the dispersibility of nanoparticles has a significant influence in their frictional properties. The tribological property of the water-based lubricant was evaluated using a pin-on-disc tester under different loading conditions. The worn surfaces of the contact elements were characterised using SEM and a Nano-tester.

5.2   Preparation of lubricants

The prepared lubricants were composed of the rare earth metal nanoparticles (Cerium Oxide) and deionised water with or without surfactant. Both CeO_2 nanoparticles and a suitable amount of surfactant Sorbitan monostearate were added into the deionised water. The blend was firstly heated up to 55°C and dispersed with an ultrasonic homogenizer for two minutes. Subsequently, the mixture was heated up to 70°C and maintained at the temperature for one hour while stirring using a rotor–stator homogenizer (Sonics VC 750) with a speed of 10k rpm. Finally, the stable milky colour suspensions were achieved and these suspensions were employed for the tests within 10 minutes. One sample with low additive concentration of

water+0.05wt% CeO2+1% surfactant, was prepared for particle size and zeta-potential measuring in order to ensure a good accuracy (low additive concentration is required). For the tribology tests, the lubricant samples with different nanoparticle concentrations were prepared in order to investigate the effects of nanoparticle concentration on the tribological properties. The surfactant concentration was doubled to 2wt% in order to ensure a good stability of the suspensions when various amounts of CeO_2 nanoparticles were applied. All additive concentrations in this study were presented in weight ratio. No sedimentation was observed in the prepared lubricants for four days.

5.3 Pon-on-disc test conditions

The anti-wear and friction reduction properties of the CeO_2 nanoparticles as a lubricant additive in water with and without surfactant Sorbitan monostearate were evaluated using a POD-2 pin-on-disc Tester. A low sliding speed of 50mm/s was used for each test to achieve boundary lubrication. Tests were carried out at room temperature with duration of 30 minutes. The bearing balls of 5mm diameter used in the tests were made of AISI52100 chrome steel with HRc of $60 - 67$, and has a surface roughness Ra of 20nm. The disc was made of the identical material, with 27mm in diameter and 12mm in thickness. The sample discs were polished using a p1200 abrasive paper to achieve a uniform surface roughness Ra of around 30nm. Before and after each test, both bearing balls and discs were cleaned with acetone in an ultrasonic water bath for five minutes.

5.4 Experimental results

5.4.1 Friction coefficient of the nanofluids

Figure 5–1 and Figure 5–2 illustrate how the different nanoparticle concentrations in the fluids affect the friction coefficients at the loads of 10N (1.54GPa Hertz pressure) and 20N (1.94GPa

Hertz pressure) without the surfactant. The friction coefficient of the pure deionised water was also obtained as a reference. Evidence collected has shown that at both loading conditions, without the surfactant, the water-based CeO_2 nanofluids did not show any obvious effect on the friction coefficient. A high friction coefficient of more than 0.4 was obtained in all lubricant samples without surfactant. After the tests, the nanoparticle sedimentation was also found in all lubricant samples without the surfactant. It suggests that the agglomeration of nanoparticles accelerates their sedimentation in water, which hugely reduces the concentration of nanoparticles in the fluids. The agglomeration also causes nanoparticles to form much bigger sized clusters, which can increase the asperity level between the contacting surfaces [181].
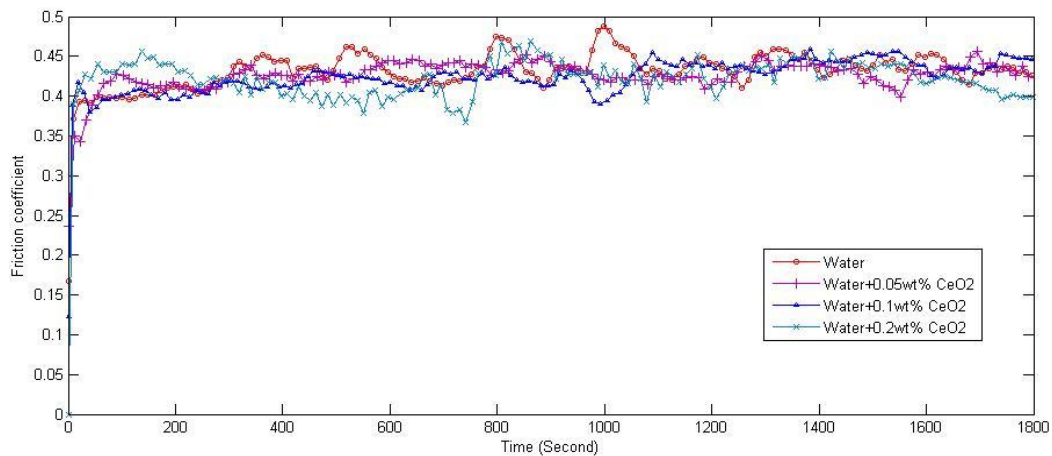
Figure 5–1 Friction coefficient of the water-based nanofluids with different CeO_2 nanoparticles concentration (without surfactant) under 10N load
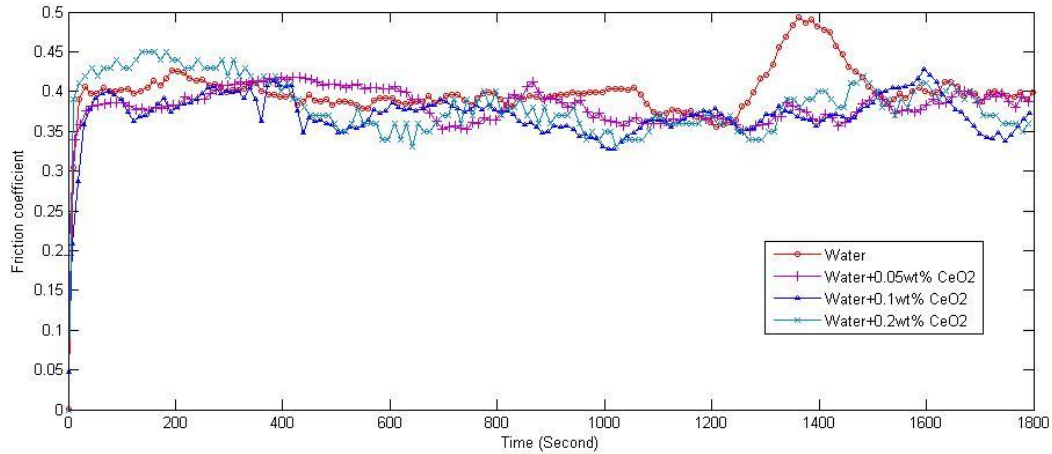
Figure 5–2 Friction coefficient of the water-based nanofluids with different CeO$_2$ nanoparticles concentration (without surfactant) under 20N load

Friction coefficients of the water-based CeO$_2$ nanofluids with 0.2wt% CeO$_2$ nanoparticles dispersed with surfactant are shown in Figure 5–3 and Figure 5–4. It is evident that at both loading conditions of 10N and 20N, with 2wt% surfactant, the friction coefficients of the water-based CeO$_2$ nanofluids with 0.2wt% CeO$_2$ were reduced sharply to below 0.1. Compared with the friction coefficient of the same nanofluids without surfactant shown in Figure 5–1 and Figure 5–2, a reduction over 75% was observed.

Because surfactants are used as an additive in the fluids, and very often they can also contribute to the tribological improvement [182]. Therefore, it is essential to clarify whether CeO$_2$ nanoparticles are responsible to the reduction of friction coefficient shown in Figure 5–3 and Figure 5–4. As illustrated in Figure 5–3, water+2wt% surfactant gives a friction coefficient around 0.079 at a load of 10N. All suspensions containing CeO$_2$ nanoparticles demonstrate lower friction coefficients at the same condition. The lowest friction coefficient of around 0.067 was observed when water+0.2% CeO$_2$+2wt% surfactant was tested, and compared with that of water+2wt% surfactant, a reduction of 15% in friction coefficient was achieved. Water+0.1% CeO$_2$+2wt% surfactant delivered the similar friction reduction performance with water+0.2% CeO$_2$+2wt% surfactant, however more fluctuations on friction coefficient were found in the experiment of using water+0.1% CeO$_2$+2wt% surfactant. Under

a load of 20N, as shown in Figure 5–4, the similar friction reduction phenomenon was also observed. Water with both CeO_2 nanoparticles and 2% surfactant has outperformed water with 2% surfactant alone. Water+0.2wt% CeO_2+2wt% surfactant demonstrated the best overall friction reduction property and a 10% reduction of friction coefficient was found in the first 900 seconds, compared with water+2wt% surfactant. In the second duration of 900 seconds, the reduction went up to more than 20%. Much stronger fluctuations on friction coefficient were obtained in the experiments under 20N load due to the more intensified stress. It is evident that much less oscillation can be noticed for the lubricants with nanoparticles as shown in Figure 5–3 and Figure 5–4. This is possibly attributed to the third body effect of nanoparticles. Entrapped nanoparticles groups between two surfaces work like a cushion, which may help smoothen the rough surfaces, diminish direct contact and reduce adhesion friction.
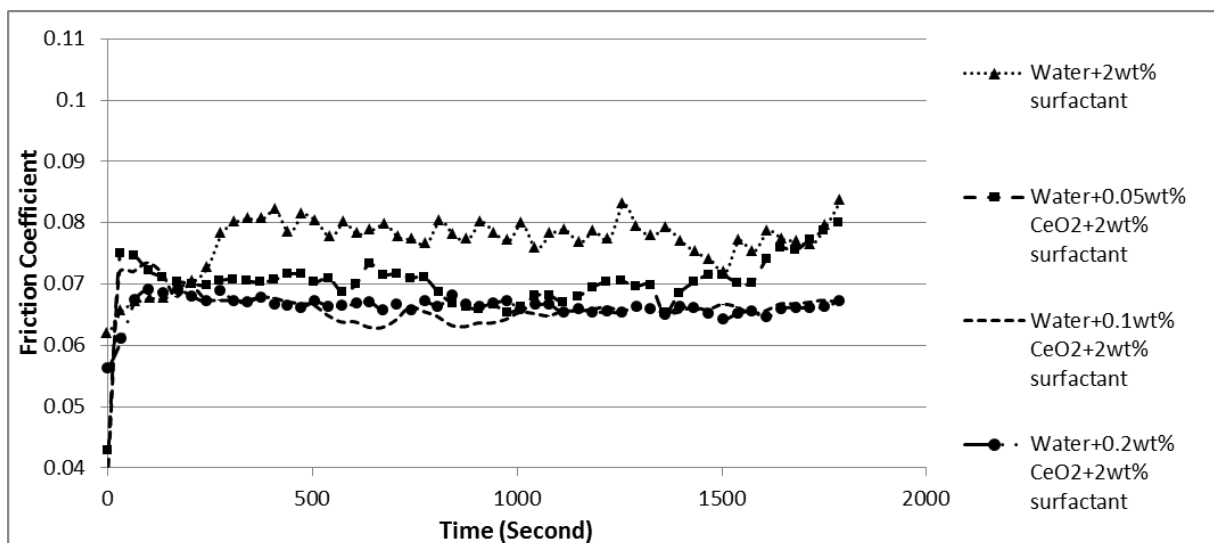
Figure 5–3 Comparison of friction coefficient of water with surfactant and the water-based CeO_2 nanofluids with surfactant under 10N load
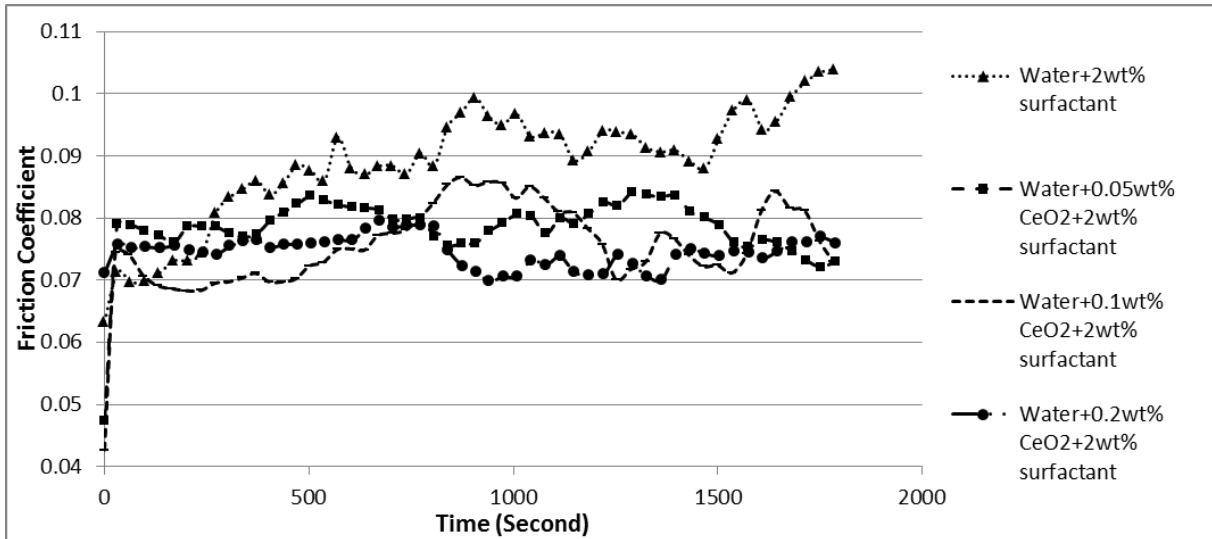
Figure 5–4 Comparison of friction coefficient of water with surfactant and the water-based CeO_2 nanofluids with surfactant under 20N load

5.4.2 Anti-wear Property

The worn surface scanning with a nano-indentation tester was performed to measure the topography of the wear tracks of the sample discs in order to reflect the anti-wear ability of the fluids. The depth of the wear tracks was determined using the scanning mode of the Nano-indentation device. The contact load and scanning speed employed in the tests were 0.1mN and 5µm/s respectively. The indenter used for scanning is a conical indenter with 60 degrees head angle and a tip size of 5µm radius. Figure 5–5 illustrates the typical depth profiles of the wear tracks generated on the discs during a test. The central positive reading peaks in Figure 5–5 indicate the depths of two wear tracks on discs.

The influence of CeO_2 nanoparticles and surfactant on the depth of wear tracks is shown in Figure 5–6. It is evident that the existence of the nanoparticles considerably reduced the depth of the wear tracks. Without surfactant, the smallest track depths of 1365nm at a load of 10N and 2495nm at 20N were found after the water-based CeO_2 nanofluids with 0.1wt% CeO_2 had been tested. Compared with the depth of wear track lubricated with water only, 49% and 38% reductions of the depth from the nanofluids were observed at the loading conditions

of 10N and 20N respectively. However, when the particle concentration of the nanofluids was increased further to 0.2wt%, without surfactant, the water-based nanofluids with 0.2wt% CeO_2 caused even higher value of the track depth than that of the water-based nanofluids with 0.1wt% CeO_2 at both loading conditions.

When 2% surfactant was used, only slight reductions were obtained with the employment of CeO_2 nanoparticles. However, the deterioration on the anti-wear performance caused by 0.2wt% CeO_2 was effectively limited with the utilization of surfactant. It is suggested that without surfactant, agglomeration caused by excessive content of nanoparticles is the possible reason for the increase of wear track depth. Agglomeration of particles may form abrasive clusters between the sliding pairs and results in an increase of wear. The improved disparity of the nanoparticles achieved by the application of surfactant reduced the extent of agglomeration, and therefore a better anti-wear performance can be observed. As a popular surfactant, Sorbitan monostearate itself has excellent friction and wear reduction ability when it is used as an additive in base lubricants [182-184]. This could be the reason for the overshadowed influence of CeO_2 nanoparticles on the reduction of wear.
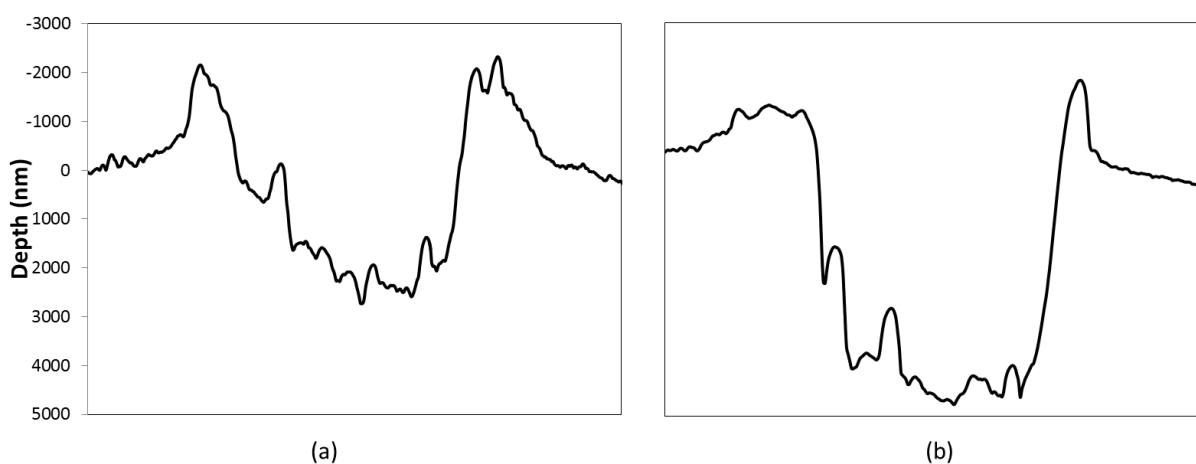
Figure 5–5 Depth profiles of wear tracks: (a) tested in water-based nanofluids
with 0.1wt% CeO_2 and (b) tested in pure water
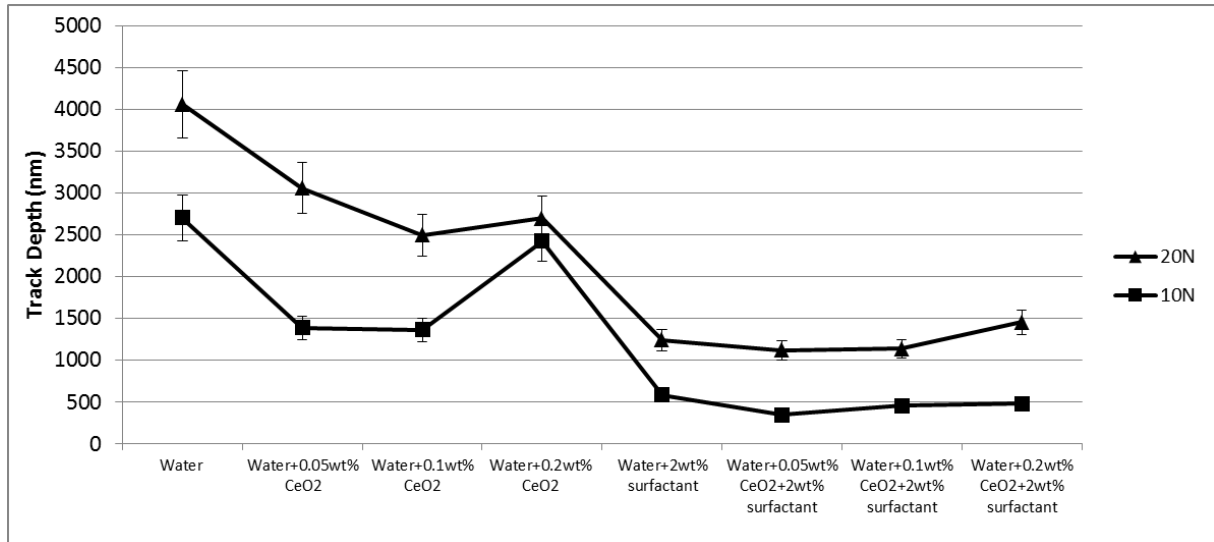
Figure 5–6 Depth of wear tracks versus different fluids with different CeO_2 nanoparticles concentration and surfactant

5.5   Interpretation and discussion of the results

5.5.1   Conglomerate size of ceria nanoparticles and zeta-potential

It is well known that particle size in a lubricant makes a huge difference in most of lubrication applications. The Conglomerate size of CeO_2 nanoparticles in water was measured by zeta-potential apparatus. Figure 5–7 and Figure 5–8 illustrate the average conglomerate sizes of 0.05wt% CeO_2 nanoparticles in the deionised water with and without 1wt% surfactant. Before each measurement, the samples were stirred vigorously using an ultrasonic homogeniser (KINEMATICA PT 10-35 GT). The average conglomerate size of CeO_2 nanoparticles dispersed in the fluids with 1wt% surfactant was around 110nm in radius. By contrast, the average conglomerate size of the CeO_2 nanoparticles in water without surfactant was 193.7nm in radius. It is suggested that CeO_2 nanoparticle clusters formedin the fluids with surfactant have a narrow size span. As shown in Figure 5–7, with surfactant, there is only one peak appeared in the distribution diagram, which suggests a uniform distribution. However, without

surfactant, CeO_2 nanoparticle clusters in the fluids have a much wider size span. As shown in Figure 5–8, two peaks appear in the distribution diagram and, the second peak indicates a size distribution of nanoparticle cluster with more than 2000nm radius.

Size Distribution by Intensity
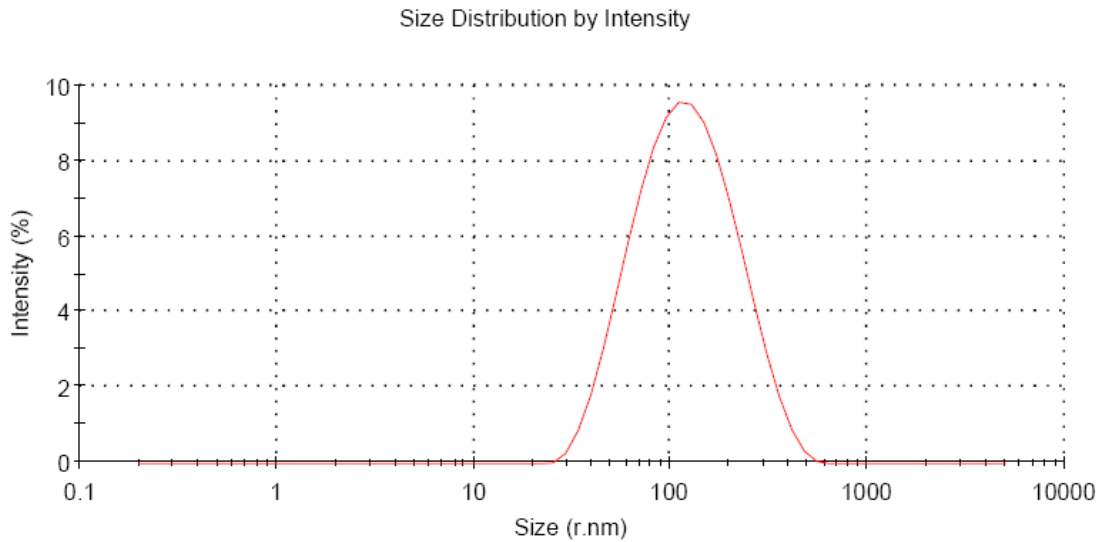
Figure 5–7 Size distribution of particle conglomerate of water+0.05wt% CeO2+1wt% surfactant (Sorbitan monostearate)

Size Distribution by Intensity
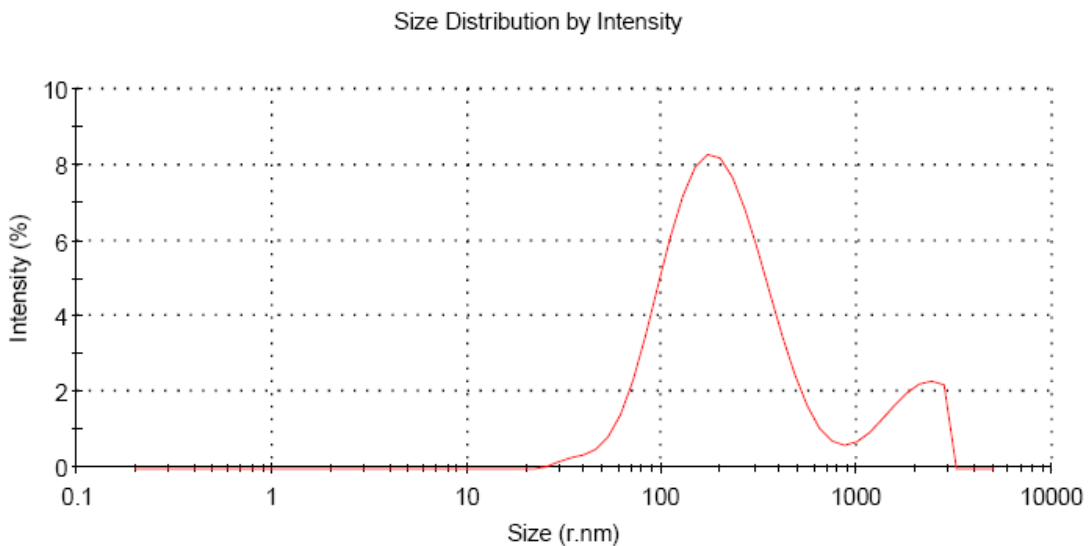
Figure 5–8 Size distribution of particle conglomerate of water + 0.05wt% CeO_2 without surfactant

PDI (Polydispersity index) and correlation function intercept also confirmed the dispersibility improvement of nanoparticles in fluids using surfactant. PDI readings in Table 5-1 indicate the regularity of conglomerate size in the fluids. The lower PDI value confers a better consistency of conglomerate size. The PDI value of the fluids, water+0.05wt% +1wt% surfactant, was 0.252 and is much lower than 0.415 of water+0.05wt% CeO_2. Therefore, it is evident that with surfactant, conglomerate size of CeO_2 in fluids was significantly reduced and also became more uniformly distributed. Correlation function intercept is the signal to noise ratio obtained for the measurement. Correlation function intercept of more than 0.8 for both suspensions indicates good data quality.

Table 5-1 Dispersibiltiy of nanoparticles in the fluids with and without surfactant

Water solution	PDI test results	Zeta-potential value	Correlation function intercept	Average conglomerate size (radius)
Water+ 0.05wt% CeO_2	0.415	+19.7 mV	0.81	193.7nm
Water+0.05wt% CeO_2+1wt% surfactant	0.252	+44.8 mV	0.88	110nm

Absolute Zeta-potential value of the fluids, water+0.05wt% CeO_2, was measured to be 19.7mV. Comparatively, the number was increased to 44.8mV for the fluids of water+0.05wt% CeO_2+1wt% surfactant. Surface charges caused by absorption of ions and molecules generate an electrostatic repulsion force between particles. For small particles, the electrostatic repulsion force can partially counteract gravitation and reduce agglomeration and sedimentation of particles [150]. Therefore, a higher absolute value of zeta-potential presents a better stability. A greater absolute Zeta-potential value for the fluids, water+0.05wt%

CeO_2+1wt% surfactant, suggests that the stability of CeO_2 nanoparticles in the water-based fluids has been greatly improved by an employment of surfactant. It was also observed that the stabilization of surfactant is reversible. As shown in Table 5-2, after 24 hours, the absolute Zeta-potential value of the prepared fluids, water+0.05wt% CeO_2+1wt% surfactant, was reduced to 36.8mV and further reduced to 35.4mV after 96 hours.

Table 5-2 Reduction of Zeta-potential value with time

Hours after dispersion	0 hour	24 hours	96 hours
Zeta potential reading	+48.8mV	+36.8mV	+35.4mV

5.5.2 SEM micrographs and EDS Analysis

The morphology and the elemental distribution on the worn surface of the tested bearing balls were studied using JEOL-6100 scanning electron microscope (SEM) equipped with energy dispersive spectra (EDS). Figure 5–9 shows the SEM morphology of the worn surface tested with the water-based CeO_2 nanofluids with 0.2wt% CeO_2. The elemental distribution analysis was also performed using SEM equipped with EDS. As shown in Figure 5–9, CeO_2 nanoparticles were found on worn surface after the pin-on-disc experiment. Element mapping shown in Figure 5–10 has also confirmed the CeO_2 nanoparticle distribution on the worn surface. Both Ce and O elements are consistently distributed in the worn area. Fe element indicates a relatively weaker signal in the area where Ce and O elements are densely accumulated. The irregular distribution of the elements is possibly due to the uneven contact stress distribution on worn surface introduced by the geometrical shape of the bearing ball. Figure 5–9 indicates that CeO_2 nanoparticles were entrapped and accumulated between contacting surfaces during the tests.
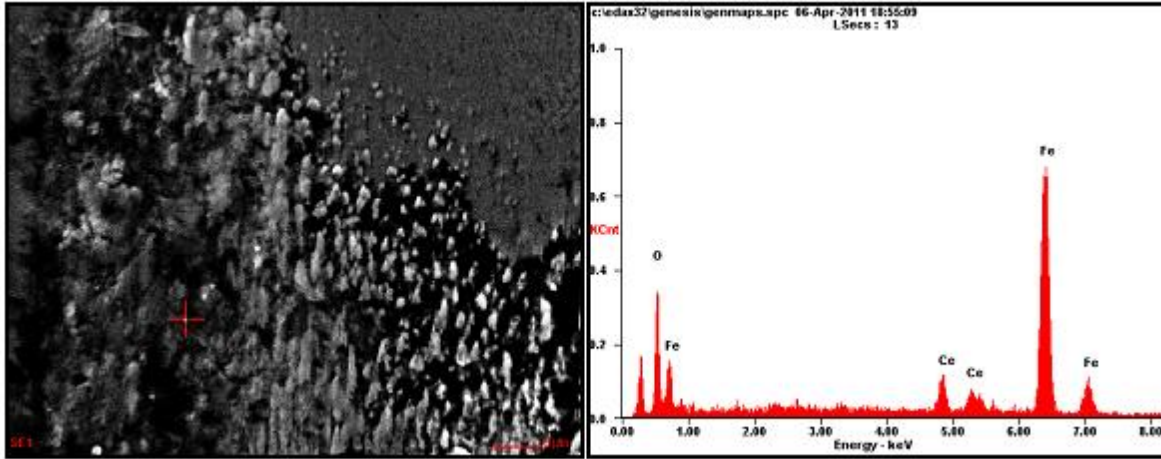
Figure 5–9 SEM morphology and element analysis of worn surface
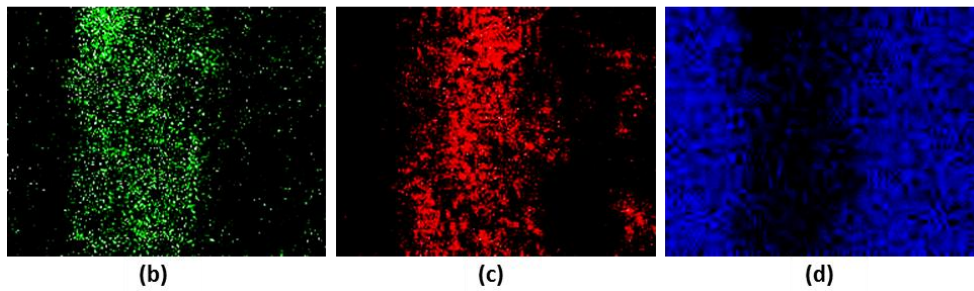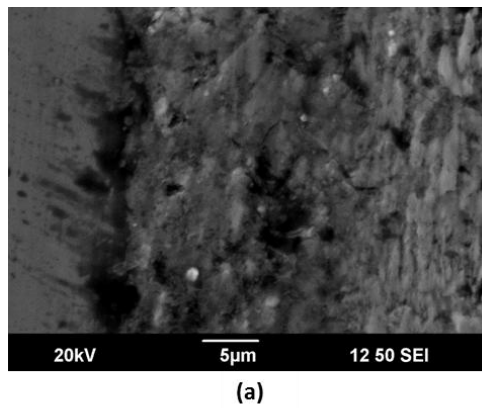
Figure 5–10 Element distribution on worn surface: (a) SEM morphology (b) distribution of Ce element; (c) distribution of O element; (d) distribution of Fe element

5.5.3 Discussion

Experimental results displayed in Figures 5–1 - 5–6 have demonstrated the friction reduction and anti-wear performance of CeO_2 nanoparticles as the lubricant additive in water. Dispersibility of solid lubricant additive in base media has been proven to be of great importance on the tribological performance. No noticeable contribution on a reduction of

102

friction was observed when CeO_2 nanoparticles alone were added in water, regardless of the variation of additive concentrations. However friction coefficient was effectively reduced when surfactant sorbitan monostearate was employed to enhance the dispersibility of CeO_2 nanoparticles in water. The improved dispersibility, indicated by the higher Zeta potential and the smaller conglomerate size of CeO_2 nanoparticles, was obtained with the application of Sorbitan monostearate.

With improved dispersibility, the influence of particle concentration on friction coefficient can be noticed. Containing 2wt% surfactant, the water based lubricant exhibited a greater reduction on friction coefficient with higher concentration of CeO_2 nanoparticles.

The anti-wear property of CeO_2 nanoparticles is independent with their friction performance. Although no reduction of friction was achieved by adding CeO_2 nanoparticle in water alone, considerable reduction on wear track depth was found without the application of surfactant Sorbitan monostearate.

SEM and EDS Analyses have clearly indicated that CeO_2 nanoparticles embedded on the worn surface after sliding contact. Based on the above observations, it is logical to suggest that the third body effect of CeO_2 nanoparticles is the dominant mechanism for their tribological performance in water. Under a friction force, CeO_2 nanoparticles are firstly entrapped and then deposited on to the contact interfaces due to shear effect. The CeO_2 nanoparticles between the contact surfaces can reduce direct metal contact and surface adhesion. Moreover deposition of CeO_2 can also fill up valleys on the surfaces, make up material loss and therefore, protect the contacting metal pairs.

5.6   Summary

In this chapter, the tribological properties of CeO_2 nanoparticles suspended in water with and without surfactant have been investigated. Base on the above test results, this chapter can be summarized as follow:

- The dispersibility of CeO_2 nanoparticles in water was improved by the employment of surfactant sorbitan monostearate. With surfactant, the average particle conglomerate size of 0.05wt% CeO_2 nanoparticles dispersed in water has been reduced from 193.7nm to 110nm. Measurement of the zeta-potential also confirmed the enhancement of the stability of suspension brought by surfactant.

- With the employment of surfactant sorbitan monostearate, CeO_2 nanoparticles in the water with improved dispersibility have demonstrated the considerable friction reduction performance. With 2wt% surfactant, the additive of 0.2wt% CeO_2 in water delivered a reduction on friction coefficient of up to 20%.

- Without surfactant, CeO_2 nanoparticles did not indicate any ability to reduce friction in the lubrication system. The agglomeration and sedimentation of ceria nanoparticles may be responsible for their poor lubricating property in water. However the anti-wear property of water was improved effectively when 0.05% and 0.1% CeO_2 nanoparticles were applied. A reduction of up to 49% on wear track depth was observed.

- Third body effect is the possible explanation for excellent anti-wear performance of the CeO_2 nanoparticles. Even when surfactant is not applied, a substantial anti-wear property was still demonstrated by the reduction of wear track depth of sample discs.

Chapter 6.   The Preparation and Tribological Properties of Surface Ceria Nanoparticles as a Lubricant Additive in Liquid Paraffin

6.1   Introduction

In this chapter Cerium dioxide (CeO_2) nanoparticles were studied as a lubricant additive in liquid paraffin and all experimental results as well as observations were presented. Oleic acid (OA) and Hexadecyltrimethoxysilane (HDTMOS) coupling agents were employed to modify CeO_2 nanoparticle surfaces in order to improve the dispersibility in base lubricant. The surface modifications of CeO_2 nanoparticles were successfully carried out and the chemical bondings between the nanoparticles and modification agents were verified by FTIR Spectrometer. The reduction in particle agglomeration size associated with the improved dispersibility of CeO_2 nanoparticles in organic solvent was measured with a Malvern Zetasizer. The tribological properties of the original and modified CeO_2 nanoparticles in liquid paraffin (LP) was evaluated and compared using a pin-on-disc tester. Worn surfaces were also examined by AFM and SEM equipped with EDS.

6.2   Surface modification of Cerium oxide nanoparticles

Surface modification techniques were employed in this part of the study to improve the stability of the solid lubricant additive in lubricant. Oleic acid (OA) and Hexadecyltrimethoxysilane (HDTMOS) were used as the surface modification agent The OA modified CeO_2 nanoparticles and HDTMOS modified CeO_2 nanoparticles were synthesized successfully in the following procedure. CeO_2 nanoparticles of 3 g were firstly dispersed in 40mL mixed solution of ethanol and water (volume ratio 1:1) using a high shear homogenizer at a rotary speed of 15K rpm for 10 minutes. A suitable amount of modifier (either OA or HDTMOS) dissolved in 10 mL of absolute alcohol was then added into the first dispersion

(mole ratio of CeO_2 nanoparticles to modifier is 10:1). Subsequently, the mixture was heated to 70°C and maintained at this temperature with vigorous stirring for 4 hours. Then, the suspension was centrifuged at a speed of 8000 rpm for 10 minutes and the white precipitate was collected. The obtained precipitate was rinsed with distilled water and ethanol alternately and centrifuged repeatedly in order to remove the excessive modifier. Finally the thoroughly washed precipitate was dried in a vacuum oven at 40°C for 6 hours and the surface modified CeO_2 were obtained.

6.2.1 Sample characterisation

The surface structure and morphology of the original and surface modified CeO_2 nanoparticles are shown in Figure 6–1. It is clear that both surface modified CeO_2 samples shared a similar particle size and morphology to the original CeO_2 nanoparticles shown in Figure 6–1(a). However, compared with the original and OA modified CeO_2 nanoparticles (Figure 6–1(a) and Figure 6–1(b)), less agglomeration was found in HDTMOS modified CeO_2 nanoparticles shown in Figure 6–1(c).
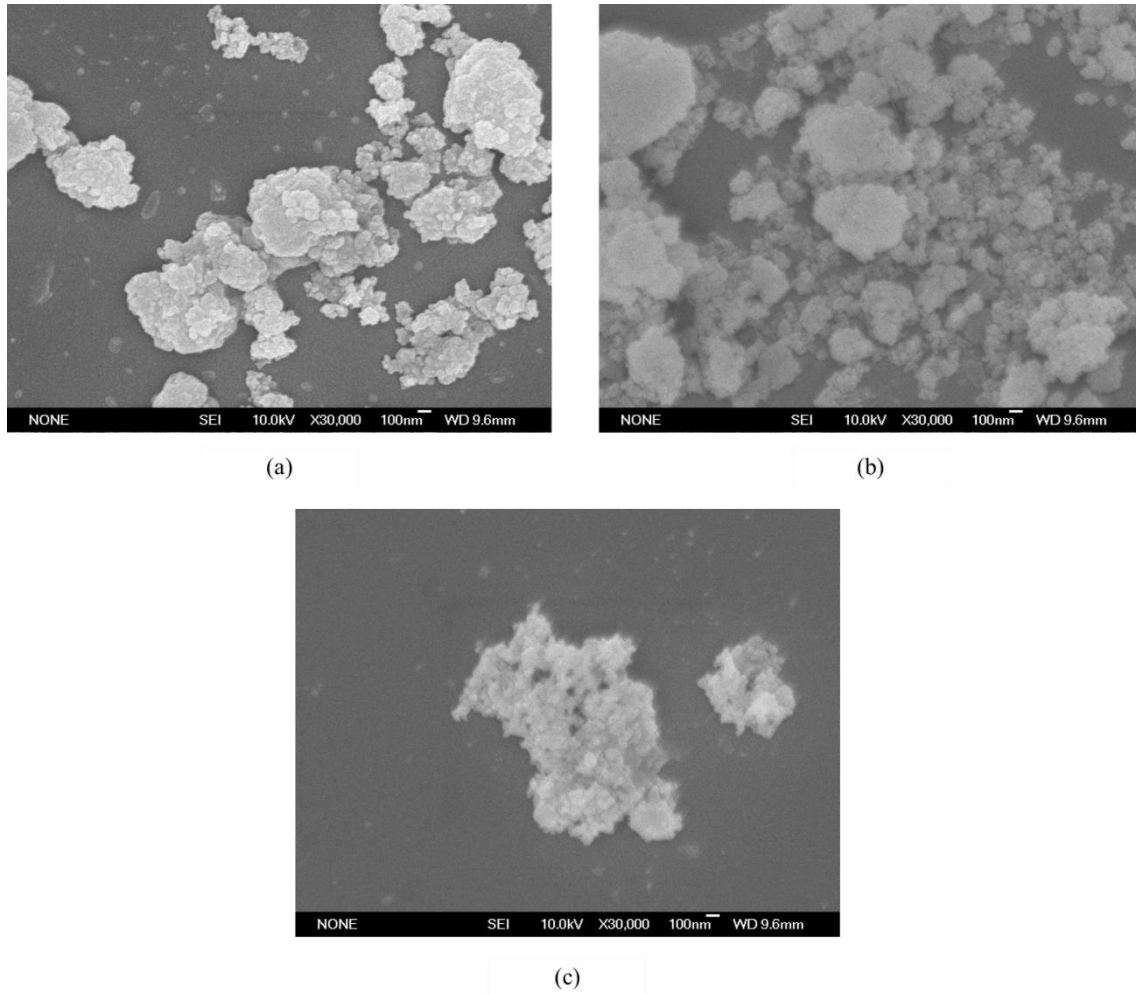
Figure 6–1 SEM micrographs of (a) the original CeO_2 nanoparticles, (b) OA
modified CeO_2 nanoparticles, (c) HDTMOS modified CeO_2 nanoparticles

Table 6-1 displays the conglomerate size and zeta-potential of the original and surface

modified CeO_2 nanoparticles in methanol. 0.05wt% samples were dispersed in methanol with

an ultrasonic homogeniser (KINEMATICA PT 10-35 GT) for 5 minutes. The average

conglomerate size of original CeO_2 nanoparticles measured in methanol was 1385nm in

diameter. Under the same condition, OA modified CeO_2 nanoparticles demonstrated a

smaller but still similar value of 1253nm in diameter. On the other hand, a considerable

reduction on the conglomeration size of HDTMOS modified CeO_2 nanoparticles to 540nm

was observed. Zeta-potential of the original CeO_2 nanoparticles dispersed in methanol was

measured to be 4.7 mV. In comparison, both OA modified CeO_2 nanoparticles and HDTMOS

modified CeO_2 nanoparticles demonstrated the higher values of 26.0mV and 38.6mV respectively. It is well known that surface charges of the particles caused by absorption of ions and molecules generate an electrostatic repulsion force between particles. This electrostatic repulsion force can partially counteract gravitation and reduce agglomeration and sedimentation of particles. The physical stability of a colloidal system can be determined by the balance between the repulsive and attractive forces that are described quantitatively by the Deryaguin–Landau–Verwey–Overbeek (DLVO) theory [158]. Therefore, a higher absolute value of zeta-potential of a suspension presents a better stability. The Zeta potential results from this study shown in Table 6-1 suggest that surface modifications using OA and HDTMOS have effectively improved the stability of CeO_2 nanoparticles in organic solvent. The highest zeta-potential value of HDTMOS modified CeO_2 nanoparticles also suggests that they have better stability than OA modified CeO_2 nanoparticles in methanol.

Table 6-1 Conglomerate size and Zeta-potential of CeO_2 nanoparticles
despersed in methanol

	Zinc borate ultrafine powders		
	Original	OA modified CeO_2 nanoparticles	HDTMOS modified CeO_2 nanoparticles
Conglomerate size (in methanol)	1385nm	1253nm	672nm
Zeta-potential	4.7 mV	26.0mV	38.6mV

The composition and structure of the OA modified CeO_2 nanoparticles and HDTMOS modified CeO_2 nanoparticles were characterised with FT-IR spectroscopy as shown in Figure 6–2. In the infrared spectrum of original CeO_2 nanoparticles shown in Figure 6–2(a), the

broad band at $3450 cm^{-1}$ is assigned to stretching of –OH, which suggests the presence of –OH groups on the surface of ceria particles and the existence superficial adsorbed water before modification. In the spectra of OA and HDTMOS displayed in Figure 6–2(b-c), two sharp peaks at 2923 and 2856 cm^{-1} are attributed to the asymmetric and symmetric $-CH_2$ stretching vibrations respectively. The same peaks were also be found in the spectra of OA modified CeO_2 nanoparticles and HDTMOS modified CeO_2 nanoparticles shown in Figure 6–2(d-e). It is evident that the positions of peaks for the distinctive functional groups observed in the spectra of OA modified CeO_2 nanoparticles and HDTMOS modified CeO_2 nanoparticles are identical with the pure modification agents of OA and HDTMOS. The infrared spectra result indicates that the surface of CeO_2 nanoparticles have been successfully modified with OA and HDTMOS.
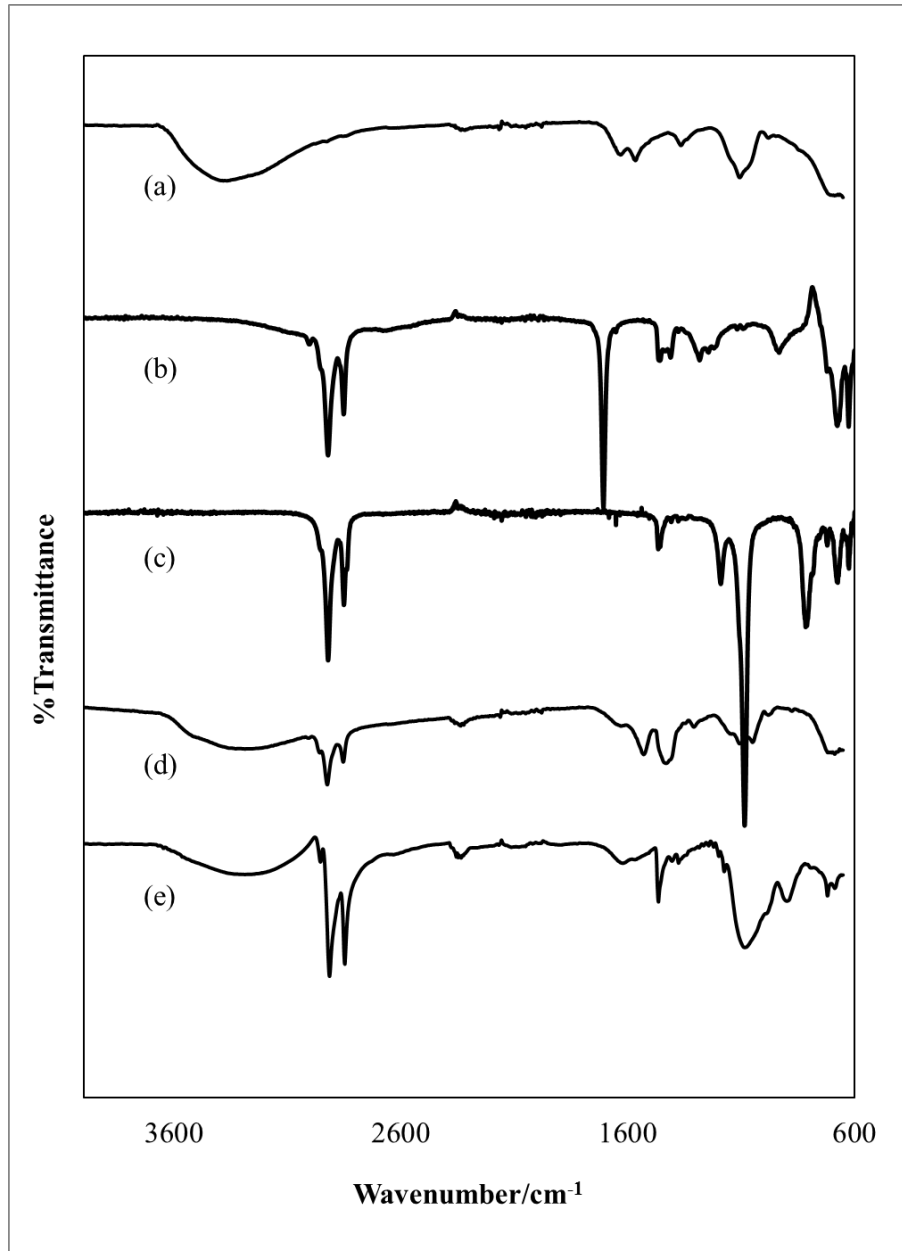
Figure 6–2 FT-IR spectra of (a) original CeO$_2$ nanoparticles, (b) OA, (c)
HDTMOS, (d) OA modified CeO$_2$ nanoparticles, (e) HDTMOS modified
CeO$_2$ nanoparticles

6.3   Preparation of lubricants

Due to the small particle size of the solid lubricant additives, an additive concentration of as

low as 0.5% can be considerably effective [80, 177]. In this study, a uniform concentration of

0.5% in weight fraction was applied for all friction and wear tests when the additive powders

were employed. Additives were dispersed in liquid paraffin (LP) with an ultrahigh shear homogenizer at the speed of 20k rpm for 20 minutes.

6.4   Pin-on-disc test conditions

The tribological properties of all lubricant samples were evaluated using a POD 2 pin-on-disc tester (Teer Coatings Ltd.). All the tests were carried out with a sliding speed of 50mm/s for a testing period of 60 minutes at the ambient temperature of 22°C. The test load was set to be 10N (1.54GPa Hertz pressure). Same bearing balls (pins) and disc samples as described in Chapter 5 were employed. Except that the thickness of the disc samples was reduced from the original 12mm to 3mm instead in order to meet the specification of the auto polishing device. Prior to each test, the disks were grounded and polished to a mirror finish and a uniform surface roughness Ra of 15nm was achieved. Before each test, both the pins (bearing balls) and the discs were cleaned with toluene in an ultrasonic water bath for five minutes to eliminate any potential grease on the surface, also a further cleaning with acetone was carried out for five minutes in the same way after this.

6.5   Experimental results

6.5.1   Friction coefficient

Friction coefficients of different lubricant samples are illustrated in Figure 6–3. Lubricant specimens with 0.5% HDTMOS modified CeO_2 nanoparticles have displayed the highest friction coefficient. Pure liquid paraffin (LP) delivered the lowest friction coefficient. Lubricant samples with HDTMOS and OA modified CeO_2 nanoparticles have displayed higher friction coefficient compared with pure LP. Highest friction coefficient was found when LP with HDTMOS modified CeO_2 nanoparticles were used as the lubricant. LP with original CeO_2 nanoparticles delivered the lowest friction coefficient. Among all lubricant

samples, pure LP demonstrated the most stable friction coefficient, whereas all lubricants that

contain CeO_2 nanoparticles presented higher level of fluctuations.
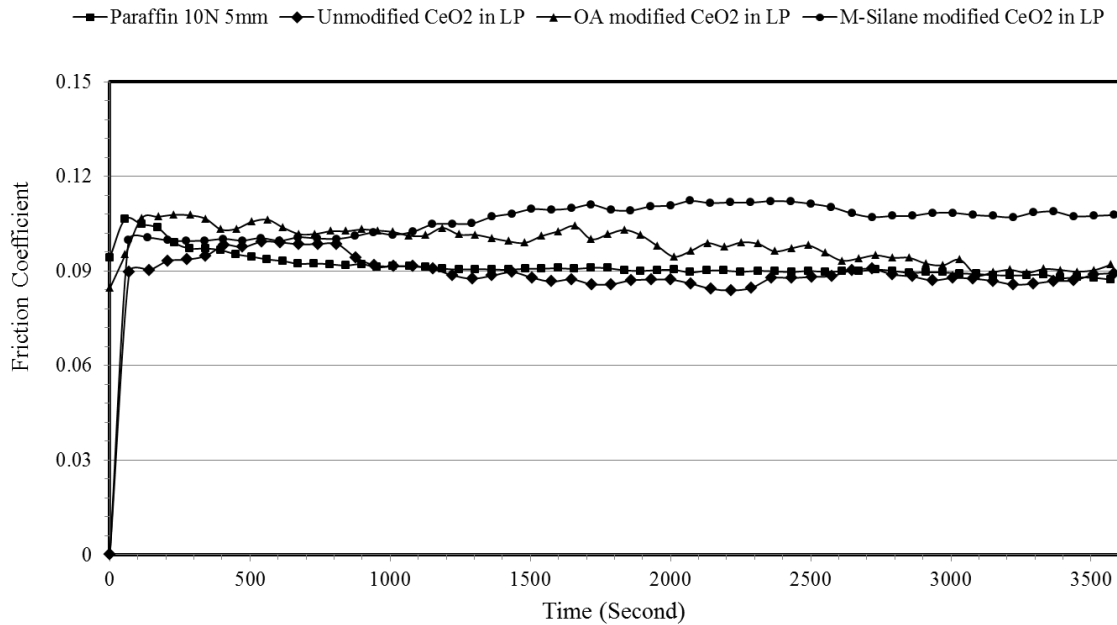
Figure 6–3 Effect of different lubricant additives on friction coefficient of LP

6.5.2 Anti-wear behaviour

Wear scar of the pins (bearing balls) used in pin-on-disc tests were firstly assessed using an

optical microscope. The morphology and wear scar diameter (WSD) of the tested pins are

shown in Figure 6–4. A smaller WSD implies a less material loss therefore the superior wear

resistance. It is evident that the applications of OA and HDTMOS modified CeO_2

nanoparticles as lubricant additives in LP have effectively reduced the WSDs of the pins

(bearing balls). Particularly, a WSD as small as 136 μm was obtained when LP with

HDTMOS modified CeO_2 nanoparticles was used as a lubricant, which is about 40% smaller

than the wear scar obtained when the LP with OA-ZB UFPs was applied, and more than 45%

smaller than that generated by pure LP. Quite the reverse, without surface modification of the

solid lubricant additive, LP with original CeO_2 nanoparticles delivered the biggest WSD of

284µm. A uniform and tenacious tribo-film was found on the wear scar lubricated with LP with HDTMOS modified CeO_2 nanoparticles, as shown in Figure 6–4(d). The formation of this tribo-film appears to have played an important role in the outstanding anti-wear performance.

Wear losses of the pins lubricated by different lubricant samples were also illustrated in Figure 6–5. The wear loss volume was calculated geometrically based on the assumption that wear scar is a flat surface. As shown in Figure 6–5, wear loss of the upper pin lubricated by LP with 0.5% HDTMOS modified CeO_2 nanoparticles is more than 11 times smaller than that lubricated by pure LP.
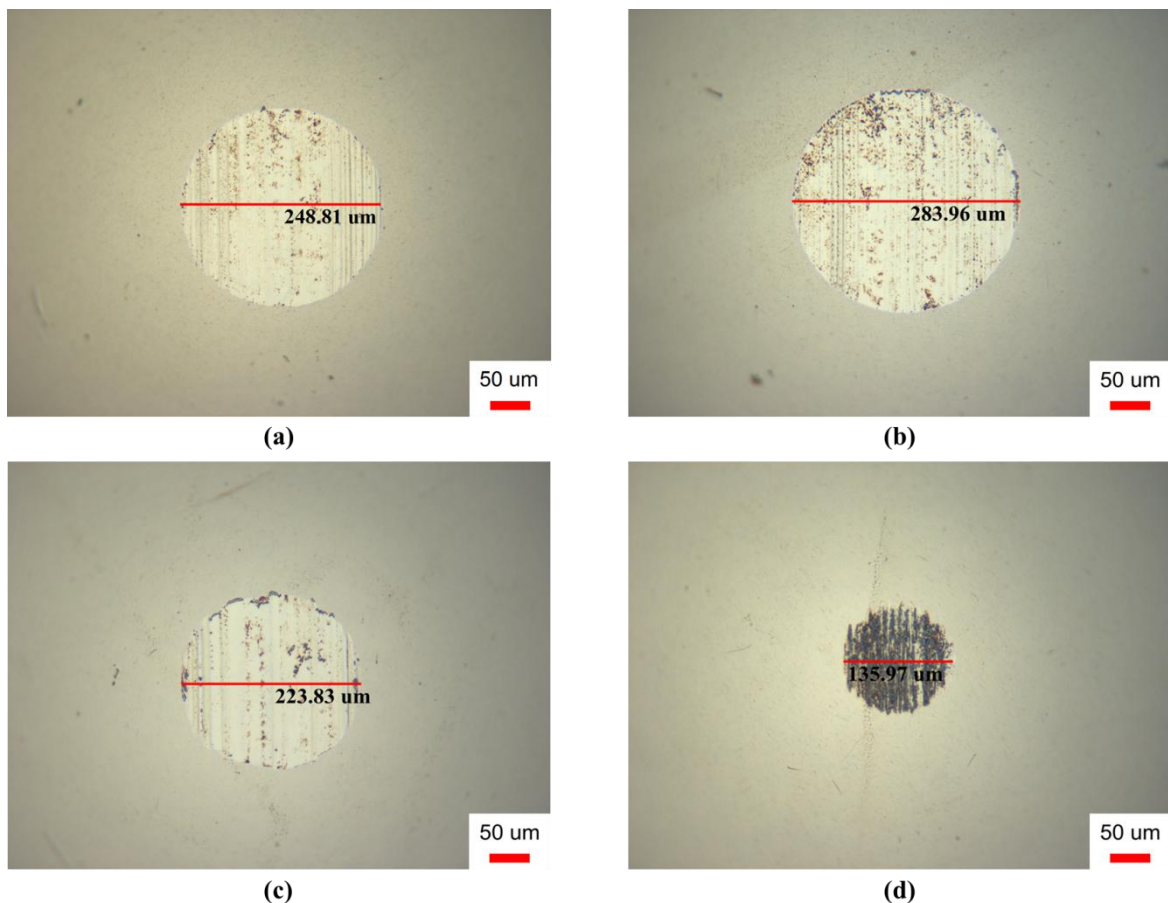
Figure 6–4 Optical micrographs of wear scars lubricated using: (a) LP, (b) LP with CeO_2 nanoparticles, (c) LP with OA modified CeO_2 nanoparticles (d) LP with HDTMOS modified CeO_2 nanoparticles

113
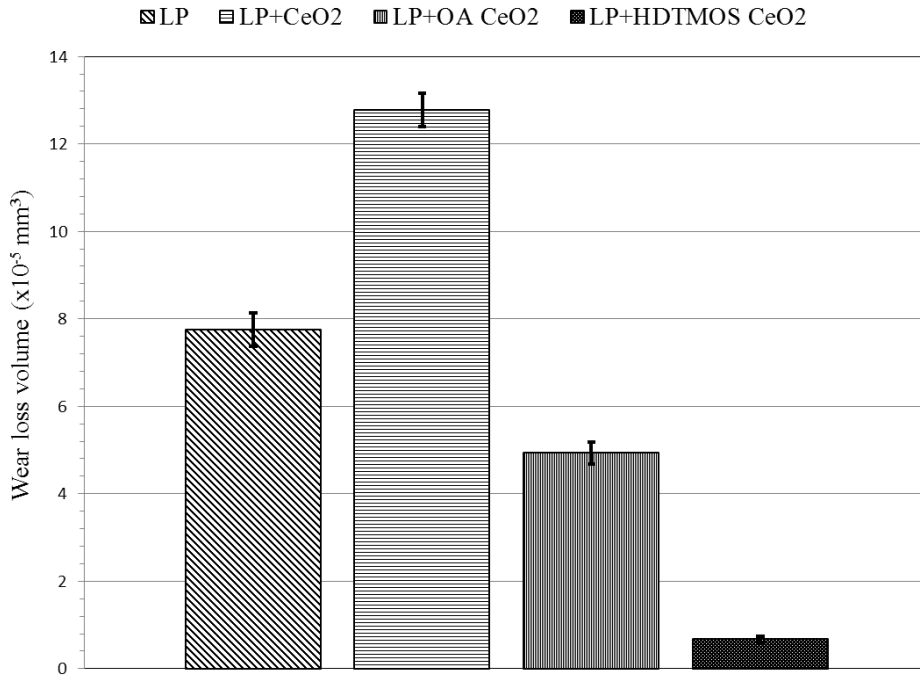
Figure 6–5 Effect of different lubricant additives on wear loss volume of the bearing balls

6.6 Interpretation and discussion of the results

6.6.1 Characterisation of the worn surfaces

Wear scars of the pins used in the pin-on-disc tests were observed using optical microscopy and scanning electron microscopy (SEM). Wear scar diameter of the pins were measured to the accuracy of 1µm. The topography of the wear scar surface was studied with atomic force microscopy (AFM).

Energy dispersive X-ray spectroscopy (EDS) were conducted to examine the chemical features and elemental composition of the tribo-film generated on the worn surfaces of the pin. Mechanical properties of the tribo-film were determined with the Nano indentation facility. A Berkovich indenter with a tip diameter of 50nm was employed throughout the experiment. For all indentation tests, a constant maximum indentation depth of 110nm was applied with the loading/unloading duration of 15 seconds in order to avoid the effect of

substrate on the measured properties of tribo-film, and the initial load was set to be 0.05mN to minimise any initial damage to the surface. Distance between each indent was not less than 15μm in order to avoid any possible interference between neighbouring indents.

6.6.1.1 Physical and mechanical properties

Figure 6–6(a) shows a magnified optical photo of the wear scar lubricated by LP with 0.5% HDTMOS modified CeO_2 nanoparticles. Figure 6–6(b-c) present the AFM images of tribo-film generated on wear scar surface as indicated in Figure 6–6(a). It appears that a tribo-film has a good coverage but is not entirely even distributed was observed. The average thickness of the tribo-film is measured to be around 190nm (see Figure A–1 in Appendix–2). The mechanical property of the tribo-film has been measured with nano-indentation. Indentations were made on both the tribo-film and the substrate. Corresponding load–depth curves are illustrated in Figure 6–7. Mechanical properties of the worn surface on the tested bearing balls were derived from further analysing the load–depth curves. The maximum indentation depth was set to be 110nm which is less than the thickness of the tribo-film. Although at this condition the mechanical properties of the tribo-film measured will receive some interference contributed by the substrate, the surface hardness and reduced modulus derived from this load-depth curve were only treated as the relative properties of the tribo-film in comparison with the substrate, and therefore the interference from the substrate will not affect the overall conclusions. In order to reach pre-set indentation depth, the indentation force required on tribo-film was 2.97mN (curve (b) in Figure 6–7), whereas under the same test conditions the indentation force required on substrate steel was 4.75 mN (curve (a) in Figure 6–7). A comparison of the surface hardness and reduced modulus of the tribo-film with those of the substrate steel is presented in Table 6-2. The test results suggest that the tribo-film is made of a softer material with lower stiffness compared with the substrate steel.

(a)

(b)

(c)
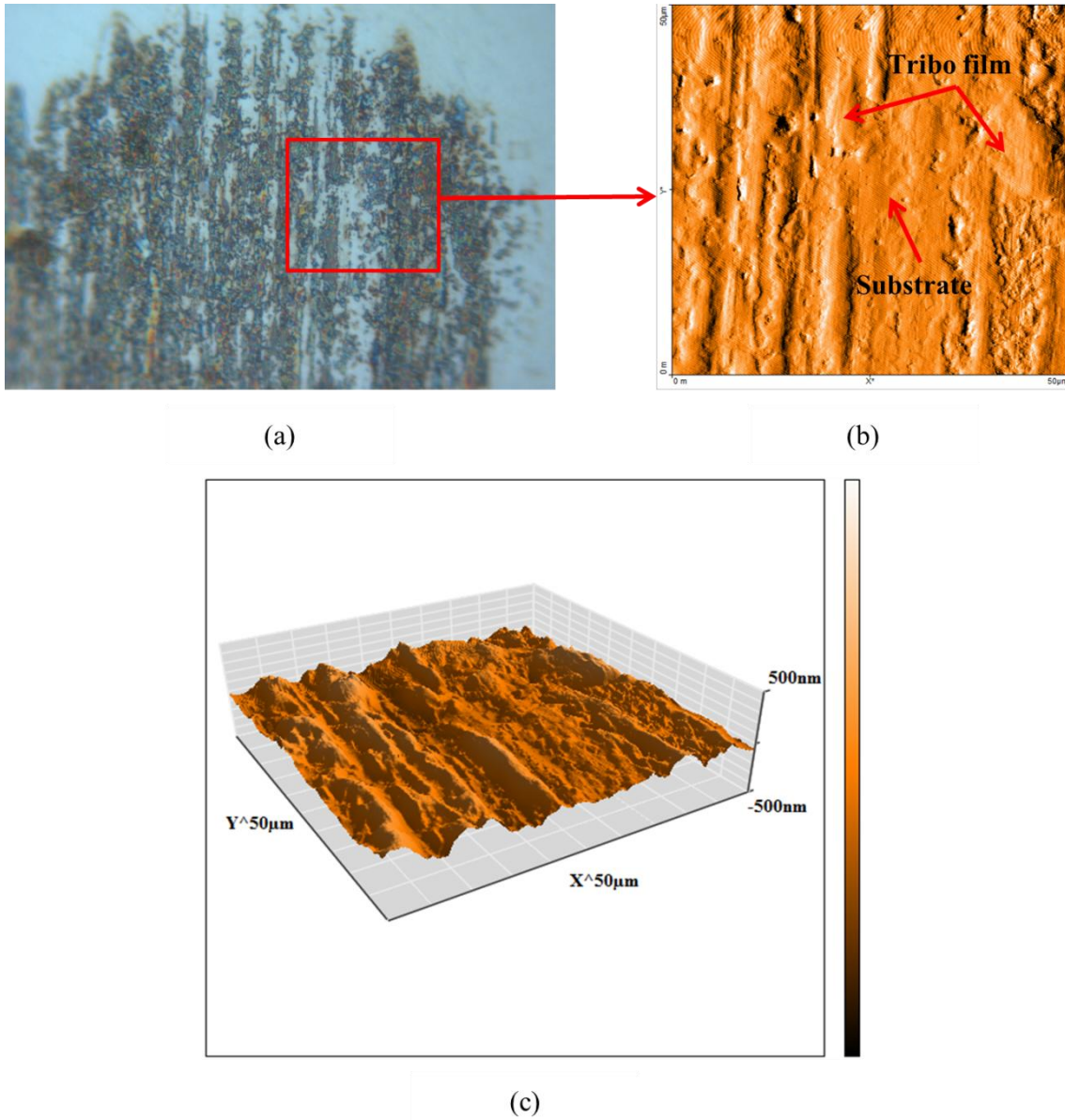
Figure 6–6 Morphologies of the tribo-film generated by LP with HDTMOS modified CeO_2 nanoparticles: (a) optical image, (b) AFM surface topographic image, (c) 3D AFM surface topographic image
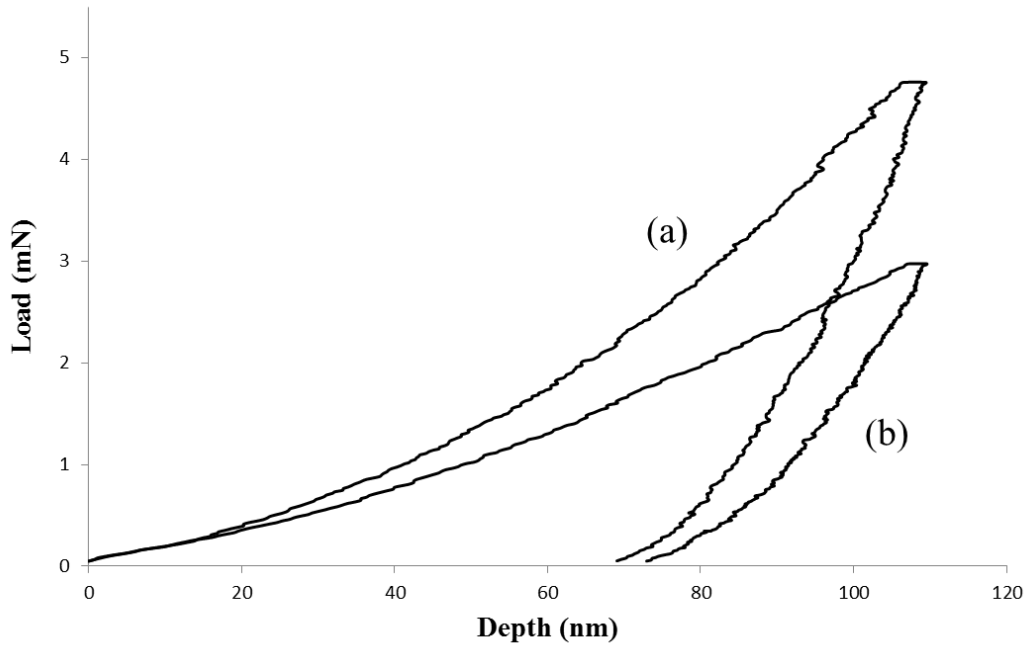
Figure 6–7 Inentation curves obtained at different domains on the worn
surface lubricated by LP with HDTMOS modified CeO$_2$ nanoparticles: (a)
on substrate, (b) on tribo-film

Table 6-2 A comparison of mechanical properties of the tribo-film and the
substrate

Indentation position	Indentation force	Hardness	Reduced modulus
Tribo-film	2.97mN	8.3GPa	186GPa
Substrate	4.75mN	13.2GPa	304GPa

Figure 6–8 shows the AFM morphologies of the worn surfaces of the pins lubricated with
different lubricant samples. Changes on the size and profile of the tribo-films were
discovered when different lubricant samples were used. When pure LP was used as the
lubricant as shown in Figure 6–8(a-b), no complete tribo-film but only small patchy pieces
were found scattering over the worn surface and some ploughings can also be seen clearly.
Similar phenomenon was also observed when LP with the original CeO$_2$ nanoparticles was
employed; very fine fragments of tribo-film can be seen spreading over the examined area.as
shown in Figure 6–8(c-d). Heavy ploughings also took place on the worn surface lubricated

117

by LP with the original CeO_2 nanoparticles, which suggests the abrasion effect contributed by the additional CeO_2 nanoparticles. The tribo-film generated on the wear scar lubricated by LP with OA modified CeO_2 nanoparticles, as shown in Figure 6–8(e-f), has a bigger fragment size and elongated shape stretching along the direction of sliding. Among all the worn surfaces, surface lubricated by LP with HDTMOS modified CeO_2 nanoparticles has the most widespread and tenacious tribo-film. Almost the whole scanned surface is covered with the tribo-film although the thickness of the tribo-film is not entirely uniform across the area as shown in Figure 6–8(h). It can be suggested that an employment of HDTMOS modified CeO_2 nanoparticles in LP enables to generate a more complete and durable tribo-film on the contact surface and this tribo-film can effectively protect the surface from wear damage.
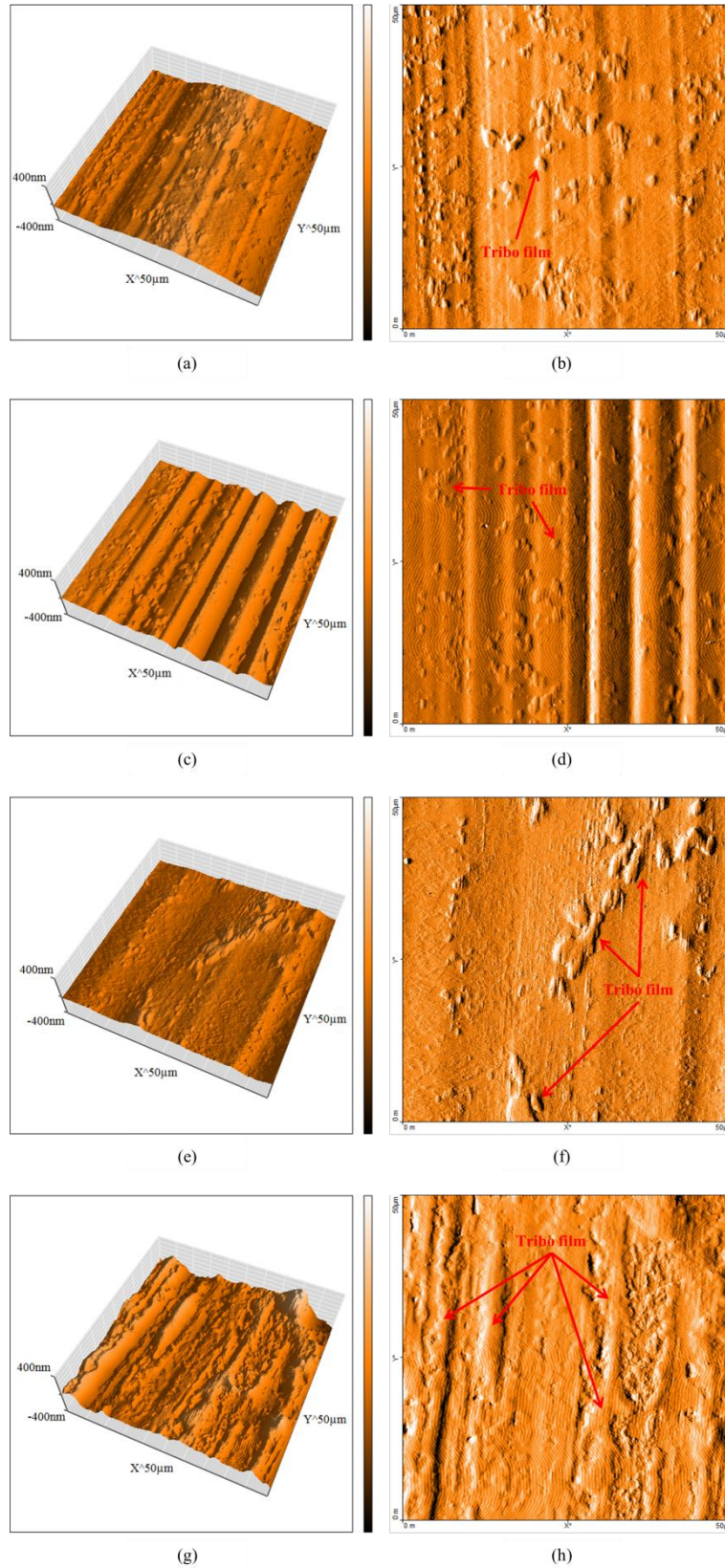
Figure 6–8 AFM surface topographic images of the worn surfaces lubricated
with different lubricants: (a, b) LP, (c, d) LP with CeO_2 nanoparticles, (e, f)
LP with OA modified CeO_2 nanoparticles, (g, h) LP with HDTMOS
modified CeO_2 nanoparticles

6.6.1.2 SEM micrographs and EDS analysis

The worn surfaces lubricated by LP with 0.5% HDTMOS modified CeO_2 nanoparticles were analysed under a scanning electronic microscope (SEM) equipped with energy dispersive X-ray spectroscopy (EDS). Typical SEM images and EDS analyses are shown in Figure 6–9. Distinctive topographical differences of the tribo-film and substrate can be seen clearly. The tribo-film displayed in Figure 6–9(a) appears in dark colour with a complex topography which makes a good contrast with the substrate displayed in brighter colour with smoother surface texture. The EDS patterns of the region highlighted on the tribo-film and the substrate are shown in Figure 6–9(d) and Figure 6–9(e) accordingly. Quantified elemental analysis results are given in Table 6-3. A considerable increase of Oxygen and Silicon contents was found on the tribo-film, compared with the element distribution on the substrate. The further amount of Oxygen and Silicon is possibly derived from Hexadecyltrimethoxysilane (HDTMOS). It is evident that HDTMOS modification agent is an important ingredient of the formation of the tribo-film. Cerium element from CeO_2 nanoparticles was detected neither on the substrate nor on the tribo film, which suggests that CeO_2 nanoparticles did not chemically contribute to the formation of tribo film. However at the same time the employment of CeO_2 nanoparticles is an essential factor to produce a tenacious and continuous tribo film with a good coverage on worn surface. Based on the test results obtained, a hypothesis can be made that although CeO_2 nanoparticles are not chemically involved in the tribochemical reaction carried out on the worn surface during sliding process, they played a role as a physical carrier to effectively deliver the HDTMOS surfactant to contact surfaces. Due to the small particle size, the HDTMOS modified CeO_2 nanoparticles can be easily entrapped into contact interface by shear effect [7]. Finally , the HDTMOS modified CeO_2 nanoparticles deposit on the worn surface result in a high concentration (localised) of HDTMOS surfactant on the worn surface. Spontaneously, tribochemical reactions take place during a sliding process due

to the local high pressure and flash temperature caused by the collision and rupture of the

asperities between the mating surfaces, and HDTMOS surfactant turns into a key ingredient

for a healthy tribo film.
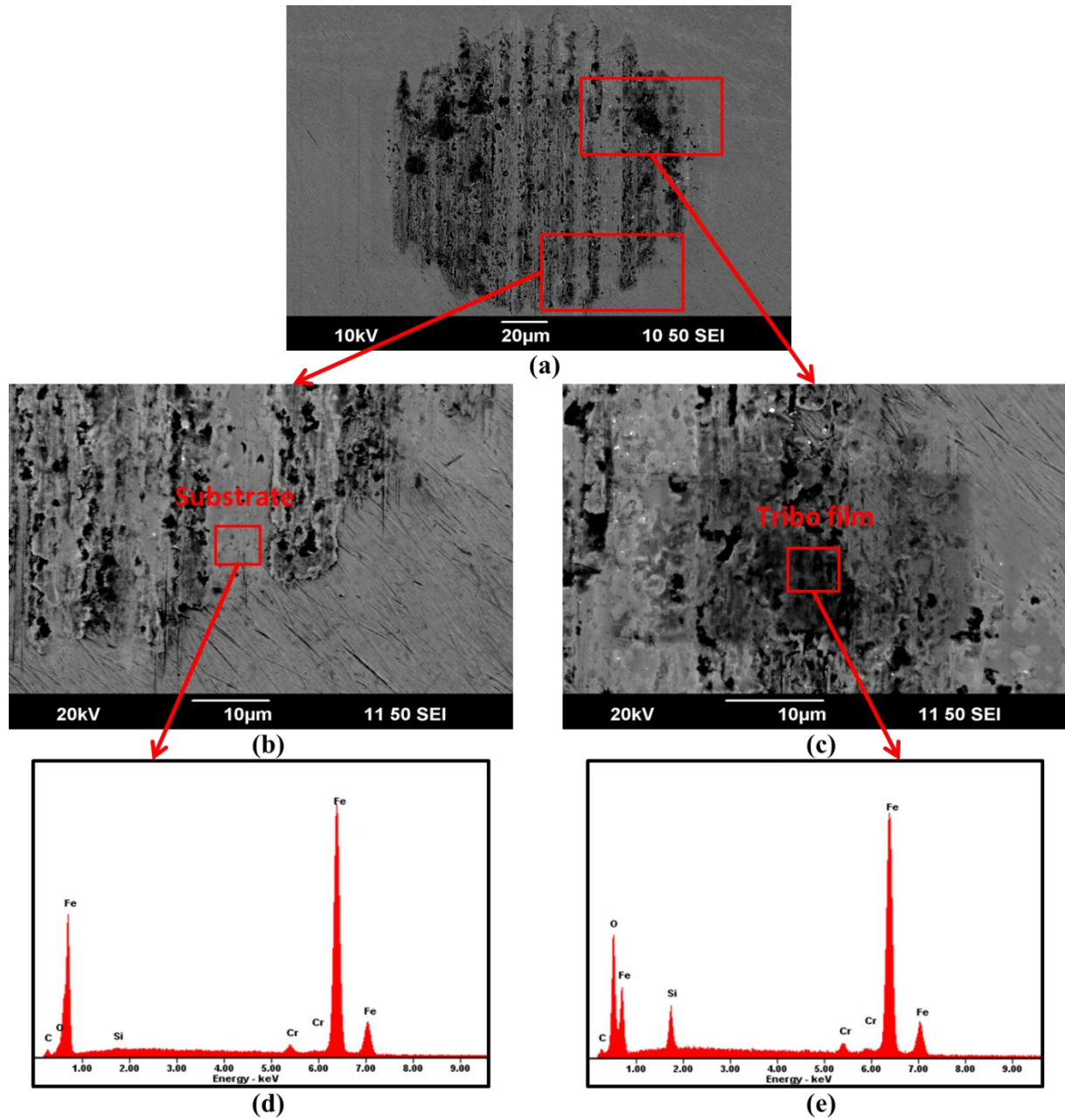
Figure 6–9 SEM images and EDS patterns of worn surfaces lubricated with
LP with HDTMOS modified CeO$_2$ nanoparticles: (a) worn surface
morphology, (b, c) magnified SEM image, (d) EDS patterns of the substrate,
(e) EDS patterns of the tribo-film

Table 6-3 Quantified elemental analysis on worn surface shown in Figure 6-9

Element	Spectrum (d) (At%)	Spectrum (e) (At%)
C	20.56	16.28
O	6.83	35.12
Si	0.50	5.22
Cr	1.36	1.08
Fe	70.76	42.31

6.6.2 Discussion

Based on the experimental results, it is clear that surface modified CeO_2 nanoparticles have demonstrated much better tribological properties as lubricant additives in LP than the original CeO_2 nanoparticles. HDTMOS modified CeO_2 nanoparticles have revealed a superior anti-wear property to OA modified CeO_2 nanoparticles. At the beginning of a pin-on-disc sliding test, direct metal contact and adhesion were reduced by the third body effect of CeO_2 nanoparticles, as the particles were entrapped into contact area as a result of friction force [7]. This is possible reason for the reduced initial friction coefficients of all lubricant samples that contain CeO_2 nanoparticles, as shown in Figure 6–3.

As the sliding continues, ploughings take place and debris is also produced. A tribo-film is formed on the contact surfaces as a result of interaction between chemical components of the lubricant with the lubricated surface. The formation of tribo-film is associated with the decrease of wear. At all times the high wear loss was associated with small and patchy tribo-film fragments observed on the worn surface. On the contrary, the low wear loss was obtained when more complete tribo-films were formed. The test results suggest that the formation of tribo-film is greatly influenced by the surface modification conducted on CeO_2 nanoparticles. Original CeO_2 nanoparticles may agglomerate in base lubricant and form clusters with big particle size. These clusters may sometime behave like abrasive particles,

which will encourage the generation of debris and destruction of tribo-film and eventually increase wear. As a result, the original CeO_2 nanoparticles demonstrated the highest wear loss due to its poor dispersibility in LP and the resultant abrasive effect.

Due to the formation of a complete and tenacious tribo-film with a lower hardness and reduced modulus than substrate steel, the best anti-wear performance was delivered when the HDTMOS modified CeO_2 nanoparticles were employed as the lubricant additive in LP. This outstanding anti-wear performance is very much coincide with *the delamination theory of wear* [105]. It is well understood that at the initial stage of sliding, wear occurs as the fatigue fracture of the deformed original asperities. This is then followed by a regime in which the wear loss is dominated by material delamination. For a homogeneous material the dislocations pile up beneath the surface layer, subsequently subsurface cracks nucleation and propagation take place when the critical shear stress is reached [185]. When the cracks reach a critical length and finally propagate to the surface, delamination (wear loss) begins. However, when a thin layer of tribo-film with low hardness and reduced modulus is generated on the hard substrate, dislocations will pile up at the interface between the tribo-film and the substrate. As the sliding continues, these dislocations escape through the surface of the tribo-film due to its very small thickness [186]. On a surface without tribo-film, dislocations will be transferred and generated within the substrate material as a result of very high stresses. On the other hand, the transfer of dislocations from tribo-film to substrate metal will be considerably less owing to the lower tangential force transmitted. Therefore the wear of material protected by tribo-film will be remarkably reduced or delayed.

EDS analysis showed that there were considerable amount Silicon content in the tribo-film, but no Cerium element could be detected. This suggests that the HDTMOS modification agent is a critical component for the formation of a robust tribo-film, but conversely CeO_2

nanoparticles were not chemically involved in the tribochemical reaction carried out on the worn surface during the sliding process.

The stability of additive particles in base oil also plays an important role in the formation of tribo-film. Compared with original CeO_2 nanoparticles, OA modified CeO_2 nanoparticles have better stability in LP although the particle size does not appear to be dramatically reduced. The HDTMOS modified CeO_2 nanoparticles have demonstrated the best stability and the smallest conglomerate size in organic solvent. It can be suggested that HDTMOS modified CeO_2 nanoparticles may have a better integration with base oil and easier access to the contact interface.

6.7   Summary

In this chapter, the tribological properties of the surface modified CeO_2 nanoparticles employed as lubricant additives in liquid paraffin (LP) were investigated. Base on the test results demonstrated in this chapter, it can be summarised that:

- Oleic acid (OA) and hexadecyltrimethoxysilane (HDTMOS) modified CeO_2 nanoparticles were successfully prepared. Without surface modification, the original CeO_2 nanoparticles did not demonstrate any noticeable friction reduction and anti-wear performance.

- The modified CeO_2 nanoparticles as lubricant additives in LP displayed much greater anti-wear performance than LP and LP with the unmodified CeO_2 nanoparticles. Compared with the OA modified CeO_2 nanoparticles, the HDTMOS modified CeO_2 nanoparticles demonstrated much greater improvement on anti-wear property when they were used in LP, and they also exhibited better stability and smaller conglomerate size in organic solvent.

- The outstanding anti-wear performance of the HDTMOS modified CeO_2 nanoparticles can be attributed to the formation of a complete and tenacious tribo-film on worn surface. Modification agent HDTMOS is a crucial ingredient for the formation of the tribo-film which has a smaller hardness and reduced modulus than the substrate material.

- The changes on the size and profile of the tribo-films were discovered when different lubricant samples were employed. It is evident that the coverage of the tribo-films on the worn surfaces has a good consistence with intensity of wear. A good coverage of tribo-film can protect the surface from wear effectively. Only small patchy pieces of film were found on the worn surfaces lubricated by LP and LP with the original CeO_2 nanoparticles. Tribo film with larger fragment size was observed on the worn surface when LP with the OA modified CeO_2 nanoparticles was used. The best coverage by tribo-film was achieved by using LP with the HDTMOS modified CeO_2 nanoparticles as the lubricant.

Chapter 7. The Tribological Properties of Zinc Borate Ultrafine Powders as a Lubricant Additive in Sunflower Oil

7.1 Introduction

In recent years, many interests have also been put on the application of borate nanoparticles as solid lubricant additive. Particularly, tribological properties of titanium borate [115], ferrous borate, magnesium borate [49] and zinc borate [89] nanoparticles together with dispersing agent sorbitan monostearate have been investigated, and the outstanding lubricating performances were observed. However the expensive and complicated preparation process of nanoparticles hinders their mass application. Compared with nanoparticles, submicron sized particles have won their attention in industrial application due to relatively low cost and simple preparation process. In this chapter, a concept of "green" lubricant was investigated, friction reduction and anti-wear properties of decomposable sunflower oil with lubricant additive zinc borate ultrafine powders (ZB UFPs) were studied using pin-on-disc tribo tester. The morphology and mechanical properties of worn surface as well as the tribo film generated on the surface were analysed using scanning electron microscopy (SEM), atomic force microscopy (AFM) and Nano-indentation facility.

7.2 Preparation of lubricants

Based on literature study, the optimal concentration of the solid lubricant additives is often between 0.5% to 2% [80, 139, 149, 187]. In this chapter, uniform and stable suspensions with three additive concentrations in weight ratio of 0.5%, 1% and 2% were prepared using an ultrasonic homogenizer for two minutes. The sample code and composition are presented in Table 7-1

Table 7-1 Sample code and composition

Sample code	Constituent
SF	Sunflower oil
SF + 0.5% ZB UFPs	Sunflower oil with 0.5 wt% zinc borate ultrafine powders
SF + 1% ZB UFPs	Sunflower oil with 1 wt% zinc borate ultrafine powders
SF + 2% ZB UFPs	Sunflower oil with 2 wt% zinc borate ultrafine powders

7.3   Pin-on-disc test conditions

The friction reduction property of the ZB UFPs in sunflower oil was evaluated using a POD 2 pin-on-disc tester (Teer Coatings Ltd.). All the tests were carried out with a sliding speed of 50mm/s for 30 minutes under 50N load (2.63GPa Hertz pressure) at the ambient temperature of 22°C. The bearing balls (pins) and sample discs were prepared with the same specifications as described in Chapter 6. Both bearing balls and discs were cleaned with acetone in an ultrasonic water bath for five minutes before each test.

7.4   Experimental results

7.4.1   Friction reduction property

Friction coefficients of sunflower oil with various additive concentrations are illustrated in Figure 7–1. The typical friction coefficient curve pattern of boundary lubrication, that has an initial temporary rise in friction caused by the original roughness or adhesion of the surface is quickly replaced by a drop in friction due to the reduction of adhesion friction or surface

conformity, was demonstrated by all lubricant samples. The highest rise in friction coefficient at the very beginning of the pin-on-disc tests was delivered by pure sunflower oil (SF). While the lubricants that contain ZB UFPs all showed lower friction coefficient values on that point. As sliding continued, the friction coefficients of SF, SF + 0.5% ZB UFPs and SF + 1% ZB UFPs were finally stabilized. However, for SF + 0.1% ZB UFPs, the descending of friction coefficient did not last long, the friction coefficient gradually climbed back up after 400 seconds. Among all the lubricant samples, the highest fluctuations in the friction coefficient were observed when SF + 2% ZB UFPs was used.

It can be seen in Figure 7–1 that pure sunflower oil exhibited the highest friction coefficient when tested using the pin-on-disc tester. SF + 0.5% ZB UFPs delivered the best friction reduction performance. Compared with using pure sunflower oil, more than 13% reduction on friction coefficient was observed by adding 0.5% ZB UFPs. SF + 1% ZB UFPs demonstrated the similar level of friction reduction to sunflower oil with 0.5% additive. When SF + 1% ZB UFPs was used as lubricant, the same friction reduction tendency was found in the first 380 seconds, and then friction coefficient gradually increased to the similar level to that when pure sunflower oil was used. Further increasing concentration of ZB UFPs to 2% did not yield any extra improvement; on the contrary, both an increase of friction coefficient and an unstable lubricating performance were obtained.
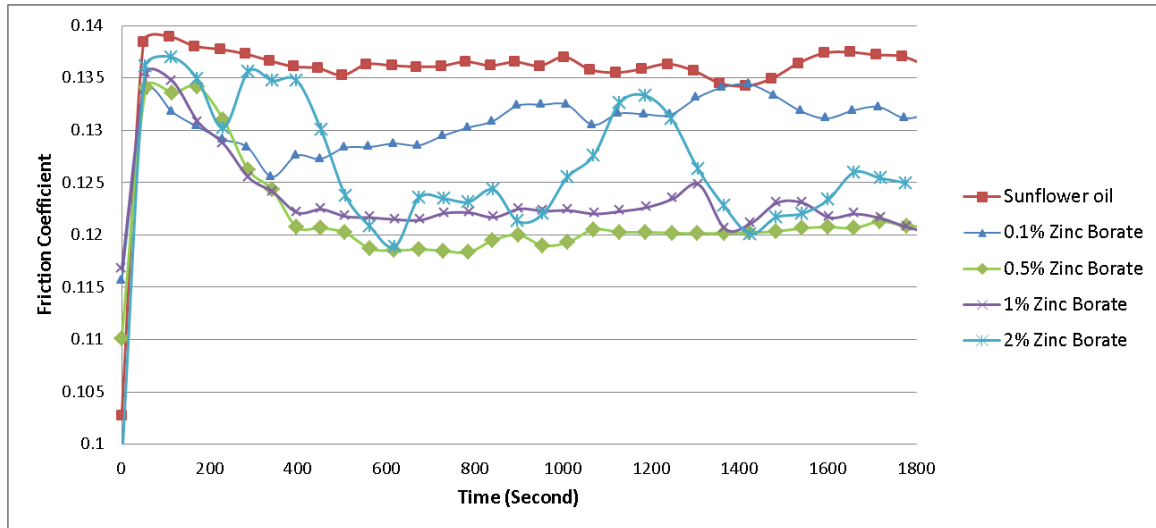
Figure 7–1 Friction coefficient as a function of testing duration

7.5 Interpretation and discussion of the results

7.5.1 Characterisation of the worn surfaces

The morphology and the elemental distribution on the wear track of the tested sample discs were studied using an optical microscope and a scanning electron microscope (SEM) equipped with energy dispersive spectra (EDS). Atomic force microscopy (AFM) was employed to characterise the tribo films generated on the worn surface.

Mechanical properties of the worn surfaces were determined using the Nano-indentation facility. The same testing parameters mentioned in Chapter 6 were applied.

7.5.1.1 Morphology analyses of the worn surfaces

Wear tracks on AISI 52100 steel discs resulted from pin-on-disc tests were firstly assessed using an optical microscope. As shown in Figure 7–2, tribo-films appeared in dark colour can be observed on all the wear tracks of the discs. They demonstrate a clear contrast to substrate materials appeared in bright colour. A clear change of the morphology on the worn surfaces was observed when different concentrations of ZB UFPs were applied. Wear tracks (*b*) and (*c*)

129

in Figure 7–2 were produced using sunflower oil containing 0.5% and 1% ZB UFPs respectively. Compared with wear track (*a*), which was lubricated by pure sunflower oil, much less dark areas (tribo-films) can be found on tracks (*b*) and (*c*). A great amount of dark areas (tribo-films) were also observed on track (*d*) which is lubricated using SF + 2% ZB UFPs. It is evident that the appearance of dark area (tribo-films) is in coincidence with an increase of friction coefficient.
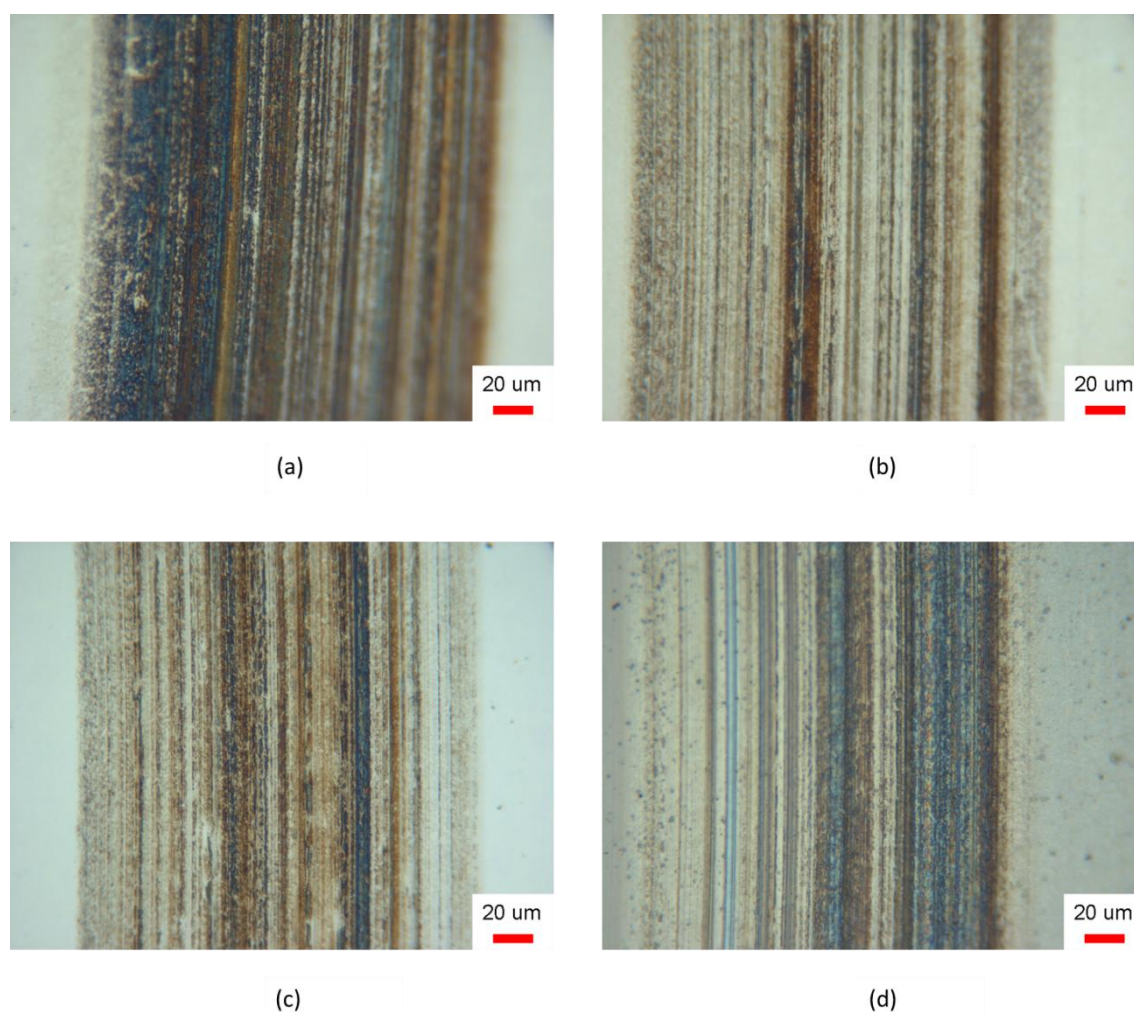
Figure 7–2. Optical micrographs of wear tracks on the discs lubricated using:
(a) pure SF (b) SF + 0.5% ZB UFPs (c) SF + 1% ZB UFPs (d) SF + 2% ZB
UFPs

Figure 7–3 shows the AFM morphologies of the tribo-films (dark area) generated on the wear tracks lubricated with different lubricant samples. The changes on the size and shape of the

tribo-films were discovered when different lubricants were used. The tribo-films generated on the worn surface lubricated with pure sunflower oil, as shown in Figure 7–3(a-b), have a relatively big fragment size and the measured thickness of the tribo-films was around 800nm (see Figure A–2 in Appendix-2). When SF + 0.5% ZB UFPs was used as the lubricant as shown in Figure 7–3(c-d), the tribo-films discovered on the worn surface established a reduced fragment size and small patchy pieces of tribo-films with irregular and stretched shapes were found scattering over the worn surface. The thickness of the measured tribo-films was around 230nm (see Figure A–3 in Appendix–2). As shown in Figure 7–3(c-d), more homogenous and evenly spread tribo-films were found when SF + 1% ZB UFPs was employed as the lubricant. The tribo-films have a thickness of around 280nm (see Figure A–4 in Appendix–2), which is similar to the one generated by SF + 0.5% ZB UFPs. The tribo-films generated by SF + 2% ZB UFPs, as shown in Figure 7–3(e-f), also have considerably bigger fragment size compared with the tribo-films generated by SF + 0.5% ZB UFPs and SF + 1% ZB UFPs. The thickness of the tribo-films around 360nm was recorded (see Figure A–5 in Appendix–2). It is evident that, to the tribo-films generated by sunflower oil containing ZB UFPs, the growths of the fragment size and thickness of the tribo-films were consistent with an increase of the zinc borate additive concentration in the lubricant base oil.

(a)

(b)

(c)

(d)

(e)

(f)

(g)

(h)
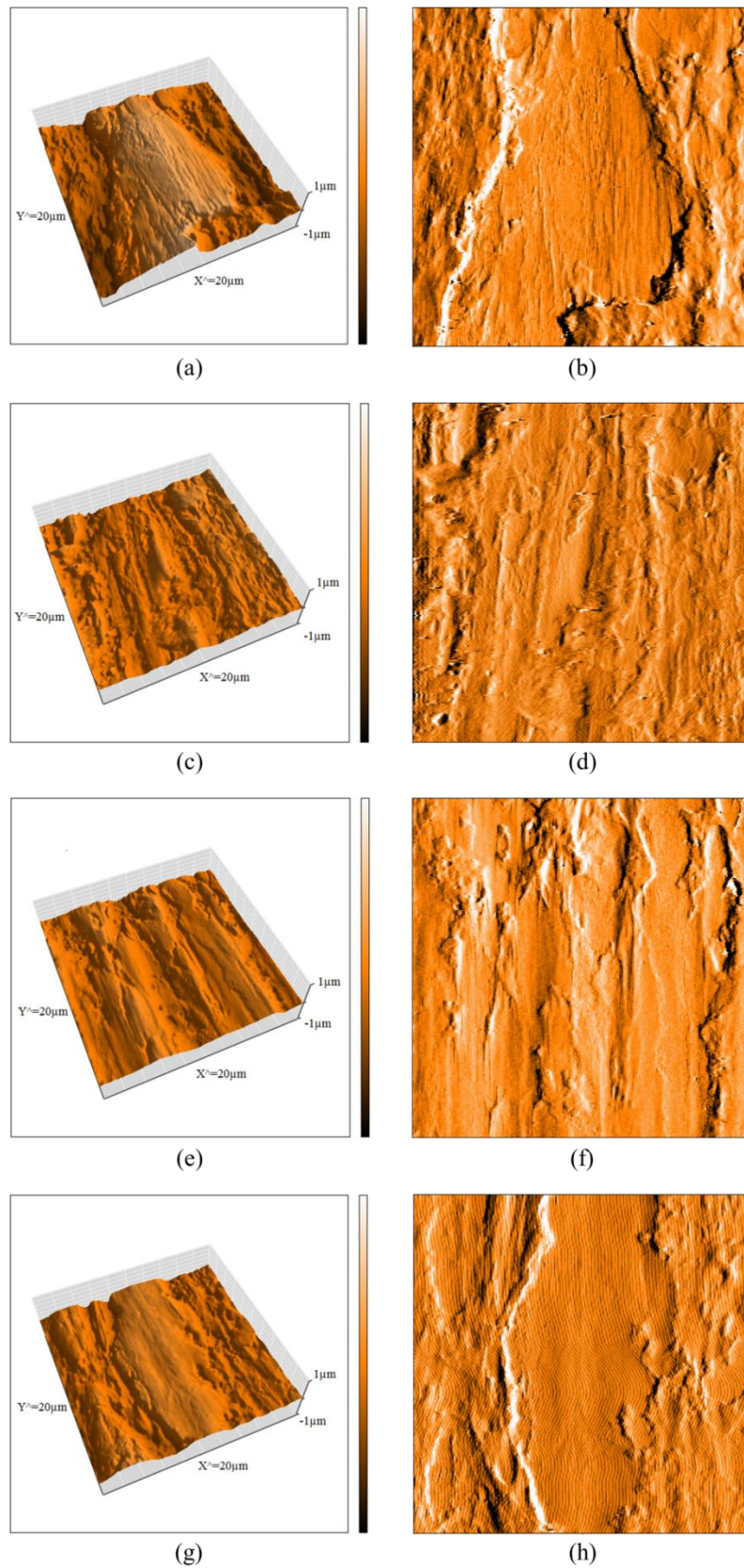
Figure 7–3. AFM surface topographic images of the worn surfaces lubricated by sunflower oil with different additive concentrations: (a, b) 0%, (c, d) 0.5%, (e, f) 1%, (g, h) 2%

7.5.1.2 Measurements of electrical contact resistance

ECR (Electrical contact resistance) measuring technique has been employed to study the contact of the two moving surfaces on the pin-on-disc tribo tester. It is well understood that a low ECR value between metallic tribo-pairs is related to the occurrence of metallic contact and a tighter contact leads to a lower ECR value. Rough surface and the existence of non-metallic substance between contact surfaces could all result in an elevated ECR value [79, 136]. ECR measurements of contact surfaces lubricated with sunflower oil in various concentrations of ZB UFPs are shown in Figure 7–4. ECR measurements were recorded once per second for 30 minutes in situ with the pin-on-disc experiment. Blanks or disconnections in Figure 7–4 indicate the data out of range (too much resistance). Figure 7–4(*a*) illustrates the ECR value of using pure sunflower oil, compared with Figure 7–4(*b*) which is lubricated using SF + 0.5% ZB UFPs, the ECR value of using pure sunflower oil has relatively lower consistency and higher rate of disconnection. The possible reasons for this are an accumulation of wear debris and formation of tribo-films between contact surfaces. However, as shown in Figure 7–4(*b*), when the 0.5% ZB UFPs was applied in sunflower oil, the ECR measurement was out of range in roughly the first 200 seconds when the friction coefficient was high, and then reduced to about 0.7 ohm almost at the same time when friction coefficient started decreasing and stayed as stable as the value of friction coefficient throughout the rest of the experiment. Similar phenomenon can also be observed in the experiment of using SF + 2% ZB UFPs, as shown in Figure 7–4(*c*). The ECR measurements have a good consistency with the friction coefficient result. Discontinuity and immeasurable of ECR measurements appeared in the periods when the friction coefficients were high and measurable ECR values were obtained in the same period when a good reduction performance of friction was observed. The ECR measurements also show a logical relationship with the thickness, coverage and the fragment size of the tribo-films generated on

worn surfaces. Combined with the morphology analysis as shown in Figure 7–3, it is easy to understand that wear track lubricated by SF + 0.5% ZB UFPs has a smoother surface compared with that using sunflower oil. Both small coverage of the tribo-films and their insignificant thickness give less contribution to the electrical resistance between contact surfaces, and therefore a better contact between the upper pin and disc can be achieved and hence a low and stable ECR value has been measured. In the cases using pure sunflower oil and SF + 2% ZB UFPs, the relatively higher surface coverage and thickness of the tribo-films are believed to be the explanation of the high ECR measurements.
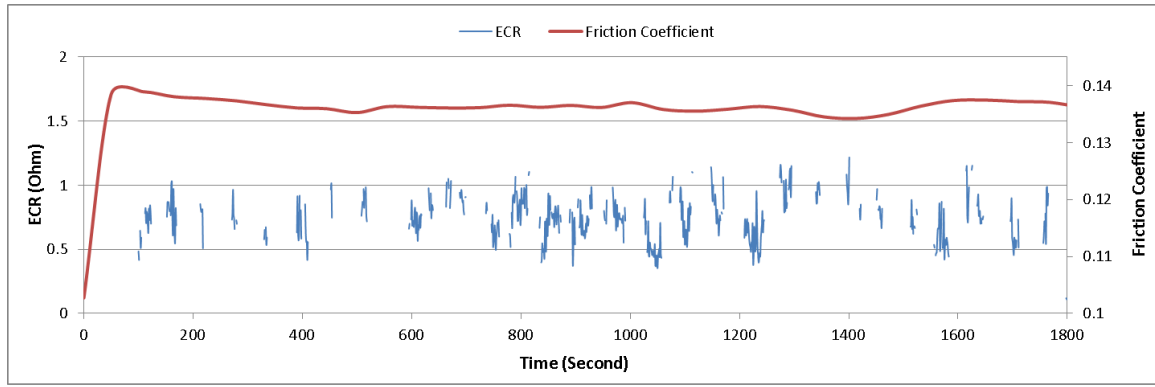
(a)
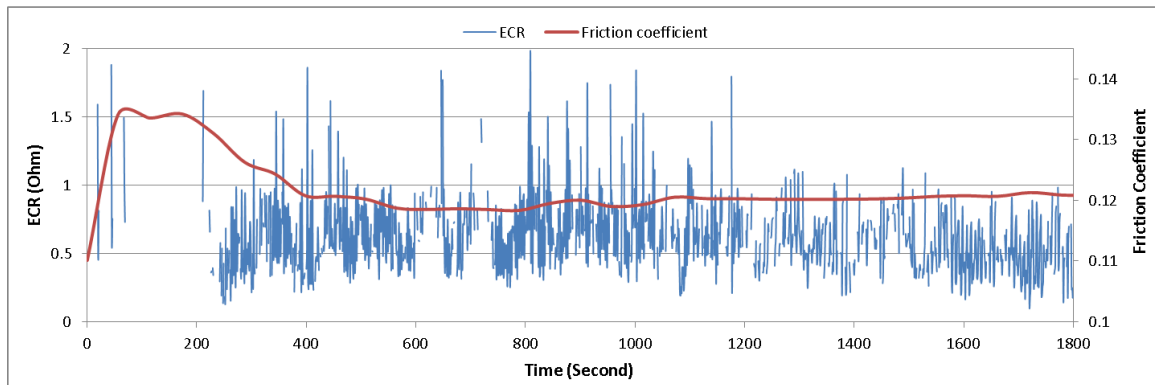
(b)
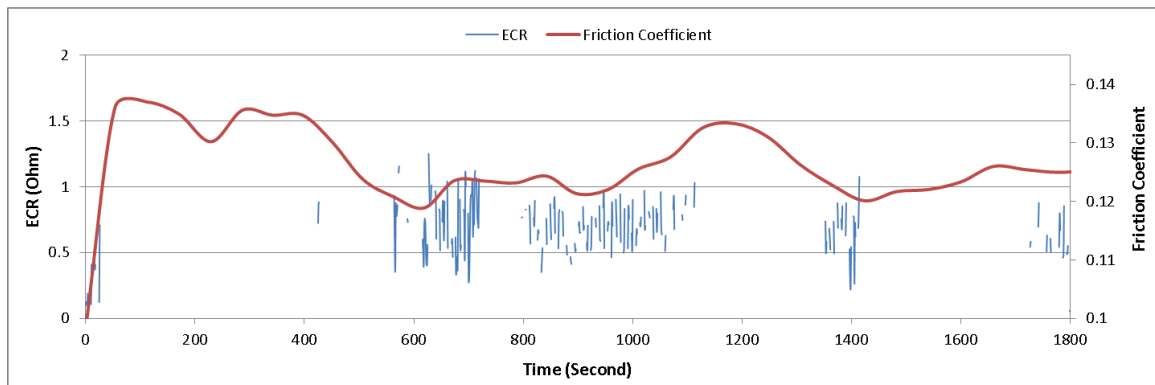
(c)

Figure 7–4. Friction coefficient and ECR value versus testing duration: (a) in pure SF (b) in SF + 0.5% ZB UFPs (c) in SF + 2% ZB UFPs

7.5.1.3 Effect of tribo-film on surface hardness

The nano-indentation tests were carried out at randomly selected positions in the bright (substrate) and dark (tribo-films) areas on a wear track. Corresponding load–depth curves of samples lubricated using sunflower oil with different concentrations of ZB UFPs are

135

illustrated in Figure 7–5 to Figure 7–8. Surface hardness of the worn surface on the tested discs can be derived from further analysis of the load–depth curves. Hardness, in this case, was calculated from the results achieved. Hardness is reflected by the indentation depth when a fixed load applied. A higher value of indentation depth suggests a softer surface. As shown in Figure 7–2, the surface properties of the wear track are not homogenous across its width span. In all experiments, indents on the substrate have smaller indentation depth (Group *A*) than the indents performed on the tribo-films (Group *B*). Compared with load–depth curves of the surfaces lubricated using pure sunflower oil (Figure 7–8) and SF + 2% ZB UFPs (Figure 7–7), load–depth curves of the surface lubricated using sunflower oil with 0.5% (Figure 7–5) and 1% (Figure 7–6) zinc borate additive are less scattered. The fluctuation in local mechanical properties could be used to reflect the homogeneity of a worn surface on a contact track, since a good lubricant may reduce the variation or fluctuation in local mechanical properties and retain a relatively homogeneous worn surface [188]. The average hardness measurements of both the substrate and tribo-films of all the samples are presented in Figure 7–9. Substrate and tribo-films on the worn surface have higher hardness values when sunflower oil containing ZB UFPs was used as the lubricant than those when pure sunflower oil was employed. As shown in Figure 7–9, the hardness of the substrate on the worn surface lubricated by the sunflower oil with ZB UFPs is relatively consistent. Compared with the result in pure sunflower oil, an average increase of 26% in hardness was observed with the application of zinc borate additive. It is suggested that the hardness increase of the substrate is the result from the tribo-chemical reaction and the iron boride generated on worn surface substrate may effectively influence its mechanical properties [84, 138, 139]. The hardness measurements of the tribo-films, however, did not show the similar consistency. When ZB UFPs was applied, the hardness of the tribo-films reduced with an increase of zinc borate additive contents. The tribo-films generated in SF + 0.5% ZB UFPs demonstrated the

highest hardness measurement of 9.3GPa, which was followed by 7.3GPa, the hardness of the tribo-films generated by SF + 1% ZB UFPs. Tribo-films generated in pure sunflower oil held the lowest hardness measurement of 5.5 GPa, which was close to 5.7 GPa obtained with additional 2% ZB UFPs.

A variation of the hardness values of the tribo-films was observed when different lubricants were used for the tests. Based on the morphology study of the worn surfaces, it is suggested that the thickness and continuity of the tribo-films are responsible for such variations. It is clear that tribo-films generated on the worn surface have a lower hardness than that on the substrate. Compared with the thicker tribo-films generated by pure sunflower oil and SF + 2% ZB UFPs, the hardness values of the tribo-films generated by SF + 0.5% ZB UFPs and SF + 1% ZB UFPs are more likely to be interfered by the high hardness of the substrate due to their thin thickness. Therefore, a reduction of the measured hardness values of the tribo-films that associated with an increase of tribo-films' thickness can be observed.
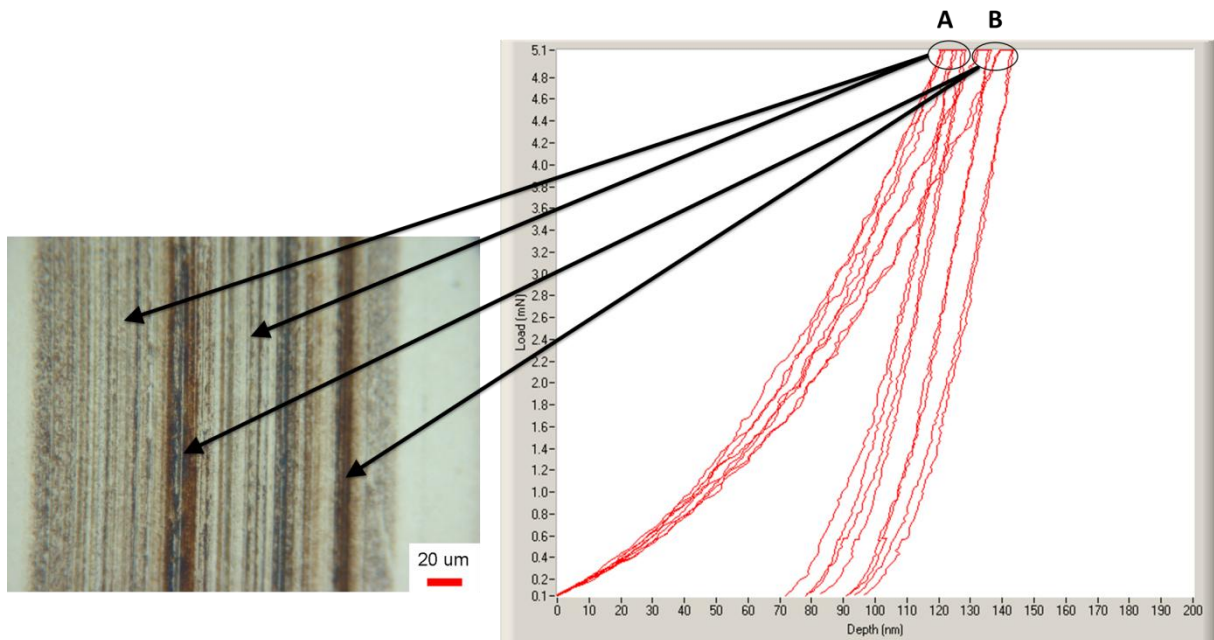
Figure 7–5. Typical load depth curves of surface lubricated by SF + 0.5% ZB UFPs (with a maximum applied load of 5mN)

137
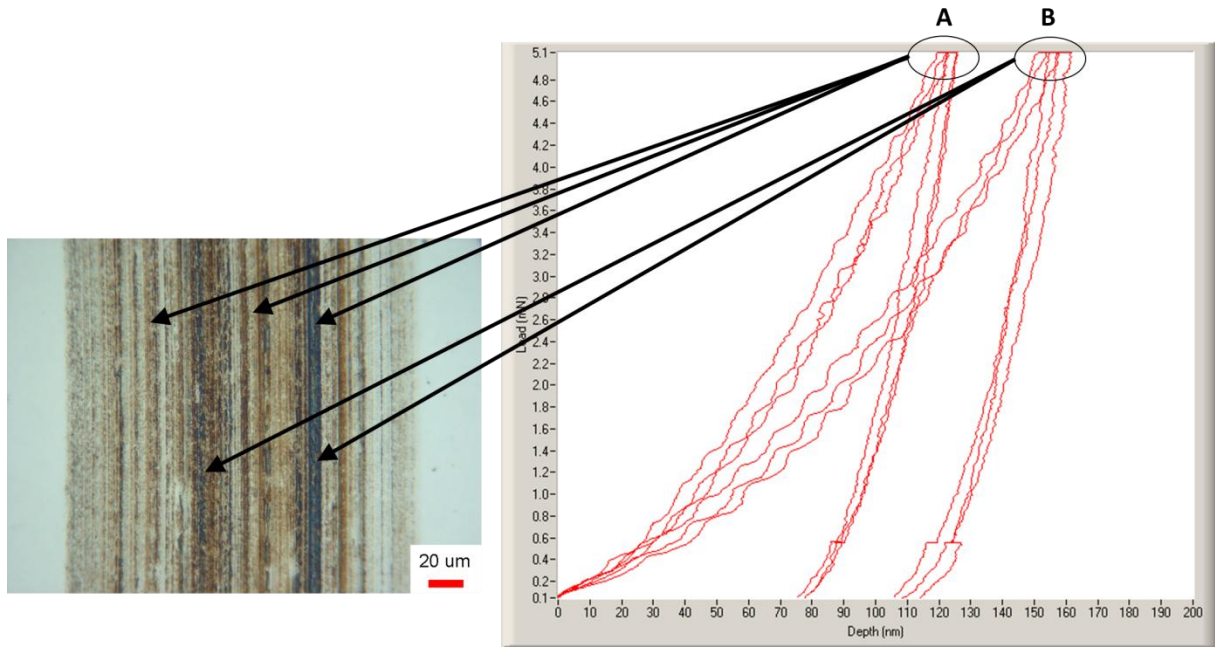
Figure 7–6. Typical load depth curves of surface lubricated by SF + 1% ZB
UFPs (with a maximum applied load of 5mN)
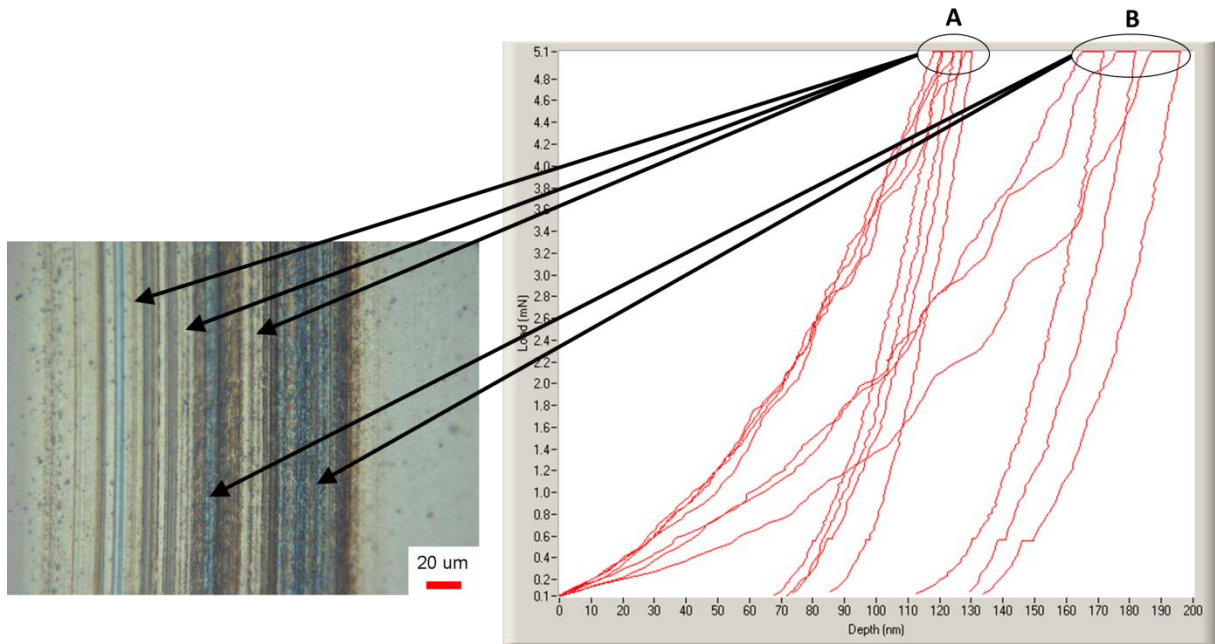
Figure 7–7. Typical load depth curves of surface lubricated by SF + 2% ZB
UFPs (with a maximum applied load of 5mN)
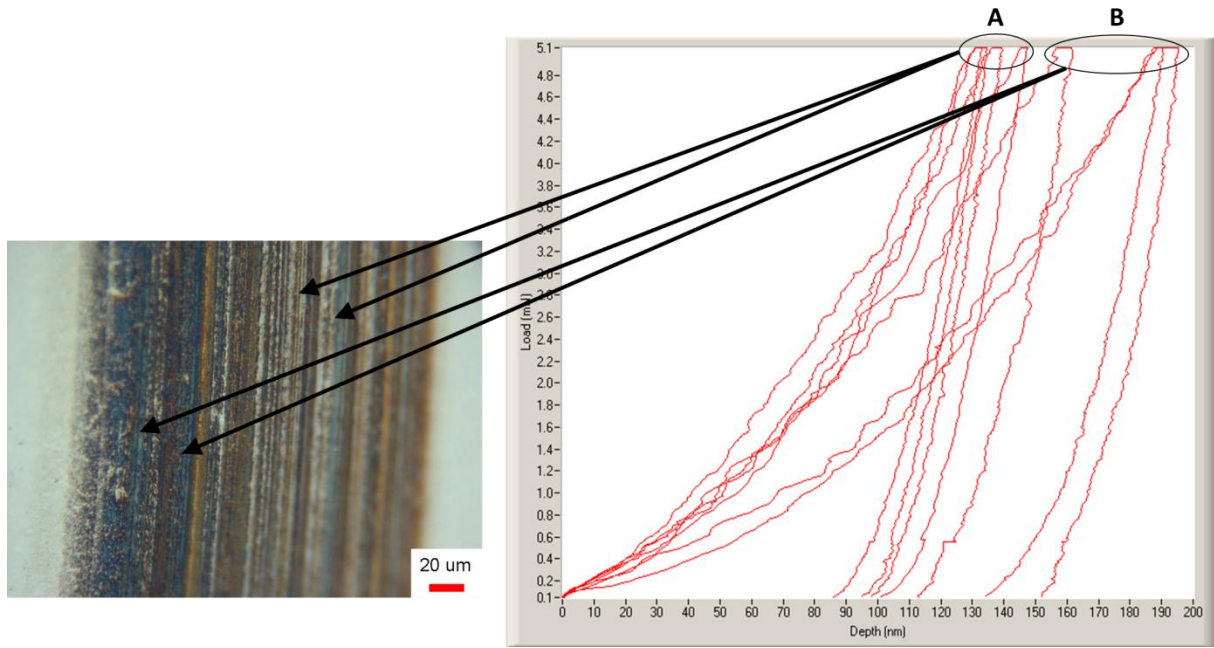
Figure 7–8. Typical load depth curves of surface lubricated by pure SF (with a maximum applied load of 5mN)
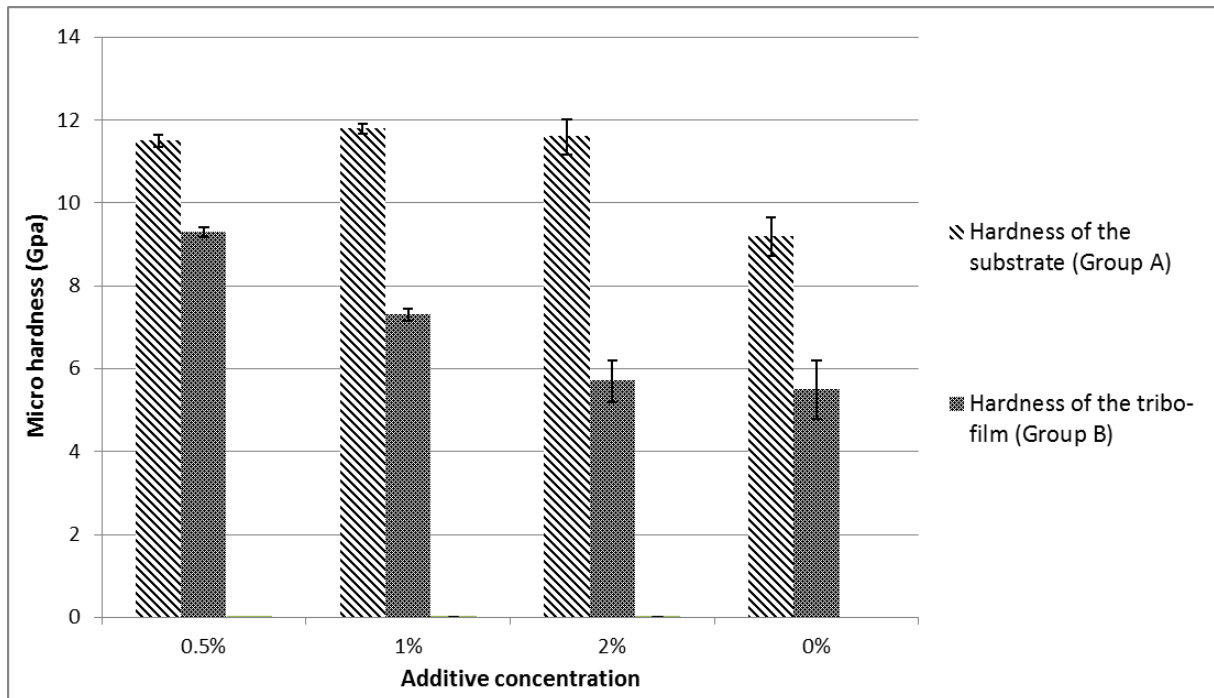
Figure 7–9. Surface hardness on the wear tracks of discs lubricated by sunflower oil with different additive concentrations (with a maximum applied load of 5mN)

139

7.5.1.4   SEM micrographs and elemental analysis

The wear tracks on the discs were analysed under a scanning electronic microscope (SEM) equipped with energy dispersive X ray spectroscopy (EDS). Typical SEM images of the worn surface lubricated by SF + 2% ZB UFPs are shown in Figure 7–10, EDS analyses were also carried out on the worn surface lubricated by SF + 2% ZB UFPs because the highest contrast of the dark (tribo-films) and bright (substrate) areas were observed on this surface. The tribo-films displayed in Figure 7–10(a) have a complex topography which make a good contrast with the substrate displayed in Figure 7–10(c) with smoother surface texture. The EDS patterns of the tribo-films and substrate are illustrated in Figure 7–10(b) and Figure 7–10(d) respectively and the associated quantified elemental analysis results are also given in Table 7-2. It is well understood that it is generally difficult to achieve an accurate Boron quantity directly using EDS due to its low atom weight, and therefore Boron quantity is not given in the table. It can be seen that a great increase of content of Carbon, Oxygen and Zinc was found on the tribo-films compared with that on the substrate. The similar phenomenon was found on the wear tracks tested in all other lubricant samples with ZB UFPs. It is suggested that the Carbon is mainly contributed by decomposed lubricant base oil (sunflower oil). The Oxygen is possibly derived from zinc borate additive and metal oxides. The Zinc is also attributed to the ZB UFPs employed as the lubricant additive in sunflower oil. These results suggest that tribo-chemical reactions may have taken place during the sliding process due to the local high contact pressure and flash temperature caused by the collision and rupture of the asperities between the mating surfaces. Consequently the tribo-films appeared in dark colour were formed on the worn surface and ZB UFPs is proven to be an important ingredient of the tribo-film formation.

(a)

(b)

(c)

(d)
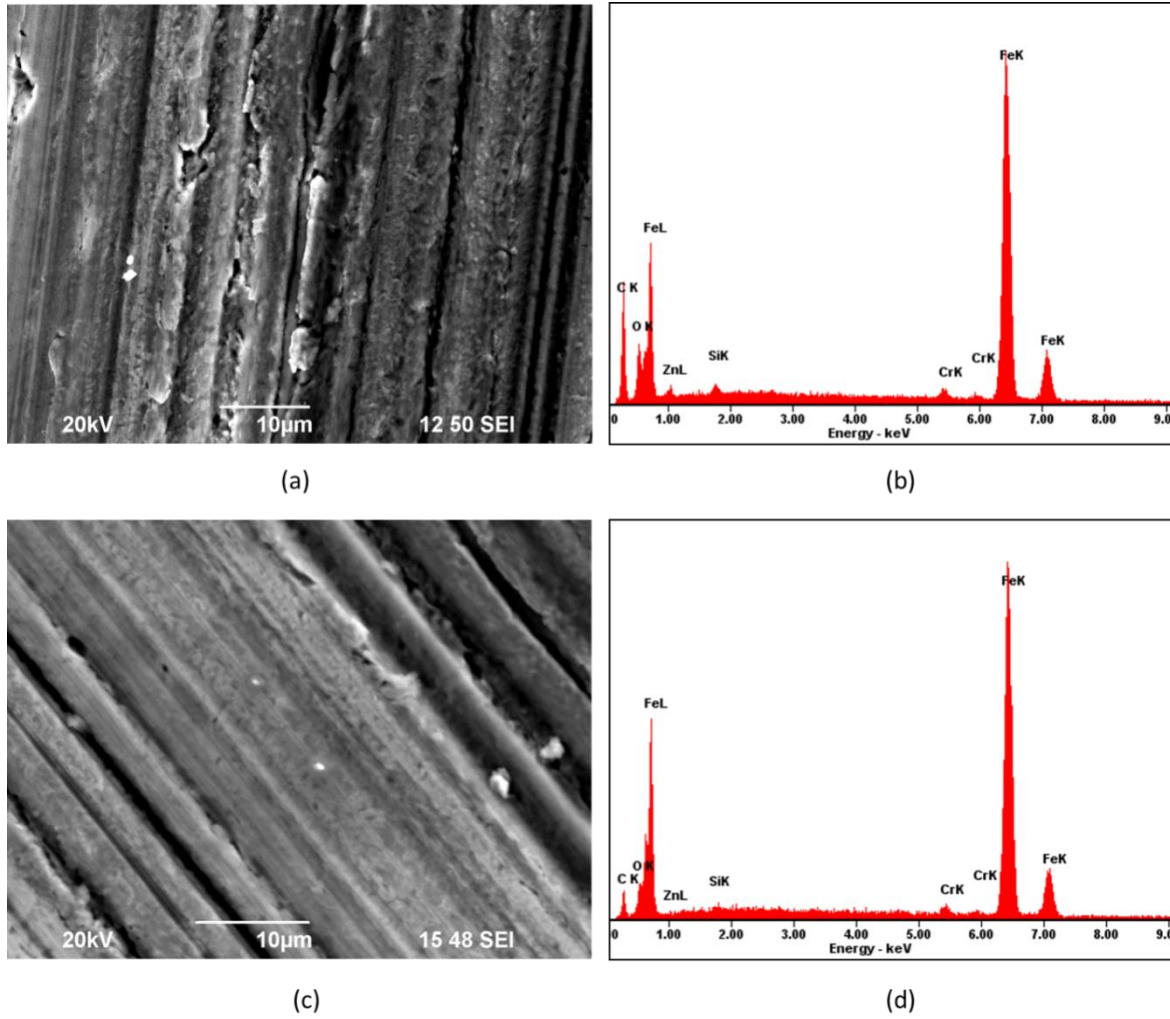
Figure 7–10. SEM micrographs and EDS patterns of worn surfaces lubricated
by SF + 2% ZB UFPs: (a, b) dark area of the wear track (c, d) bright area of
the wear track

Table 7-2 EDS element analysis of the worn surface lubricated by SF + 2%
ZB UFPs

Element composition (wt%)	Bright area	Dark area
C	11.21	29.65
O	3.57	5.48
Zn	0.39	2.86
Si	0.45	0.58
Cr	1.22	0.95
Fe	83.16	60.49

7.5.2 Discussion

Experimental data from the current study have demonstrated the excellent tribological properties of zinc borate ultrafine powders (ZB UFPs) employed as a lubricant additive in sunflower oil. Under a friction force, ZB UFPs is firstly entrapped and then deposit on to contact interfaces due to shear effect. The third body effect of the ultrafine particles between contact surfaces can reduce direct metal contact and consequently adhesion [7]. A reduction of adhesion is directly responsible for the reduction of friction and wear, especially at the beginning of the experiment when both friction and wear caused by adhesion were dominant. When ploughing and debris are generated at the contact interface, ZB UFPs entrapped in contact areas could deliver mechanical filling and polishing effects on the rubbed surface and reduce the mechanical lockup between contact surfaces.

As the sliding continues, it is clear that tribo-chemical reactions took place due to the local high contact pressure and flash temperature caused by the collision and rupture of the asperities between the mating surfaces. Tribo-films appeared in dark colour were then generated on the worn surface, which have a lower hardness than that on the substrate material. It is evident that the properties of the tribo-films play an important role in the tribological performance. The best friction reduction and anti-wear performances were observed when sunflower oil with 0.5% and 1% zinc borate powder was used as the lubricants, accompanied with the thin and patchy tribo-films with small coverage on the worn surface. The friction reduction performance of the two lubricants can be attributed to the diboron trioxide and iron boride formed by tribo-chemical reactions [84, 138, 156, 166, 189]. The outstanding anti-wear performance can be associated with the high hardness of the substrate and the formation of trio-films [105]. As stated in the discussion section of Chpter 6,

when a thin layer of tribo-film with low hardness and reduced modulus is generated on the hard substrate, dislocations will pile up at the interface between the tribo-film and the substrate. As the sliding continues, these dislocations escape through the surface of the tribo-film due to its small thickness [186]. As a result, the wear of material protected by tribo-film will be remarkably reduced or delayed. For the same reason, with an increase of additive concentration, the anti-wear performance of the lubricants containing ZB UFPs was further improved due to the formation of more healthy and complete tribo-films. Interestingly, an increase of additive concentration demonstrated different effects on the friction reduction performance. A slight rise on friction coefficient was detected after the additive concentration was increased from 0.5% to 1%. When the additive concentration was further raised to 2% the ability of friction reduction of the lubricant was weakened considerably. The possible reason for this is the intensified plastic deformation and mechanical lockup promoted by the thickened and better spread tribo-films. As a result of plastic flow, soft tribo-films easily pile up in front of the asperities and cause more resistance for manoeuvre. When sunflower oil with 2% zinc broate ultrafine powder was used as the lubricant, the big fluctuation in friction coefficient reflects the breakdown and replenishment process of the tribo-films.

Without ZB UFPs, the pure sunflower oil demonstrated the highest friction coefficient and the worst anti-wear behaviour. The morphology of the tribo-films and low hardness of the substrate could be responsible for the bad performance. The complex surface topography introduced by very thick tribo-films may also cause a barrier effect which leads to local breakage of oil film [86, 190].

7.6   Summary

This chapter presents an investigation on the tribological properties of zinc borate ultrafine powder employed as a lubricant additive in sunflower oil. The stable dispersions of 0.5 wt%,

1 wt% and 2 wt% zinc borate ultrafine powder in sunflower oil were achieved by using an ultrasonic homogeniser. A pin-on-disc tester was employed to evaluate friction reduction capability of zinc borate ultrafine powder. Post-test surface analyses of wear tracks on the rotating disc were conducted. Tribo-films with dark colour were generated on the worn surfaces and showed a good contrast with the substrate displayed in bright colour. The worn surface with different morphologies reflected as the colour alterations on the worn surface were observed when different lubricants were applied. The morphology and elemental analysis of the worn surfaces were studied using atomic force microscopy (AFM) and SEM equipped with EDS. Mechanical properties of the tribo-films and substrates were studied with a nano-indentation tester. Test results suggest that tribo-films generated on the worn surface have a relatively low hardness compared with the steel substrate. The substrates on the worn surfaces lubricated in sunflower oil with zinc borate ultrafine powder demonstrated higher hardness than that of the substrate lubricated with pure sunflower oil due to the possible tribo-chemical reaction between the zinc borate additive and substrate. The combination of sunflower oil with 0.5% zinc borate ultrafine powder has delivered the most balanced performance in friction and wear reduction. Base on the above results, this chapter can be summarized as follow:

- Zinc borate ultrafine powder with a particle size of 500-800nm has demonstrated excellent friction reduction performance as a lubricant additive in sunflower oil. The most noticeable tribological improvement was observed when 0.5% zinc borate ultrafine powder was applied when more than 14% reduction of friction coefficient was found.

- The outstanding tribological performance of zinc borate ultrafine powder as lubricant additive in sunflower oil can be attributed to the increased hardness of the substrate and the formation of tribo-films due to the tribo-chemical reactions occurred on the worn surfaces.

These tribo-films with content of Fe, O, C, Zn, and B elements have a smaller hardness than the substrate material.

- The changes on the size and profile of the tribo-films were discovered when the different lubricant samples were employed. The physical and chemical properties of the tribo-films play an important role in the tribological behaviour.

Chapter 8.   The Preparation and Tribological Properties of Surface Modified Zinc Borate Ultrafine Powders as a Lubricant Additive in Liquid Paraffin

8.1   Introduction

The recent studies have shown that some of the submicron sized particles have demonstrated good advantages to be employed as the lubricant additives in oil. However, the poor dispersibility of these solid particles in base oil restrains from their tribological properties and development in practical applications. In this chapter, ZB UFPs were firstly surface modified with Oleic acid (OA) and Hexadecyltrimethoxysilane (HDTMOS) coupling agents to improve the dispersibility. Tribological properties of liquid paraffin with original and modified ZB UFPs were investigated and compared using a Pin-on-disc tribo tester. Post analysis of the worn surface and tribo film was carried out in a similar fashion as mentioned in Chapter 6. Moreover, surface modification of zinc borate ultrafine powder was verified using FTIR Spectrometer and Thermogravimetric analyser (TGA), also conglomerate size and stability of the original and modified samples in methanol were studied with a Malvern Zetasizer.

8.2   Surface modification of zinc borate ultrafine powder

The Oleic acid modified zinc borate ultrafine powder (OA-ZB UFPs) and Hexadecyltrimethoxysilane modified zinc borate ultrafine powder (HDTMOS-ZB UFPs) were synthesized in this study using the same technique described in Chapter 6.

The surface structure and morphology of the original and surface modified ZB UFPs are shown in Figure 8–1. It can be seen that ZB UFPs modified by OA shown in Figure 8–1(b) shares a similar particle size and morphology to the original ZB UFPs shown in Figure 8–1(a). However, compared with the unmodified specimen, more complicated surface texture with

less sharp edges can be observed from the OA-ZB UFPs. The HDTMOS-ZB UFPs shown in

Figure 8–1(c) demonstrates the smallest particle size.
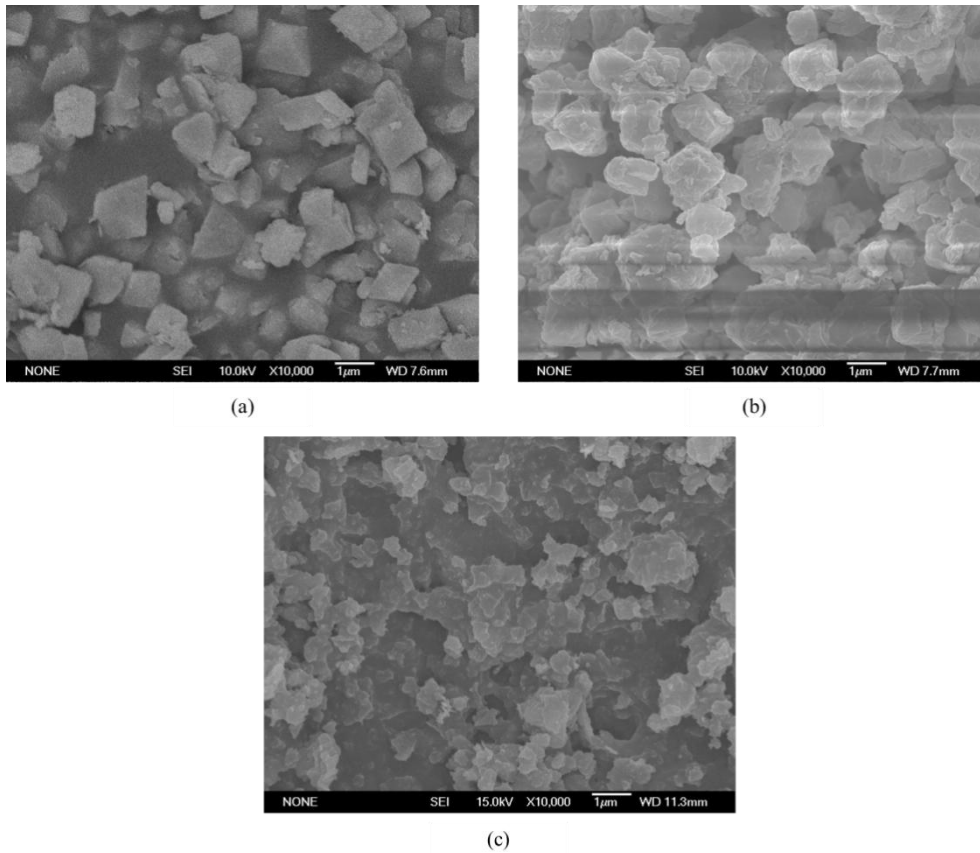
Figure 8–1. SEM micrographs of (a) the original ZB UFPs, (b)OA-ZB UFPs,
(c) HDTMOS-ZB UFPs

Table 8-1 displays the conglomerate size and zeta-potential values of the original and surface

modified ZB UFPs in methanol. 0.05wt% samples were dispersed in methanol with an

ultrasonic homogeniser (KINEMATICA PT 10-35 GT) running for 5 minutes. The average

conglomerate size of original ZB UFPs measured in methanol was 2150nm in diameter.

Under the same condition, OA-ZB UFPs demonstrated a similar value of 2470nm in diameter.

By contrast, the conglomerate size of HDTMOS-ZB UFPs was reduced to 540nm when

HDTMOS was employed as the modification agent. Zeta-potential of the original ZB UFPs

dispersed in methanol was measured to be 6.81 mV. In comparison, both OA-ZB UFPs and

HDTMOS-ZB UFPs demonstrated the higher values of 27.9mV and 35.8mV respectively. It

is well known that surface charges of the particles caused by absorption of ions and molecules generate an electrostatic repulsion force between particles. This electrostatic repulsion force can partially counteract gravitation and reduce agglomeration and sedimentation of particles. Based on the Deryaguin–Landau–Verwey–Overbeek (DLVO) theory [158], a higher absolute value of zeta-potential of a suspension presents a better stability. With the Zeta potential results from this study shown in Table 8-1, it can be suggested that surface modifications of the ZB UFPs carried out with OA and HDTMOS have effectively improved the stability of ZB UFPs in organic solvent. The highest zeta-potential value of HDTMOS-ZB UFPs also suggests that it has better stability than OA-ZB UFPs in methanol.

Table 8-1 Conglomerate size and Zeta-potential of zinc borate powders
despersed in methanol

	Zinc borate ultrafine powders		
	Original	OA-ZB UFPs	HDTMOS-ZB UFPs
Conglomerate size (in methanol)	2150nm	2470nm	540nm
Zeta-potential	6.81 mV	27.9mV	35.8mV

The composition and structure of the OA-ZB UFPs and HDTMOS-ZB UFPs were characterised with FT-IR spectroscopy as shown in Figure 8–2. In the infrared spectrum of original ZB UFPs shown in Figure 8–2(a), the band at $3458 cm^{-1}$ is assigned to stretching of –OH. The band at $1650 cm^{-1}$ is attributed to the H–O–H bending mode, which indicates the existence of crystal water. The peaks observed between $1450–1300 cm^{-1}$ and $1200–1000 cm^{-1}$ are related to asymmetric stretching vibrations of trihedral borate (BO3) and tetrahedral

borate (BO4) groups respectively and the peaks between 960–740 cm^{-1} are related to the symmetric stretching vibrations of (BO3) and (BO4) groups [191]. In the spectra of OA and HDTMOS displayed in Figure 8–2(b-c), two sharp peaks at 2923 and 2856 cm^{-1} are attributed to the asymmetric and symmetric –CH$_2$ stretching vibrations respectively. The same peaks with lower intensity can also be found in the spectra of OA-ZB UFPs and HDTMOS-ZB UFPs shown in Figure 8–2(d-e). It is evident that the positions of peaks for the distinctive functional groups observed in the spectra of OA-ZB UFPs and HDTMOS-ZB UFPs are identical with the pure modification agent OA and HDTMOS. The infrared spectra result indicates that the surface of ZB UFPs has been successfully modified with OA and HDTMOS.
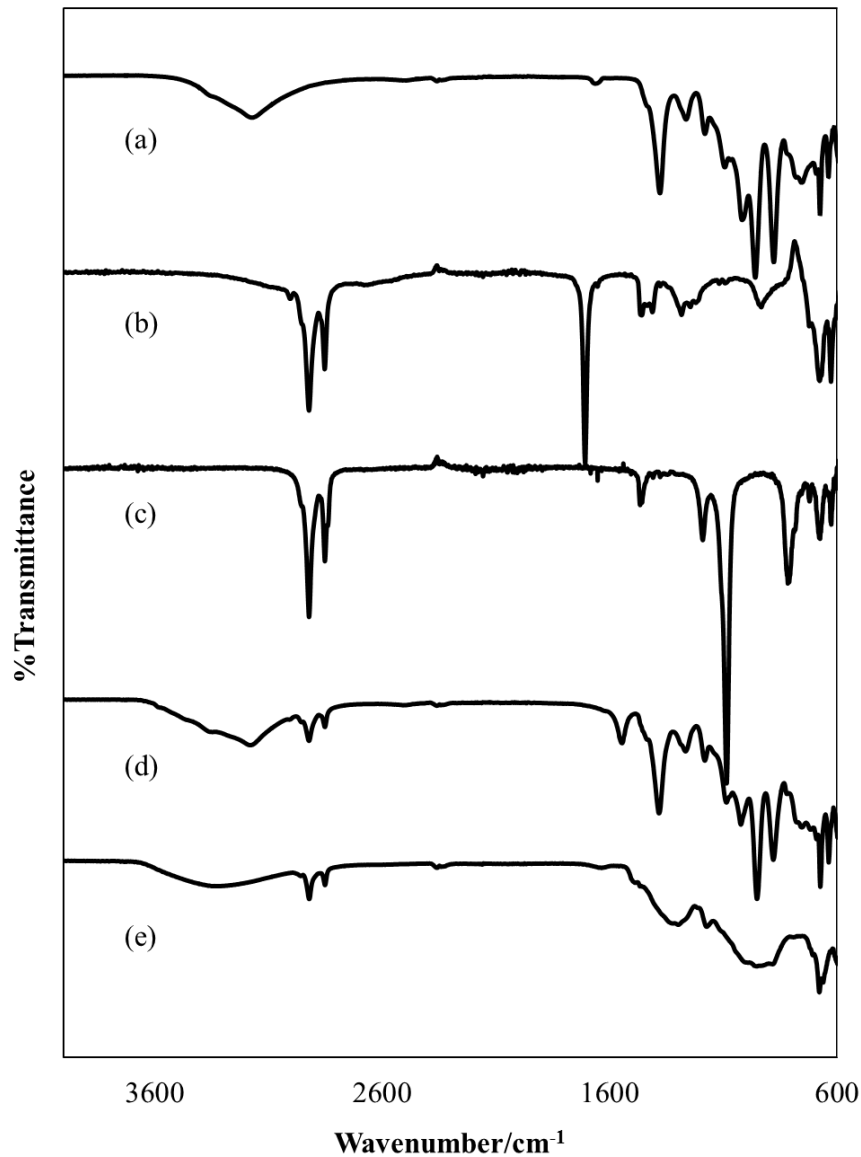
Figure 8–2. FT-IR spectra of (a) original ZB UFPs, (b) OA, (c) HDTMOS, (d)
OA-ZB UFPs, (e) HDTMOS-ZB UFPs

Thermal gravimetric (TG) analysis of OA-ZB UFPs and HDTMOS-ZB UFPs is demonstrated in Figure 8–3 in order to verify the surface modification conducted and to calculate the amount of organic substance covered on the surface of ZB UFPs. As shown in curve (a) of Figure 8–3, the weight of the original ZB UFPs reduced sharply with an increase of temperature due to the loss of crystal water. The decrease on sample weight started at 140 °C and a weight loss of 15% was observed when the reduction stopped at 230 °C. Curves

150

b-c in Figure 8–3 show the TGA results of HDTMOS-ZB UFPs and OA-ZB UFPs respectively when they were heated from 80 °C -500 °C. It can be seen that the weight of both samples began to reduce at the almost same temperature about 95 °C and the reduction completed accordingly at 480 °C and 445 °C. Compared with the original ZB UFPs, HDTMOS-ZB UFPs and OA-ZB UFPs have a higher ratio of weight loss of 20% and 25% respectively because of the decomposition of the organic groups covered on the surface of the modified particles. The results of TG analysis confirm that ZB UFPs have been successfully covered with organic groups of HDTMOS and OA modification agents. Based upon the fact that OA-ZB UFPs have a higher weight loss in TG analysis compared with HDTMOS-ZB UFPs, it is suggested that a bigger coverage of organic groups on the surface of ZB UFPs has been achieved when OA is employed as the modification agent.
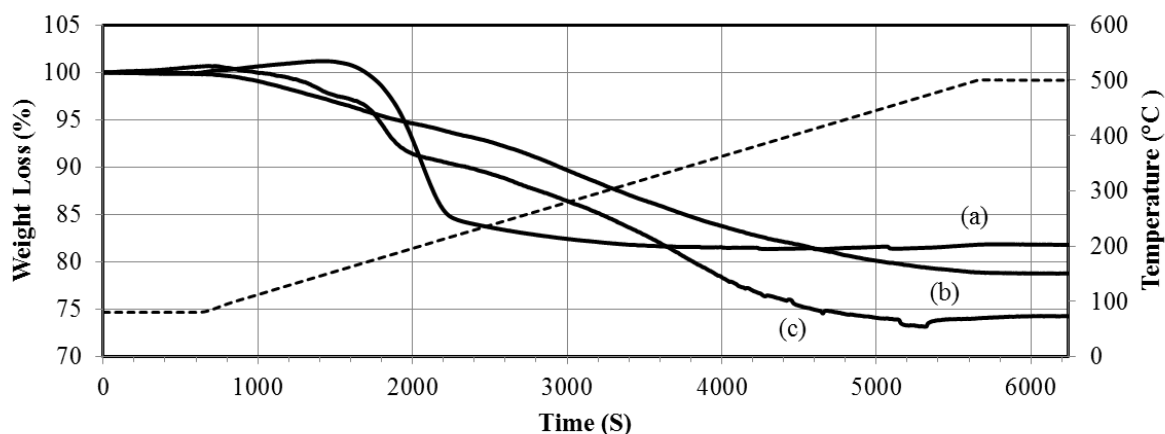
Figure 8–3. Thermal gravimetric analysis (TGA) of (a) original ZB UFPs, (b) HDTMOS-ZB UFPs, (c) OA-ZB UFPs

8.3 Preparation of lubricants

In this study, a uniform concentration of 0.5% in weight fraction was applied for all friction and wear tests when the additive powders were employed (additive concentration was decided base on literature study). Additives were dispersed in LP with an ultrahigh shear

homogenizer at the speed of 20k rpm for 20 minutes. The lubricants prepared in this study are

presented in Table 8-2.

Table 8-2 The lubricants prepared in the tests

Sample code	Constituent
LP	Liquid paraffin
LP + ZB UFPs	Liquid paraffin with 0.5 wt% original zinc borate ultrafine powders
LP + OA-ZB UFPs	Liquid paraffin with 0.5 wt% oleic acid modified zinc borate ultrafine powders
LP + HDTMOS-ZB UFPs	Liquid paraffin with 0.5 wt% hexadecyltrimethoxysilane modified zinc borate ultrafine powders

8.4   Pin-on-disc test conditions

The tribological properties of all lubricant samples were evaluated using a POD 2 pin-on-disc

tester (Teer Coatings Ltd.). All the tests were carried out with a sliding speed of 50mm/s for a

testing period of 60 minutes at the ambient temperature of 22°C. The test load was set to be

10N (1.54GPa Hertz pressure). The bearing balls (pins) and sample discs were prepared with

the same specifications as described in Chapter 6.

8.5   Experimental results

8.5.1   Friction coefficient

Friction coefficients of different lubricant samples are illustrated in Figure 8–4. The typical

friction coefficient curve pattern of boundary lubrication was demonstrated by all lubricant

samples. The highest rise in friction coefficient at the beginning of the pin-on-disc tests was

delivered by pure LP and it was followed by LP with ZB UFPs and LP with OA-ZB UFPs.

As sliding continued, the friction coefficients for each lubricant sample were finally

stabilized, except for LP with ZB UFPs. More fluctuations were observed in the friction

coefficient curves of LP with OA-ZB UFPs and LP with ZB UFPs

As shown in Figure 8–4, lubricant samples with HDTMOS-ZB UFPs and OA-ZB UFPs have

displayed higher friction coefficient compared with pure LP. Highest friction coefficient was

found when LP with HDTMOS-ZB UFPs was used as the lubricant. LP with ZB UFPs

delivered the lowest friction coefficient. Among all the lubricant samples used in these tests,

LP with ZB UFPs is the only one that failed to demonstrate a stable friction coefficient in the

pin-on-disc tests. When LP with ZB UFPs was used as the lubricant, a clear descending

tendency of friction coefficient against a testing period can be observed and at the end of the

test, and a maximum reduction of 25% on friction coefficient was found compared with the

pure LP.
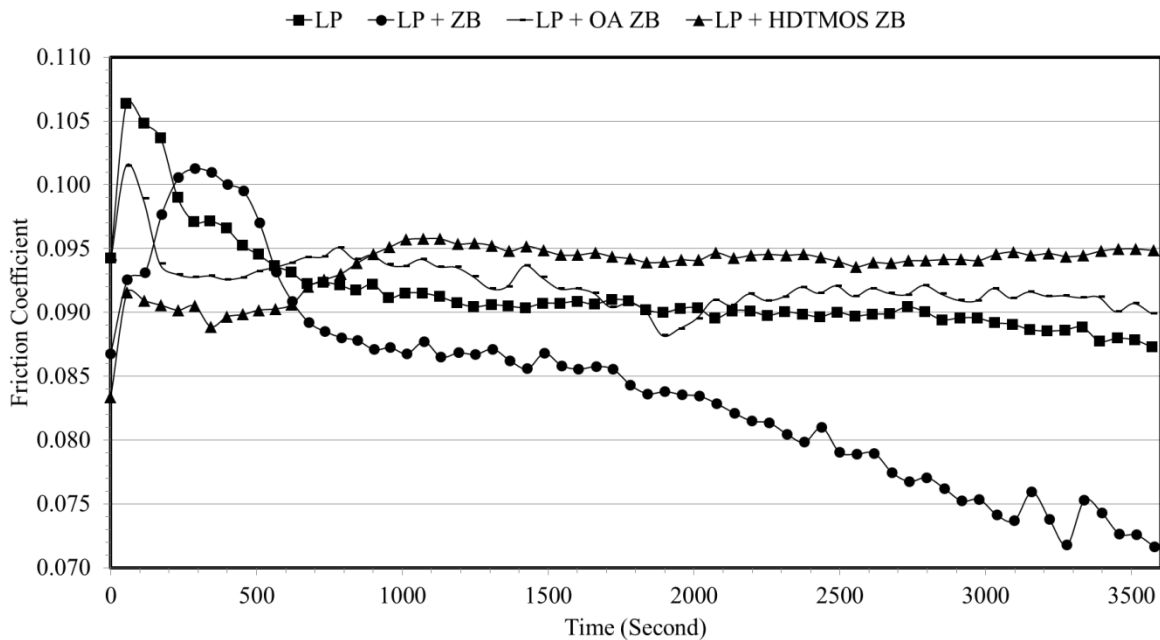
Figure 8–4. Effect of different lubricant additives on friction coefficient of LP

8.5.2 Anti-wear behaviour

Wear scar of the pins (bearing balls) used in pin-on-disc tests were firstly assessed using an optical microscope. The morphologies and wear scar diameters (WSD) of the tested pins are shown in Figure 8–5. A smaller WSD implies a less material loss therefore the superior wear resistance. It is evident that with the employment of OA-ZB UFPs and HDTMOS-ZB UFPs, WSDs of the pins have been reduced. Particularly, a WSD of as small as 123µm was obtained when LP with HDTMOS-ZB UFPs was employed as a lubricant. This WSD of 123µm is approximately 45% smaller than the wear scar obtained when the LP with OA-ZB UFPs was applied, and more than 50% smaller than that generated by pure LP. On the contrary, LP with ZB UFPs delivered the biggest WSD of 373µm. A uniform and tenacious tribo-film was found on the wear scar lubricated with LP with HDTMOS-ZB UFPs, as shown in Figure 8–5(d) and the formation of this tribo-film appears to have played an important role in the outstanding anti-wear performance.

Wear losses of the pins lubricated by different lubricant samples were also presented in Figure 8–6. The wear loss volume was calculated geometrically based on the assumption that wear scar is a flat surface. As shown in Figure 8–6, the addition of 0.5% HDTMOS-ZB UFPs in LP has led to a more than 15 time decrease on wear loss of the upper pin.
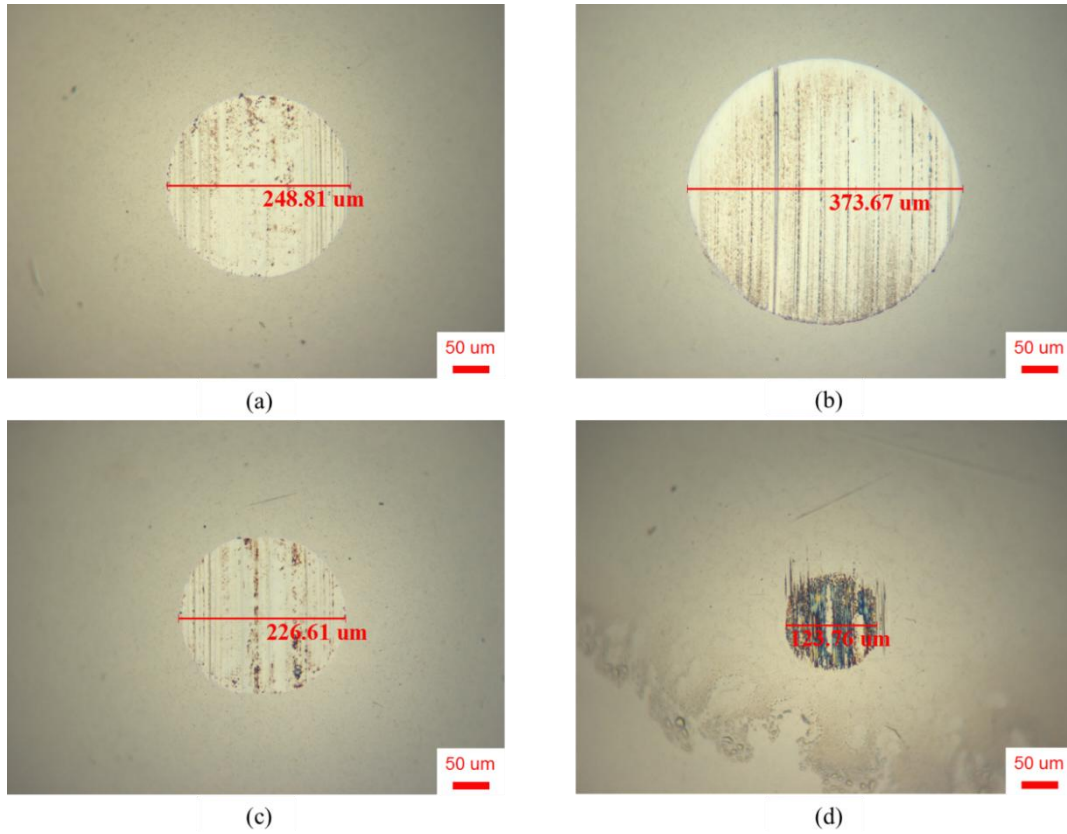
Figure 8–5. Optical micrographs of wear scars lubricated using: (a) LP, (b) LP with ZB UFPs, (c) LP with OA-ZB UFPs (d) LP with HDTMOS-ZB UFPs
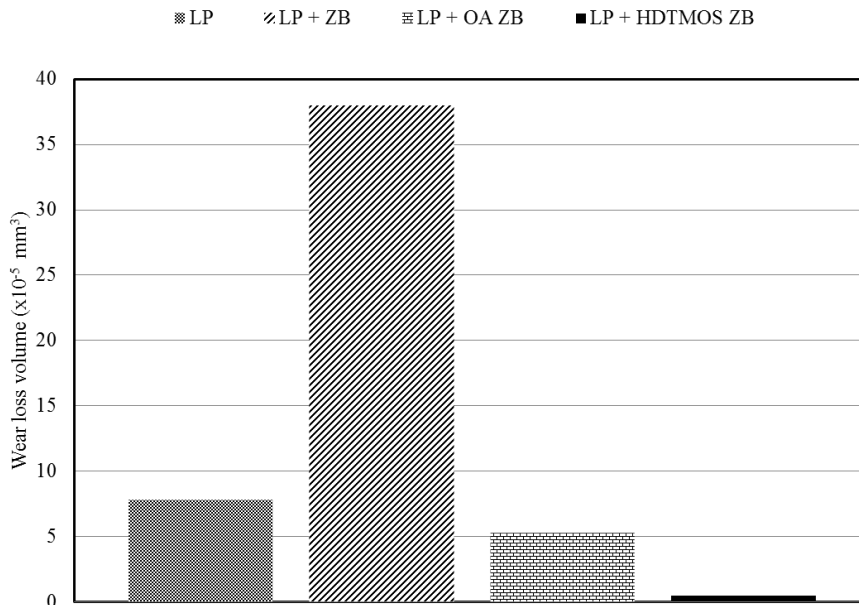
Figure 8–6. Effect of different lubricant additives on wear loss volume of the bearing balls

155

8.6   Interpretation and discussion of the results

8.6.1   Characterisation of the worn surfaces

The same surface characterisation techniques used in Chapter 6 were applied. It involves the employment of optical microscopy, scanning electron microscopy (SEM), atomic force microscopy (AFM), Energy dispersive X-ray spectroscopy and Nano-indentation facility.

8.6.1.1   Physical and mechanical properties

Figure 8–7(a) shows a magnified optical photo of the wear scar of a pin (a bearing ball) lubricated by LP with HDTMOS-ZB UFPs. Figure 8–7(b-c) present the AFM images of tribo-film generated on wear scar surface as marked in Figure 8–7(a). Clearly a uniform and complete tribo-film was observed. The thickness of the tribo-film is measured to be around 315nm (see Figure A–6 in Appendix–2). The mechanical property of the tribo-film has been measured with nano-indentation device. Indentations were made on both the tribo-film and the substrate steel. Figure 8–8(a) shows the patch of tribo-film that had the indentation on. Corresponding load–depth curves are illustrated in Figure 8–8(b). Mechanical properties of the worn surface on the tested bearing balls can be derived from further analysing the load–depth curves. With a maximum indentation load of 5mN, the indentation depth on tribo-film reached 155nm (curve (ii) in Figure 8–8(b)) which is not greater than the thickness of the tribo-film. At this condition the mechanical property of the tribo-film measured will not receive much interference from the substrate. Therefore the surface hardness and reduced modulus derived from this load-depth curve only represent the property of the tribo-film alone. A comparison of the surface hardness and reduced modulus of the tribo-film and substrate steel is presented in Table 8-3. Based upon the test results, it can be suggested that tribo-film is made of a softer material with lower stiffness compared with substrate steel.
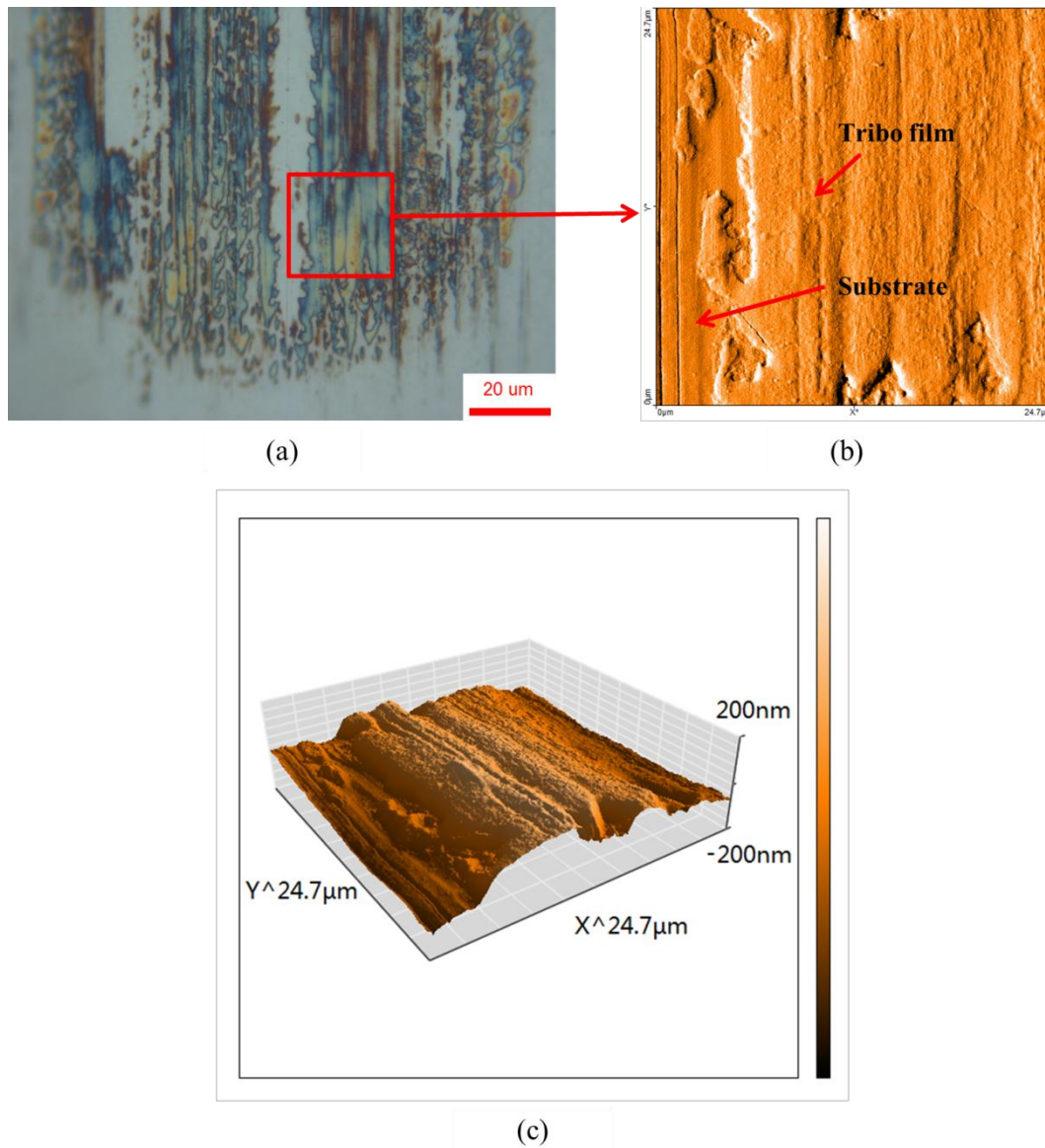
Figure 8–7. Morphologies of the tribo-film generated by LP with HDTMOS-ZB UFPs: (a) optical image, (b) AFM surface topographic image, (c) 3D AFM surface topographic image
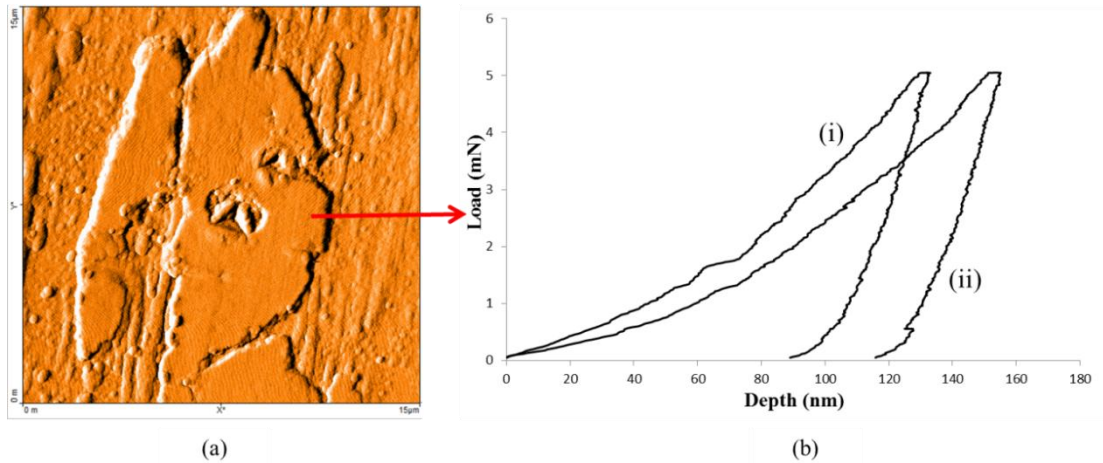
Figure 8–8 Morphology of a piece of tribo-film generated by LP +
HDTMOS-ZB UFPs and corresponding inentation curves obtained from
different domains: (i) on substrate, (ii) on tribo-film

Table 8-3 A comparison of mechanical properties of the tribo-film and the
substrate

Indentation position	Indentation depth	Hardness	Reduced modulus
Tribo-film	155nm	7.2GPa	228GPa
Substrate	132nm	9.8GPa	260GPa

Figure 8–9 shows the AFM morphologies of the worn surfaces of the pins lubricated with the

different lubricant samples. Changes on the size and profile of the tribo-films were

discovered when the different lubricant samples were used. When pure paraffin was used as

the lubricant as shown in Figure 8–9(a-b), no complete tribo-film but only small patchy

pieces were found scattering over the worn surface, some ploughings were also seen clearly.

Similar phenomenon was also observed when LP with the original ZB UFPs was employed,

as shown in Figure 8–9(c-d). Very fine fragments of tribo-film can be seen spreading over the

examined area. The tribo-film generated on the wear scar lubricated by LP with OA-ZB

UFPs, as shown in Figure 8–9(e-f) have a bigger fragment size and elongated shape

stretching along the direction of the sliding. Among all the samples, the tribo-film generated

by LP with HDTMOS-ZB UFPs was the most widespread and tenacious. Almost the whole

scanned surface was covered with the tribo-film, and the thickness of the tribo-film was fairly uniform across the area. As marked in Figure 8–9(h), the main part of the tribo-film is continuous and smooth, while the other areas demonstrate the trace of disintegrating of the tribo-film. Cracks can be seen propagating in the tribo-film in this area and gradually breaking a complete piece of tribo-film into small fragments. No outstanding change of film thickness was found on a disintegrating part of the tribo-film compared with the other completely covered area. It is suggested that the employment of HDTMOS-ZB UFPs in LP enables to generate a more complete and durable tribo-film on the contact surface and this tribo-film can effectively protect the surface from wear damage.
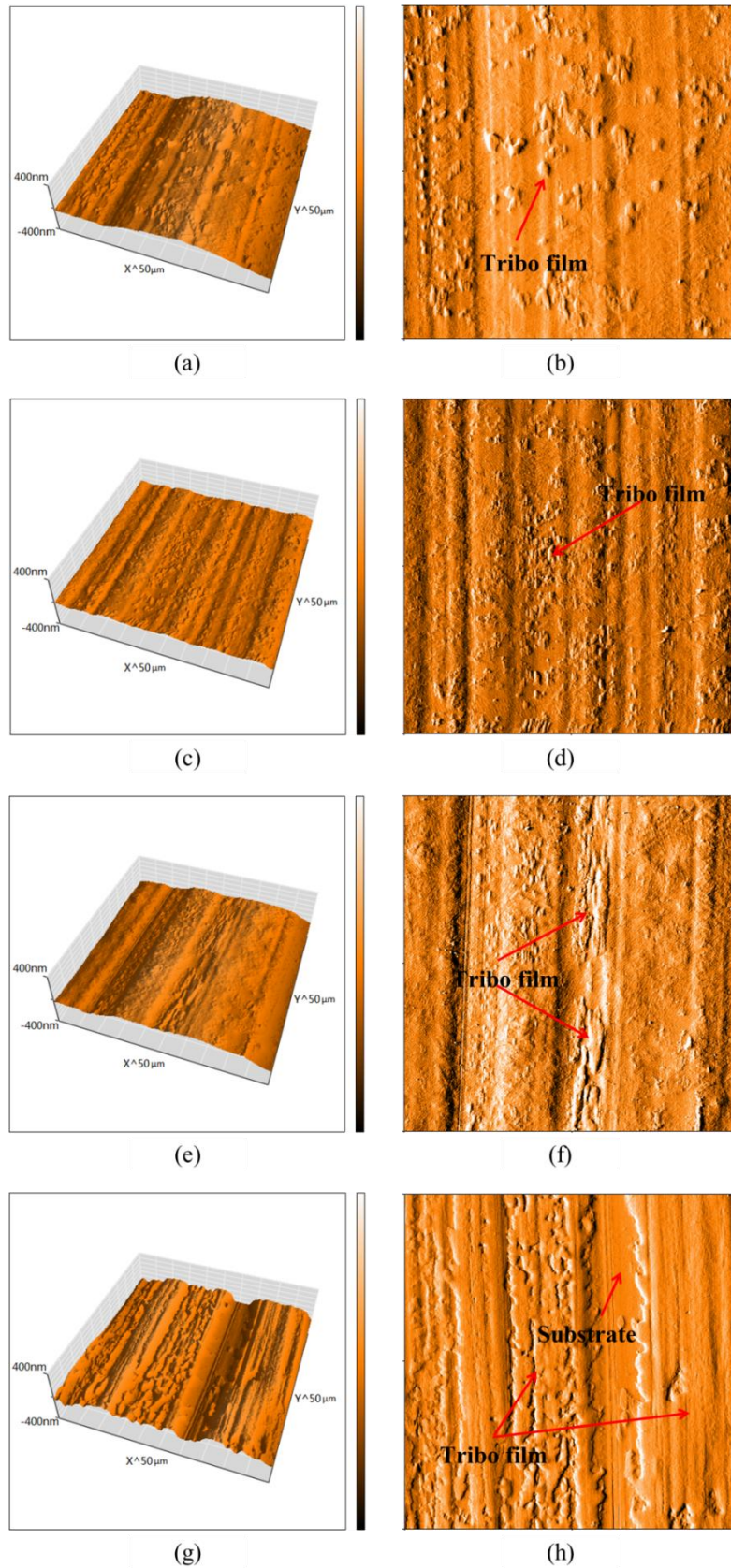
Figure 8–9 AFM surface topographic images of the worn surfaces lubricated
with different lubricants: (a, b) LP, (c, d) LP with ZB UFPs, (e, f) LP with
OA-ZB UFPs, (g, h) LP with HDTMOS-ZB UFPs

8.6.1.2   SEM micrographs and EDS analysis

The worn surfaces lubricated by LP with HDTMOS-ZB UFPs were analysed under a scanning electronic microscope (SEM) equipped with energy dispersive X-ray spectroscopy (EDS). Typical SEM images and EDS analyses are shown in Figure 8–10. Distinctive topographical differences of the tribo-film and substrate can be seen clearly. The tribo-film displayed in Figure 8–10(a) appears in dark colour with a complex topography which makes a good contrast with the substrate displayed in brighter colour with smoother surface texture. The EDS patterns of the region highlighted on the tribo-film and the substrate are shown in Figure 8–10(b) and Figure 8–10(c) respectively. Quantified elemental analysis results are also given in Table 8-4. It is obvious that a considerable increase of Oxygen and Zinc contents was found on the tribo-film compared with the element distribution on the substrate. The Oxygen is possibly derived from ZB UFPs and metal oxides. The Zinc is attributed to the ZB UFPs. The elemental analysis also showed that slight more Born was found on substrate rather than on tribo-film and the reason for this is still not clear; however it is generally difficult to achieve an accurate Boron quantity by EDS due to its low atom weight. It is evident that HDTMOS-ZB UFPs are an important ingredient of the formation of the tribo-film. These results suggest that some tribochemical reactions may have taken place during the sliding process due to the local high pressure and flash temperature caused by the collision and rupture of the asperities between the mating surfaces.

(a)

(b)

(c)
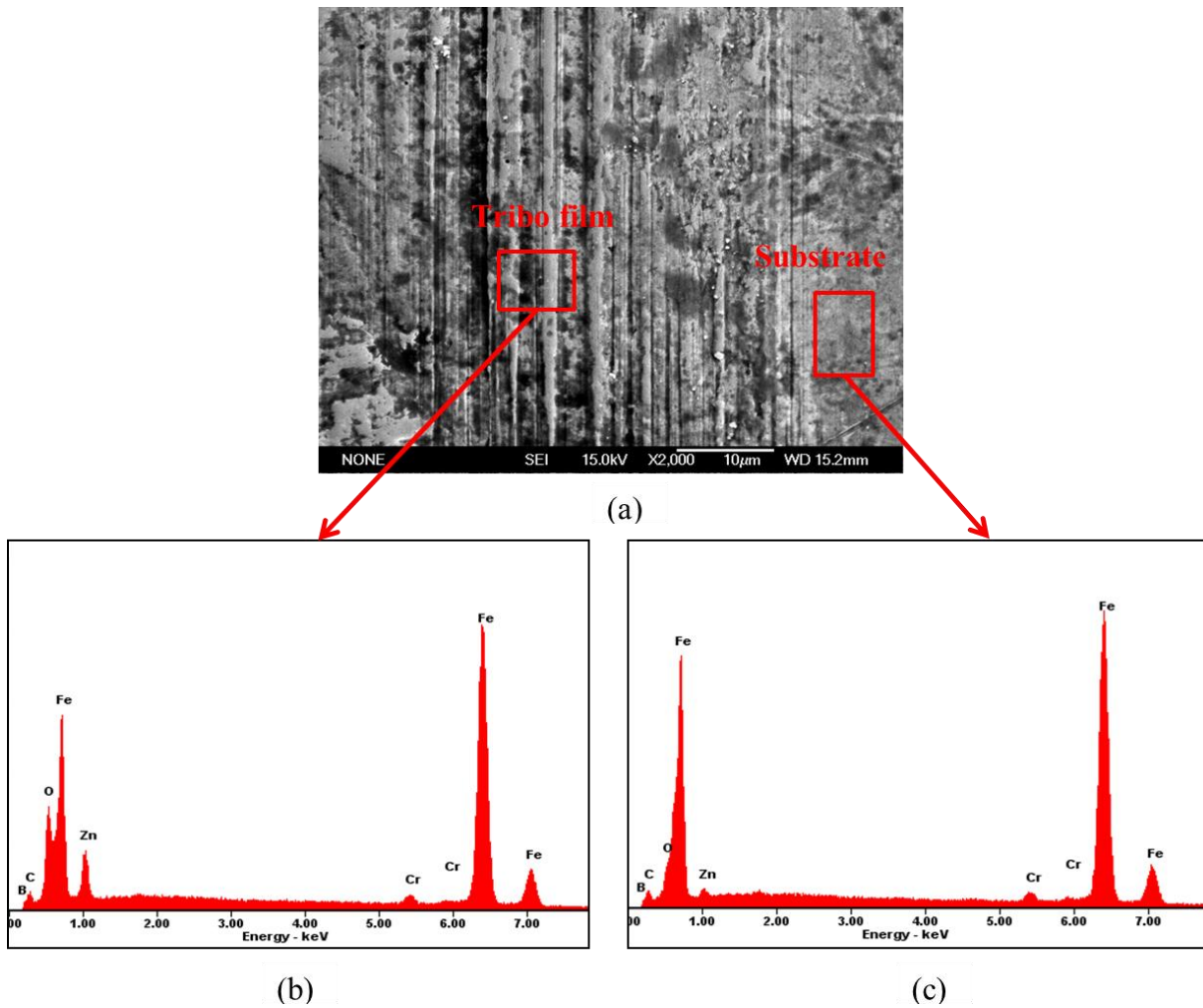
Figure 8–10. SEM images and EDS patterns of worn surfaces lubricated with
LP with HDTMOS-ZB UFPs: (a) worn surface morphology; (b) EDS
patterns of the tribo-film; (c) EDS patterns of substrate

Table 8-4 Quantified elemental analysis on worn surface shown in Figure 8–
10

Element	Spectrum (b) (At%)	Spectrum (c) (At%)
B	24.53	26.54
C	25.10	22.78
O	15.67	12.11
Zn	4.63	1.78
Cr	0.62	0.77
Fe	29.45	36.02

8.6.2   Discussion

Surface modified ZB UFPs have demonstrated the excellent tribological properties as lubricant additives in LP. HDTMOS-ZB UFPs have revealed a superior anti-wear property to conventional OA-ZB UFPs. Direct metal contact and adhesion were reduced by the third body effect of ZB UFPs, when the particles were entrapped into contact area as a result of friction force [7]. As discussed in Chapter 7, a reduction of adhesion is directly responsible for the reduction of friction and wear, especially at the beginning of the experiment when both friction and wear caused by adhesion were dominant. This explains why the initial friction coefficients of all lubricant samples that contain either original or modified ZB UFPs are lower than the friction coefficient of pure LP as shown in Figure 8–4.

As the sliding continues, ploughings take place and debris is also produced. A tribo-film is formed on the contact surfaces as a result of interaction between chemical components of the lubricant with the lubricated surface. The formation of tribo-film is associated with a decrease of wear. At all times the high wear loss was associated with small and patchy tribo-film fragments observed on the worn surface. On the contrary, the low wear loss was obtained when more complete tribo-films were formed. The test results suggest that the formation of tribo-film is greatly influenced by the dispersibility of ZB UFPs in LP. Solid lubricant additives with big particle size may sometime behave like abrasive particles, which will encourage the generation of debris and destruction of tribo-film and eventually increase wear. Whereas an increase of the amount of debris and tribo-film fragments in the lubricant can be beneficial to a reduction of friction coefficient. As a result, original ZB UFPs demonstrated the highest wear loss due to its poor dispersibility in LP and still the lowest friction coefficient was observed when this lubricant sample was applied.

When HDTMOS-ZB UFPs were employed as the lubricant additive in LP, the best anti-wear performance was delivered due to the formation of a complete and tenacious tribo-film with a lower hardness and reduced modulus than substrate steel. This outstanding anti-wear performance can be explained with *the delamination theory of wear* [105]. As stated in the discussion section of Chapter 6, dislocations will pile up at the interface between the tribo-film and the substrate, when a thin layer of tribo-film with low hardness and reduced modulus is generated on the hard substrate. As the sliding continues, these dislocations escape through the tribo-film on the surface due to its very small thickness [186]. For a surface without tribo-film, the dislocations will be transferred and generated within the substrate material as a result of very high stresses, on the other hand, the transfer of dislocations from tribo-film to substrate metal will be considerably less owing to the lower tangential force transmitted. Therefore the wear of material protected by tribo-film will be remarkably reduced or delayed.

EDS analysis suggests that zinc borate additive is a critical component for the formation of a robust tribo-film. For this reason, the stability of additive particles in base oil plays an important role in the formation of tribo-film. Compared with original ZB UFPs, OA-ZB UFPs have better stability in LP although the particle size does not appear to be reduced. HDTMOS-ZB UFPs have demonstrated the best stability and the smallest conglomerate size in organic solvent, which suggests that HDTMOS-ZB UFPs may have better integration with base oil and easier access to the contact interface. Therefore, the film forming ability and completeness of the tribofilm can be improved when HDTMOS-ZB UFPs are used as a lubricant additive.

8.7   Summary

This chapter presents the effects of surface modification of zinc borate ultrafine powders (ZB UFPs) on their tribological properties as lubricant additives in liquid paraffin (LP). ZB UFPs

were successfully modified with an employment of oleic acid (OA) and hexadecyltrimethoxysilane (HDTMOS). The modified ZB UFPs were characterised by means of infrared spectroscopy (IR) and Thermal gravimetric analysis (TGA). Compared with other additive samples, HDTMOS modified zinc borate ultrafine powder (HDTMOS-ZB UFPs) delivered a smaller conglomerate size and superior stability in the organic solvent. Tribological properties of LP with original and modified ZB UFPs were investigated using a pin-on-disc tribo tester. The highest wear reduction was observed when the HDTMOS–ZB UFPs were used in liquid paraffin. The worn surfaces of the tested pins were analysed by atomic force microscopy (AFM) and scanning electron microscopy (SEM). A continuous and tenacious tribo-film was generated on the worn surface when HDTMOS–ZB UFPs were employed as the lubricant additive in LP. The mechanical properties and elemental composition of the tribo-film were studied with nano-indentation and energy-dispersive X-ray spectroscopy (EDS). The test results suggest that this tribo-film with content of Fe, O, C, Zn, and B elements has a smaller hardness and reduced modulus than substrate material. The formation of this tribo-film appears to have played an important role in the outstanding anti-wear performance. This investigation suggests that with the appropriate surface modifications the tribological properties of zinc borate ultrafine powders as lubricant additives in liquid paraffin can be improved. Base on the above results, this part can be summarized as follow:

- Oleic acid (OA) and hexadecyltrimethoxysilane (HDTMOS) modified UFPs were successfully prepared. Without surface modification, original ZB UFPs did not demonstrate any anti-wear performance although the friction coefficient of LP was considerably reduced with the employment of the unmodified lubricant additive.

- The modified ZB UFPs as lubricant additives in LP displayed superior anti-wear performance to LP and LP with ZB UFPs. Compared with O-ZB UFPs, the HDTMOS-ZB

UFPs demonstrated much greater improvement on anti-wear property when it was used in LP, and it also exhibited better stability and smaller conglomerate size in organic solvent.

- The outstanding anti-wear performance of HDTMOS-ZB UFPs is attributed to the formation of a complete and tenacious tribo-film on worn surface. This tribo-film with content of Fe, O, C, Zn, and B elements has a smaller hardness and reduced modulus than the substrate material.

- The changes on the size and profile of the tribo-films were discovered when different lubricant samples were employed. It is evident that the coverage of the tribo-films on the worn surfaces has a good consistence with wear intensity. A good coverage of tribo-film can protect the surface from wear effectively. Only small patchy pieces of film were found on the worn surfaces lubricated by LP and LP with ZB UFPs. The larger fragments with elongated shape were observed on the worn surface when LP with OA-ZB was used. The best coverage by tribo-film was achieved by using LP with HDTMOS-ZB as the lubricant.

Chapter 9.   Conclusions and Suggestion for Future Work

9.1   Conclusions

The work in this thesis was carried out to investigate the influence of solid particle additives on the tribological properties of lubricants. Two types of solid particles, Ceria nanoparticles and Zinc borate ultrafine powders, were employed as the lubricant additives in this study. Although extensive research has been done on the applications of solid lubricant additives in the past, information on these two types of solid particles, Ceria nanoparticles and Zinc borate ultrafine powders, is still very limited. Surface modification technique was employed to improve the dispersibility of these particles in base lubricants. Conventional modification agent Oleic acid (OA) and the novel modification agent Hexadecyltrimethoxysilane (HDTMOS) were used to modify the solid particle surfaces and their modification performances were also compared in this study. The friction and wear behaviours of these two types of solid lubricant additives (with or without surface modification) in different base lubricants were identified. The distinctive friction and wear behaviours of Ceria nanoparticles and Zinc borate ultrafine powders reflected the different functionalities of these two solid lubricant additives in base lubricants.

This section concludes this study with regard to the tribological performance, the tribo film properties, surface modification of the solid lubricant additives, and the functionalities of the solid lubricant additives.

9.1.1 Tribological performance of ceria nanoparticles and zinc borate ultrafine powders

9.1.1.1 Friction reduction

9.1.1.1.1 Original solid particles without surface modification

The two types of solid particles behave differently when they are used as lubricant additive without surface modification. In the application of Ceria (CeO_2) nanoparticles, CeO_2 nanoparticles did not show a noticeable contribution to the reduction of friction when they were used alone. However when surfactant Sorbitan monostearate was employed to enhance the dispersibility of CeO_2 nanoparticles in water, the application of this additive was capable of reducing friction coefficient of water effectively. Different phenomenon was found in the application of Zinc borate ultrafine powders (ZB UFPs) as lubricant additive. Evident friction reduction was observed when original ZB UFPs were added in sunflower oil and liquid paraffin. These differences in friction reduction performances of CeO_2 nanoparticles and ZB UFPs can be attributed to the dissimilar properties that the two particles hold. As a metal oxide, CeO_2 nanoaprticles are chemically inert and reactions with substrate and base lubricants are not expected. During friction, the agglomeration of CeO_2 nanoparticles forms much bigger sized clusters, which can increase the asperity level between the contacting surfaces and cause more abrasive friction. On the other hand, it has be widely reported that when zinc borate particles were used as lubricant additive, diboron trioxide and iron boride can be formed by tribo-chemical reactions. These tribo chemical reactions that take place during sliding of two surfaces are possibly responsible for the reduction on friction coefficient observed when ZB UFPs were used as lubricant additive.

9.1.1.1.2   Surface modified solid particles

An increase on friction coefficient was noticed when OA and HDTMOS modified CeO_2 nanoparticles and ZB UFPs were used as lubricant additives. The application of HDTMOS modified particles in base lubricant have resulted in the greatest growth in friction. The improved tribo film coverage and enlarged fragment size of tribo film are the possible explanation for this phenomenon. During sliding, as a result of plastic flow, soft tribo-films could easily pile up in front of the asperities and cause more resistance for manoeuvre. At the same time the change on surface topography introduced by the piled-up thick tribo-films may also cause a barrier effect and lead to local breakage of oil film.

9.1.1.2   Antiwear performance

Very consistent wear performances were observed for both types of solid particles. Unmodified solid particles caused the most severe wear when they were used as lubricant additives in liquid paraffin (LP), while the surface modified solid particle effectively improved the wear resistance of the base lubricant. Especially, LP with HDTMOS modified particles delivered the most remarkable antiwear performance. Also the antiwear performance is closely related with the morphology and coverage of the tribo-films generated on the contact interface. Outstanding antiwear performance is always associated with a tenacious tribo film of good surface coverage.

9.1.2   Tribo film properties

The mechanical property of the tribo-films generated on the surface lubricated by lubricant samples were analysed by a nano indentation device. It is evident that tribo-film is made of a softer material with lower stiffness compared with the substrate steel. The thickness of the tribo-films was also determined and was in the scale of few hundred nanometres.

9.1.3   Surface modification of solid particles

Surface modification of the solid particles was involved in the study to improve the dispersibility of these particles in base lubricants. Oleic acid (OA) and Hexadecyltrimethoxysilane (HDTMOS) were selected as the modification agents. Compared with OA, HDTMOS has demonstrated a superior performance in stabilizing solid particles and reducing wear as the surface modification agent of solid lubricant additives.

As demonstrated by the experimental results, surface modified particles have all given higher Zeta-potential measurements in organic solvent, which suggests that surface modification have successfully improved the stability of solid particles in an organic solvent. Between the two modification agents, HDTMOS modified solid particles revealed higher Zeta-potential values than OA modified solid particles. Furthermore, OA modified particles failed to show a consistent reduction of particle conglomerate size. However, the particle conglomerate size was considerably reduced when HDTMOS was used as the modification agent. Therefore, it can be concluded that HDTMOS performs better as a surface modification agent than the conventional OA.

9.1.4   Functionality of solid lubricant additives

In this study, CeO_2 nanoparticles and ZB UFPs have all demonstrated the good potentials to be employed as solid lubricant additives. Depending on the intrinsic character of each type of particles, the way they perform as solid lubricant additive also varies. Third body effect is the common functionality shared by CeO_2 nanoparticles and ZB UFPs. The phenomenons associated with this effect, particularly the reduction in adhesion friction, are mostly contributed by the physical characteristics of the two solid particles. As the sliding continues, ZB UFPs are capable of assisting in the tribochemical reaction with substrate steel and

surrounding lubricant, and form diboron trioxide and iron boride which are potentially important on improving the lubricating performance of a system. Although, no evidence was found to support that CeO_2 nanoparticles would be able to encourage the tribochemical reaction directly, it is clearly demonstrated that CeO_2 nanoparticles function as a physical carrier to effectively deliver the HDTMOS surfactant to contact surfaces and increase localised concentration of HDTMOS surfactant. In this way CeO_2 nanoparticles become an essential ingredient for the generation of a healthy tribo film.

9.2 Future work

Although the present work have systematically investigated the tribological properties of the original and surface modified Ceria nanoparticles and Zinc borate ultrafine powders, there is still a plenty of work for further development. The recommendations are outlined below:

Base lubricant

In the present study, original and surface modified Ceria nanoparticles and Zinc borate ultrafine powders were used as the only lubricant additive in base lubricants. It is still an unknown question how they would behave in a commercial lubricant environment where a package of lubricant additives is used and the interactions of solid lubricant additives with other lubricant additives are inevitable.

Surface modification

Surface modifications of Ceria nanoparticles and Zinc borate ultrafine powders using modification agents, Oleic acid and Hexadecyltrimethoxysilane, were conducted and a consistent modification procedure was applied throughout the present study. Modification procedures and controlling parameters are of great importance to the performance of the final

171

products. However in current study it is still an open question that how these parameters affect the modification reaction.

Chemical analysis of tribo-film

Elemental analysis of the tribo-film was carried out with Energy-dispersive X-ray spectroscopy (EDS), however the accuracy of the spectrum can be easily affected by the nature of the sample such as homogeneity and roughness. Also not enough information can be provided by this analysis technique to identify a complex chemical compound. In comparison, X-ray photoelectron spectroscopy (XPS) and Secondary ion mass spectrometry (SIMS) are going to be particularly helpful on identifying the composition of a tribo film and its forming mechanisms.

Influence of the experimental conditions

Influences of the experimental conditions such as sliding speed, contact pressure are proven to be the important influential factors for the performance of solid lubricant additives. Further work in the future is required to identify the effect of sliding speed and contact pressure.

References

1. SunQing, Q., D. JunXiu, and C. Guoxu, *Wear and friction behaviour of CaCO₃ nanoparticles used as additives in lubricating oils.* Lubrication Science, 2000. 12(2): p. 205-212.

2. Peng, D., et al., *Tribological properties of diamond and SiO₂ nanoparticles added in paraffin.* Tribology International, 2009. 42(6): p. 911-917.

3. Bhushan, B., et al., *Fullerene (C60) films for solid lubrication.* Tribology Transactions, 1993. 36(4): p. 573-580.

4. Ouyang, Q. and K. Okada, *Nano-ball bearing effect of ultra-fine particles of cluster diamond.* Applied Surface Science, 1994. 78(3): p. 309-313.

5. Chen, L., et al., *Nanofluids containing carbon nanotubes treated by mechanochemical reaction.* Thermochimica acta, 2008. 477(1–2): p. 21-24.

6. Wu, Y.Y. and M.J. Kao, *Using TiO₂ nanofluid additive for engine lubrication oil.* Industrial Lubrication and Tribology, 2011. 63(6): p. 440-445.

7. Godet, M., *The third-body approach: a mechanical view of wear.* Wear, 1984. 100(1-3): p. 437-452.

8. Tao, X., Z. Jiazheng, and X. Kang, *The ball-bearing effect of diamond nanoparticles as an oil additive.* Journal of Physics D: Applied Physics, 1999. 29(11): p. 2932.

9. Zhou, J., et al., *Tribological behavior and lubricating mechanism of Cu nanoparticles in oil.* Tribology Letters, 2000. 8(4): p. 213-218.

10. Dowson, D., *History of tribology*1979: Longman London.

11. Thomas, T.R., *Rough surfaces*1999: World Scientific.

12. Whitehouse, D.J., *Handbook of surface and nanometrology*2010: CRC.

13. Buckley, D.H., *Surface effects in adhesion, friction, wear, and lubrication*. Vol. 5. 1981: Elsevier.

14. Bhushan, B., *Introduction to tribology*2002: Wiley.

15. Samuels, L.E., *Damaged surface Layers: Metals*, in *The surface Chemistry of Metals and Semiconductors*, e. H.C. Gatos, Editor 1960, Wiley: New York. p. 82-103.

16. Bhushan, B., *Tribology and mechanics of magnetic storage devices*1996: Springer New York.

17. Shaw, M.C., *Metal cutting principles*. Vol. 19. 2005: Oxford University Press Oxford.

18. Cook, N. and B. Bhushan, *Sliding surface interface temperatures(Solid-solid interface temperature rise during sliding from model with surface topography statistics, frictional conditions, surface hardness and thermal parameters).* ASME, Transactions, Series F-Journal of Lubrication Technology, 1973. 95: p. 59-64.

19. Ling, F.F., E.E. Klaus, and R. Fein, *BOUNDARY LUBRICATION.* 1969: p. 39-60.

20. Hayward, D.O. and B.M.W. Trapnell, *Chemisorption*1964: Butterworths London.

21. Rivière, J.C., *Surface analytical techniques*1990: Clarendon Press. Oxford University Press.

22. Montaser, A., et al., *An introduction to ICP spectrometries for elemental analysis.* Inductively coupled plasma mass spectrometry, 1998: p. 1-31.

23. Osán, J., et al., *Light element analysis of individual microparticles using thin-window EPMA.* Microchimica Acta, 2000. 132(2): p. 349-355.

24. Hofmann, S., *Practical surface analysis: state of the art and recent developments in AES, XPS, ISS and SIMS.* Surface and Interface Analysis, 1986. 9(1): p. 3-20.

25. Leroy, V., *Metallurgical applications of surface analytical techniques.* Materials Science and Engineering, 1980. 42(0): p. 289-307.

26. Heuberger, R., A. Rossi, and N.D. Spencer, *XPS study of the influence of temperature on ZnDTP tribofilm composition.* Tribology Letters, 2007. 25(3): p. 185-196.

27. Minfray, C., et al., *Chemistry of ZDDP tribofilm by ToF-SIMS.* Tribology Letters, 2004. 17(3): p. 351-357.

28. Bennett, J. and L. Mattsson, *Introduction to surface roughness and scattering.* Introduction to Surface Roughness and Scattering by Jean Bennett, Lars Mattsson Washington DC: Optical Soceity of America, 1989, 1989. 1.

29. KELLNER, H.L. *MEASUREMENT OF SURFACE SMOOTHNESS*. in *Proceedings of the... Annual Convention*. 1950. The Society.

30. Liu, J.J., Y. Chen, and Y.Q. Cheng, *The generation of wear debris of different morphology in the running-in process of iron and steels.* Wear, 1992. 154(2): p. 259-267.

31. Fuller, K. and D. Tabor, *The effect of surface roughness on the adhesion of elastic solids.* Proceedings of the Royal Society of London. A. Mathematical and Physical Sciences, 1975. 345(1642): p. 327-342.

32. Texture, S., *Surface Roughness, Waviness and Lay.* American Society of Mechanical Engineers Standard B, 1995. 46: p. 1.

33. Zhang, J., *Influence of succinimide dispersants on film formation, friction and antiwear properties of zinc dialkyl dithiophosphate*, 2012, Imperial College London (University of London).

34. Wen, S. and P. Huang, *Principles of tribology*2012: Wiley.

35. Svahn, F., Å. Kassman-Rudolphi, and E. Wallén, *The influence of surface roughness on friction and wear of machine element coatings.* Wear, 2003. 254(11): p. 1092-1098.

36. Persson, B., et al., *On the nature of surface roughness with application to contact mechanics, sealing, rubber friction and adhesion.* Journal of Physics: Condensed Matter, 2004. 17(1): p. R1.

37. Organization, I.S., *Instruments for the Measurement of Surface Roughness by Profile Methods*, 1975.

38. Bhushan, B., *Contact mechanics of rough surfaces in tribology: multiple asperity contact.* Tribology Letters, 1998. 4(1): p. 1-35.

39. Hironaka, S., *Boundary lubrication and lubricants.* Three Bond Technical News, 1984. 9.

40. Hertz, H., *Über die Berührung fester elastischer Körper.* J. für die reine u. angew. Math., 1882. 92.

41. Johnson, K., K. Kendall, and A. Roberts, *Surface energy and the contact of elastic solids.* Proceedings of the Royal Society of London. A. Mathematical and Physical Sciences, 1971. 324(1558): p. 301-313.

42. Pashley, M., *Further consideration of the DMT model for elastic contact.* Colloids and surfaces, 1984. 12: p. 69-77.

43. Dowson, D., *A generalized Reynolds equation for fluid-film lubrication.* International Journal of Mechanical Sciences, 1962. 4(2): p. 159-170.

44. Christensen, H., *A theory of mixed lubrication.* Proceedings of the Institution of Mechanical Engineers, 1972. 186(1): p. 421-430.

45. Blok, H., *Fundamental mechanical aspects of boundary lubrication.* SAE Journal, 1940(2).

46. Lindsay, N., et al., *Characterization of films formed at a lubricated cam/tappet contact.* Spectrochimica Acta Part A: Molecular Spectroscopy, 1993. 49(13): p. 2057-2070.

47. Klaus, E., et al. *The Adsorption of Tribochemical reaction products at solid surfaces.* 1987.

48. Stribeck, R., *Kugellager für beliebige Belastungen*1901: Buchdruckerei AW Schade, Berlin N.

49.   Stribeck, P., *Die wesentlichen Eigenschaften der Gleit-und Rollenlager*. Z. Ver. Dt. Ing, 1902. 46(38): p. 1341-1348.

50.   Bieber, H., E. Klaus, and E. Tewksbury, *A study of tricresyl phosphate as an additive for boundary lubrication*. ASLE TRANSACTIONS, 1968. 11(2): p. 155-161.

51.   Cann, P. and A. Cameron, *Studies of thick boundary lubrication — influence of zddp and oxidized hexadecane*. Tribology International, 1984. 17(4): p. 205-208.

52.   Heyes, D.M., *Molecular aspects of boundary lubrication*. Tribology International, 1996. 29(8): p. 627-629.

53.   Hsu, S.M. and R.S. Gates, *Boundary lubricating films: formation and lubrication mechanism*. Tribology International, 2005. 38(3): p. 305-312.

54.   Zhang, Y., *Boundary lubrication—An important lubrication in the following time*. Journal of Molecular Liquids, 2006. 128(1–3): p. 56-59.

55.   Lu, X., M. Khonsari, and E. Gelinck, *The Stribeck curve: experimental results and theoretical prediction*. Journal of tribology, 2006. 128: p. 789.

56.   Wells, H.M., Southcombe, J.E., *The theory and practice of lubrication: The "Germ-Process"*. J. Soc. of Chem. Lond., 1920. 39: p. 51T-60T.

57.   Boye, H.a., K o l l o i d - Z., 1932. 59: p. 153.

58.   Frewing, J.J., *The heat of adsorption of long-chain compounds and their effect on boundary lubrication*. Proceedings of the Royal Society of London. Series A. Mathematical and Physical Sciences, 1944. 182(990): p. 270-285.

59.   Daniel, S., *The adsorption on metal surfaces of long chain polar compounds from hydrocarbon solutions*. Transactions of the Faraday Society, 1951. 47: p. 1345-1359.

60.   Greenhill, E., *The adsorption of long chain polar compounds from solution on metal surfaces*. Transactions of the Faraday Society, 1949. 45: p. 625-631.

61.   Hardy, W. and I. Doubleday, *Boundary lubrication. The paraffin series*. Proceedings of the Royal Society of London. Series A, 1922. 100(707): p. 550-574.

62.   Langmuir, I., *The mechanism of the surface phenomena of flotation*. Transactions of the Faraday Society, 1920. 15(June): p. 62-74.

63.   Bailey, A.I. and J. Courtney-Pratt, *The area of real contact and the shear strength of monomolecular layers of a boundary lubricant*. Proceedings of the Royal Society of London. Series A, Mathematical and Physical Sciences, 1955: p. 500-515.

64.   Roberts, G., *Langmuir-Blodgett films*. Contemporary Physics, 1984. 25(2): p. 109-128.

65.   Bowden, F.T., *Friction and lubrication of solids, Part I*1950, Oxford, UK: Clarendon Press.

66. Zisman, W.A., *Durability and Wettability Properties of Monomolecular Films on Solids*, in *Friction and Wear*1959, Elsevier: Amsterdam. p. 110-148.

67. Owens, D.K., *Friction of polymer films. I. Lubrication.* Journal of Applied Polymer Science, 1964. 8(3): p. 1465-1475.

68. Fein, R.S. and K.L. Kreuz, *Chemistry of Boundary Lubrication of Steel by Hydrocarbons.* A S L E Transactions, 1965. 8(1): p. 29-38.

69. Smeeth, M., H. Spikes, and S. Gunsel, *Boundary film formation by viscosity index improvers.* Tribology Transactions, 1996. 39(3): p. 726-734.

70. Yamaguchi, E., et al., *Boundary film formation by ZnDTPs and detergents using ECR.* Tribology Transactions, 1998. 41(2): p. 262-272.

71. Hsu, S.M. and R. Gates, *Boundary lubricating films: formation and lubrication mechanism.* Tribology International, 2005. 38(3): p. 305-312.

72. Habboush, A.E., S.M. Farroha, and H.I. Khalaf, *Extraction-gas chromatographic method for the determination of organophosphorus compounds as lubricating oil additives.* Journal of Chromatography A, 1995. 696(2): p. 257-263.

73. Spikes, H., *Low‐and zero‐sulphated ash, phosphorus and sulphur anti‐wear additives for engine oils.* Lubrication Science, 2008. 20(2): p. 103-136.

74. Godfrey, D., *The lubrication mechanism of tricresyl phosphate on steel.* ASLE TRANSACTIONS, 1965. 8(1): p. 1-11.

75. Fox, M. and M. Priest, *Tribological properties of ionic liquids as lubricants and additives. Part 1: synergistic tribofilm formation between ionic liquids and tricresyl phosphate.* Proceedings of the Institution of Mechanical Engineers, Part J: Journal of Engineering Tribology, 2008. 222(3): p. 291-303.

76. Li, B., et al., *Tribochemistry and antiwear mechanism of organic–inorganic nanoparticles as lubricant additives.* Tribology Letters, 2006. 22(1): p. 79-84.

77. Gunsel, S., H.A. Spikes, and M. Aderin, *In-Situ Measurement of ZDDP Films in Concentrated Contacts.* Tribology Transactions, 1993. 36(2): p. 276-282.

78. Spikes, H., *The history and mechanisms of ZDDP.* Tribology Letters, 2004. 17(3): p. 469-489.

79. Zhang, M., et al., *Performance and anti-wear mechanism of $CaCO_3$ nanoparticles as a green additive in poly-alpha-olefin.* Tribology International, 2009. 42(7): p. 1029-1039.

80. Hernández Battez, A., et al., *CuO, ZrO_2 and ZnO nanoparticles as antiwear additive in oil lubricants.* Wear, 2008. 265(3-4): p. 422-428.

81. Huang, H., et al., *An investigation on tribological properties of graphite nanosheets as oil additive.* Wear, 2006. 261(2): p. 140-144.

82. Xue, Q., W. Liu, and Z. Zhang, *Friction and wear properties of a surface-modified TiO2 nanoparticle as an additive in liquid paraffin.* Wear, 1997. 213(1-2): p. 29-32.

83. Zhou, J., et al., *Study on an antiwear and extreme pressure additive of surface coated LaF₃ nanoparticles in liquid paraffin.* Wear, 2001. 249(5-6): p. 333-337.

84. Dong, J. and Z. Hu, *A study of the anti-wear and friction-reducing properties of the lubricant additive, nanometer zinc borate.* Tribology International, 1998. 31(5): p. 219-223.

85. Swalen, J.D., et al., *Molecular monolayers and films. A panel report for the materials sciences division of the department of energy.* Langmuir, 1987. 3(6): p. 932-950.

86. Cusano, C. and H. Sliney, *Dynamics of solid dispersions in oil during the lubrication of point contacts, Part I—Graphite.* ASLE TRANSACTIONS, 1982. 25(2): p. 183-189.

87. Olomolehin, Y., *The influence of zinc dialkyldithiophosphate and other lubricant additives on soot-induced wear*, 2009, Imperial College London.

88. Guangteng, G. and H. Spikes, *Boundary film formation by lubricant base fluids.* Tribology Transactions, 1996. 39(2): p. 448-454.

89. Cao, L.L., Y.M. Sun, and L.Q. Zheng, *Chemical structure characterization of the boundary lubrication film using X-ray photoelectron spectroscopy and scanning Auger microprobe techniques.* Wear, 1990. 140(2): p. 345-357.

90. Chen, B., et al., *Friction and wear performances of borates and lanthanum chloride in water.* Journal of Rare Earths, 2008. 26(4): p. 590-593.

91. Hu, Z., et al., *Preparation and tribological properties of nanometer magnesium borate as lubricating oil additive.* Wear, 2002. 252(5-6): p. 370-374.

92. KONG, L., et al., *Synthesis and surface modification of the nanoscale cerium borate as lubricant additive.* Journal of Rare Earths, 2011. 29(11): p. 1095-1099.

93. Zhao, F., et al., *Tribological properties of serpentine, La(OH)₃ and their composite particles as lubricant additives.* Wear, 2012. 288(0): p. 72-77.

94. Guangteng, G. and H.A. Spikes, *The Control of Friction by Molecular Fractionation of Base Fluid Mixtures at Metal Surfaces.* Tribology Transactions, 1997. 40(3): p. 461-469.

95. Foord, C.A., W.C. Hammann, and A. Cameron, *Evaluation of Lubricants Using Optical Elastohydrodynamics.* A S L E Transactions, 1968. 11(1): p. 31-43.

96. Johnston, G., R. Wayte, and H. Spikes, *The measurement and study of very thin lubricant films in concentrated contacts.* Tribology Transactions, 1991. 34(2): p. 187-194.

97. Spikes, H.A., *Direct Observation of Boundary Layers†.* Langmuir, 1996. 12(19): p. 4567-4573.

98. Spikes, H., *Thin films in elastohydrodynamic lubrication: the contribution of experiment.* Proceedings of the Institution of Mechanical Engineers, Part J: Journal of Engineering Tribology, 1999. 213(5): p. 335-352.

99. Spikes, H. and P. Cann, *The development and application of the spacer layer imaging method for measuring lubricant film thickness.* Proceedings of the Institution of Mechanical Engineers, Part J: Journal of Engineering Tribology, 2001. 215(3): p. 261-277.

100. Binnig, G. and H. Rohrer, *Scanning tunneling microscopy.* Surface Science, 1983. 126(1): p. 236-244.

101. Hutchings, I.M., *Tribology: friction and wear of engineering materials* 1992: Butterworth-Heinemann Ltd.

102. Khruschov, M.M., *Principles of abrasive wear.* Wear, 1974. 28(1): p. 69-88.

103. Vinsbo, O. *Wear and Wear Mechanisms.* in *Wear of Materials Conf. ASME.* 1979. New York.

104. Rabinowicz, E., *Friction and wear of materials.* Vol. 2. 1965: Wiley New York.

105. P Suh, N., *The delamination theory of wear.* Wear, 1973. 25(1): p. 111-124.

106. Xu, J., K. Kato, and T. Hirayama, *The transition of wear mode during the running-in process of silicon nitride sliding in water.* Wear, 1997. 205(1): p. 55-63.

107. Brown, R.D., *Test Method*, in *BOUNDARY LUBRICATION. AN APPRAISAL OF WORLD LITERATURE* F.F. Ling, E.E. Klaus, and R. Fein, Editors. 1969, ASME: New York. p. 341-392.

108. Blau, P.J. and K.G. Budinski, *Development and use of ASTM standards for wear testing.* Wear, 1999. 225: p. 1159-1170.

109. Schöfer, J. and E. Santner, *Quantitative wear analysis using atomic force microscopy.* Wear, 1998. 222(2): p. 74-83.

110. Jagtap, R. and A. Ambre, *Overview literature on atomic force microscopy (AFM): Basics and its important applications for polymer characterization.* Indian Journal of Engineering and Materials Sciences, 2006. 13(4): p. 368.

111. Cameron, A. and R. Gohar, *Theoretical and experimental studies of the oil film in lubricated point contact.* Proceedings of the Royal Society of London. Series A. Mathematical and Physical Sciences, 1966. 291(1427): p. 520-536.

112. Dawson, T.G. and T.R. Kurfess, *Quantification of tool wear using white light interferometry and three-dimensional computational metrology.* International Journal of Machine Tools and Manufacture, 2005. 45(4–5): p. 591-596.

113. Gåhlin, R. and S. Jacobson, *A novel method to map and quantify wear on a micro-scale.* Wear, 1998. 222(2): p. 93-102.

114. Asher, J., et al., *Thin layer activation: A technique for monitoring material loss during high temperature surface degradation processes.* Materials Science and Engineering, 1987. 88(0): p. 143-150.

115. Boumans, P.W.J.M., *Inductively coupled plasma emission spectroscopy. Part II: applications and fundamentals. Volume 2.* Other Information: From review by Edward H. Piepmeier, Oregon State Univ., in J. Am. Chem. Soc., Vol. 110, No. 11 (1988)1987. Medium: X; Size: Pages: 498.

116. Fan, J. and H. Spikes, *New Test for Mild Lubricated Wear in Rolling-Sliding Contacts.* Tribology Transactions, 2007. 50(2): p. 145-153.

117. Bowden, F.P. and D. Tabor, *The friction and lubrication of solids.* Clarendon Press, 1986, 1986: p. 374.

118. Amontons, G., *De la résistance causée dans les machines.* Mémoires de l'Académie des Sciences, 1699: p. 257-282.

119. Coulomb, *Théorie des machines simples, en ayant égard au frottement de leurs parties et la roideur des cordages.* Mémoires de Mathématique et de Physique, presentés à L'Académie Royales des Sciences, 1785. 10: p. 161-342.

120. Bowden, F. and D. Tabor, *The friction and lubrication of solids, part II*, 1964, Clarendon Press, Oxford.

121. Courtney-Pratt, J.S. and E. Eisner, *The Effect of a Tangential Force on the Contact of Metallic Bodies.* Proceedings of the Royal Society of London. Series A. Mathematical and Physical Sciences, 1957. 238(1215): p. 529-550.

122. Greenwood, J. and D. Tabor, *The friction of hard sliders on lubricated rubber: the importance of deformation losses.* Proceedings of the Physical Society, 1958. 71(6): p. 989.

123. Rigney, D.A. and J.P. Hirth, *Plastic deformation and sliding friction of metals.* Wear, 1979. 53(2): p. 345-370.

124. Moore, D.F., *The Friction and Lubrication of Elastomers*1972, Oxford, UK: Pergamon.

125. Suh, N.P. and H.C. Sin, *The genesis of friction.* Wear, 1981. 69(1): p. 91-114.

126. Buckley, D.H., *Surface films and metallurgy related to lubrication and wear.* Progress in Surface Science, 1982. 12(1): p. 1-153.

127. Blau, P.J., *On the nature of running-in.* Tribology International, 2005. 38(11–12): p. 1007-1012.

128. Blau, P.J., *Friction and wear transitions of materials*1989. Medium: X; Size: Pages: (476 p).

129. Port Huron, P.H., *GRAPHITE DISPERSIONS*, 1967: U.S.

130. James B. Peace, J.B.P., *SOLID LUBRICANT AND PIGMENT DISPERSIONS*, 1967: U.S.

131. Donald L. DeVries, J.M.D., *Solid particles containing lubricating oil composition*, 1978, Atlantic Richfield Company.

132. Apikos, D.A., *Graphited gear oils*, 1982, Atlantic Richfield Company: U.S.

133. Hong, R., et al., *Synthesis and surface modification of ZnO nanoparticles.* Chemical Engineering Journal, 2006. 119(2): p. 71-81.

134. Hu, Z., J. Dong, and G. Chen, *Study on antiwear and reducing friction additive of nanometer ferric oxide.* Tribology International, 1998. 31(7): p. 355-360.

135. Zhou, X., et al., *Study on the tribological properties of surfactant-modified MoS< sub> 2</sub> micrometer spheres as an additive in liquid paraffin.* Tribology International, 2007. 40(5): p. 863-868.

136. Yu, H., et al., *Effect of thermal activation on the tribological behaviours of serpentine ultrafine powders as an additive in liquid paraffin.* Tribology International, 2011.

137. Zhang, Z., et al., *The effect of LaF3 nanocluster modified with succinimide on the lubricating performance of liquid paraffin for steel-on-steel system.* Tribology International, 2001. 34(2): p. 83-88.

138. Chen, G., et al., *Preparation and tribology of ultrafine and amorphous strontium borate.* Proceedings of the Institution of Mechanical Engineers, Part L: Journal of Materials: Design and Applications, 2001. 215(3): p. 133-140.

139. Hu, Z., et al., *Preparation and tribological properties of nanoparticle lanthanum borate.* Wear, 2000. 243(1-2): p. 43-47.

140. Tarasov, S., et al., *Study of friction reduction by nanocopper additives to motor oil.* Wear, 2002. 252(1–2): p. 63-69.

141. Rapoport, L., et al., *Mechanism of friction of fullerenes.* Industrial Lubrication and Tribology, 2002. 54(4): p. 171-176.

142. Liu, G., et al., *Investigation of the Mending Effect and Mechanism of Copper Nano-Particles on a Tribologically Stressed Surface.* Tribology Letters, 2004. 17(4): p. 961-966.

143. Rapoport, L., et al., *Tribological properties of WS$_2$ nanoparticles under mixed lubrication.* Wear, 2003. 255(7): p. 785-793.

144. Xu, T., et al., *Study on the structure of surface-modified MoS$_2$ nanoparticles.* Materials research bulletin, 1996. 31(4): p. 345-349.

145. Kimura, Y., et al., *Boron nitride as a lubricant additive.* Wear, 1999. 232(2): p. 199-206.

146. Gansheimer, J. and R. Holinski, *Molybdenum Disulfide in Oils and Greases Under Boundary Conditions.* Journal of Lubrication Technology, 1973. 95(2): p. 242-246.

147. Rapoport, L., N. Fleischer, and R. Tenne, *Applications of WS2 (MoS2) inorganic nanotubes and fullerene-like nanoparticles for solid lubrication and for structural nanocomposites.* Journal of Materials Chemistry, 2005. 15(18): p. 1782-1788.

148. Yu, H.-l., et al., *Tribological properties and lubricating mechanisms of Cu nanoparticles in lubricant.* Transactions of Nonferrous Metals Society of China, 2008. 18(3): p. 636-641.

149. Chou, R., et al., *Tribological behavior of polyalphaolefin with the addition of nickel nanoparticles.* Tribology International, 2010. 43(12): p. 2327-2332.

150. Gao, Y., et al., *Study on tribological properties of oleic acid-modified TiO$_2$ nanoparticle in water.* Wear, 2002. 252(5–6): p. 454-458.

151. Hernández Battez, A., et al., *Wear prevention behaviour of nanoparticle suspension under extreme pressure conditions.* Wear, 2007. 263(7-12): p. 1568-1574.

152. Hu, Z. and J. Dong, *Study on antiwear and reducing friction additive of nanometer titanium oxide.* Wear, 1998. 216(1): p. 92-96.

153. Chen, Q., et al., *Enhanced tribology properties of ZnO/Al$_2$O$_3$ composite nanoparticles as liquid lubricating additives.* Journal of Sol-Gel Science and Technology, 2012. 61(3): p. 501-508.

154. Chunxiang, L.W.X.Q.H. and Z.X.W. Hanqing, *Study of the Antiwear Properties of Potassium Borate as an Oil Additive [J].* Tribology, 1992. 2: p. 010.

155. Normand, V., et al., *Micellar calcium borate as an antiwear additive.* Tribology Letters, 1998. 5(2-3): p. 235-242.

156. Hu, Z. and J. Dong, *Study on antiwear and reducing friction additive of nanometer titanium borate.* Wear, 1998. 216(1): p. 87-91.

157. Verwey, E.J.W., *Theory of the Stability of Lyophobic Colloids.* The Journal of Physical and Colloid Chemistry, 1947. 51(3): p. 631-636.

158. Yu, W., H. Xie, and L.H. Liu, *A Review on Nanofluids: Preparation, Stability Mechanisms, and Applications.* Journal of Nanomaterials, 2011. 2012(711): p. 128.

159. Kopperud, H.M., F.K. Hansen, and B. Nyström, *Effect of surfactant and temperature on the rheological properties of aqueous solutions of unmodified and hydrophobically modified polyacrylamide.* Macromolecular Chemistry and Physics, 1998. 199(11): p. 2385-2394.

160. Zhang, Z.J., J. Zhang, and Q.J. Xue, *Synthesis and Characterization of a Molybdenum Disulfide Nanocluster.* The Journal of Physical Chemistry, 1994. 98(49): p. 12973-12977.

161. Chen, S., W. Liu, and L. Yu, *Preparation of DDP-coated PbS nanoparticles and investigation of the antiwear ability of the prepared nanoparticles as additive in liquid paraffin.* Wear, 1998. 218(2): p. 153-158.

162. Chen, S. and W. Liu, *Preparation and Characterization of Surface-Coated ZnS Nanoparticles.* Langmuir, 1999. 15(23): p. 8100-8104.

163. Li, Z. and Y. Zhu, *Surface-modification of SiO_2 nanoparticles with oleic acid.* Applied Surface Science, 2003. 211(1-4): p. 315-320.

164. Fekete, E., et al., *Surface modification and characterization of particulate mineral fillers.* Journal of Colloid and Interface Science, 1990. 135(1): p. 200-208.

165. Papirer, E., J. Schultz, and C. Turchi, *Surface properties of a calcium carbonate filler treated with stearic acid.* European polymer journal, 1984. 20(12): p. 1155-1158.

166. Jia, Z. and Y. Xia, *Hydrothermal Synthesis, Characterization, and Tribological Behavior of Oleic Acid-Capped Lanthanum Borate with Different Morphologies.* Tribology Letters, 2011. 41(2): p. 425-434.

167. Liu, W., J.L. Duda, and E.E. Klaus, *Wear property of silicon nitride in steel-on-Si_3N_4 and Si_3N_4-on-Si_3N_4 systems.* Wear, 1996. 199(2): p. 217-221.

168. Sheng, C., S. Xiaodong, and L. Benlan, *Surface organic modification of Fe_3O_4 nanoparticles by silane-coupling agents.* Chinese Journal of Rare Metals, 2006. 25(z1).

169. Li, X., et al., *Surface-modification in situ of nano-SiO_2 and its structure and tribological properties.* Applied Surface Science, 2006. 252(22): p. 7856-7861.

170. Arkles, B., *Tailoring Surfaces with Silanes.* Chem Tech, 1977. 7: p. 13.

171. Lee, S.Y., et al., *Amino acid side chain-like surface modification on magnetic nanoparticles for highly efficient separation of mixed proteins.* Talanta, 2012. 93(0): p. 160-165.

172. Tanguchi, J., H. Murata, and Y. Okamura, *Analysis of aggregation and dispersion states of small particles in concentrated suspension by using diffused photon density wave spectroscopy.* Colloids and Surfaces B: Biointerfaces, 2010. 76(1): p. 137-144.

173. Sze, A., et al., *Zeta-potential measurement using the Smoluchowski equation and the slope of the current–time relationship in electroosmotic flow.* Journal of Colloid and Interface Science, 2003. 261(2): p. 402-410.

174. Borm, P.J.A., et al., *The potential risks of nanomaterials: a review carried out for ECETOC.* Particle and fibre toxicology, 2006. 3(1): p. 11.

175. Jiao, D., et al., *The tribology properties of alumina/silica composite nanoparticles as lubricant additives.* Applied Surface Science, 2011.

176. Hernandez Battez, A., et al., *The tribological behaviour of ZnO nanoparticles as an additive to PAO6.* Wear, 2006. 261(3–4): p. 256-263.

177. Hernández Battez, A., et al., *Friction reduction properties of a CuO nanolubricant used as lubricant for a NiCrBSi coating.* Wear, 2010. 268(1–2): p. 325-328.

178. Gu, C., et al., *Study on application of CeO2 and CaCO3 nanoparticles in lubricating oils.* Journal of Rare Earths, 2008. 26(2): p. 163-167.

179. Ru Yang, J.L., Ming Li, *Synthesis of mesoporous ceria using a non-surfactant template approach.* Journal of the Chinese Rare Earth Society, 2004. 22(6).

180. Evans, D.R., *Cerium Oxide Abrasives – Observations and Analysis.* MRS Online Proceedings Library, 2004. 816: p. null-null.

181. Yu, H., et al., *Tribological behaviors of surface-coated serpentine ultrafine powders as lubricant additive.* Tribology International, 2010. 43(3): p. 667-675.

182. Wasilewski, T. and M.W. Sulek, *Paraffin oil solutions of the mixture of sorbitan monolaurate–ethoxylated sorbitan monolaurate as lubricants.* Wear, 2006. 261(2): p. 230-234.

183. Savrık, S.A., D. Balköse, and S. Ülkü, *Synthesis of zinc borate by inverse emulsion technique for lubrication.* Journal of Thermal Analysis and Calorimetry, 2011. 104(2): p. 605-612.

184. Sułek, M. and T. Wasilewski, *Antiseizure properties of aqueous solutions of ethoxylated sorbitan esters.* Mat. Sci, 2003. 9: p. 187-190.

185. Hirth, J.P. and J. Lothe, *Theory of dislocations.* John Wiley and Sons, Inc., 1982, 1982: p. 857.

186. Ttsuya, Y. and R. Takagi, *Lubricating properties of lead films on copper.* Wear, 1964. 7(2): p. 131-143.

187. Yang, G.-b., et al., *Preparation and tribological properties of surface modified Cu nanoparticles.* Transactions of Nonferrous Metals Society of China, 2012. 22(2): p. 366-372.

188. Wang, X., H. Zhang, and D. Li, *Characterization of lubricated worn surfaces using a nano/micro-indenter.* Materials Science and Engineering: A, 2004. 371(1): p. 222-228.

189. Tian, Y., et al., *Synthesis of hydrophobic zinc borate nanodiscs for lubrication.* Materials letters, 2006. 60(20): p. 2511-2515.

190. Cusano, C. and H. Sliney, *Dynamics of Solid Dispersions in Oil During the Lubrication of Point Contacts, Part II—Molybdenum Disulfide.* ASLE TRANSACTIONS, 1982. 25(2): p. 190-197.

191. Jun, L., X. Shuping, and G. Shiyang, *FT-IR and Raman spectroscopic study of hydrated borates.* Spectrochimica Acta Part A: Molecular and Biomolecular Spectroscopy, 1995. 51(4): p. 519-532.

List of publications

- C Zhao, G. Ren and *Y.K. Chen, *Frictional properties of cerium oxide nanoparticles in water*, Proceedings of 2011 World Congress on Engineering and Technology, ISBN 978-1-61284-365-0, Shanghai, 4, 139, (2011).

- C. Zhao, G. G. Ren and Y. K. Chen, *A Study of Tribological Properties of Water-Based Ceria Nanofluids.* Tribology Transaction (accepted in November 2012)

- C. Zhao, Y. Jiao, Y. K. Chen and G. G. Ren, *The tribological properties of zinc borate ultrafine powder as a lubricant additive in sunflower oil*. (revision submitted to special issue of WEAR on the 4th UK-China Tribology Symposium in September 2012)

Appendix – 1

Malvern Zetasizer-Nano Series device specifications

Measurement type:	Particle size	Zeta potential
Measurement type:	Particle size and molecular size	Zeta potential (and optional Protein Mobility)
Measurement range:	0.3nm – 10.0 microns (diameter).	3.8nm – 100 microns (diameter)
Measurement principle:	Dynamic Light Scattering	Electrophoretic Light Scattering
Minimum sample volume:	12µL	150µL (20µL using diffusion barrier method)
Accuracy:	Better than +/-2% on NIST traceable latex standards	0.12µm.cm/V.s for aqueous systems using NIST SRM1980 standard reference material
Precision/Repeatability:	Better than +/-2% on NIST traceable latex standards	10mg/mL (BSA).

SETARAM TG-DSC 1600 device specifications

Temperature Range	Ambient to 1 600 °C
Isothermal temperature accuracy	+/- 1 °C
Programmable temperature scanning rate (heating and cooling	0.01 to 100 °C.min-1
Furnace cooling	32 min (1600°C to 50°C)
Maximum balance capacity	20 g
Weight range	+/- 1 000 mg - +/- 200 mg
Weighing precision	+/- 0.01 %
TG resolution	0.2 μg - 0.02 μg
Auto Sampler	30 samples and 6 references 4-prong gripper
DSC rod - Resolution	0.4 μW / 10 μW dependent on sensor
3D Cp rod - Cp Accuracy	< 2 %
Vacuum	< 10-1 mbar
Evolved gas	simultaneous MS, FTIR couplings (option)
Gases	Two inlets for gas scanning (inert or reactive) OR 3 carrier gases (option) (MFC from 4 to 200 ml/min) + 1 auxiliary or reactive gas (MFC from 0.3 to 16 ml/min)
Weight	55 kg / 121 lbs
Dimensions (Height / Width / Depth)	56 closed, 76 opened / 53 / 58 cm (22.0 closed 29.9 opened / 20.8 / 22.8 in)
Power requirements	230 V - 50/60 Hz

Appendix – 2

In this section, the thickness measurements of the tribo-films generated by different lubricants samples are displayed. Morphologies of the tribo films were firstly constructed by an atomic force microscope (AFM) used in this study, 'Nanosurf Easyscan 2' from Nanosurf (Liestal, Switzerland). The 2-D cross section profiles of the tribo-films were later created using the dedicated softerware. The thickness of the tribo-films can then be measured as the distance from the top surface of the tribo-films to the bottom substrates.
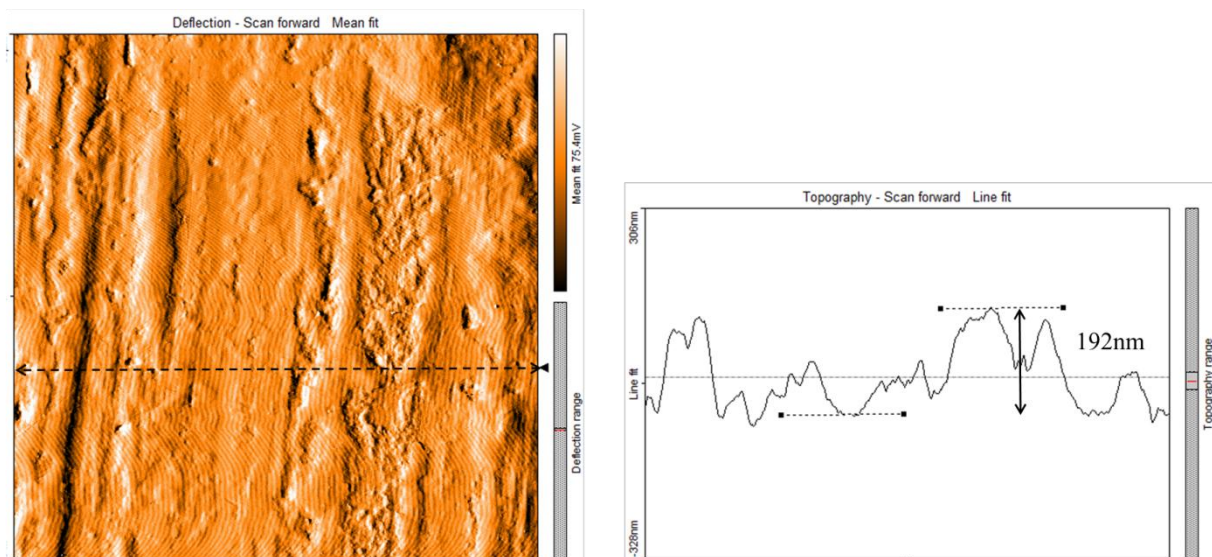
Figure A–1 The thickness of the tribo-film generated by liquid paraffin with 0.5% HDTMOS modified CeO_2 nanoparticles
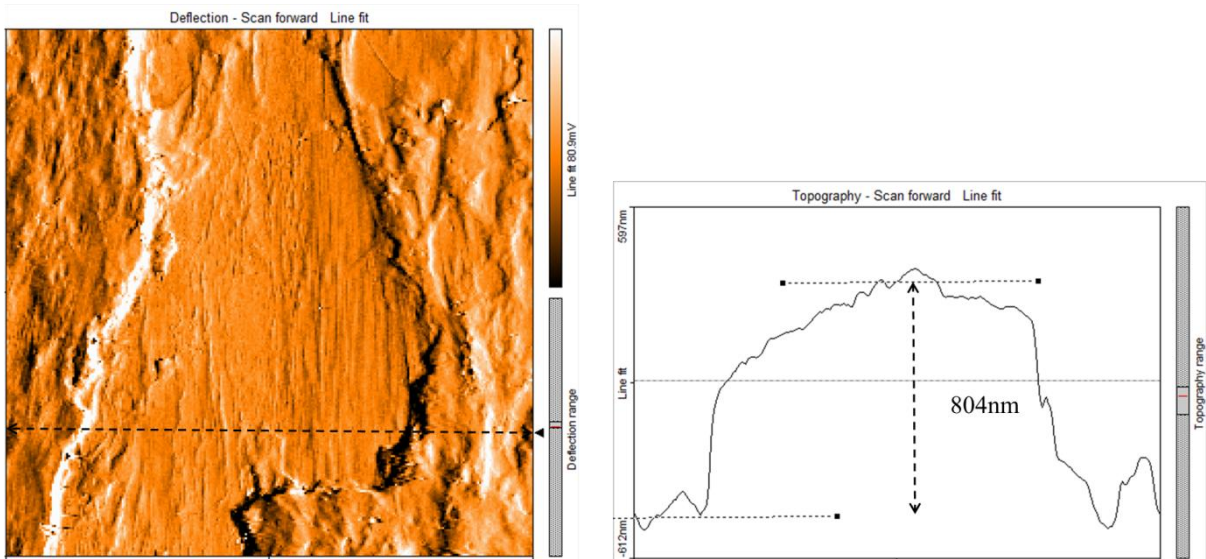
Figure A–2 The thickness of the tribo-film generated by pure sunflower oil
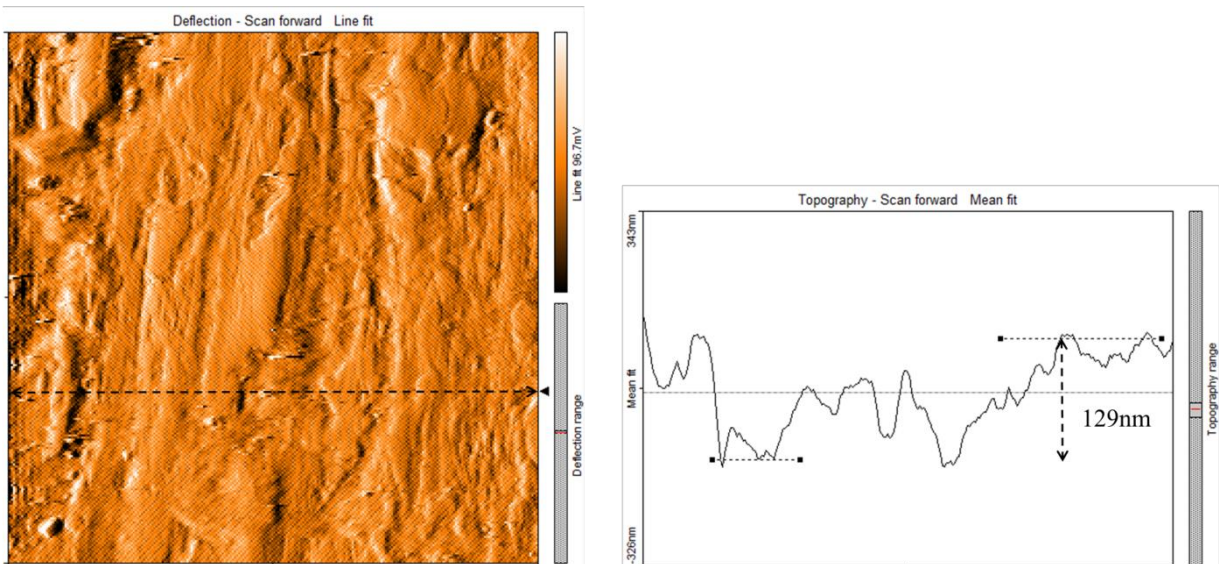

Figure A–3 The thickness of the tribo-film generated by sunflower oil with 0.5% ZB UFPs
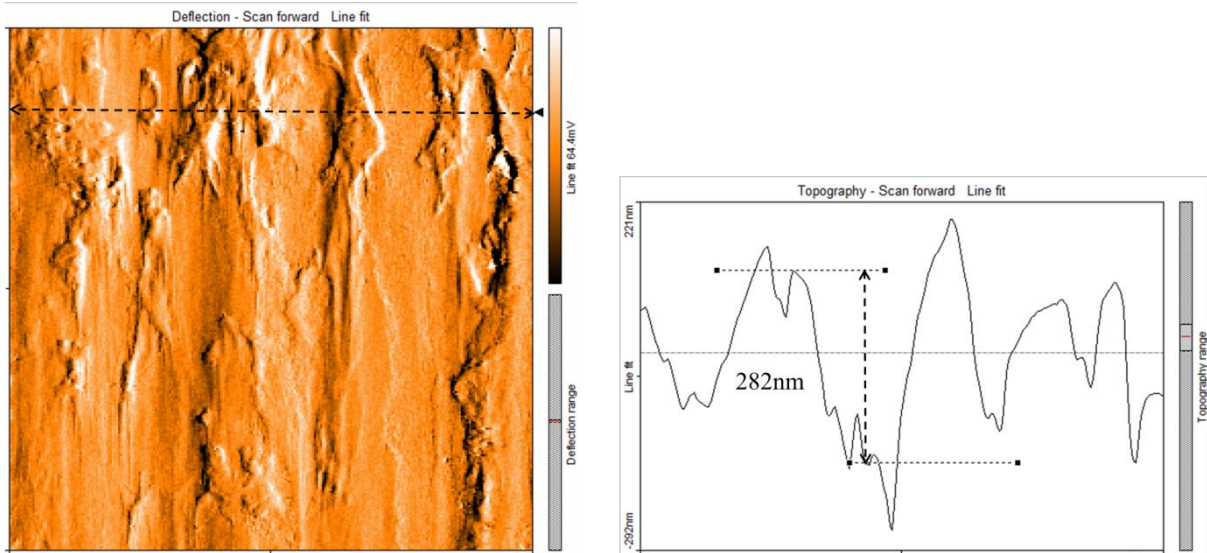
Figure A–4 The thickness of the tribo-film generated by sunflower oil with 1% ZB UFPs
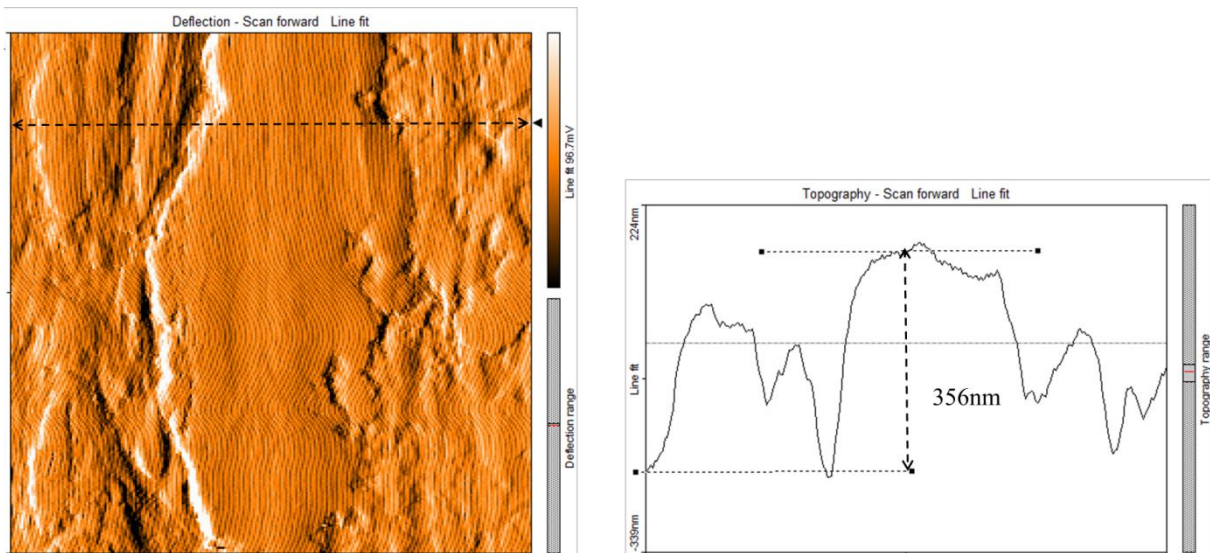

Figure A–5 The thickness of the tribo-film generated by sunflower oil with 2% ZB UFPs
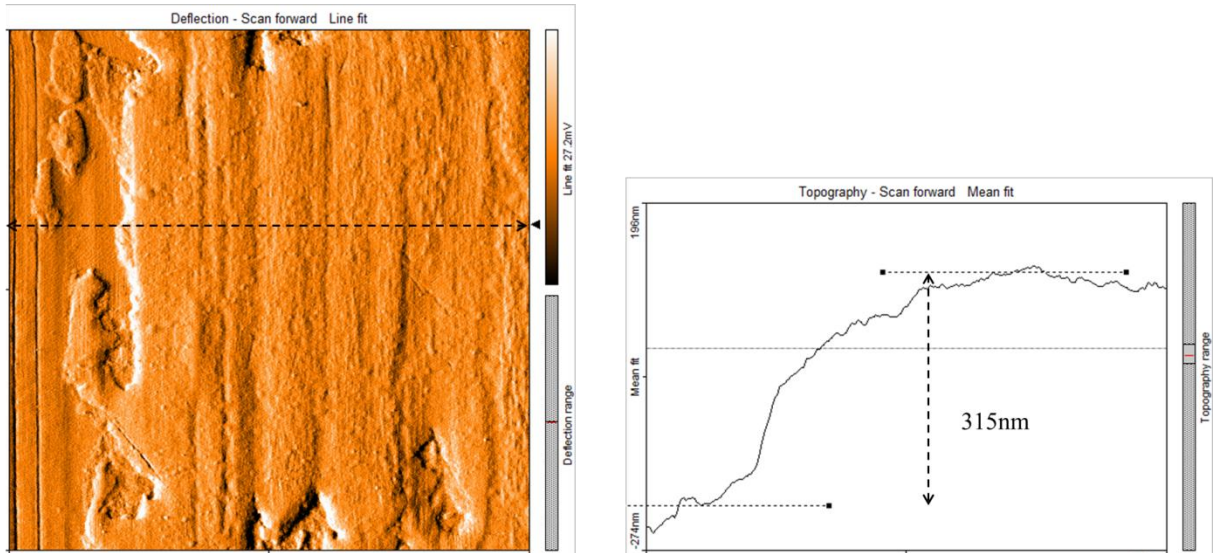
Figure A–6 The thickness of the tribo-film generated by liquid paraffin with
0.5% HDTMOS modified ZB UFPs